PHYSICOCHEMICAL STUDIES ON LIPOSOME MIMETIC SYSTEMS AND THEIR COMPLEXES WITH BIOLOGICALLY RELEVANT POLYMERS

Thesis submitted

to the

University of North Bengal

For the award of

Doctor of Philosophy

In Chemistry

By

Pritam Guha (M. Sc. in Chemistry)

GUIDE

Prof. Amiya Kumar Panda

Department of Chemistry

University of North Bengal

P.O: University of North Bengal, DT: Darjeeling

PIN: 734013, W. B., INDIA

February-2018

DECLEARTION

I declare that the thesis entitled **"PHYSICOCHE MICAL STUDIES ON LIPOSOME MIMETIC SYSTEMS AND THEIR COMPLEXES WITH BIOLOGICALLY RELEVANT POLYMERS"** has been prepared by me under the supervision of Prof. Amiya Kumar Panda.

No parts of this thesis have formed the basis for the award of any degree or fellowship previously.

Pritam Guha

Pritam Guha

Department of Chemistry

University of North Bengal

Darjeeling- 734013

West Bengal

India

Date: 09/02/2018

CERTIFICATE FROM THE SUPERVISOR

I certify that Mr. **Pritam Guha** has prepared the thesis entitled **"PHYSICOCHE MICAL STUDIES ON LIPOSOME MIMETIC SYSTEMS AND THEIR COMPLEXES WITH BIOLOGICALLY RELEVANT POLYMERS"** for the award of Ph.D. degree from the University of North Bengal, under my guidance. He has carried out the work at the Department of Chemistry, University of North Bengal.

No parts of this thesis have formed the basis for the award of any degree or fellowship previously.

Amiya Kumar Panda

Date: 09/02/2018

URKUND

Antiplagiarism Report of Ph.D Thesis

Title of the Thesis: PHYSICOCHEMICAL STUDIES ON LIPOSOME MIMETIC SYSTEMS AND THEIR COMPLEXES WITH BIOLOGICALLY RELEVANT POLYMERS

Urkund Analysis Result

Analysed Document:	Pritam_Chemistry.pdf (D35476192)
Submitted:	2/9/2018 12:18:00 PM
Submitted By:	nbuplg@gmail.com
Significance:	1 %

Sources included in the report:

Prasant_Chemistry.docx (D27172807)
https://aaltodoc.aalto.fi/handle/123456789/2456
http://www.academia.edu/29412230/Ion_Pair_Amphiphile_A_Neoteric_Substitute_that_Modulates_the_Physico-Chemical_Properties_of_Biomimetic_Membranes
http://www.mdpi.com/2306-5354/4/4/84/pdf

Instances where selected sources appear:

16

Pritam Guha
Signature of the Candidate

Signature of the Supervisor

09/02/18
Signature of the HOD, Chemistry

Dedicated to My Parents…….

ACKONOWLEDGEMENT

The field of research is full of uncertainty with little hope to invent or to discover the undisclosed object. However in my field of research I have been motivated encouraged and supported by several individuals who actually assist me in the course of research.

I wish to express my most sincere gratitude to my supervisor; Prof. Amiya Kumar Panda, former Professor, Department of Chemistry, University of North Bengal, Darjeeling for his incalculable planning in the field of research and its presentation, extreme guidance and continuous support to my entire research work. Sir it is because of you my dream comes true.

I express my sincere thanks to the authorities of University of north Bengal for providing the resources and accessibilities related to my research work.

I would like to convey my cordial gratitude to Prof. Boris A. Noskov and his group; Department of Colloid Chemistry, St. Petersburg State University, St. Petersburg, Russia, for their valuable assistance in my research work.

I offer my special thanks to Prof. Chien- Hsiang Chang, Department of Chemical Engineering, National Chen Kung University, Taiwan for carrying out Small angle x-ray scattering studies.

I would like to express my special sincere thanks to Prof M. N. Roy, Prof. P. Ghosh, Prof. A. Mishra and Prof, S. K. Saha for their constant support and motivation during my research work.

I express my profound sense of gratefulness to the Head and all of my respected Teachers, Department of Chemistry, University of North Bengal for their assistance and motivation during my entire research work. I am also grateful to all the non-teaching stuff for their contentious cooperation.

I am sincerely thankful to UGC-BSR for the research fellowship under the scheme of BSR fellowship.

I convey my gratitude to my Parents for their continuous support, motivation and encouragement during my entire life. Without them I would not be here today.

I also convey my sincere gratitude to Dr. Animesh Pan for the assistance in the field of monolayer investigation.

I would like to express gratitude to my past and present fellow colleagues Dr. Kausik Manna, Dr. Sujoy Paul, Dr. (Mrs.) Moumita Chakraborty, Banita Sinha, Sudarshana di, Prasant, Biplab, Gourab, Priyam, Suraj, Manish, Amrit, Ravi, Anup, Manas Barai, Atanu, Manas Mondol, Sujit Patra, Habiba Sultana and Emili Manna for their valuable support during my research work.

My special thanks go to my fellow lab mates Dr. Prasenjit Ghosh, Bittu Saha, Tanushree Sutradhar, Sudip sarkar and Gulmi Chakroborty for their kind assistant during my research work.

At this time I would express my sincere thanks to SAIF, North Eastern Hill University, for providing TEM micrographs of my research sample.

My sincere gratitude goes to Prof. Kanjiro Torigoe, Department of Pure and Applied Chemistry, Tokyo University of Science for carring out FF-TEM investigation of my research samples.

I also express my deep sense of appreciation to my cherished friend Ms. Moumita Sarkar for lends a selfless hand in preparation of Graphical Abstract and her continuous love and support.

Finally I would express my sincere appreciation to CSIR, DST, UGC and DBT, Govt. of India for the research fund for procuring chemicals and instruments. Because of these

funds, Instrument facilities like DLS, DSC, UV-VIS spectrophotometer, Langmuir Blodegt balance, and ultra sonicators are made possible.

Pritam Guha
Department of Chemistry
University of North Bengal
Darjeeling - 73413

ABSTRACT

The research work embodied in this thesis entitled **"PHYSICOCHEMICAL STUDIES ON LIPOSOME MIMETIC SYSTEMS AND THEIR COMPLEXES WITH BIOLOGICALLY RELEVANT POLYMERS"** is primarily focused on to develop stable, non toxic and biodegradable drug delivery medium, viz liposome mimetic system, known as vesicles with the aid of naturally occurring phospholipids soylecithin (SLC) and synthetic amphiphiles. Finally their interaction with biological macromolecules like dendrimer has been investigated. The whole thesis work is divided into three chapters and their brief discussion is given below.

Chapter I describes the physicochemical characterization of vesicles. vesicles were prepared at different ratio of soylecithin (SLC) and IPA with additional30 mol% cholesterol (with respect to SLC and IPA) in PBS. Impact of IPA on SLC monomolecular film was studied by Langmuir monolayer technique (surface pressure – area isotherms). Hydrodynamic size (d_h), zeta potential (Z. P.) and polydispersity index (PDI) which describes the dispersion behaviour vesicles were measured through dynamic light scattering (DLS) technique. Vesicles Morphological properties also successfully recognized by electron microscopic (normal TEM as well as FF-TEM) studies. Thermotropic behaviours of the bilayers were scrutinized by differential scanning calorimetry (DSC). Structural changes of bilayer, caused by IPA, were further scrutinized by using fluorescence spectroscopy using 1, 6-diphenyl-1, 3, 5-hexatriene (DPH) and 7-hydroxycoumarin (7HC) as the fluorescent probes to get knowledge about the micro viscosity of the bilayer wall. Entrapment efficiency (E. E.) of the vesicles using cationic dye methylene blue (MB) was also evaluated. Such systems are expected to have superior properties as potent vectors for drug delivery.

Chapter II illustrates physicochemical investigation on cationic hybrid vesicles and its toxicity relate to Neuroblastoma cell line. As biological cell membranes are

negatively charged, non-toxic, biodegradable vesicles could be served as an excellent drug delivery agent. Cationic vesicles were prepared using bi-tail cationic surfactants with varying hydrocarbon chain length (bis-C_{12} to C_{18}) in combination with soy lecithin (SLC) and ion pair amphiphile (IPA). Bi-tail cationic surfactants were chosen to progressively substitute with previously established three sets of SLC/IPA combinations (1:0, HCV1; 9:1, HCV2 and 7:3, HCV3; M/M). Interaction between hybrid membrane and Piroxicame (Px), a Non Steroidal anti inflammatory Drug were analyzed in the form of monolayer, bilayer and solid supported bilayer.

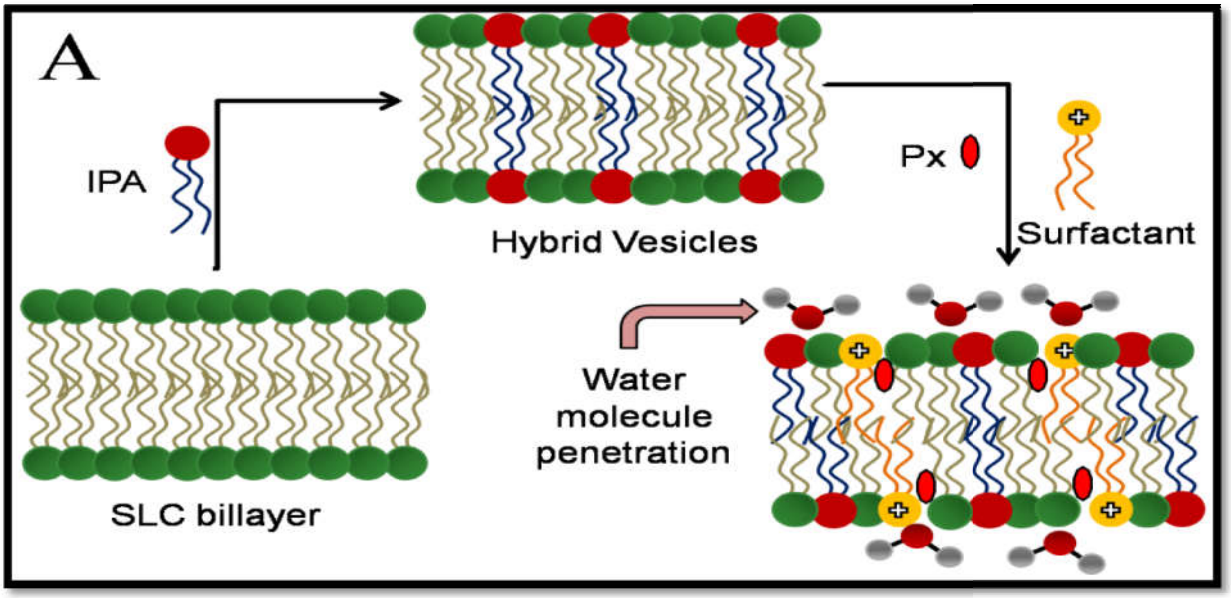

Finally optimised Px encapsulated formulations were analysed for biological activity. Mutual miscibilities among the components were studied by way of the surface pressure – area measurements. Physicochemical characterizations of the different hybrid vesicles with and without Px were assessed by combined dynamic light scattering, zeta potential, electron microscopy, atomic force microscopy, differential scanning calorimetry, FTIR, UV-VIS absorption and emission sepctroscopic studies. Entrapment efficiency and the release kinetics of Px from the vesicles were analyzed by conventional dialysis bag approach. Finally the toxicity and biocompatiblity of the drug loaded formulations were assessed. And could shed

further light in the development of drug delivery systems in the treatment of brain – tumors targeted drug delivery.

Chapter III presents the physic-chemistry between the interaction of cationic vesicles and PAMAM succinimaci acid, 1, 4-diaminobutane core dendrimers generation 5 (G5-SA) which is negatively charged. Previously prepared cationic vesicle comprised of SLC, IPA and DHDAB in three different combinations was taken to investigate the impact of dendrimers. Increasing hydro dynamic size and reduced Z. P. measurement suggests the formation of vesicles/dendrimers aggregates. The formation of aggregates was further confirmed by turbidity measurement. Morphological state of the vesicles with and without dendrimers was analysed via TEM studies. Vesicles disintegration kinetics measurement also has been done to understand the pattern of interaction using varying concentration of dendrimers. A surface pressure – time isotherm developed due to the vesicle disintegration upon the inclusion of dendrimer. The rate kinetics of such disintegration process was found to be depending on the dendrimers concentration.

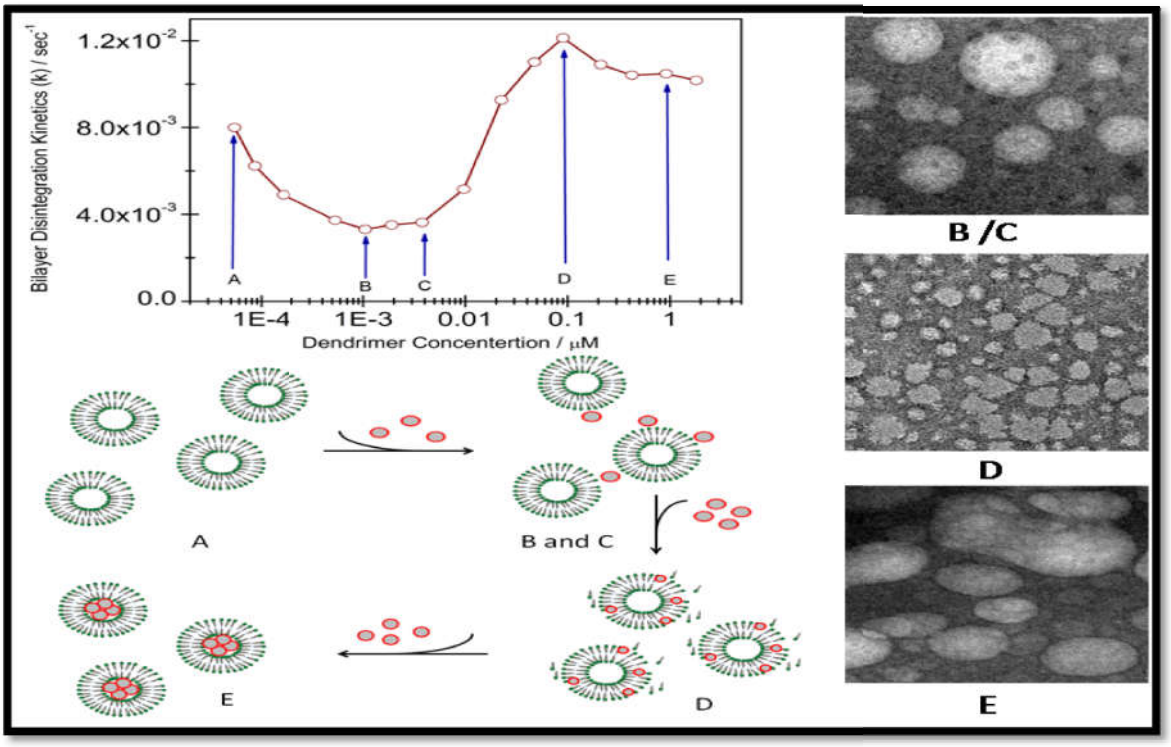

The effect of dendrimers on solid supported cationic bilayer was further scrutinized via AFM studies that help to understand stoichiometry depended aggregate formation. Finally DSC studies was performed which specifically enlighten the features of bilayer in presence of dendrimers as well it describe the point of interaction induced by dendrimer on the bilayer region. Steady state fluorescence anisotropy measurements also lead us to recognize that at lower concentration, dendrimer porn to attack on the surface of the bilayer and thereby rigidify membrane packing. However at higher concentration, it interdigited into the bilayer segment. Overall interaction studies put IPA on the map as it tries to restore the bilayer morphology by providing hydrophobic interaction. Bilayer embedded dendrimer forms supramolecular aggregates that can be promoted in the field of drug, gene, and vaccine delivery.

PREFACE

Vesicle base formulations have extensively used in the field of therapeutics because of its fantastic charisma to host both hydrophilic and lipophilic drug molecules into it. Literature study revel numerous type of liposome or vesicles and their characterization, application in different fields. It is known that amphiphile molecules like lipids are one of the primary components for the preparation of liposome mimetic system. However liposome or vesicle suffers through some major limitations like oxidation, bacterial attack and room temperature instability.

Chapter I summarizes the preparation and characterisation of vesicular formulation comprised of SLC and IPA. Investigations suggest IPA; a superior surrogate for the SLC bilayer. By providing extra hydrophobic effect, it rigidifies bilayer packing and was found to be stable at room temperature for a period of 100 days. **Chapter II** describes a process of modification in SLC/IPA vesicle by introducing double tailed cationic surfactant with varying chainlength (bis- C_{12}-C_{18}) to formulate hybrid cationic vesicles (HCV). Most stable vesicular formulations were chosen to incorporate Non Steroidal Anti Inflammatory Drug (NSAID), Piroxicam (Px). The drug loaded vesicles were employed for cytotoxicity measurement. Formulations were hemocompatable and non toxic to normal human blood cell lymphocytes. However it confirms considerable toxicity for Neuroblastoma cell line (Cancer cell line), hence could be benefitted in the field of cancer treatment. **Chapter III** explores the impact of biologically relevant polymer, dendrimer on hybrid cationic vesicles (HCV). PAMAM-succinamic acid dendrimers, 1,4-diaminobutane core, Generation 5, (G5-SA) was added in various range of concentration to a fixed quantity of vesicle formulation. Investigations suggest G5-SA at low concentration adsorb on the surface of the vesicles driven by ionic interaction. Although at higher concentrations, it disrupts the bilayer and creates an opportunity to produce dendrimer/vesicles supramolecular complex.

TABLE OF CONTENTS

CHAPTER I

Ion Pair Amphiphile: A Neoteric Substitute that Modulates the Physico-Chemical Properties of Biomemetic Membranes

CHAPTER II

Exploring the Dual Impact of Hydrocarbon Chainlength and the Role of Piroxicam a Conventional NSAID on Soylecithin/Ion pair Amphiphiles Mediated Hybrid Vesicles for Brain – Tumors Targeted Drug Delivery

CHAPTER III

Ion Pair Amphiphile in preserving Bilayer Integrity: An account of PAMAM dendrimer induced Morphological adaption of Hybrid cationic vesicles

LIST OF TABLES

LIST OF FIGURES

Chapter I

Chapter III

LIST OF APPENDICES

APPENDIX A:

List of research publications

APPENDIX B:

List of Oral and Poster presentation

APPENDIX A

List of Publications (Related to Thesis work)

1. **Guha, P**.; Roy, B.; Karmakar, G.; Nahak, P.; Koirala, S.; Sapkota, M.; Misono, T.; Torigoe, K.; Panda, A. K., Ion-Pair Amphiphile: A Neoteric Substitute That Modulates the Physicochemical Properties of Biomimetic Membranes. *The Journal of Physical Chemistry B* **2015,** *119* (11), 4251-4262.

2. **Guha, P**.; Roy, B.; Nahak, P.; Karmakar, G.; Chang, C-H.; Bikov, A. G.; Akentiev, A. B.; Noskov, B. A.; Mandal, A. K.; Kumar, A.; Hassan, P. A.; Aswal, V. K.; Misono, T.; Torigoe, K.; Panda, A. K., Exploring the dual impact of hydrocarbon chainlength and the role of Piroxicam a conventional NSAID on Soylecithin/Ion pair amphiphiles mediated hybrid vesicles for brain – tumors targeted drug delivery. (Communicated)

3. **Guha, P**.; Roy, B.; Nahak, P.; Karmakar, G.; Bikov, A. G.; Akentiev, A. B.; Noskov, B. A.; Panda, A. K., Ion Pair Amphiphile in preserving Bilayer Integrity: An account of PAMAM dendrimer induced Morphological adaption of Hybrid cationic vesicles. (Manuscript is under preparation)

List of Publications (Not related to Thesis work)

1. Nahak, P.; Karmakar, G.; Roy, B.; **Guha, P**.; Sapkota, M.; Koirala, S.; Chang, C.-H.; Panda, A. K., Physicochemical studies on local anaesthetic loaded second generation nanolipid carriers. *RSC Advances* **2015,** *5* (33), 26061-26070.

2. Sapkota, M.; Karmakar, G.; Nahak, P.; **Guha, P**.; Roy, B.; Koirala, S.; Chettri, P.; Das, K.; Misono, T.; Torigoe, K.; Panda, A. K., Effect of polymer charge on the formation and stability of anti-inflammatory drug loaded nanostructured lipid carriers: physicochemical approach. *RSC Advances* **2015,** *5* (81), 65697-65709.

3. Bhattarai, R.; Roy, B.; **Guha, P**.; Bista, A.; Bhadra, A.; Karmakar, G.; Nahak, P.; Chettri, P.; Panda, A. K., Spectroscopic Investigation on the Interaction of Curcumin with Phosphatidylcholine Liposomes. *Journal of Surface Science Technology* **2015,** *31* (1-2), 1-9.

4. Koirala, S.; Roy, B.; **Guha, P**.; Bhattarai, R.; Sapkota, M.; Nahak, P.; Karmakar, G.; Mandal, A. K.; Kumar, A.; Panda, A. K., Effect of double tailed cationic surfactants on the physicochemical behavior of hybrid vesicles. *RSC Advances* **2016,** *6* (17), 13786-13796.

5. Nahak, P.; Karmakar, G.; Chettri, P.; Roy, B.; **Guha, P**.; Besra, S. E.; Soren, A.; Bykov, A. G.; Akentiev, A. V.; Noskov, B. A.; Panda, A. K., Influence of Lipid Core Material on Physicochemical Characteristics of an Ursolic Acid-Loaded

Nanostructured Lipid Carrier: An Attempt To Enhance Anticancer Activity. *Langmuir* **2016**.

7. Karmakar, G.; Nahak, P.; **Guha, P**.; Roy, B.; Chettri, P.; Sapkota, M.; Koirala, S.; Misono, T.; Torigoe, K.; Ghosh, S.; Panda, A. K., Effects of Fatty Acids on the Interfacial and Solution Behavior of Mixed Lipidic Aggregates Called Solid Lipid Nanoparticles. *Journal of Oleo Science* **2016,** *65* (5), 419-430.

8. Roy, B.; **Guha, P**.; Bhattarai, R.; Nahak, P.; Karmakar, G.; Chettri, P.; Panda, A. K., Influence of Lipid Composition, pH, and Temperature on Physicochemical Properties of Liposomes with Curcumin as Model Drug. *Journal of Oleo Science* **2016,** *65* (5), 399-411.

9. Bhadra, A.; Karmakar,G.; Nahak, P.; Chettri, P.; Roy, B.; **Guha, P**.; Mandal, K. A.; Nath, K. R.; Pnda, A. K., Impact of detergents on the physiochemical behavior of itraconazole loaded nanostructured lipid carriers. Colloids surfaces A; **2017**, *516*, (5), 63–71.

APPENDIX B

List of Oral presentation

1. "*Physico-chemical studies of liposome mimetic systems and their interaction with biologically relevant polymers*" **Pritam Guha** and Amiya Kumar Panda, in the seminar "*Trends in Surface Scienceand Related Areas*" held at Presidency University, Kolkata on July 24, 2014.

2. "*Membrane tunability achieved by the addition of double tailed cationic surfactants on soylecithin+ ion pair amphiphile: A hybrid vesicle*" **Pritam Guha** and Amiya Kumar Panda in the seminar of "*North East Regional Seminar on Trends in Colloid and Interface Science*" held in North Eastern Hill University, Shillong on November 27-28, 2014.

3. "*Membrane tenability achieved by the addition of double tailed cataionic surfactants on Soylecithin+ Ion Pair Amphiphile: A hybrid Vesicle*" **Pritam Guha** and Amiya Kumar Panda in the "*17th National Conference on Surfactants, Emulsions and Biocolloids*" held in Pt. Ravishankar Shukla University, Raipur on November 4-6, 2015 and received First Prize award for the oral presentation.

List of poster presentation

1. "Impact of Ion Pair Amphiphile on Soylecithin Vesicles" **Pritam Guha** and Amiya Kumar Panda in the "*5th Asian Conference of Colloid and Interface Science*" held in University of North Bengal, Darjeeling. November 20-23, 2013.

2. "*Physicochemical Investigation on Vesicles comprising Soylecithin and Ion Pair Amphiphile: An innovative media for Drug Delivery*" **Pritam Guha** and Amiya Kumar Panda in the "*Indo- UK International Workshop On Advanced Materials And Their Applications In Nanotechnology*" at BITS Pilani KK Birla Goa campus during May 17- 19, 2014.

3. "*Effect of Ion Pair Amphiphile and surfactant chain length on artificial vesicles: A comparative study*" **Pritam Guha** and Amiya Kumar Panda in the "*19th CRSINational Symphosium in Chemistry*" held at University of North Bengal, Darjeeling, July 14-16, 2016.

4. "*Effect of Hydrocarbon Chain Length on Hybrid Bilayer Towards the Formation of Stable Vesicular System with Special Addition to Non-Steroidal Anti-Inflammatory Drug Piroxicam*"

Pritam Guha and Amiya Kumar Panda in the "*International Conference on Challenges in Drug Discovery and Delivery*" held at Birla Institute of Technology and science, Pilani, March 2–4, 2017.

ABBRIVIATION

1,6- diphenyl – 1, 3, 5- hexatriene	DPH
7- hydroxycumarin	7-HC
1, 2 - dipalmitoyl-snglycero -3-phosphocholin	DPPC
1, 2 - dipalmitoyl-snglycero -3-phosphogylcerol	DPPG
1-palmitoyl-2-oleoyl-sn-glycero-3- phosphocholin	POPC
Atomic Force Microscopy	AFM
Critical Packing Parameter	Cpp
diacylglycerol	DAG
Didlkylaminomethyl rutin	DAMR
Disodium hydrogen phosphate	Na_2HPO_4, $12H_2O$
Differential Scanning Calorimetry	DSC
didodecyldimethylammonium bromide	DDDAB
dimethylditetradecyldiammonium bromide	DTDAB
dihexadecyldimethylammonium bromide	DHDAB
dioctadecyldimethylammonium bromide	DODAB
Dynamic Light Scattering	DLS
Drug Delivery System	DDS
Entrapment Efficiency	E. E.
Freeze-fracture TEM	FF-TEM
Hexadecyltrimethylammonium bromide	HTMAB
Hybrid cationic vesicle	HCV
Interaction Parameter	I. P.
Isothermal Caloremetry	ITC
Ion Pair Amphiphile	IPA

Langmuir Boldget	LB
Long-circulating liposome	LCL
Large unilamellar vesicles	LUV
Methelene Blue	MB
Multilamellar vesicles	MUV
National Centre for Cell Science	NCCS
Phosphatidyl choline	PC
Phosphatidyl glycerol	PG
Phosphatidyl ethanolamine	PE
Phosphatidyl serine	PS
Phospholipid	PL
Polyamidoamine	PAMAM
Polydispersity index	PDI
Phosphate buffer solution	PBS
PAMAM succinamic acid dendrimer,Generation 5	G5-SA
Piroxicam	Px
Sodium dodecylsulfate	SDS
Soylecithin	SLC
Small Unilamellar vesicles	SUV
Solid lipid nanoparticle	SLN
Scanning Electron Microscope	SEM
Small Angle Neutron Scattering	SANS
Small angle x-ray scattering	SAXS
Sodium hydrogen phosphate	$NaH_2PO_4.2H_2O$
Transmission Electron Microscope	TEM
Zeta Potential	Z. P.

1. Amphiphile

Amphiphiles have special structural features that simultaneously possess the hydrophilic (water loving) and hydrophobic part (water hating/fat loving). The hydrophilic portion generally consist ions (anionic, cationic, zwitter ionic) or uncharged polar groups whereas lipophilic parts are generally long chain hydrocarbon, such in the form of $CH_3(CH_2)_n$, with n > 8.

Carboxylate (COO^-), sulphates (SO_4^{2-}), sulfonates (SO_3^{2-}), phosphate (PO_4^-), *etc.*, are the anionic and the quaternary ammonium (NH_4^+) ion is the cationic group that attached with the lipophilic hydrocarbon chain. Alcohols are the class of polar uncharged group often attaché with long chain hydrocarbons, such as diacyl glycerol. In aqueous medium they spontaneously form self-assembled structures. Schematic diagram of amphiphile and its self assemble structure in water, commonly known as "micelle" (Figure 1).

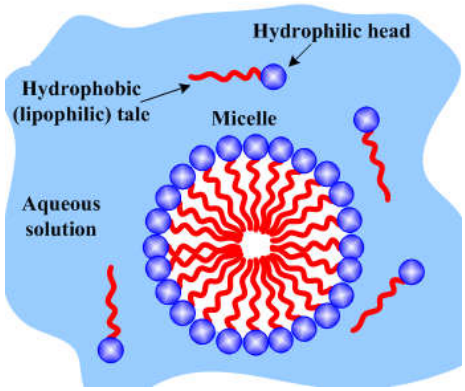

Figure 1. Structure of amphiphile and its self assembled structure (Micelle). Source: www.substech.com.

Because of the hydrophilic-lipophilic charisma, it has diverse range of applications, *viz.,* in detergent[1], paint, pharmaceutics[2-4] food[5,6] to mention a few. The variety of self-assembled structures made amphiphiles to be useful in different areas. Throughout the dissertation work, hybrid lipid bilayer is the most highlighted aggregate structure. Naturally

occurring phospholipids, synthetic amphiphiles and double tail cationic surfactants will extensively be considered in this dissertation in preparing liposome mimetic systems, here in hybrid vesicles.

1.1. Self Assembly and Aggregate Structure

Self assembly of amphiphiles is a spontaneous process, leading to the formation of aggregate having various morphologies from a variety of building blocks. Being the aggregated form, the process of self assembly can include verity of complexities. It can be a simple process of dimeriztion of two amphiphiles or as complicated as biological membranes. Among the various building blocks, amphiphiles draw the attention most over the others as its superiority to form robust assemblies.[7]

Amphiphiles having hydrophilic and lipophilic part renders dual preferences for solvents. Due to amphiphilicity, the polar head group interacts with water (or polar solvent) while the lipophilic part tends to reside out of the contact of water and thus try to orient in the air water interface. In water, it first dissolves as normal solute into the form of a monomer, after a threshold concentration is reached; they form micro-structure or assemblies to avoid the unfavourable solvent hating interaction between water and lipophilic parts. The course of self organization is spontaneous, as the overall entropy increases in the process.[8,9] The increased entropy begins from water-hydrocarbon interaction when amphiphiles are present as monomer. As monomer it forces water molecules in an order state around the lipophilic part. When concentration of amphiphiles is increased two possible scenarios are developed. Either they have to move at air-water interface or to form aggregate structure. The brakeage of ordered water molecules enhance the process of entropy that leads to an overall gain of free energy that drives the amphiphiles to form aggregate structure by virtue of self-assembly.[8,10] The aggregation of amphiphile is generally driven by hydrophobic interaction, hydrogen bond, steric effect and electrostatic interaction.

1.2. Critical Packing Parameter and Aggregate Morphology

Self assembling is a spontaneous process; where amphiphilic building blocks governed by mutual interactions form ordered structure. The shape and the size, or better to say morphology of the aggregates not only depend on above mentioned forces, but also depend on the structure, molecular geometry and concentration of the amphiphiles, extent of hydration, pH and ionic strength of the dispersion medium. Critical packing parameter (C_{pp})[11,12] which takes into account the parameters like polar head group cross-sectional area (a_0), hydrocarbon chain length (l_c) and hydrophobic volume (v) are related as:

$$C_{pp} = \frac{v}{a_0 . l_c} \qquad (1)$$

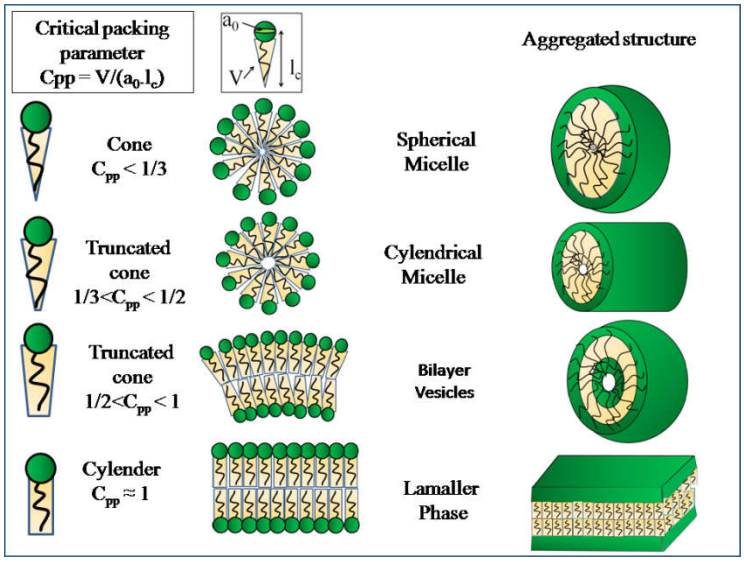

Figure 2: Summary of aggregate structure predicted from critical packing parameter C_{pp}

These parameters together hold the information about the geometrical structure of the aggregates. With increasing C_{pp}, the structure of the aggregated form could be spherical (C_{pp}< 1/3), cylindrical (1/3< C_{pp}< 1/2) and lamellar (C_{pp} = 1). In case of vesicles, the range of C_{pp} is 1/2 to 1 with an inner cavity encapsulating the dispersion medium. A summary of the aggregated structure predicted from critical packing parameter (C_{pp}) is represented in Figure 2.

2. Lipids

Lipid is one of the most significant or important constituents that helps to make the building blocks for all the varieties of animal and plants. Because of its high calorific values, lipids are important dietary components.[13] Lipids are naturally occurring carbon compounds, related to fatty acids and esters of fatty acids. Lipids belong to a diverse and large number of non polar organic compounds having non polar hydrocarbon chain or acyl chain attached with the polar head groups. During the process of aggregation, its head group gets exposed towards the polar solvent medium keeping the non polar acyl chain shielded inside. Lipids, along with proteins and nucleic acids, are essential biomolecules for the structure and function of living matter. The common lipids are fats, oils, waxes, steroids, terpins, phospholipids and glycolipids. Phospholipids are the predominant building blocks of biological membranes and herein considered in the dissertation for the preparation of liposome mimetic systems or hybrid vesicles.

2.1. General Classification and Structure of Lipids.

Lipid can be classified into three categories.

2.1.1. Simple lipids (Homolipids)

2.1.2. Compound lipids (Heterolipids)

2.1.3. Derived Lipids (Simple and Compound lipids)

2.1.1. Simple Lipids

Simple lipids are the alcohol esters of fatty acids including neutral fats and waxes. Even number of carbon atoms in the fatty acyl chain may contain saturation or unsaturation. Simple lipids are known as triglycerides or triacyl glycerols. Glyceride bond is formed when the –COOH group of fatty acid and the –OH group of glycerol is attached by the removal of one water molecule to form –C-O-C- bond. Depending upon the extent of esterification, it

can be monoglyceride, diglyceride and triglyceride. Lipids having solid or liquid state at room temperature are known as fat and oil respectively. Schematic structure of simple glyceride is shown in Figure 3.

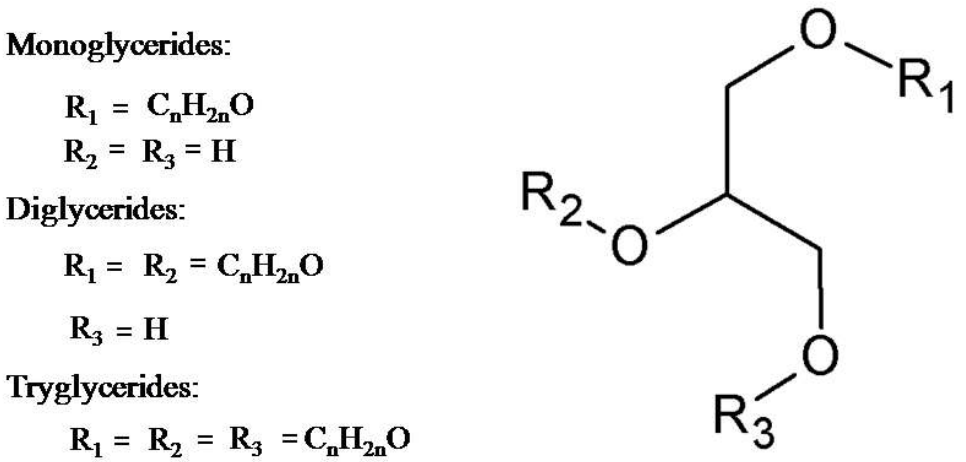

Figure 3. General structure of glycerides.

- **Waxes**

Waxes are the ester of long chain saturated or unsaturated fatty acid with long chain monohydric alcohol. The fatty acids range between C_{14} and C_{36} and the alcohols range between C_{16} and C_{36}. Because of the long hydrocarbon chains, it has high molecular mass with relatively high melting point (above 40 ^{o}C). They are mainly lipophilic in nature. Few examples are: Bee's wax secreted by bees is an ester of palmitic acid and aliphatic alcohol ($C_{30}H_{61}OH$), Lanoline wool (or) fat: Palmitic acid (or) Stearic acid (or) Oleic acid ester of cholesterol, obtained from wool.

2.1.2. Compound Lipids

Compound lipids are the fatty acid esters of glycerol in combinations with the additional groups such as phosphoric acid, nitrogen containing bases and other substituent. It can be categorized into two classes.

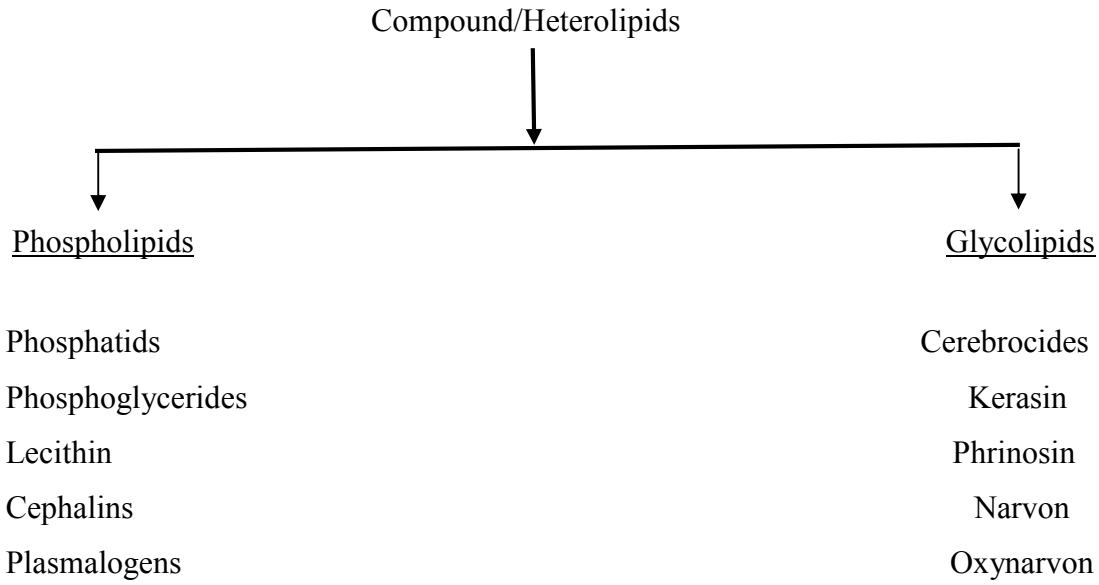

2.1.2.1. Phospholipids

Phospholipids are a class of lipids that are the major components of all cell membranes. It usually has two fatty acid chains attached to a glycerol backbone. The third carbon atom in the glycerol moiety is attached with the phosphate ion via C-O-P bond. The number of carbon atoms in the acyl chain is even and can be varied. Different phospholipids have different modified functional groups attached with the phosphate ion which eventually controls the functions of lipid. Few examples are: a nitrogen containing compound (choline), an amino acids contain phosphate (serine) an ethanol amine group linked with phosphate ion (ethanolamine) *etc*. The general structures of phospholipids with different head groups are given Figure 4.

Lecithins and cephalins are the common example of phospholipids found in the nerve cell[14] and animal liver. Egg yolks, yeast, soybeans, *etc.,* are also rich in phospholipids. Soylecithin (SLC) was one of the major components in the dissertation because of its natural abundance in the cell membrane. The structure of soylecithin is shown in Figure 5.

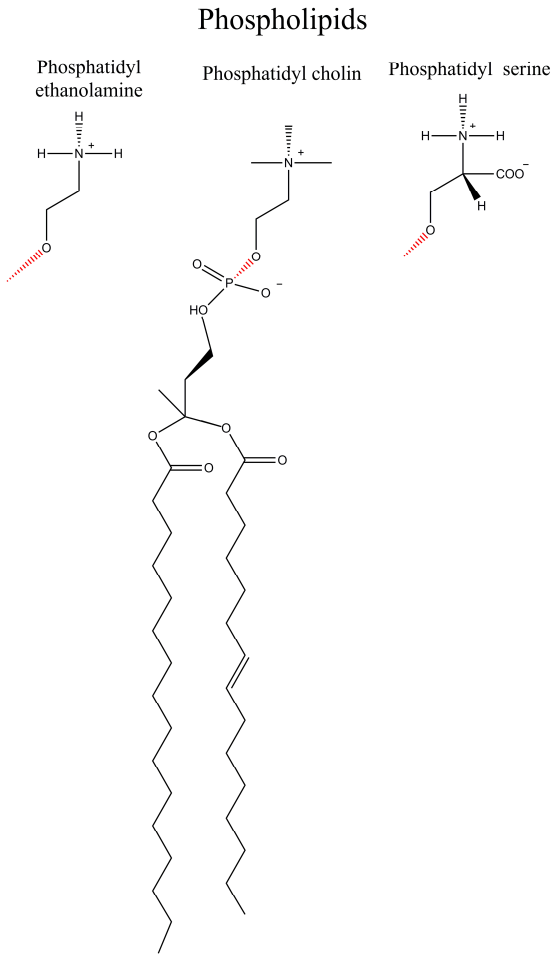

Figure 4. Molecular structure of Phospholipid with different head groups.

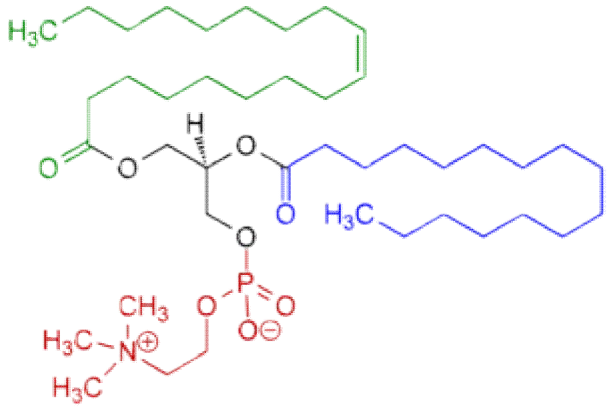

Figure 5. Structure of Soylecithin.

A general description about few phospholipids having different head groups are discussed next.

- **Phospahtidylcholine (PC)**

PC is derived from natural and synthetic sources. It is also known as lecithin. The two glycerol moiety attached with fatty acyl chain via ester linkage and the remaining one hydroxyl group linked with phosphate ion, which is further, connect with choline group. Common source of PC includes egg-yolk and soybean; although bovine heart and spinal cord are rich in PC, however its extraction is not so convenient. Lecithin is chemically inert and zwitter ionic. Besides the chemical properties, the low cost of lecithin has made it as one of the major phospholipid in liposome formulation. Lecithin from vegetable oils contains one or multiple unsaturation in its fatty acyl chain. On the other hand lecithin from animal fat produces fully saturated hydrocarbon chain.

- **Phosphatidylglycerol (PG)**

PG or glycerophospholipid are generally found in pulmonary surfactant, in bacteria and others[15]. It consist an L-glycerol 3-phosphate backbone. Two fatty acyl chains, either saturated or unsaturated, are connected through ester linkages. The head group region constituted with glycerol molecule bonded with phosphomonoester (Figure 6).

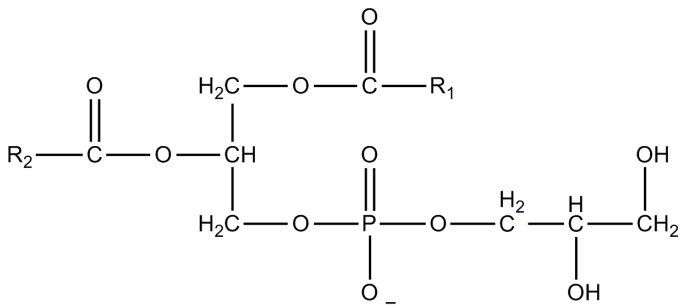

Figure 6. Structure of phosphatidylglycerol.

It is readily available in natural sources and can readily be prepared semi-synthetically form other lipids by means of phospholipase D in presence of glycerol. This type of phospholipids carries a net negative charge in the biological pH range.[16]

- **Phosphatidylethanolamine (PE)**

PE is also found in almost all the living cells and amounts to ~ 25% of phospholipids. In human body, they are found particularly on nerve tissue and spinal cord.[17] It has similar structure to the PC except three hydrogen atoms are directly attached with nitrogen of the ammonium group. These hydrogen atoms allow interaction with other molecules around the membrane via hydrogen bonding. At low or neutral pH, the ammonium group becomes protonated, leading to a resultant zwitter ionic lipid.

- **Phosphatidylserine (PS)**

Ps is another important component of mammalian cell membrane. Hydrocarbon chains are similarly attached to first two carbon atoms of glycerol via ester linkages. The phosphate group linked with the remaining hydroxyl group is also attached to serine moiety. The head group carries net negative charge due to the presence of the negative charge on phosphate. PS collected from plants and animals are different in terms of their fatty acyl chain length.

2.1.2.2. Glycolipids

Glycolipids are the glycoconjugates of lipids and generally found on the extracellular eukaryotic cell membrane. It functions to maintain the stability of membrane and to facilitate cell-cell interaction. (Source: https://www.nature.com/subject/glycolipids). Here glycolipids tail connected with one or more hydrophilic sugar head group through glycosidic bond. It acts as a rcognizing site for specific chemicals and also maintain the stability of the membrane by attaching with tissue. The general structure of glycolipids is shown in Figure 7.

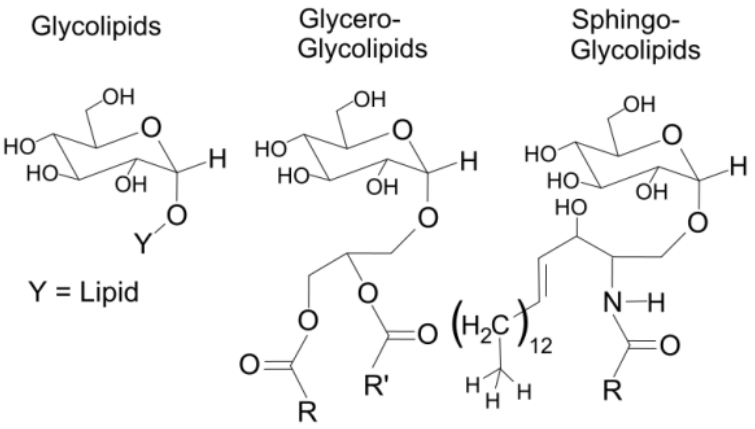

Figure 7. General structure of glycoplipids.

2.1.3. Derived Lipids

These are the class of lipids derived from simple or compound lipids via hydrolysis. Examples include cholesterol, coprostanol, cholestanol, ergosterol, different types of terpenes, lycopene, carotenese, xanthophylls, *etc*., Steroids, terpenes and carotenoieds are the most common class of derived lipids.

- **Steroids**

Steroids are the class of organic compound having four rings arranged in a specific orientation. Nucleus of the steroids has 17 carbon atoms bonded to form four fused rings; three six member cyclohexane rings (A, B and C) and one cyclopentane ring (D) as shown in Figure 8.

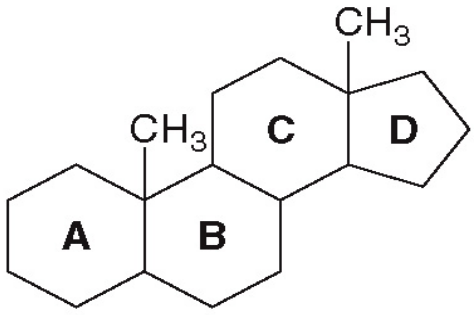

Figure 8. Steroid ring system.

Steroids do not contain any fatty acid and are hydrolyzed on heating.

Sterols are the derivatives of steroid with a hydroxyl group attached in position 3. It is also known as solid alcohol.

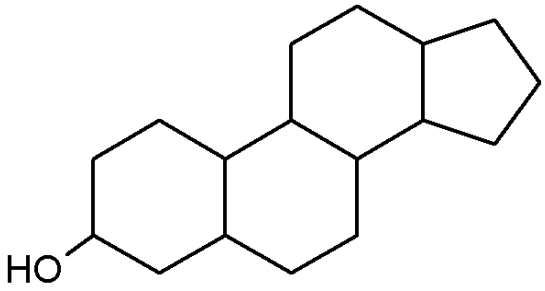

Figure 9. Core structure of sterol.

They occur naturally in the cell membrane of all type animals, plant fungi. One of the most important and familiar type of animal sterol is cholesterol which is vital to animal cell membrane as it regulates the membrane rigidity and fluidity.[18,19] It also acts as a precursor to fat-soluble vitamin and steroid hormones. Throughout this research work cholesterol have been used in preparing the liposomes. Cholesterol along with ergosterol, sex harmons, bile acids are all sterol derivatives. The structure of cholesterol is shown in Figure 10.

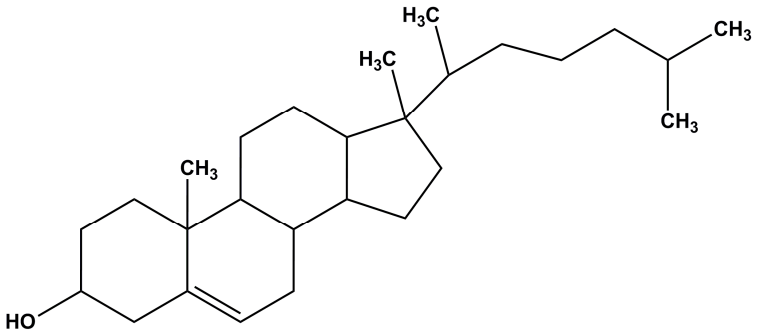

Figure 10. Structure of cholesterol.

Animal cell membrane is composed of cholesterol with a maximum of 30 mol%. It controls the membrane fluidity at all physiological temperature. Cholesterol is essential in our body as it produce hormones, vitamin D and other substances that help us to digest food. It is usually produces in our body, only a limited amount of body cholesterol comes from the diet. Unsaturated fatty acids from vegetable oil help to reduce cholesterol synthesis in our body system. On the other hand, saturated fatty acids from animal fat enhance the amount of

cholesterol in the blood as well as triglycerides. Brain, nervous tissues, solid alcohol from bile, adrenal glands, *etc*., are the sources of cholesterol.

2.2. Biological Role of Lipids

The biological functions of lipids are the following:

- Phospholipids act as the structural material to form cell wall.
- Fat is the important food storage for animals and plants.
- It acts as an important energy source through food supply.
- Transport of fat within the body is directly not possible; lipids act as detergent to emulsify the fat and thereby transport to the different parts of the body.
- Simple lipids protect intracellular organism as a heat insulators. It is also essential for fat soluble vitamin like A, D, E and K.

3. Synthetic Amphiphiles

Naturally occurring phospholipid based liposomes are common in clinical[20,21] and cosmetic formulations.[22] However liposomes formulation draw considerable issues as per as stability is concerned. Areal oxidation, bacterial attack and limited room temperature stability are some of the major concern.[23,24] Ion pair amphiphile (IPA), structurally resemble with double tail phospholipids are considered to be novel substitute that can be prepared in laboratory by stoichiometric mixing of aqueous solution of cationic and anionic surfactants.[25,26] Reports suggest that in aqueous medium few of these lipids like IPA molecules form vesicle structure, better known catanionic vesicles or "catanosome".[28] Ionic surfactants are easily available and commercially cheap relative to the phospholipids. Thus IPA prepared in combination of various type of cationic and anionic surfactants draw much attention of the researchers. However for long term storage, catanionic vesicles from IPA

easily fuse together and cannot maintain their uniformity in size. Investigation pointed out two aspects, inter-vesicles and intra-vesicle interaction that assist the process of fusion.[29] In order to improve the physical stability of catanionic vesicles, IPAs were designed by changing the hydrocarbon chain length and/or by altering the polar head group of the constituent ionic surfactant as is shown in Figure 11.

(HTMA-DS) is one of the widely investigated IPA prepared by mixing stoichiometric amount of hexadecyltrimethylammonium bromide (HTMAB) and sodium dodecylsulphate (SDS) in water. Although it possesses poor vesicular stability, however introduction of specific molecule such as phospholipid, cholesterol or double tail ionic surfactants can impact additional stability. IPA designed with different alkyl chain length or polar head groups were widely investigated in the form of ^{1}H-NMR, X-ray diffraction and FTIR.[26] Due to its similarities to the phospholipid, HTMA-DS has been frequently used to prepare hybrid vesicles throughout the dissertation.

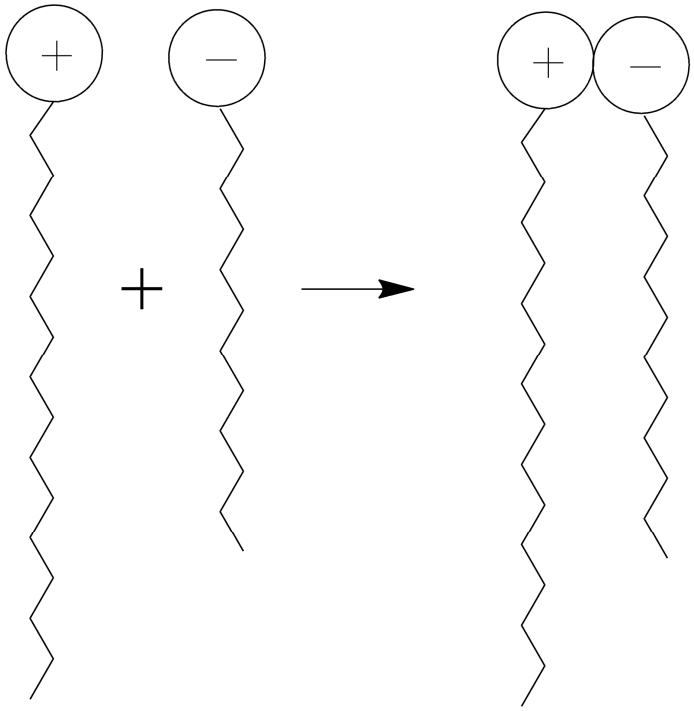

Figure 11. Schematic diagram of IPA.

4. Liposomes

Liposomes are the spherical shaped vesicles consisting one or more phospholipid bilayer. Amphiphilic molecules like lipids, cholesterol, *etc.,* are the main constituents. The word liposome comes from Greek words: “lipo” means fat and “soma” means body. Liposomes were first described in the year of 1961 by British haematologist Alec D. Bangham.[30-32] Today, liposomes become one of the important tools in different scientific discipline, including mathematics, theoretical physics, chemistry, colloid science, biochemistry and in various clinical trials.[33,34] Schematic diagram of liposome is shown in Figure 12.

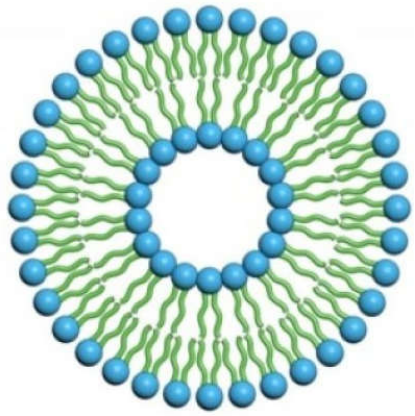

Figure 12. Structure of a liposome.

Due to its unique hydrophilic - lipophilic environment, liposome can host both the hydrophilic drug into the polar head group region or into the interior whereas lipophilic drug could be trapped inside the hydrocarbon region.[35,36] Thus artificially prepared vesicles become one of the important agents to improve the delivery of the large number of molecules; like enzyme vaccines,[37,38] genetic material,[34] drugs against microbial agents, anti cancer drug,[39,40] antifungal drugs,[34] peptide hormones, *etc*.[41]

In many cases with many drugs, the direct oral administration may always not lead to the better result. Most of the drugs are not good enough to tolerate the resistance of enzymes that it encounters during its journey through the digestive tracts. Bile salt, intestinal flora produced in human body, alkaline solution, digestive juices and free radicals in human body, *etc.*,[34] can substantially reduce the efficacy of a drug and may promote the side effect. In such cases liposome can make its mark as a protecting vehicle in transferring the drug to its desire target with controlled release. Its unique inert behaviour towards the entrapped drug (hydrophilic and lipophilic) along with ease of biodegradability and non-toxicity results in the improved bio-distribution of the drug with fewer side effects. Life time of the entrapped drug is also increased as the liposome shields the drug from different physiological environment.

4.1. Preparation of Liposome

Aforementioned lipids can be considered as the major components of cell mimetic system like liposome. The main goal in liposome formulation would be to prepare drug loaded liposome or hybrid vesicles with superiority. Narrow size distribution and long term stability of the dispersion are the primary concern in choosing the method for liposome preparation. Generally all the methods involve the lipid film hydration followed by sizing of the particle that eventually follows the removal of the non-encapsulated entities. Two major methods are involved in liposome preparation: passive loading mechanical dispersion method and active loading methods.

In passive loading mechanical dispersion method, the drug either in aqueous phase or organic phase is encapsulated by adding it before or during liposome preparation. One can expect high drug encapsulation efficiency by such liposomes. On the other hand, in active loading method, a diffusion gradient of the ions or drugs around the inner and outer phase of the aqueous layer is generated. Drugs, through the process of diffusion thus get loaded into

the liposome. Some of the commonly used methods in preparing the liposome are: thin-film hydration method, injection methods, sonication, membrane extrusion, micro emulsification, reverse phase evaporation method and calcium induced fusion method.[23,34,42]

4.1.1. Thin Film Rehydration Method

It is one of the most commonly used methods in preparing liposomes. Requisite quantities of lipidis are taken in a round bottom flask; dissolved in solvent like chloroform, dichloromethane[43], ethanol[44] and chloroform-methanol mixture (2:1 v/v; 9:1 v/v; 3:1 v/v).[45,46] A thin lipidic layer is generated by evaporating the solvent under vacuum. Traces/minute quantity of organic solvent was further removed by the stream of nitrogen at 4 ºC[47]. Distilled water, phosphate buffer solution with varying pH and normal saline buffer solution is subsequently added for the hydration of the thin film. It is then hydrated at 60-70 ºC for 1h (usually above the chain melting temperature). Total lipid hydration of the liposomal dispersion was done by allowing the lipid film to hydrate overnight.

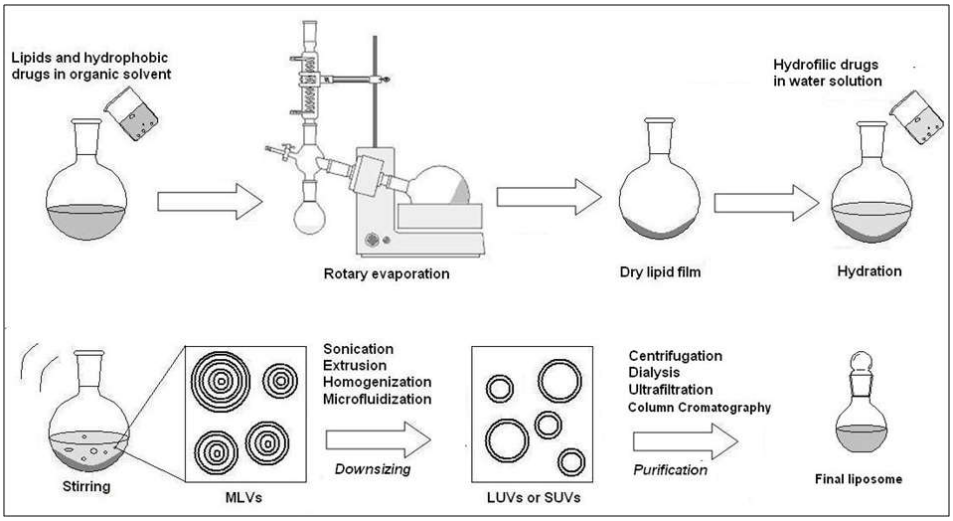

Figure 13. Schematic diagram of thin film rehydration technique.

All kinds of lipid mixture can be used in this method for the preparation of liposome. One of the important drawbacks of this method is the irregularity of the particle size which leads to the formation of heterogeneous system.

4.1.2. Injection Method

- **Ether Injection Method**

Solution of lipids dissolved in ether or ether/methanol mixture is slowly mixed into an aqueous solution of encapsulated materials at 55-65ºC with reduced pressure. At higher temperature (above the boiling point of the solvent) evaporation or removal of the organic layer leads to the formation of liposome. Major drawbacks of this method include the exposure of the encapsulated material to the organic solvent and high temperature. Irregular particle size distribution also leads to the heterogeneity.[16,48]

- **Ethanol Injection Method**

A lipid solution of ethanol is rapidly injected to a huge amount of buffer or distilled water. Immediately, the liposomes are formed in the mixture. Major disadvantages of this method are the heterogeneity in liposome size. Liposomes are very dilute and the removal of ethanol is very difficult as it forms azeotrope mixture with water. Formation of the azeotrope restricts this kind of liposomes to apply in biological system.[49,50]

4.1.3. Sonication Method

This method includes the size transformation of liposomes. Multi lamellar vesicles (MLV), prepared by in thin film rehydration technique, is sonicated by bath or probe sonicator to prepare homogeneous dispersion of small unilamellar vesicles. Major difficulties

associated with this method include low drug encapsulation due to smaller size, overheating that can degrade the components.[51]

4.1.4. Reverse Phase Evaporation Method

This method involves the formation of water-in-oil emulsion by means of brief sonication of a two phase system. The two phase system comprises the lipids dissolved in an organic solvent (diethyl ether, isopropyl ether or mixture of isopropyl ether-chloroform) and aqueous phase. Phosphate buffer solution or citric-Na_2HPO_4 buffer is sometimes added to the aqueous phase to improve the efficiency of the liposomal dispersion. The final liposomal gel was formed by the evaporation of the organic solvent under vacuum. The residual solvent is then removed by continued rotary evaporation under reduced pressure. The principle advantage of this method is high encapsulation efficiency. However a disadvantage includes the possible existence of the reminiscent solvent in the formulation restricts its application.[52,53]

Size of the vesicles ranges from 20 nm to several micrometers depending upon the pattern of aggregations. However liposome's properties could be changed by altering or tuning the charge of the head group, acyl chainlength, addition of other amphiphiles, *etc*. The properties of liposome could be altered by altering the type of phospholipid charge on the polar head group, size, hydrocarbon chain saturation-unsaturation, *etc*. Liposome of various types can thus be formulated. Apart from the precursor, few different ways of liposome preparation also leads to create different type of liposome.

4.2. Classification of Liposome

4.2.1. On the basis of composition

Liposomes are the aggregates product of natural and/or synthetic lipids along with cholesterol. The major focus on liposome relates to its capability as a drug delivery agent.

Being a drug delivery agent, its efficacy towards the target cells and effect on normal cell, tissues are the primary concerns. Depending upon the composition and mechanism of drug delivery, it could be classified into five different types:

(1) Conventional liposome (ii) pH-sensitive liposome (iii) Cationic liposomes

(iv) Immunoliposomes and (v) Long-circulating liposomes (LCL).

4.2.2. On the Basis of Hydrodynamic Size

The size of the liposome can range from 50 to 1000 nm. Size of the liposome is a vital parameter to determine its circulation life time. Bilayer controls the incorporation of the drug; a direct size dependent phenomenon.[16] Depending on the size, liposome is divided into three categories: (i) small unilamellar vesicles (SUV) (ii) large unilamellar vesicles (LUV) and (iii) multilamellar vesicles (MLV). For SUV, the size is less than 50 nm, whereas for LUV it's higher than 50 nm. MLV consists of more than one bilayer, size range from few hundred nanometre to microns.

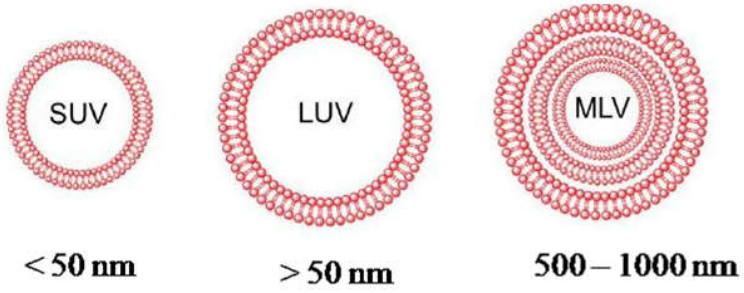

Figure 14. Representative images of SUV, LUV and MLV.

4.3. Lipid Bilayer and Lamellar Phases

Throughout the dissertation, lipid bilayer is the most frequently used system. Bilayer aggregate is formed when lipids are dispersed in water. According to the geometrical packing concept, cylindrical structure of some lipids prefer to self-aggregate into bilayer in water.[54] Higher lipid concentration usually forms two dimensional bilayer with lamellar phase. The

lamellar phase of phospholipid bilayer may exist in different states, depending on bilayer component and the environmental temperature.[55,56] For example, liposome with unsaturated phospholipids like soylecithin (SLC) produces more permeable and less stable bilayer due to its fluid (or liquid crytaline) nature. Whereas the bilayers of saturated lipid like DPPC are less permeable and more stable due to rigidity.[57,58] Temperature certainly does control the physical state of the lamellar phase. At low temperature, it exists in the gel phase (L_{β}')[59,60] where the hydrocarbon chains are closely attached with each other that forms more or less like a frozen state. When the temperature is increased, thermal energy after a threshold limit, becomes sufficient enough to transform the rigid bilayer moieties into a fluid like state. At higher temperature the randomness of the hydrocarbon chain get increased and thus form more permeable liquid-crystaline or fluid phase (L_{α}).[61,62]

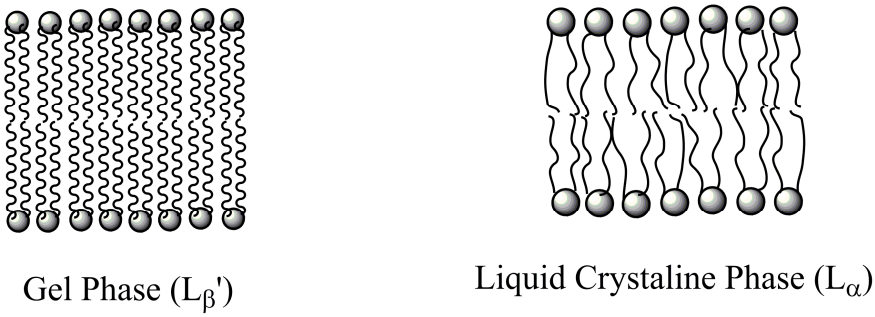

Figure 15. Gel and liquid crystalline phase of bilayer aggregate.

In gel phase all the hydrocarbon chain is in trans form whereas in liquid crystalline phase, the lipid chain is in gauche conformation.[63-65] Being in gauche conformer, the randomness of the bilayer hydrocarbon region increased which eventually holds the fate of the bilayer. Transformation of the bilayer from gel to liquid crystalline phase is known as phase transition and very much substantial to understand the thermodynamics associated with it.[66-68] The temperature at which the physical state of the bilayer transforms from L_{β}' to L_{α} is known as the phase transition temperature (T_m). Transformation or the existence of liquid crystalline

phase involves the process of interdigitation of the lipid acyl chain. Alteration in hydrocarbon chain and head group greatly affects the interdigitation and the physical property of the bilayer. Herein the bilayers that have extensively been studied are the mixture of SLC, IPA and surfactant in combination with cholesterol.

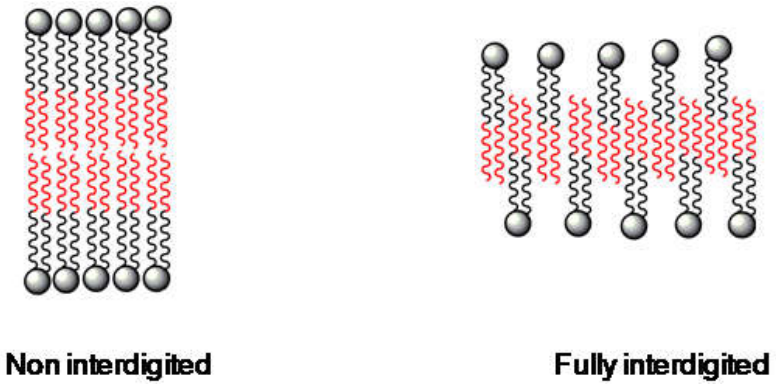

Figure 16. Schematic representation of non-interdigited and fully interdigited lamellar phase.

Interdigitation could occur in multiple ways. Structure and symmetry of the hydrocarbon chain deeply holds the nature and extent of interdigitation. Lipid often conflict its characteristics and ability to form interdigited system and thus so far no general rule has developed to fully understand the process of interdigitation.

4.4. Liposome in Drug Delivery

A drug delivery system (DDS) is capable to conduct therapeutic substances or drugs to the target tissue and thus can improve its life time and efficacy by controlling the release of the drug.[2,23, 33-35,37,45,69-71] With the help of advance technologies, several new drug-therapies have been invented, but efficacy and steady concentration of the drug in *in vivo* condition is still a challenging issue. On the other hand, some drugs have an optimum concentration range in which it shows maximum efficacy, below or above this concentration it may produce toxic effect or may not show any therapeutic activity. Liposome formulations have widely been used as an effective drug delivery system.

Table 1. Commercially available liposome based drug formulation.

Product Name	**Drug**	**Drug form/Storage time**	**Approved indication**
Ambisome	Amphotericin B	Liposome powder/36 months	Sever fungal infections
Doxil	Doxorubicin	PEGylated liposome suspension/20 months	Kaposil's sarcoma, ovarian/breast cancer
DepoDur	Morphine sulphate	Liposome suspension/24 months	Pain management
Myoset	Doxorubicin	Liposome powder/18 months	Metastatic breast cancer
Visudyne	Vertiporfin	Liposome powder/48 months	Age related molecular degradation

4.4.1. Drug Delivery Routes

Several drug delivery routes have been adopted to introduce the drug in human body. Choices of the routes of drug administration depend on the type of disease, infected zone of the body. A classification of systematic drug delivery by anatomical route is summarized as:

- **Gastrointestinal System:**
  - Oral
  - Rectal
- **Parenteral:**
  - Subcutaneous injection
  - Intramuscular injection
  - Intravenous injection
  - Intra-arterial injection
- **Transmucosal:** Buccal and through mucosa lining the rest of gastrointestinal track
- **Transnasal**
- **Pulmonary: drug delivery by inhalation**
- **Transdermal drug delivery**
- **Intra-osseous infusion**

4.4.1.1. Oral Delivery

Oral route of drug delivery has been the most acceptable and widely used process for drug administration. It is more convenient because of the easy route of administration and is also widely accepted by the patients.[72-74] However, there are some drugs that suffer major problems during oral administration, like

(i) Presence of digestive enzyme may damage the activity of the drug.

(ii) The high acid content and presence of digestive enzyme in the digestive tract can degrade some drug before they reach to the target cell or tissue.

(iii) Many drugs having structure like macromolecules or polar compound are incapable to effective traverse across the cell of the epithelial membrane in the small intestine to reach the blood stream.

(iv) Many drugs are insoluble in low pH and there by non effective towards digestive track as they are not absorbed by bloodstream.

4.4.1.2. Parenteral Delivery

This involves the administration of drugs to the body by other routs than gastrointestinal tract.[34,69,75-78] The drug is injected to the body through intramuscular, intravenous, subcutaneous and intra-arterial routes. Some advantages and disadvantages of parenteral administration are presented in Table 2.

4.4.1.3. Transdermal Delivery

The drug is administrated into the body surface such as skin or mucous for therapeutic use.[79] This route of delivery is alternative to oral, intravascular, subcutaneous and transmucosal route. It is significantly associated with local effect rather than systematic

effect.[79] The mode of drug delivery is advantageous the drug can directly affect the active site avoiding gastrointestinal and liver metabolism.

Table 2. Advantages and Disadvantages of Parental and Nasal Drug Delivery.

Routes	Advantage	Disadvantage
. Parenteral Delivery	Gastrointestinal track is avoided	Involvement of pain complaint by the patient
	Rapid onset action	For the subcutaneous process the size of the molecule does matter. Bigger molecule has slower penetration rate than smaller one.
	Almost complete bioavailability	Diffusion of the drug into the body fluid may get hamper by the viscosity.
	Proficient route for comatose patient who are unable to ingest drug by oral administration	To avoid the accumulation of the drug the sites of injection have to be changed.
Nasal Delivery	Compared to epidermis or gastrointestinal mucosa, nasal mucosa shows higher permeability.	Dose is limited as the available area for the absorption of the drug is small
	Highly vascularised sub epithelial tissue	Time available for absorption is limited
	. Rate of absorption high, usually within half an hour	Diffusion of the drug into the body fluid may get hamper by the viscosity.
	Gastric stasis and vomiting can be avoided.	During common cold or a nose with surplus watery rhinorrhea, the nasal routes get blocked.
	Most feasible roué for the delivery of peptides	Degradation of the drug due to enzymatic effect

4.4.1.4. Nasal Delivery

For systematic and topical effect, drug can be administrated nasally for several years. For nasal delivery the drug is adsorbed via the aqueous channel of the membrane. As long as the drug is in solution phase and small molecular size, it will be absorbed rapidly via aqueous path of the membrane.[80,81] With increasing molecular size of the drug, the absorption through nasal cavity decreases. The rate and extent of absorption of the drug through nasal cavity depends on several factors. Some advantages and disadvantages of parenteral administration are presented in Table 2.

5. Different Drug Delivery System

Colloidal drug delivery systems like micelle, vesicle, liquid-crystalline system and nanoparticle with diameter 10 to 400 nm are considered to be promising agents as drug carrier.[82-86] With the aid of advance technologies, researchers have been developing drugs with high and promising activity. Most of the drug, DNA and/ or protein and are characterized on the basis of its bioactivity; liberation of their bioactive material at right time with right concentration and limited toxicity.[87-89] While developing a drug carrier, the aim is to get an optimized system with better encapsulation efficiency, long shelf-life and low toxicity with controlled release of the drug. Carriers like colloids get special attraction due to the biocompatibility, biodegradability and biomimiking phenomena. General description about different drug carrier system is discussed in the following section.

5.1. Microemulsions and Nanoemulsions

Microemulsions is composed of water, oil, surfactant and co-surfactant are transparent and optically isotropic single –phase liquid solution.[90-92] The system is bi-continuous with

low viscosity and is thermodynamically stable. The solubilisation of both hydrophilic and lipophilic drug in microemulsions could be achieved. The limited use of microemulsions for dermal and oral application is a significant drawback.

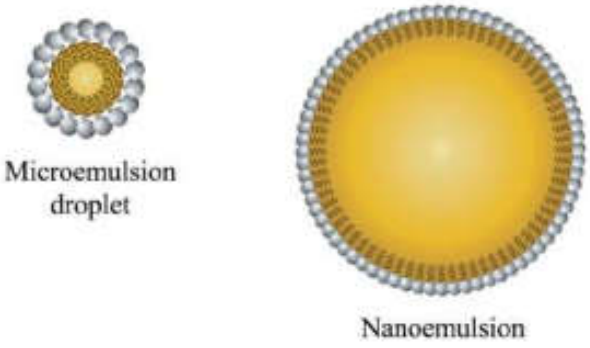

Figure17. Schematic representation of Micro and Nano emulsion. Source: Nano emulsions versus micro emulsions: Terminology, differences, and similarities, Soft Matter, 2012.

Nano emulsions come into the picture in 1950's to the need of parenteral nutrition.[93] It has been introduced into the market as various pharmaceutical products, such as: disoprivan, Etomidat lipuro, diazepam lipure, steasolid and lipotalon.[93,94] Nano emulsions are the two component heterogeneous system where one liquid is dispersed as droplets in the other one. As a drug delivery agent, it reduces the local and systematic side effect. However it has some limitation when lipophilic drug is concerned as the presence of oil solubilises the drug.

5.2. Nanoparticle

It includes nanocapsuls and nanospheres having size 10 – 200 nm and is crystalline or amorphous. They have the capabilities to encapsulate or absorb the drug and act as a protective barrier. In the recent years it draws researcher's attention because of the controlled release of the drug and targeting drug delivery. It has the ability to deliver genes, proteins and peptide through the oral route.[95]

5.3. Solid lipid nanoparticles.

Solid lipid nanoparticles (SLN) are composed with solid lipid core matrix that can solubilise lipophilic molecules. It is spherical shape and has the diameter 10 – 1000 nm. Lipids such as triglycerides, diglycerides, monoglycerides, faty acids, wasex, and steroids are used to prepare SLN. The lipid core is stabilized by adding surfactants based on the charge and molecular weight. SLN is used in various applications such as parental, pulmonary, ocular deliver of drugs.[96-98]

5.4. Liposome

The details of the liposome and its superiority as a drug delivery agent have already been discussed. Apart from the aforementioned DDS, a new class of hyper branch, polymeric molecule known as dendrimer have been using for some while. In the dissertation, dendrimer is one of the important aspects to study the interaction with liposome. The detail of dendrimer is described below.

6. Dendrimer

Dendrimers are three dimensional, hyperbranched tree-like polymeric architectures whose size and shape can be precisely controlled.[99] Dendrimers are fabricated from monomers by step growth polymerisation process. The term dendrimer arises from Greek words “dendron” meaning “tree” and “meros” meaning “branches”.[100] Dendrimer can be fabricated by controlling its molecular weight, degree of branching, and surface functionalities whose measured size reported as ranging from 2.5 nm to 10 nm.[101] Representative molecular structure of dendrimer is shown in Figure 18. Size of dendrimers can be regulated by controlling the polymeric branch which is extended outward like a tree producing spherical shape nanometre size particle leaving cavities inside.[33] Thus

encapsulation of drug inside a dendrimer cavities and transport to the target cell can be achieved.

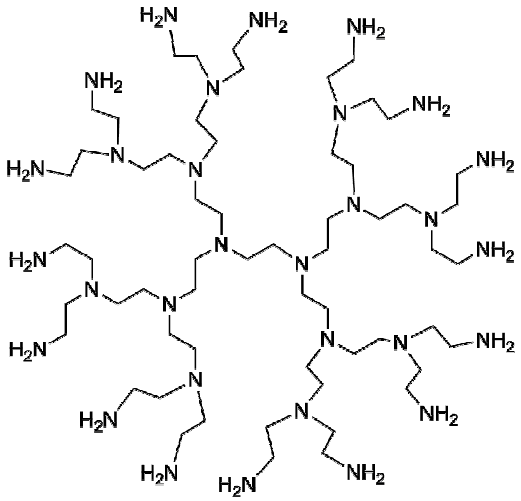

Figure 18. Schematic structure of dendrimer.

Besides the internal cavities, surface end group of dendrimer can also actively conjugate with other molecules. Molecule having amide containing cascade of polymers with amine surface group is known as PAMAM dendrimer works effectively as antibacterial agent[102], antifungal, drug[103] and gene delivery.[104]

6.1. General Properties of Dendrimer

As discussed earlier, dendrimers are polymeric, hyperbranched three dimensional tree-like architectures widely used in the field of nano science. The properties of dendrimers are mainly controlled by the surface groups; however internal core can also play a decisive role.[105-107] It is also possible to make dendrimer water soluble unlike some other polymers by introducing polar groups. It also possesses other controllable properties like toxicity, crystallinity and chirality.[106,108] It exhibits homogeneous symmetrical monodisperse structure with a typical core inside, involving an inner shell and outer shell structure. Dendrimers with hydrophilic surface groups are soluble in polar solvent like water whereas surface group with hydrophobic moieties are soluble in non-polar solvent.[109] Interaction with other entities can

takes place either with the groups inside called “endorecepters” or the groups on the periphery known as “exorecepters” depending on the type of host-guest.[110] Dendrimer structure can be categorized into three parts. (i) a multifunctional core moiety connecting the dendrons, (ii) radially linked repeating layer of branches connected with the core and (iii) terminal surface groups.

6.2. Classification of Dendrimer

The layer of the branches represents dendrimer generation. Higher the number of the branches, higher is the generation of the dendrimer. Synthesis of each new generation increases the molecular weight exponentially and doubles the number of the terminal groups.

Table 3. Generation based physicochemical properties of dendrimers.

Generation	Molecular weight	Measured diameter	Surface group
0	517	15	4
1	1,430	22	8
2	3,256	29	16
3	6,909	36	32
4	14,215	45	64
5	28,826	54	128
6	58,048	67	256

The generation of the dendrimers are represented as G1, G2, G3 etc indicating generation 1, 2 and 3 respectively. Generation of the dendrimer governs the morphology as lower generation (G0 to G4) dendrimer exhibited planner or elliptical shape whereas higher generation shows spherical conformation.[111] PAMAM is an example of dendrimers having polyamide branch into the core with different amine terminal group and can be replaced with alcohols,

carboxylate ions *etc*. Classification of dendrimer based on generation and their subsequent properties are summarized in Table 3.

6.3. General Methods of Dendrimer Synthesis

The first report on the synthesis of dendrimer was given by Vogtle and co-workers. Relying on the same protocol, amide containing cascade of polymers also known as PAMAM dendrimer was synthesised by Tomalia's group.[112] It can be categorized it three parts; a core, an inner shell and outer moieties. Different functionalities like solubility and thermal stability can be induced during dendrimer synthesis. Commonly use two methods for dendrimer synthesis are given below.

6.3.1. Divergent Method

This method was first reported by Tomalia group[112]. The method involves growth of dendrimer from the core that builds out in step wise fashion towards the periphery through polymerization process. Repetition of each steps generate a new branch which define the number of generation of dendrimer. As the growth of dendrimer originates form the core, alteration of surface group can easily be achieved. It is one of the popular methods for the synthesis of dendrimers as it leads to the formation of highly symmetrical molecules.[113]

6.3.2. Convergent Method

This process follows the opposite route of the divergent method, where the growth of dendrimer starts at the terminal functional groups and proceeds into the core. This process was pioneered by Hawker and Frechet in 1994.[114] The dedritic segment is prepared by coupling the monomers by "one to one" fashion. Different segment can be coupled to the core in this method and hence widely used in formulation of asymmetric dendrimers.

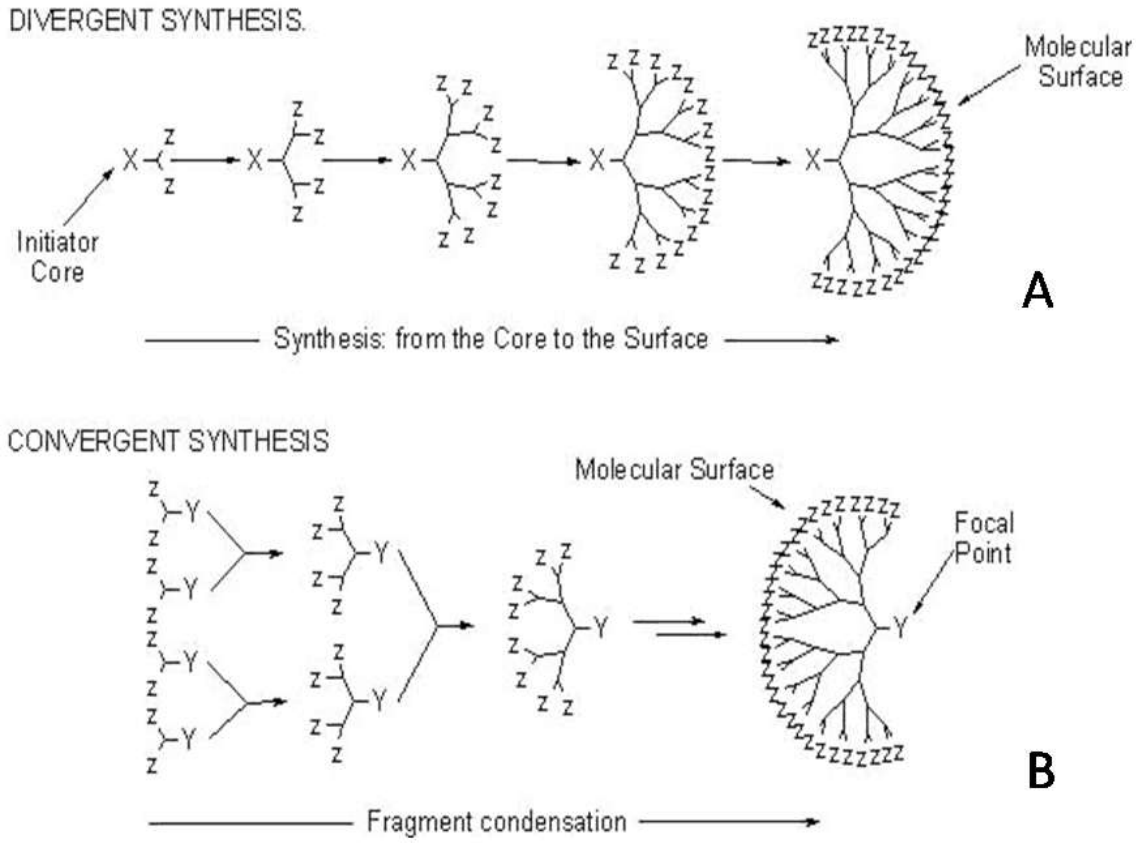

Figure 19. Synthetic routes of dendrimer. (A) Divergent synthesis and (B) Convergent synthesis. Source: http://www4.utsouthwestern.edu/jdebralab/dendrimer.html

6.4. Application of Dendrimers

Dendrimers are the promising macromolecules effectively used in drug delivery or gene delivery. Compared to other polymeric drug delivery architectures, dendrimers offer number of advantages like nanometer size morphology that allows them to pass through vascular endothelial tissue.[110] PAMAM dendrimers efficient in the field of transdermal drug delivery as reported by Cheng *et al*., where PAMAM-NSAIDs complex shows improved permeation of the drug through the skin.[115] Chauhan *et al*. has studied PAMAM-indomethcin complex for transdermal drug delivery.[116] D'Emanuele and his research group had made an

investigation on the monolayer of human colon adenocarcinoma cell line and the impact of dendrimer generation and concentration on it.[117] Bai *et al*. has shown that positively charged dendrimers are suitable agent for enoxaparin pulmonary delivery.[118]

Apart from these, dendrimers are also the point of interest for the targeted drug delivery. Thomas *et al*. has reported the use of dendrimers in the field of targeted delivery as they are able to couple with multiple components such as targeting tissue, drug and cancer imaging agent.[119] DNA assembled dendrimer conjugates have also been developed for targeting drug delivery.[120] Not only DNA, dendrimers are also employed as a gene transfection device as extensively reviewed by Broeren *et al.*[121] Dendrimer-based MRI contrast agents were used first time in *in vivo* diagnostic imaging applications.[122] G5 dendrimers with 64 Gd(III) ions gives lowest concentration detection limit made G5 as an promising dedritic MRI contrast agent.[123]

7. Characterisations of Liposome (or vesicle) and Their Aggregates with Dendrimer

Once a liposome is formulated and purified one could measure its size, surface charge (or zeta potential) and polydispersity by using dynamic light scattering (DLS) studies. Surface pressure (π)-area (a) isotherm measurement assists to understand the mutual miscibility among the components of mixed monolayer at air-water interface. Electron microscopy, small angle neutron scattering (SANS), small angle x-ray scattering (SAXS) and atomic force microscopy (AFM) studies are also helpful in determining the morphology and bilayer thickness. Bilayer phase transition and subsequent thermodynamics could be assessed by differential scanning calorimetry (DSC). Vesicles hosted drug molecules can also be scrutinized by measuring their entrapment efficiency, release kinetics and cytotoxicity. In case of vesicle/dendrimer interaction, apart from the above mentioned studies, one could

perform vesicles disintegration kinetics and Isothermal calorimetry (ITC) measurement to shed light on such interaction.

7.1. Dynamic Light Scattering

Vesicles are known as colloidal particles render surface charge and have hydrodynamic size in nano dimension. Being in dispersion state, it involves in Brownian motions. DLS technique is useful in determining the hydrodynamic size, zeta potential as well as polydispersity of the medium. It is worthy to mention that the hydrodynamic diameter is the hypothetical diameter of the hydrated particles that diffuse through the medium. In practice the colloidal particles are non-spherical, solvated and tumbling. Hence based on diffusion properties of particles, DLS calculates the apparent dynamic hydrated size of the particles; known as hydrodynamic size. Figure 20 represents particle size measurement curve.

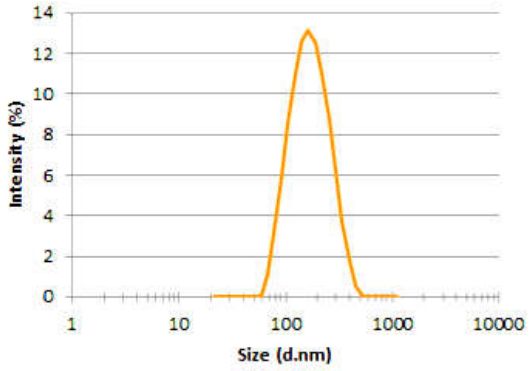

Figure 20. Hydrodynamic size distribution as function of intensities. Source: https://inanobotdresden.github.io/results.html.

A He- Ne leaser light with an emission wavelength 628 nm at an angle 90º collide with particles involved in the process of diffusions. It measures the translational diffusion coefficient (D) by collecting the light scattered by the diffused particles. Based on Stokes-Einstein's equation.

$$d_h = \frac{kT}{3\pi\eta D} \quad (2)$$

where, k, T and η indicate the Boltzmann constant, temperature and viscosity of water respectively.

Z. P. is one of the crucial parameter that maintains the stability of the vesicle. It prevents particle collision wing to the repulsion and hence it could be understood, higher the Z. P., higher is the stability of the particles. Substitution of other substances in vesicle bilayer may often change the value of Z. P. Thus measurement of Z. P. could be useful in determining the role of other components in the bilayer. Like any charge particles, vesicles can also involve in of electrophoresis under the influence of an applied electric field. The speed of the particles depends on the size, Z. P., viscosity and dielectric of the dispersion medium.

7.2. Surface Pressure (π) – Area Isotherm (a) Measurement

Bilayer could be viewed as superimposition of two monolayer's. Hence through investigation of monolayer would shed light on hydrocarbon chin miscibility, bilayer compressibility, free energy of chain mixing which helps to understand the role of hydrocarbon wall in bilayer.[124] Excess area of mixed monomolecular film where more than one amphiphiles are present are often lead to understand the associative or repulsive interaction between the hydrocarbon chain of the amphiphiles. π-a Isotherm is measured in a A Langmuir–Blodgett trough (LB trough that is used to compress monolayer of amphiphiles molecules on the surface of a given subphase (usually water) and measures surface phenomena (viz. surface pressure, surface potential *etc*.) due to this compression. Water must be purified to remove impurities. Impurities as small as 1ppm can radically change the behaviour of a monolayer. Representative image of π-a isotherm is given in Figure 21.

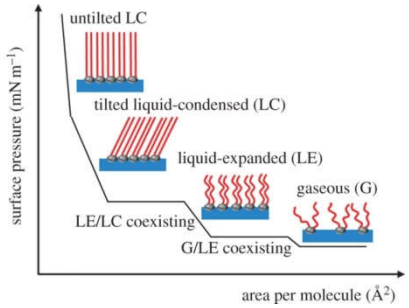

Figure 21. Representative surface pressure – area isotherm of lipids. {Schöne, 2017 #340}Source: Anne-Christin Schöne, Toralf Roch, Burkhard Schulz, Andreas Lendlein. J. Royal Soc. Interface **2017**, 14, 83-110.

After careful addition of lipidic materials to the subphase the trough was closed by a glass box to avoid the entrance of dust. 30 min after addition the compression starts with a speed 5 mm per sec. Due to the compression, surface pressure increases as the lipidic molecules come closer. As reflected from the figure, the isotherm consist of four differ parts and each describe the state of the monolayer. In gaseous state, the molecules are apart from each other whereas in liquid expanded and in liquid condense phase, they orient themselves in a same fashion. Finally in the solid state, most of the molecules are very close to each other that beyond this no further addition of molecule would not be possible and will break the pattern. Thus characterisation of bilayer would not be successful unless one performed monolayer study.

7.3. Morphology Measurement

Although DLS provides the information regarding apparent hydrodynamic size of the particle, however fully not adequate to tell the story of size and shape in detail. In the filled of nanoparticles, they are often scrutinized by using microscopic technique. Transmission Electron microscopy (TEM), Scanning Electron microscopy (SEM) and Atomic Force Microscopy (AFM) are useful in determining vesicles morphology, size, topology as well as

bilayer thickness and phase behaviour of the hydrocarbon wall.[125,126] Representative TEM, SEM and AFM images of vesicles are given in Figure 22.

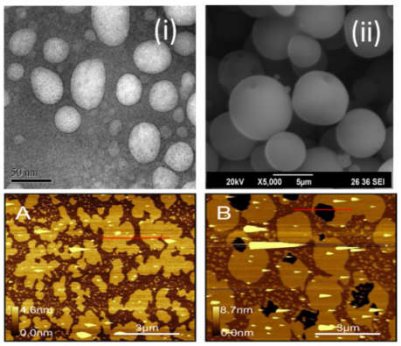

Figure 22. (i) TEM and (ii) SEM image of vesicles. Lower panel: AFM micrograph and height analysis of solid supported bilayer. Source: AFM: S. J. Attwood, Y. Choi and Z. Leonenko, *Int. J. Mol. Sci.*, **2013**, 3514-3539

Thus the micrographs of TEM and SEM provide exact morphology of the vesicles and its type of distribution. Side by side AFM also shed light on bilayer aggregation and its thickness as measured from height profile diagram. Not only microscopic analysis, small angle neutron scattering (SANS)[127-129] and small angle x-ray scattering (SAXS)[130-132] studies also help full in deterring the state of the bilayer thickness.

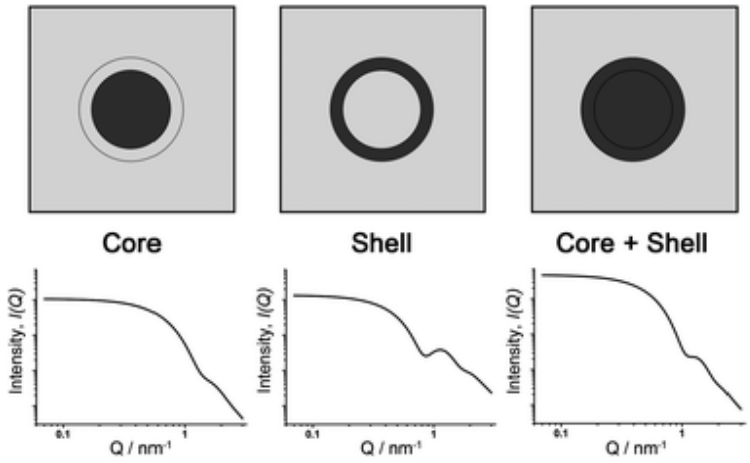

Figure 23. SANS plot of different kind of lipidic aggregates. Source: Martin J. Hollamb, *Phys. Chem. Chem. Phys.*, **2013,** 10517- 11144.

In SANS, neutron particles are made to collide with lipid bilayer or shell. In Figure 23, the intensity of the scattered neutron was plotted against scattering. The pattern of plot tells the architect of the lipidic assembly. Similarly in SAXS, electrons are being used instead of neutron that can scattered by the electron cloud around the bilayer, and hence present the bilayer morphology.

7.4. Differential Scanning Calorimetry

DSC is useful techniques that can detect the hydrocarbon chain melting process also known as phase transition. The temperature at which chain melts, known as chain melting temperature (T_m). By measuring T_m one could also get other thermodynamic parameters like enthalpy change, change in heat capacity, crystalinity of hydrocarbon chain etc. In this experiment, the vesicle bilayer were heating or cooling with desire temperature range. In chain melting process, the orientation of hydrocarbon chains get tilted leading the creation of endothermic event as reflected in the Figure 24. Hence bilayer strength and other thermodynamical entities are heavily depending on bilayer composition and the process of chain melting.

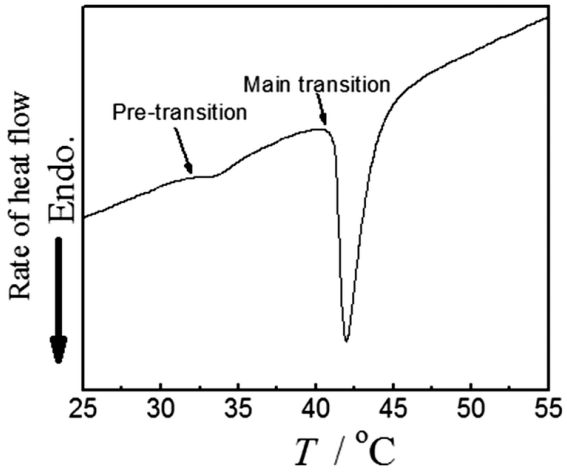

Figure 24. DSC thermogram of SLC vesicle. Scan rate: 2 ºC/min. Source: S. K. Kundu, S. Choe, K. Sasaki, R. Kita, N. Shinyashiki and S. Yagihara, *Phys. Chem. Chem. Phys.***2015**, *17*, 18449-18455.

7.5. FTIR Spectroscopy

IR spectroscopy is one of the important techniques towards chemist. Bilayer constituting lipidic molecules contains numbers of functional groups that are responsive to IR field. Group Such as –CH, -CH_2, -PO^{4-}, CO *etc*., are important that eventually control the fate of the bilayer.[133] Each of this functional groups have their own stretching frequency and slight deflection of it would tell us the situation of the concerning region of the lipids that eventually make impact on bilayer. Figure 25 describe a FTIR spectrum of DMPC liposome on the values of stretching frequencies of the functional groups. $-CH_2$ stretching frequency of the hydrocarbon chain is one of the primary concerned as it depicts the trans/gauche isomerisation of the acyl chain. The stretching frequency of $-CH_2$ at 2853 and 2924 cm^{-1} represent the antisymmetric and symmetric stretching frequency respectively.

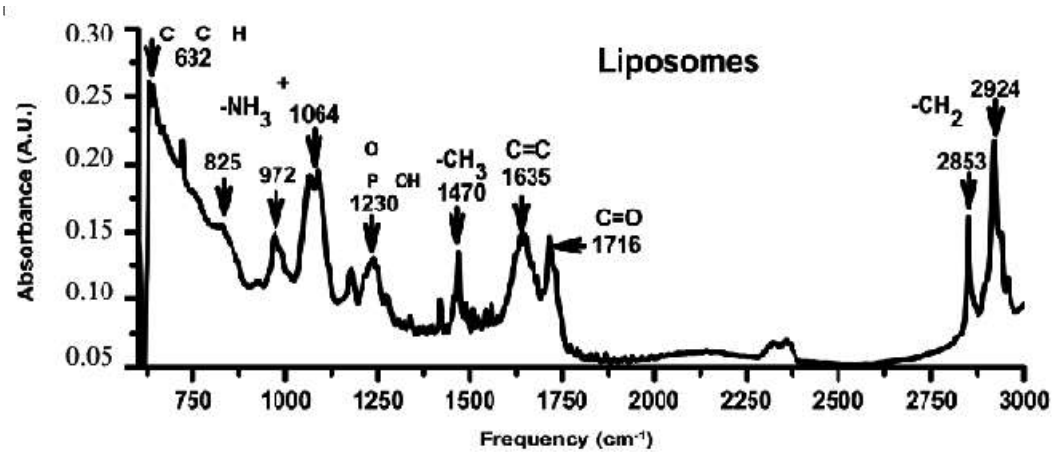

Figure 25. FTIR spectra of DMPC liposome. Source: F. R. M. Julieta, S. Macarena, I. Daniela, P. M. Jimena, A. S. D. Valle, C. N. Silvial, *Open Journal of Medicinal chemistry*, **2013**, *3*, 31-39.

Upshift of the frequencies indicates more disorderness into to the bilayer hydrocarbon zone. Head group polarity could also be checked from such studies. Phosphate stretching frequency appears at 1230 cm^{-1} and may alter depending on the surrounding medium and bilayer components. Increase in the value of stretching frequency indicates less hydration in aqueous medium and vice-versa.[133]

7.6. Fluorescence Study

Fluorescence study can be used to get idea about bilayer packing. Exogenously added compound may often changes the bilayer packing, caused either fluidity or rigidify of the membrane. Hence judicially chosen fluorescence probe like DPH or 7-hydroxycumarine (7-HC) can assert the rigidity of the non-polar chain as well as palisade layer of the membrane respectively. Steady state fluorescence spectra of 7-HC loaded vesicles would tell the polarity of the head region. Also anisotropy measurement of liposome loaded with either DPH or 7-HC would reflect the micro viscosity of the hydrocarbon and polar head region respectively. Anisotropy value of the embedded probe inside the bilayer was determined by using following equation.

$$r = \frac{I_{VV} - GI_{VH}}{I_{VV} + 2GI_{VH}} \quad (3)$$

where, I_{VV} and I_{VH} were the fluorescence intensities, the subscripts indicate the position of the excitation and emission polarizer. $G = \frac{I_{HV}}{I_{HH}}$ was the grating correction factors.

Apart from the anisotropy, one could measure membrane polarity through steady state fluorescence spectra by incorporating fluorescence probe into the palisade layer.

7.7. Drug Entrapment Efficiency (E. E.).

It is known that vesicle can accommodate both hydrophilic and lipophilic drug. Hence Drug loading capacity of vesicles need to be determined. Once drug loaded vesicle dispersion was prepared, it filled into the cellulose dialysis bag (MWCO 12 KDa) and dialyzed in PBS or water with constant stirring (50 rpm) under sink conditions for about 20 min.[134] The un-entrapped drug was removed from the formulations and the absorption spectra of collected samples were recorded through UV-VIS spectrophometer. The EE was calculated by considering the following equation:

$$\text{E.E. (\%)} = \frac{T-C}{T} \times 100 \quad (4)$$

where, T is the total amount of drug presents both in the sediment and supernatant, C is the amount of drug identified only in the supernatant. T and C values were determined colorimetrically.

7.8. Drug Release Kinetics

Vesicles are marked to be specific when they liberate the drug in target cell with sustained release. Hence drug incorporated vesicles often undergo such kinetics measurement. Dialysis method is generally used where the drug loaded samples were placed in dialysis bag and immersed in the same medium or solvent that was used in vesicle preparation. UV-VIS spectra of the sample were recorded with time which reveals the release pattern of the drug. Figure 26 put on a view of such release kinetics of drug loaded vesicles.

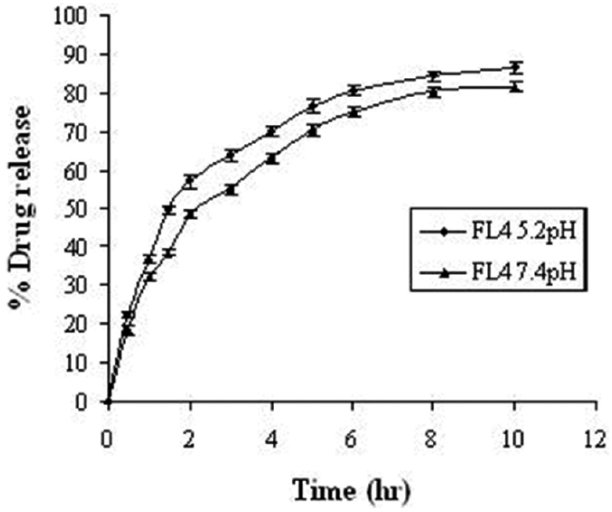

Figure 26. Representative image of % of drug release with time form vesicles bilayer. Source: K. Sasaki, R. Kita, N. Shinyashiki and S. Yagihara, *Phys. Chem. Chem. Phys.* **2012**, 13, 1442-1449

From Figure 26, one could easily get the idea of maximum drug release and the times to achieve sustain drug release.

Although several investigations have been made on liposome and dendrimers, however the exact mechanism of their interaction fully not understood. With a motive to get knowledge about physicochemical properties of vesicles and dendrimers and in particularly their aggregates, investigations have been carried out and the dissertation work has divided into three parts.

Vesicles were prepared at different combination of soylecithin (SLC) and IPA with 30 mol% cholesterol. Impact of IPA on SLC was studied by Langmuir-Blodget and spontaneity of the hydrocarbon chain mixing was found to be dependent on the amount of IPA. Hydrodynamic size (d_h), zeta potential (Z. P.) and polydispersity index (PDI) which describes the dispersion behaviour vesicles were measured through dynamic light scattering (DLS) technique. Vesicles Morphological properties also successfully recognized by electron microscopic (normal TEM as well as FF-TEM) studies. Thermotropic behaviours of the bilayer were scrutinized by differential scanning calorimetry (DSC). Structural changes of bilayer, caused by IPA, were further scrutinized by using fluorescence spectroscopy using 1, 6-diphenyl-1, 3, 5-hexatriene (DPH) and 7-hydroxycoumarin (7HC) as the fluorescent probes to get knowledge about the micro viscosity of the bilayer wall. Entrapment efficiency (E.E.) of the vesicles using cationic dye methylene blue (MB) was also evaluated. Such systems are expected to have superior properties as potent vectors for drug delivery.

As biological cell membranes are negatively charged, non-toxic, biodegradable vesicles could be served as an excellent drug delivery agent. Cationic vesicles were prepared using bi-tail cationic surfactants with varying hydrocarbon chain length (bis-C_{12} to C_{18}) in combination with soy lecithin (SLC) and ion pair amphiphile (IPA). Bi-tail cationic surfactants were chosen to progressively substitute with previously established three sets of SLC/IPA combinations. Interaction between hybrid membrane and piroxicame (Px), a Non Steroidal anti inflammatory Drug were analyzed in the form of monolayer, bilayer and

solid supported bilayer. Finally optimised Px encapsulated formulations were analysed for biological activity. Mutual miscibility among the components was studied by way of the surface pressure – area measurements. Physicochemical characterizations of the different hybrid vesicles with and without Px were assessed by combined dynamic light scattering, zeta potential, electron microscopy, atomic force microscopy, differential scanning calorimetry, FTIR, UV-VIS absorption and emission spectroscopic studies. Entrapment efficiency and the release kinetics of Px from the vesicles were analyzed by conventional dialysis bag approach. Finally the toxicity and biocompatibility of the drug loaded formulations were assessed. And could shed further light in the development of drug delivery systems in the treatment of brain – tumors targeted drug delivery.

The last chapter gives us an idea of physic-chemistry between the interaction of cationic vesicles and PAMAM succinamic acid, 1, 4-diaminobutane core dendrimer generation 5 (G5-SA) which is negatively charged. Previously prepared cationic vesicle comprised of SLC, IPA and DHDAB in three different combinations was taken to investigate the impact of dendrimer. Increasing hydro dynamic size and reduced Z.P. measurement suggests the formation of vesicle/dendrimer aggregates. The formation of aggregates was further confirmed by turbidity measurement. Morphological state of the vesicles with and without dendrimer was analysed via TEM studies. Vesicles disintegration kinetics measurement also has been done to understand the pattern of interaction using varying concentration of dendrimer. A surface pressure – time isotherm developed due to the vesicle disintegration upon the inclusion of dendrimer. The rate kinetics of such disintegration process was found to be depending on the dendrimer concentration. The effect of dendrimer on solid supported cationic bilayer was further scrutinized via AFM studies that help to understand stoichiometry depended aggregate formation. Finally DSC studies was performed which specifically enlighten the features of bilayer in presence of dendrimer. Overall

interaction studies put IPA on the map as it tries to restore the bilayer morphology by providing hydrophobic interaction.

7. Reference.

References are given in BIBLIOGRAPHY under Introduction (pp.142-150).

Ion Pair Amphiphile: A Neoteric Substitute that Modulates the Physico-Chemical Properties of Biomemetic Membranes

Abstract: Ion-pair-amphiphiles (IPAs) are neoteric pseudo double tailed compounds with potentials as novel substitute of phospholipid. IPA, synthesized by stoichiometric mixing of aqueous solution of hexadecyltrimethylammonium bromide (HTMAB) and sodium dodecyl sulphate (SDS) was used as potential substituent of naturally occurring phospholipids, soylecithin (SLC). SLC and IPA were mixed in different mole ratio along with 30 mol% cholesterol to produce stable vesicle dispersion. Cholesterol, being interdigited into the bilayer, controls the rigidity or fluidity of the membrane. Impacts of IPA on different SLC+IPA vesicles were firstly examined by monolayer studies by way of surface pressure (π) – area (A) measurements. Associated thermodynamic parameters were evaluated and the miscibility between the components was dependent on the ratio of SLC and IPA. Solution behaviour of the bilayer, in the form of vesicles, were investigated by monitoring the hydrodynamic diameter, zeta potential and polydispersity index over a period of 100 days. Systems comprising 20 and 40 mol% IPA exhibited anomalous behaviour. Thermal behaviours of the vesicles, as scrutinized by differential scanning calorimetry were correlated with the hydrocarbon chain as well as the head group packing. Steady state fluorescence spectroscopy and anisotropy analyses further supported the DSC results. Entrapment efficiency (E.E.) of the vesicles towards the cationic dye methylene blue (MB) was also evaluated. Vesicles were smart enough to entrap dye and the efficiency was found to vary with IPA concentration and the E.E. was found to be well above 80% for some stable

dispersions. Morphological behaviours of the vesicles were documented by TEM measurement and the results were well correlated with DLS study.

1. Introduction

Intracellular components are compartmentalized by thin bio membranes which commonly behave like a physical boundary to separate the respective compartments from the surrounding continuous environments.[1] Biological cells are directly responsible for numerous physico-chemical processes that depend on the composition of the membrane bilayer. Researches on the biological and biomemitc membranes resulted in the generation of substantial useful information in order to understand its subtle structure and its relevance in physiological environments. Bio membranes have diversity in potential because of the functional interface; it can bind to DNA, peptides, control the enzymes, *etc*.[2,3] Further researches on the membranous components suggest that bio membranes can actively play role in biochemical processes, *e.g.,* adhesion, signalling, controlling the Na^+/ K^+ balance, fusion, *etc.*[4] The resultant activity or potential of bio membranes largely depends on their components (phospholipids, cholesterol and regulatory protein, *etc*.).

The major components of the cell membranes are phospholipids that are capable to form vesicles spontaneously when they are hydrated.[5] Because of their amphiphilic nature, naturally occurring phospholipids are widely used in the synthetic formulation of vesicles in order to have further insight into their different physico-chemical properties. Researches on biomemetic membranes over the past few decades have revealed its potential application towards drug delivery, gene therapy, DNA transfection, *etc.*[6] Drug caring capabilities arise because of its unique hydrophilic and hydrophobic charisma. So last few years, vesicles have been the subject of focus for its biocompatibility and stability.

Stability of the vesicles are highly dependent on the amphiphile composition, surface charge (zeta potential) and hydrodynamic size.[7] Additionally 'rigidity' and 'fluidity' of the membranes' micro-environment also play a crucial role for its stability as they are highly dependent on the nature of the phospholipids and cholesterol. Cholesterol is one of the key components of the cell membranes as it can judiciously control the fluidity and rigidity of the bilayer.[8] Unsaturated phospholipids from natural sources, like palmitooleylphosphatidylcholine (POPC) forms less stable fluidic and permeable bilayers, whereas saturated phospholipids, *viz*., dipalmitoylphasphotidylcholine (DPPC), dimyristylphosphatidylcholine (DMPC) can form rather stable, however, rigid bilayers.[9] It is reported that vesicles comprising naturally occurring phospholipids exhibit poor stability at normal condition.[10] However strategies have been adapted by researchers in order to improve the stability of vesicles for its better performance.

Vesicles comprising different types of phospholipids have been the research of interest for past few decades.[7,11,12] Double tail and single tail surfactants which also form self-assembled structures were also introduced to produce stable vesicles dispersion. Kaler *et al*.[13] first reported about a neoteric phospholipid mimic amphiphile, which spontaneously form vesicles. This was synthesized from single chain mixed cationic and anionic surfactants, known as ion pair amphiphile (IPA). Vesicles comprising catanionic surfactants, also known as catanosomes, find its excellence for drug delivery,[6] binding with DNA,[14,15] nanoparticle synthesis[15,16] *etc*. Easy laboratory preparation of IPA marked its implication in membrane mimetic studies. However the impact of IPA on naturally occurring phospholipids (unsaturated) on monolayer and consequently on the bilayer needs some extra attention as it may produce stable vesicular dispersion for drug delivery. Such studies could shed further light on the possible yet unexplored application potentials as well as from the understanding of the fundamentals on the membranous interfaces.

In our present set of experiments, we choose to formulate stable vesicular dispersion with soylecithin (SLC) and IPA (prepared by equimolar mixing of HTMAB and SDS) with overall 30 mol% cholesterol in physiological buffer, phosphate buffer solution (PBS, pH 7.4). Formulations were prepared by varying the molar ratio of SLC and IPA. Cholesterol, which is a key component of bilayers, regulates the rigidity and fluidity of the membrane.[17] The effect of IPA on SLC in the form of monomolecular film was investigated by Langmuir monolayer technique (surface pressure – area isotherms). Bilayer, in the form of vesicles, could be viewed as the superimposition of two monolayers, so thorough study of monolayer could explain the nature of interaction between SLC and IPA. Ideality/non ideality in mixing, film compressibility and associated thermodynamic parameters were evaluated from such studies. Hydrodynamic size (d_h), zeta potential (Z. P.) and ploydispersity index (PDI) of the vesicles were measured by dynamic light scattering (DLS) technique. Thermotropic behavior of the bilayer was scrutinized by differential scanning calorimetry (DSC). Such studies helped in evaluating the chain melting of mixed acyl chains of SLC+IPA. Additionally, formation and deformation of water overlayer surrounding the lipidic head groups were confirmed from such study and could well be correlated with the composition of (molar ratio of IPA and SLC) the bilayer. Structural changes that occur in the bilayer due to the incorporation of IPA were further scrutinized by using fluorescence spectroscopy where extrinsic fluorescent probes 1, 6-diphenyl-1, 3, 5-hexatriene (DPH) and 7-hydroxycoumarin (7HC) were introduced. Variation in the crystalinity of the membrane as well as the head group packing with the composition could be correlated from the fluorescence spectroscopic analyses. Entrapment efficiency (E.E.) of the vesicles towards the cationic dye methylene blue (MB) was also evaluated. Morphological behaviours of the vesicles were successfully documented by TEM measurement and the results obtained, were also correlated with the size that obtained from DLS study.

2. Experimental Section

2.1. Materials

L-α-phosphatidylcholine (soylecithin, SLC, from soybean) was obtained from EMD Chemicals, Germany. A. R. grade sodium dodecylsulfate (SDS) [$CH_3(CH_2)_{11}SO_4Na$], hexadecyltrimethylammonium bromide (HTMAB) [$C_{16}H_{33}N(CH_3)Br$], 1,6-diphenyl-1,3,5-hexatriene (DPH), 7-hydroxycoumarin (7HC) and (3β)-cholest-5-en-3-ol (cholesterol) were the products of Sigma-Aldrich Chemicals Pvt. Ltd. (USA). A.R. grade disodium hydrogen phosphate (Na_2HPO_4, $12H_2O$), sodium hydrogen phosphate ($NaH_2PO_4.2H_2O$), sodium chloride (NaCl), methylene blue (MB) and chloroform (HPLC grade) were the products from Merck Specialities Pvt. Ltd, India. All the chemicals were stated to be more than 99% pure and were used as received. Double distilled water with a specific conductance 2-4 μS (at 25 ^oC) was used for the preparation of solutions.

2.2. Methods

2.2.1. Preparation and Isolation of IPA

Stoichiometric amount of aqueous HTMAB solution was added drop wise to a 0.1M aqueous solution of SDS under constant stirring. The white precipitate obtained, was extracted using chloroform.[18] Vacuum drying technique was introduced to remove the organic solvent. The white powder was then redissolved in chloroform and dried again. The process was followed for three cycles.[18] Fine white powders HTMA-DS (IPA) was then obtained and stored in vacuum desiccators.

2.2.2. Preparation of Vesicles.

Small unilamellar vesicles (SUVs) were prepared by conventional thin film technique.[12,19] Molar ratio of SLC: IPA was set at 10:0, 9:1. 8:2. 7:3, 6:4 and 5:5 along with

30 mol% cholesterol. Quantitative amount of SLC, IPA and cholesterol were dissolved in chloroform in a round bottom flask followed by solvent evaporation in a rotary evaporator. Finally trace amount of solvent was removed by the stream of nitrogen (N_2). The thin film obtained was then rehydrated for 1h in PBS (0.1 M Na_2HPO_4, 0.1M NaH_2PO_4, 100mM NaCl, pH 7.4) at 70 ^oC, well above the chain melting temperature of all the lipidic components. It was then frozen at −20 ºC and thawed in an ultrasonic water bath at room temperature for 15 min. Freeze-thaw process was repeated for another 4 cycles. Finally it was extruded using 0.45 μM cellulose nitrate membrane filter (Whatman Gmbh, Germany). Dye loaded vesicles were obtained by mixing appropriate amount of dye (DPH and 7-HC) into the lipid mixture before the generation of the thin film such that the final ratio of lipid and dye was 200:1. The total phospholipid concentration was kept at 2mM and was diluted depending on the type of experiment.

2.2.3. Surface pressure (π) – Area (A) Isotherm Measurement

Surface pressure (π) – area (A) isotherms were recorded with a Langmuir balance (M/S Apex Instrument Co. India, Model LB2000C) with a stated resolution of 0.01 mMm^{-1}. The trough and the barrier were made up of teflon (both hydrophobic and lyophobic) to avoid any contamination.[18] To prevent the entry of dust particles, a Plexiglass box was used which covered the stage and trough. The trough was filled with the PBS solution at pH = 7.4 with iconicity 100mM NaCl. A lipid monolayer film was formed by careful spreading of quantitative amount of the lipid ± IPA (with 30 mol% cholesterol) solutions dissolved in chloroform (1.0 $mgmL^{-1}$) with a Hamilton syringe (USA) onto the air-buffer interface. The solvent was allowed to evaporate approximately for 20min. Surface of the subphase was pre-cleaned using a micropipette aspirator, before spreading the monomolecular film. All the π – A isotherms were recorded at a subphase temperature of 25±0.5 ^oC with a lateral compression

rate of 5.0 mm min^{-1}. For each set of experiments, the curve was repeated at least twice to achieve the reproducible result. Further details are available in the literature.[20,21]

2.2.4. Dynamic Light Scattering (DLS) Studies

DLS studies were carried out to determine the hydrodynamic diameter (d_h), polydispersity index (PDI) and zeta potential (Z.P.) of different vesicle formulations.[16, 22] A dynamic light scattering spectrometer (Zetasizer Nano ZS90 ZEN3690, Malvern Instruments Ltd, U. K) was used for such studies. A He-Ne laser with an emission wavelength of 632.8 nm was used and all the data were recorded at a scattering angle of 90^0. The translational diffusion coefficient (D) was actually measured by this instrument which is correlated with the diameter (d_h) of vesicles according to Stokes-Einstein's equation:[22]

$$d_h = \frac{kT}{3\pi\eta D} \quad (1)$$

where, k, T and η indicate the Boltzmann constant, temperature and viscosity of water respectively. Polydispersity index (PDI) is another informative parameter which could be obtained from the DLS studies. Zeta potential (Z.P.) values were measured using folded capillary cells. All the measurements were carried out at temperature 25 ^oC and each reported zeta potential value was an average of four measurements.

2.2.5. Transmission Electron Microscopy (TEM)

Synthesized vesicles with varying composition of SLC+IPA were prepared as described earlier. One drop of liposomal dispersion was placed on Formver™ carbon-coated 200mesh copper grid.[23] The excess drop was removed by using a piece of filter paper from the edge of the grid. The grid was then dried for 10 minutes before performing the measurement. The dry sample loaded grid was then viewed through Hitachi H-600

transmission electron microscopic (Japan) using the standard procedure. The voltage was set at 80KV.

2.2.6. Differential Scanning Calorimetry (DSC) Studies

DSC studies were performed to evaluate the chain melting temperature/phase transition temperature (T_m) and related thermodynamic parameters of the bilayer which eventually control the physical states of vesicles. Experiments were carried out in a Mettler Toledo differential scanning calorimeter (DSC 1, STAR^e system, Switzerland). The dry thin films were rehydrated in 40 μL sealed Al pan. Each sample was scanned two times with a scanning rate 5 ^oC /min and 2 ^oC /min for complete heating and cooling cycles. The reference pan was sealed with PBS (pH 7.4). The obtained results were calculated by StarE software.

2.2.7. Fluorescence Spectroscopic Studies

Solvatochromic dye 7-HC and hydrophobic probe DPH were employed to investigate membrane polarity and bilayer packing respectively. Having some oxygeneous moiety, coumarine derivatives accommodate itself into the palisade layer of vesicles.[24] Overall membrane polarity was thus determined from the steady-state spectra of 7-HC comprising systems. The spectra were recorded by using a bench-top spectrofluorimeter (Quantummaster-40, Photon Technology International Inc., NJ, USA). Steady-state fluorescence spectra of 7-HC under different conditions were recorded in the range 350-600nm with an excitation wavelength of 330nm (λ_{ex}). Fluorescence anisotropy of 7-HC was determined by recording the emission data at 379 nm. Fluorescence anisotropy values for the probe embedded in the liposomal bilayer were obtained using the following equation:[25,26]

$$r = \frac{I_{VV} - GI_{VH}}{I_{VV} + 2GI_{VH}} \quad (2)$$

where, I_{VV} and I_{VH} were the fluorescence intensities, the subscripts indicate the position of the excitation and emission polarizer. G = $\frac{I_{HV}}{I_{HH}}$ was the grating correction factors. DPH, being a hydrophobic dye, is expected reside inside the bilayer.[27-29] Steady-state fluorescence anisotropy technique was employed to measure the membrane rigidity. All the anisotropy data were recorded at room temperature with excitation wavelength 351nm and the emission was set to 421 nm for DPH where as that for 7- HC, excitation and emission wave length were set to 330 nm and 379 nm respectively.

2.2.8. Entrapment Efficiency

Entrapment efficiency (E.E.) reveals the dye entrapment capacity of the vesicles. To determine the entrapment efficiency, lipidic components (SLC, IPA and cholesterol) were dispersed in PBS (pH 7.4) containing known amount of methylene blue (MB).[23] Three cycles of freeze-thawing technique, as mentioned earlier, was adopted so that the dye concentration inside and outside vesicle remained the same. 40μM MB loaded vesicles were made in such a way so that final concentration of lipid: MB becomes 50:1. MB loaded samples were centrifuged at 10, 000 rpm for 2h. The supernatant containing free MB molecules were analyzed in UV-visible spectrophotometer (Spectro UV-VIS double beam PC scanning spectrophotometer, UVD-2950, Labomed INC., USA) and the absorbance values were recorded for different sets of vesicles. The entrapment efficiency was calculated by using the following equation:[30]

$$\text{E.E. (\%)} = \frac{T-C}{T} \times 100 \qquad (3)$$

where, T is the total amount of dye presents both in the sediment and supernatant, C is the amount of drug detected only in the supernatant. T and C values were determined colorimetrically.

3. Results and Discussion

3.1. Surface Pressure (π) – Area (A) Isotherm

Using a Langmuir-Blodgett trough, pure and mixed lipidic monolayers were conveniently studied at the desired combination, which is otherwise not possible in the form of bilayer. Besides, different physicochemical parameters, *viz.*, molecular organization and subsequent interaction between the different components, limiting area, excess thermodynamic potential, film compressibility, *etc.*, were evaluated from such measurements.[18] Despite the fact that the monolayers effectively being only half a bilayer, with a flat rather than curved structure, information from the monolayer studies can effectively be translated into liposome or cell membrane systems.[31] With this background, surface pressure-area isotherms for SLC +IPA mixtures (in presence of 30 mol% cholesterol) were recorded at the air-PBS buffer (pH 7.4) interface. π-A isotherms for different combinations of SLC+IPA, along with 30 mol% cholesterol, have been shown in Figure 1. The limiting area appeared at 1.07 $nm^2molecule^{-1}$ for SLC while that for the IPA was at 1.08 $nm^2molecule^{-1}$. Results were found to be comparable with the previously published reports.[18,32] Monolayers with unsaturated lipid, exhibit as a single homogenous liquid expanded (fluid) phase.[17,20,32] The limiting area of IPA was found to be 1.08 $nm^2molecule^{-1}$ at zero surface pressure, that means, at the interface the limiting area per alkyl chain or in other words the half of the limiting area of an IPA was then about 0.54 $nm^2molecule^{-1}$; which was found to be larger than the theoretically proposed value, ~ 0.20 $nm^2molecule^{-1}$ per single chain.[20] This larger limiting value suggests that the molecular packing at the interface was somehow correlated to the bulky head groups of the IPA. Additionally, non-parallel orientations of the hydrocarbon chains were responsible for such differences. Cholesterol with a relatively smaller lift-off (0.3 nm^2) area has a propensity to interdigitize itself into the bilayers with parallel orientation.[17]

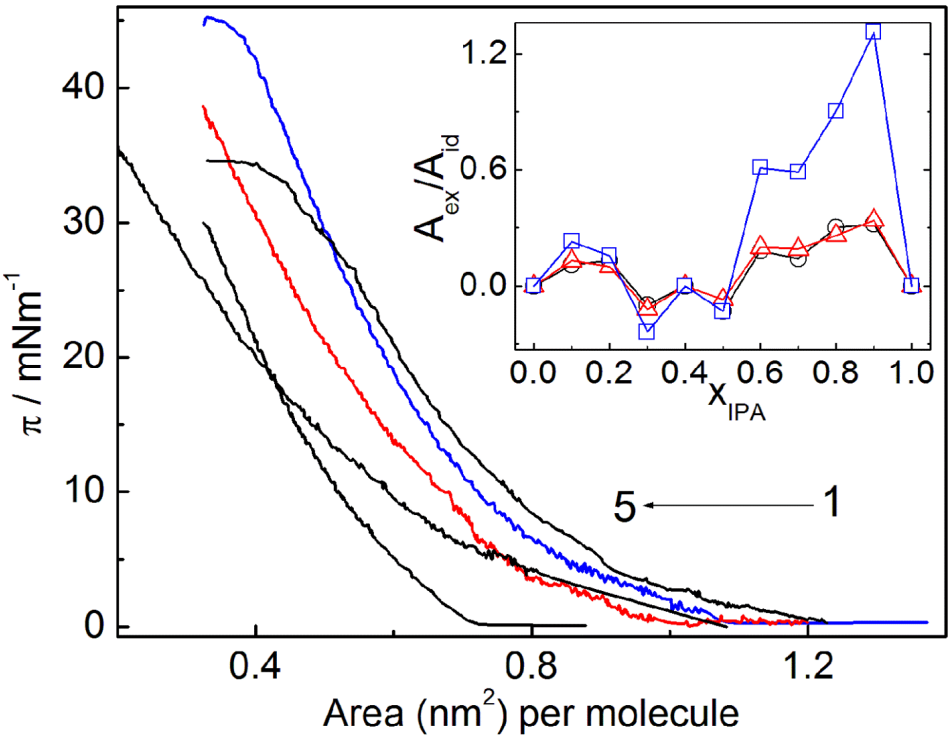

Figure 1. Surface pressure (π) – area (A) isotherm for the monomolecular films of SLC+IPA (in presence of 30 mol% cholesterol) at the air-buffer interface. Temp. 25 ^{o}C. Mole fraction of IPA (x_{IPA}): 1,0.2; 2, 0.0; 3,0.4; 4,1.0 and 5,0.5. Inset: A_{ex}/A_{id} *vs.* x_{IPA} profile at π = O,0; Δ, 20 and □, 30 mNm^{-1}. A 0.1 mM PBS buffer (pH 7.4) in 100 mM NaCl was used as the subphase.

Isotherms of mixed monolayers ((SLC+IPA) were different from that of the individual components. Expanded isotherms were noticed for the systems with x_{IPA} = 0.2; where the limiting area was found to be highest, 1.21 nm^{2}molecule^{-1}. Comparably condensed states for the mixed monolayer were initiated for x_{IPA} ~ 0.3 and this trend followed upto 0.5. The isotherms for the mixed monolayers shifted to lower area region from that of the pure isotherms with gradual increment of IPA and indeed the limiting area was reduced from 1.21 nm^2 molecule^{-1} (x_{IPA} = 0.2) to 0.71 nm^{2}molecule^{-1} where x_{IPA} being 0.5 as estimated from the π – A isotherms. Such studies clearly indicate the renovation/reorganization of the molecular packing at the interface to a more condensed state when the IPA mole fraction was higher (x_{IPA} > 0.2). The unusual variation in the lower mole fraction range of IPA can be

rationalized as follows: the Columbic forces of repulsion between bulky choline head groups of SLC were dominant in the presence of lower amount of IPA leading to the expanded (fluidic) monolayer. Increasing amountof IPA (> 20 mol%) in the mixed monolayer, assist the hydrogen bonding or some sort of van der Waal's forces of attraction between SLC and IPA which overcome the columbic force exerted by the choline head groups, thus condensed mixed monolayer was resulted.

Da-Cheng et al.[32] reported that C_8- substituted alkylaminomethyl rutin (DAMR) and SLC were miscible but exhibit intermolecular repulsive force over the entire range of DMAR mole fraction. Reports on the monomolecular film studies in combination with different amphiphiles are available in the literature. Chang *et al*.[6] studied the monolayer behavior of IPA in presence of double tail cationic surfactant dihexadecyldimethylammoniumbromide (DHDAB), where the dissociation of the IPA was confirmed at x_{DHDAB} = 0.5.[20] Characterization of IPA was further reported by Panda *et al*.[18] where solubilisation of IPA in presence of additives like cholesterol and bile salt were confirmed and the distinguished properties of IPA with the variation of alkyl chain length were observed. In all of their studies film functionality were found to be dependent on the composition of the lipid mixture.

Isotherms of the pure components lead to calculate ideal isotherms for the mixed systems according to additivity rule:[33]

$$A_{id} = x_1 A_1 + x_2 A_2 \quad (4)$$

where, A_{id} is the average theoretical area per molecule, x_1 and x_2 being mole fractions of the components 1 (SLC+30 mol% cholesterol) and 2 (IPA+30 mol% cholesterol) respectively. A_1 and A_2 are the corresponding area per molecule for the individual components. Mixed monolayer which follow equation 5 were said to be ideal in nature. Deviation of the

experimental value (A_{ex}) from the ideal one can be obtained through the calculation of the excess area per molecule as:[21]

$$A_{ex} = A_{12} - A_{id} \quad (5)$$

where, A_{12} is the experimental area per molecule of the mixed monolayer. Any deviation from linearity or any incidence of the appearance of maximum or minimum with varying composition would produce the extent of deviation from ideality.[34] In the case of an ideal mixture, the calculated value (A_{id}) should be equal to that of the measured value (A_{12}) and should vary linearly with mole fraction of any components. On the other hand, for immiscible/noninteractive systems, each component hangs about as individual/separate clusters containing substantial/considerable amount of molecules. A negative deviation from the ideal behavior signifies associative interaction between lipidic hydrocarbon chains and the IPA. While a positive deviation (positive A_{ex}) signifies repulsive interaction.[35] Representative plots for the variation of A_{ex}/A_{id} with composition are shown in the inset of Figure 1.

Initial positive deviation (up to x_{IPA} = 0.1 to 0.2) from the linearity was the outcome of repulsive interaction between SLC and IPA. Columbic repulsion which prevails at low x_{IPA} causes the system to deviate positively from the ideality. However associative interactions were validating for the systems where x_{IPA} were 0.3 and 0.5 respectively. Strong van der Waal's force of interaction along with some sort of hydrogen bonding results in the formation of associative type interaction which over crossed the Columbic repulsion for these systems. Significant divergence from the trend line was observed for x_{IPA} 0.2 and 0.4, suggesting some anomalous interactions than other combinations. The calculated values of A_{ex}/A_{id} for the former were found to be ~ 0.117 and that for the later was 0. This constancy was found for the entire range of surface pressure for the two. Loss of molecules from the monolayer into the subphase through the formation of vesicles and micelle could be the reason for this

peculiar behavior; as been reported by Chang *et al*.[6] Dissociation of $HTMA^+$ from IPA was the outcome when amphiphile concentration was higher and some sort of stress on IPA was initiated.[20] Accordingly, positively charged quaternary amine group of the zwitterionic choline moiety could exert strong electrostatic interaction with unbound DS^- at the interface with the desorption of $HTMA^+$. $HTMA^+$, because of its reasonable water soluble characteristics, would not be able to withstand high surface pressure at interface after being dispatched by the choline moiety. Reports are supporting the fact that the dissociation of excess ionic surfactant from the mixed cationic/anionic monolayers with non equimolar ratio, whereas stably existed monolayer was confirmed with a mixture of equimolar ratio. Thus, it could be inferred that dissociation of $HTMA^+$ from IPA (HTMA-DS) was one of the reasons for the abnormal behaviour that generate excess area curve.

The condensation of mixed monolayer (area contraction) at higher x_{IPA} was revealed form Figure 1 and the subtle structure of the monolayer could further be scrutinized from various factors such as ordering of chain, tilting of polar head and molecular packing. To obtain the state of the investigated film and the consequent molecular ordering, compression modulus was calculated (according to equation 6) for different mixed monolayers. Film compressibility (C_s) is a measure of the resistance of the monolayer against compression; in other words it can be defined as the amount of pressure needed to cause a change in the molecular area.[33] The reciprocal of compressibility,C_S^{-1}, known as compression modulus, is also another route to demonstrate the phase transition.

$$C_S^{-1} = -A\,(\delta\pi/\delta A)_T \qquad (6)$$

Such a representation is depicted in Figure 2. It is known that the monomolecular film with compressibility modulus in the range of 12.5- 50mNm^{-1} are in the liquid- expanded (LE) phase, whereas for the liquid states the value lie in the range of 50-100 mNm^{-1}.[18]

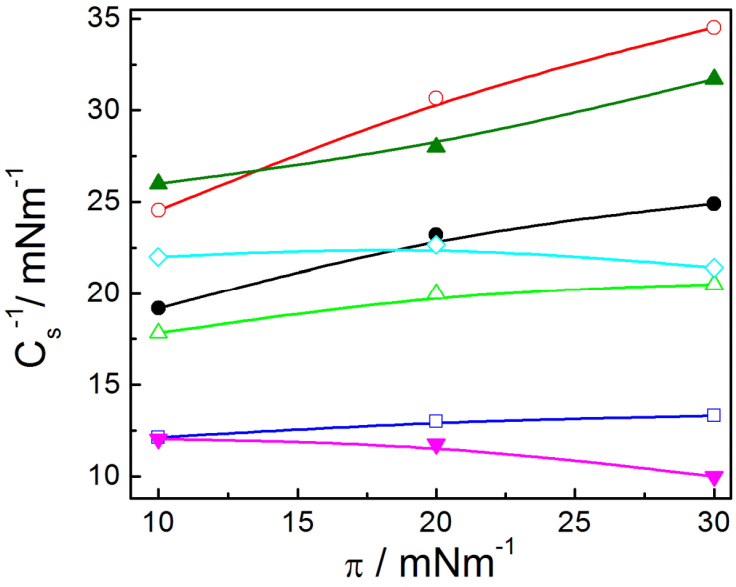

Figure 2. Variation in the compressibility modulii (C_S^{-1}) with the surface pressure for pseudo binary monomolecular films of SLC+IPA. A 30 mol% cholesterol was used. Temp. 25 ^{o}C. Mole fraction of IPA (x_{IPA}): ●, 0; O, 0.1; Δ, 0.2; □, 0.3; ◊, 0.4; ▲, 0.5 and ▼ 1.0

In our present set of studies, all the mixed monolayers were in the LE phase as the compression modulus were in between 12.5 - 50 mNm^{-1}. C_S^{-1} values were found to be larger for x_{IPA} = 0.1 and little smaller for 0.5, which then increased with increasing surface pressure. Surface pressure independence of C_S^{-1} was noted for the mixed monolayers comprising 20 and 40 mol% IPA which indeed was in good agreement with previous findings. Lowest C_S^{-1} values were found for the system comprising 30 mol% IPA as well as the system comprising IPA alone. Because of the unsaturation, these monolayers were more compressible than their saturated analogue. IPA, with the acyl chain, being saturated, experienced less compressibility than SLC. Such an observation is not uncommon.

Mixed monolayer study could be useful to formulate stable liposomal dispersions by considering different thermodynamic parameters of the interaction processes. The spontaneity that associated with hydrophobic interactions between the hydrocarbons chains of SLC–IPA

can also viewed by evaluating the excess free energy change as given the following equation:[31]

$$\Delta G_{ex}^{0} = \int_{0}^{\pi} (A_{12} - A_{id})\, d\pi \qquad (7)$$

Quantitative assessment of the magnitude of the mutual interaction between SLC and IPA could be best studied by considering ΔG_{ex}^{0} values. Figure 3 describes the variation in the excess free energy with the composition of the mixed monolayer (x_{IPA}).

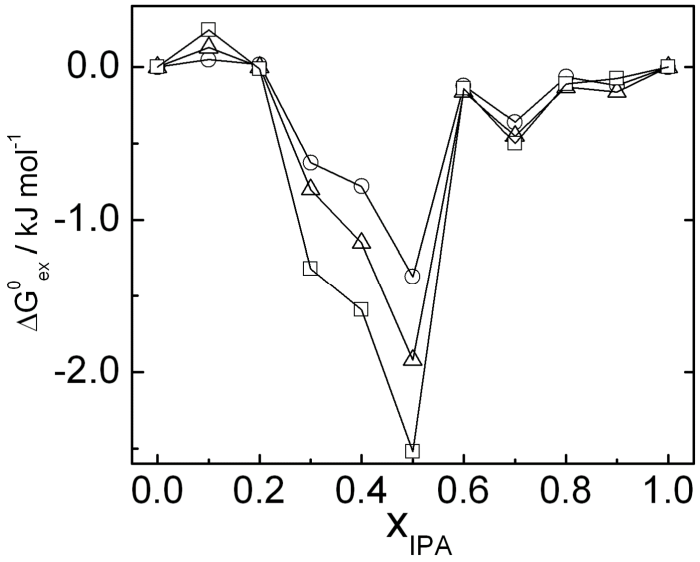

Figure 3. Variation of excess free energy (ΔG_{ex}^{0}) for the SLC+IPA mixed monolayer systems (in presence of 30 mol% cholesterol) with the mole fraction of IPA (x_{IPA}) at different surface pressure (mNm^{-1}) : O, 10 ; Δ, 20 and □, 30. Temp. 25 ^{o}C.

Non ideal mixing behaviour between SLC and IPA was confirmed from the run of the curves; positive deviation from the ideal behaviour was observed for the system comprising < 20 mol% IPA. Columbic force of repulsive interaction between the polar head groups and the dissociation of $HTMA^{+}$ from IPA could be associated in the process of mixing. Again the cis orientation of one of the fatty acyl chains of SLC could resist the IPA to get condensed and subsequent non spontenity in the mixing processes were observed. Negative values of

ΔG_{ex}^{0} for x_{IPA} = 0.3, 0.4 and 0.5 indicate that the supplement of IPA into SLC monolayer grounds the formation of stable monolayer at their favourable arrangement. Because of the saturation of IPA, strong van der Waals force of interaction and hydrogen bonding among SLC and IPA result in an associative manner. Thus stable mixed monolayer was resulted at higher mole fraction of IPA. Unlike the systems with 30 and 50% IPA, monolayer with 40 % IPA did not follow the same trend and produced relatively lower negative value of ΔG_{ex}^{0} compared to the other two. Unfavorable interaction between SLC and IPA could be the reason as $HTMA^{+}$ has a propensity to dissociate (when x_{IPA} is higher) in the presence of quaternary ammonium ion of the choline group and get solubilised into the subphase. Thus the small negative ΔG_{ex}^{0} that originate for the system with 40% IPA could be due to the associative electrostatic interaction between ammonium ion and DS^{-}.

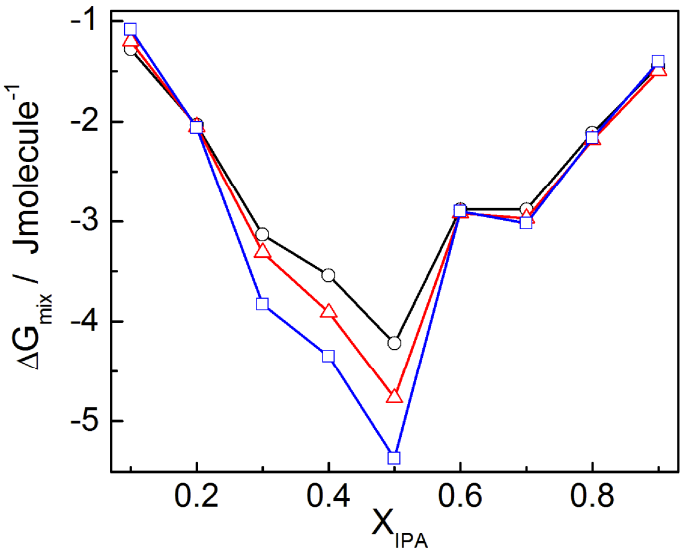

Figure 4. Variation of ΔG_{mix} as a function of composition for mixed monolayers of SLC+IPA at 25 °C. Surface pressures (π / mNm^{-1}) are: O, 10; Δ, 20 and □, 30.

The extent of hydrocarbon chain mixing among SLC and IPA was further calculated in terms of free energy of mixing (ΔG_{mix}). Figure 4 illustrates the free energy of mixing for the mixed monomolecular film of SLC and IPA as a function of IPA mole fraction.

In order to further scrutinize the interaction between SLC and IPA in their monolayer forms, apart from conventional monolayer thermodynamic parameters, regular solution theory was adopted. Interaction parameter (I. P.) describes the extent of interaction between SLC and IPA in mixed monolayer state and can be derived by using following equation:[32]

$$\text{W} = \frac{\Delta G_{ex}^{0}}{x_1 \, x_2} \tag{8}$$

$$\text{I.P.} = \frac{W}{RT} \tag{9}$$

I. P. as a function of π was plotted in Figure 4 and shows some fascinating points regarding the interaction process. Figure 5 indicates that interaction was maximum for x_{IPA} = 0.1 and increasing linearly with π, whereas that for x_{IPA} = 0.3 and 0.4, I.P. independence of mixing on the surface pressure for the system comprising 20 mol% IPA was further established through its parallel propagation along the X- axis. Relatively high extent of interaction for x_{IPA} = 0.1, was due the presence of least amount of IPA in the monolayer. Presence of one IPA molecule for nine other combinations was a state where IPA was assumed to be interdigited by huge amount of SLC. Cholesterol, being an additive, played an important role for the interaction process. With increasing π, cholesterol pushes the acyl chains of SLC which in turn hold the saturated hydrocarbon chain of IPA firmly to produce reasonable I.P. for this mixed monolayer. It could be stated as "arresting the IPA by lipids assembly through the lipophilic solvation in monolayer". On the contrary, we noticed relatively lower I.P. values for the systems with higher proportion of IPA. To address the corollary, one must need to consider the influence of head group packing between SLC and IPA. It is now been known that IPA constitutes bulky head groups which produce lesser tight packing when mixed with SLC (as choline group is also a bulky head group). Again desorption of $HTMA^+$ from IPA and its subsequent solubilisation was the reason that we could not find any changes in the values of I. P.

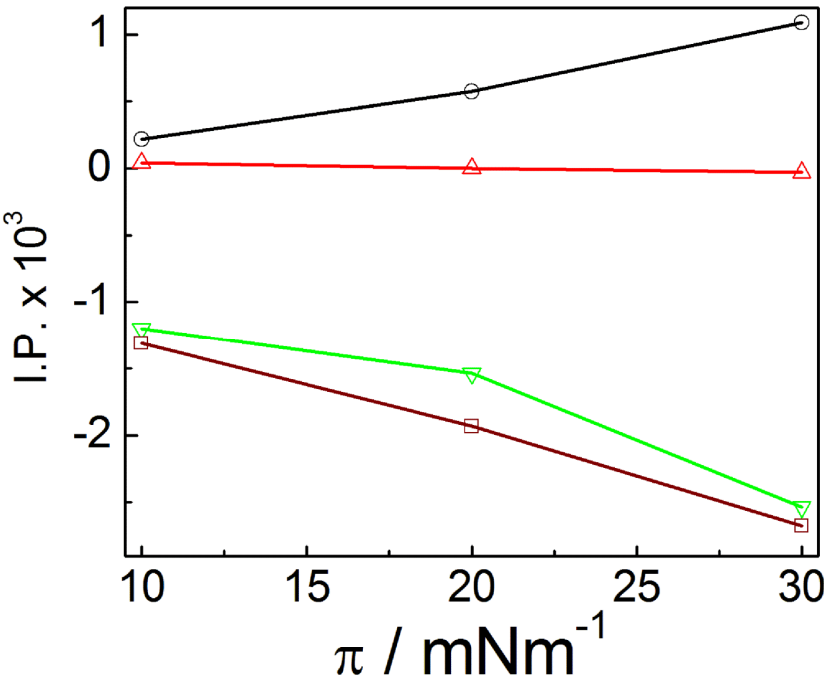

Figure 5. Relationship between interaction energy (I. P.) and surface pressure (π) at different IPA mole fraction. x_{IPA}: ○, 0.1; Δ, 0.2; ∇, 0.3 and □, 0.4. Temperature was set on 25 ^{o}C.

Lipid assemblies in the monolayer and bilayer forms are different. While the former having linear orientation that for the later show curvature. Although there are some structural differences, mixed monolayer studies could be informative to explain the stability and biodiversity of SLC-IPA vesicles. It was concluded from π – A study that increasing proportion of IPA made the system more rigid although 10 mole % of IPA exhibited repulsive interaction. Some aberration for 20 and 40 mol% of IPA were observed. Such anomalous behaviours are beyond explanation with the present level of knowledge. The mechanisms of such interactions are yet to be cleared and could be explained on the basis of molecular dynamics simulation which is considered as one of the future perspectives.

3.2. Dynamic Light Scattering (DLS) Studies

Hydrodynamic diameter (d_h) is an important parameter towards the direction of stability and bio distribution of vesicle formulations. Apart from the size, polydispersity index (PDI) is considered to be another important parameter as it describes the size distribution of dispersions having range from zero for a monodispersed system upto unity for completely polydispersed systems. Stability of the vesicles with different compositions of SLC and IPA, in combination with 30 mol% cholesterol, was investigated through the size measurement for a time period over 100 days starting from the day of sample preparation. Representative sizes vs. time (day) profiles are presented in Figure 6. Some important information could have been achieved from such plots. Size of the vesicles passed through a minimum at ~ 10 – 12 days (except the system with x_{IPA} = 0.2), which depended on the composition. This time period may be viewed as the equilibration time for the vesicles. Flipping and reorganization of liposomal components occurred during this time period which led to the decrease in size. Initial observation shows that progressive addition of IPA to the SLC resulted in the size increment of vesicles. System comprising 40 mol% IPA exhibited completely different behaviour. Additionally it was observed that the equilibration time increased with increasing mole fraction of IPA. Initial size contraction for equilibration (for x_{IPA} = 0.1, 0.2 and 0.3) may be attributed to the presence of saturated hydrocarbon chain of IPA which produces more hydrophobic environment in the bilayers. However permanent size contraction was involved for the liposome with x_{IPA} = 0.1, as also reflected from highest C_S^{-1} and I. P. (shown earlier) that demonstrate the strong interaction between SLC and IPA. Vesicles with 30 and 50% IPA showed exceptional stability upto 100 days; the spontaneity of the interaction that arise for these two systems, as revealed from the excess Gibbs potential (ΔG_{ex}^0) value from monolayer study, also support the fact. Size of the vesicles with x_{IPA} = 0.2 and 0.4 monotonously increased with time; such systems also exhibited relatively higher PDI

value. Such a different behavior could be rationalized through the surface pressure independent repulsive interaction between SLC and IPA as already reflected from the monolayer studies. Dissociation of $HTMA^+$ from IPA could lead unfavourable orientation for lipid acyl chain which could lead the way of destabilization. However the modes of interactions for these two sets of vesicles are yet to be revealed and cannot be explained with the present level of knowledge.

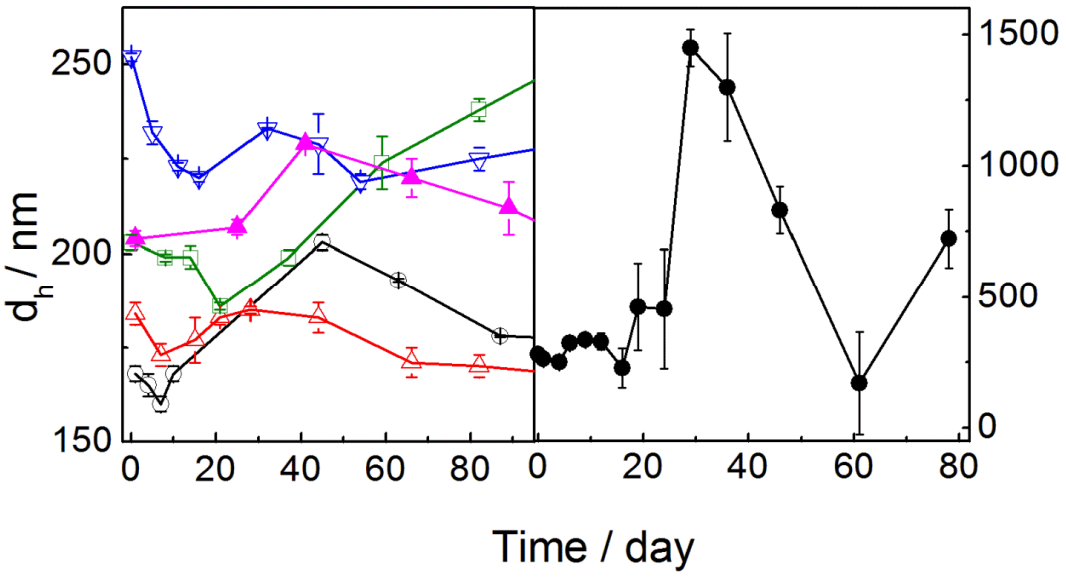

Figure 6. Variation in the hydrodynamic diameter (d_h) for SLC +IPA (in presence of 30 mol% cholesterol) vesicles with time at 25 ^oC. Mole fraction of IPA (x_{IPA}): O, 0; Δ, 0.1; □, 0.2; ∇, 0.3; ▲ ,0.5 and ●, 0.4

Change in the PDI values with time have been graphically presented in Figure 7. Results on the DLS data recorded day 45 are shown in Table 1 as representative. Stable liposomal dispersions were formed for the systems with the following compositions of SLC/IPA (M/M): 10:0, 9:1, 7:3 and for 5:5. d_h – time profile for the different systems have been graphically presented in Figure 6. Addition of IPA (except x_{IPA} = 0.4) resulted in the decrease in polydispersity which remained almost constant with time.[36] It could therefore be

concluded that the IPA plays an important role in stabilizing the vesicles by imparting monodispersity for which the IPA could be considered as novel substitutes of the conventional phospholipids.

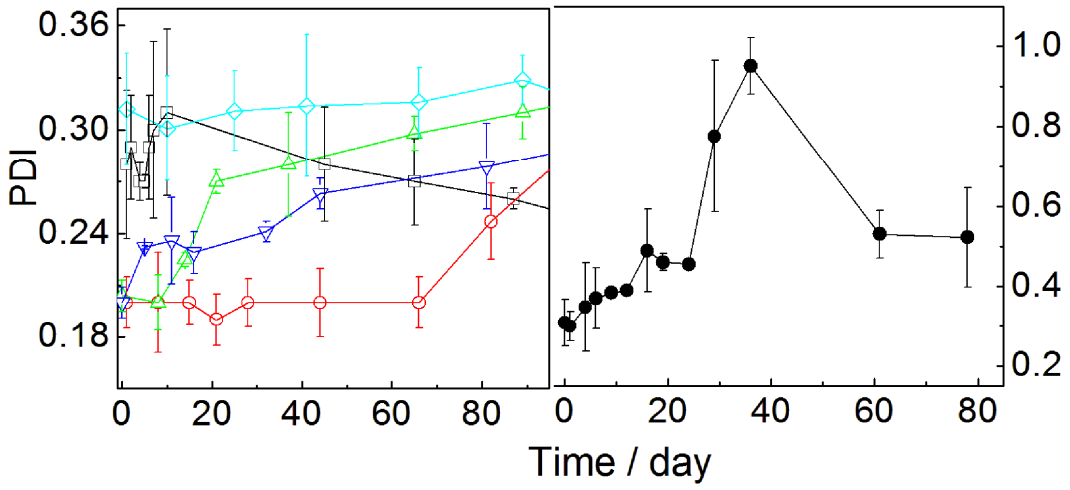

Figure 7. Variation of polydispersity index for the SLC+IPA (in presence of 30 mol% cholesterol) vesicles with time. Mole fraction of x_{IPA}: □, 0; O, 0.1; Δ, 0.2; ∇, 0.3; ●, 0.4 and ◊, 0.5.

Zeta potential (Z. P.) is another major parameter that holds the physical stability and subtle structure of vesicles as it determines the electrostatic repulsion between the vesicles.[12] Table 1 represents the zeta potential of the vesicles with different SLC+IPA molar ratio recorded on day 45 of the sample preparation. Generally the zeta potential values were found to be negative, which accounts for the electrostatic stabilization among the lipidic dispersion and thus prevent vesicles from fusion or aggregation (the mean size did not change much as reflected from hydrodynamic size measurement study). With gradual increasing proportion of IPA in the vesicles (with respect to SLC), negative zeta potential values moved towards the positive range. SLC, a naturally occurring phospholipid exhibited Z.P. ~ −20.7 mV. The negative value of Z. P. was found to decrease with increasing IPA mole fraction. Variation of Z.P. with composition was non linear and followed two degree (2^0) polynomial equation with $R^2 = 0.95$.

Table 1. Hydrodynamic diameter (d_h), Zeta potential (Z. P.) and Polydispersity index (PDI) values for the different vesicle formulations at 25 ^oC. Values correspond to the data acquired on day 45 of the sample preparation

SLC:IPA	d_h / nm	Z. P. /mV	PDI
10:0	203.0±2	-20.7± 1.41	0.28 ± 0.03
9:1	182.4±4	-7.17 ± 1.30	0.20 ± 0.02
8:2	207.8±2	-1.59 ± 0.45	0.28 ± 0.03
7:3	227.8±8	-1.53 ± 0.79	0.24 ± 0.006
6:4	877.5±89	+3.02 ± 0.87	0.95 ±0.07
5:5	228.4±1	-1.71 ± 1.41	0.31 ± 0.04

Although we could prepare vesicles with 40 mol% IPA which showed positive zeta potential, however was certainly a discrepancy that was due to the dissociation of $HTMA^+$ from IPA. The dispatched $HTMA^+$ into the aqueous medium resulted in the formation of some micelle like structure which pushed the Z. P. in the positive range. The instability of the vesicle having x_{IPA} = 0.4 now could well be realized and could be correlated from the monolayer studies.

3.3. Transmission Electron Microscopy

Both normal TEM and freeze fractured TEM (FF-TEM) studies were carried out with an aim to confirm the formation of vesicles as well as their morphologies[37-40,21,30,31,44] also the impact of IPA on vesicles size could be evidenced from such measurements.[37,38,21,44,42] Representative TEM image of the vesicle with 30 mol% IPA has been shown in Figure 8. Spherical morphology and bilayer structure of the vesicles were confirmed from the image. In

the inset, the magnified image of the selected vesicle further revealed the existence of the bilayer.

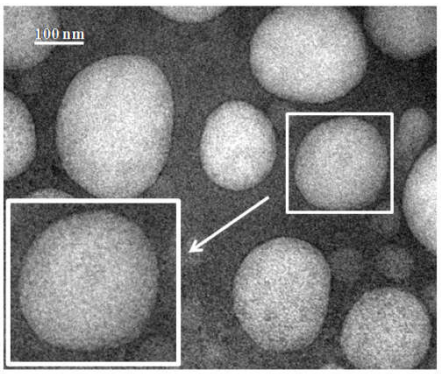

Figure 8. Representative TEM image of SLC+IPA (7:3, M/M) vesicles. Inset: Magnified image of the selected area. Scale bar is indicated in the figure.

Thus TEM measurement could be considered as a useful tool to characterize a vesicular system. FF-TEM studies were carried out to further support the normal TEM measurements, presented in Figure 9 as representatives.[39-41] Both the images in panel A (pure SLC) and B (7:3 SLC+IPA system) put on a view of spherical morphology as well as bilayer section around the vesicles. A distinct bilayer structure could be visualized as shown in the inset of panel A.

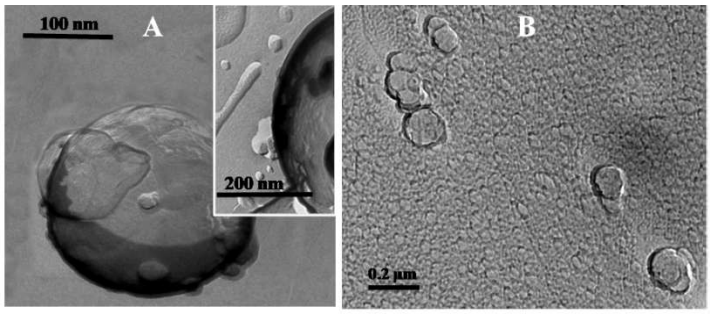

Figure 9. Freeze fractured TEM images of SLC+IPA (10:0, M/M, panel A) and SLC+IPA (7:3, M/M, panel B) vesicles. Scale bars are indicated in each panel.

Vesicle sizes were found to be comparable in both normal TEM and in FF-TEM. Impact of IPA on SLC bilayer have been explored by means of different instrumentation, like DLS study; the fate of the vesicles were found to be same here also as we have witnessed minor size enhancement for 7:3 SLC+IPA. Spherical morphology of the vesicles was confirmed from the images and the clustered form so obtained was not uncommon for the vesicular systems.

3.4. Differential Scanning Calorimetry (DSC) Studies

Chain melting temperature (T_m) of the bilayer dispersion, its crystalinity, enthalpy of the transition processes (ΔH) as well as the heat capacity values (ΔC_p), *etc.*, can suitably be evaluated by DSC studies. Such studies are exceedingly responsive in presence of exogenously added compounds (herein the IPA).[37] Exogenously added compound may alter the half peak width ($\Delta T_{1/2}$). In the present set of studies, DSC measurements were carried out in the temperature range -25 to 25 ^{o}C with a scan rate of 2 ^{o}C min^{-1}. Representative thermograms are shown in Figure 10. Vesicles of different compositions with 30 mol% of cholesterol generated three distinct separate events. Two endotherms appeared at "a" in the temperature range -20 to -19 ^{o}C and another and "c" in the temperature range 3 to 6 ^{o}C respectively. The exothermic one, "b" appeared in the temperature range 0 to 3 ^{o}C. SLC, with an unsaturation in one of its fatty acyl chains, exhibited the T_m at around -20 ^{o}C .The value was found to be comparable with the previously published report.[42] Endotherm "a" was due to the 'phase transition' or 'chain melting' of mixed acyl chains of SLC.[42] IPA has discrete effect on the thermograms. The bilayer chain melting temperature (T_m), width at half-peak height ($\Delta T_{1/2}$),[43] enthalpy change (ΔH) and corresponding heat capacities (ΔC_p) for the different formulations have been summarized in Figure 11.

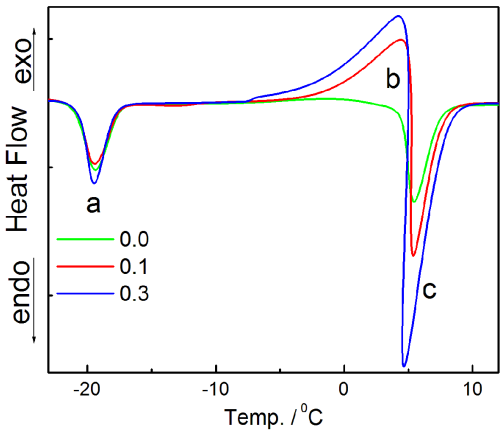

Figure 10. DSC thermograms of SLC+IPA vesicles at different SLC/IPA ratio (in presence of 30 mol% cholesterol). Scan rate: 2 ^{o}C min^{-1}. Mole fractions of IPA are mentioned inside the figure.

Incorporation of 10 mol% IPA enhanced T_m (0.8%) and lowered the $\Delta T_{1/2}$ (1.3%) values at ~ −20 ^{o}C mildly, but a significant increase in the negative value of ΔH (11%) and positive value of ΔC_p (16%) were noticed. It was found that progressive addition of IPA into the SLC bilayers decreased the $\Delta T_{1/2}$ while increased ΔC_p in the transition region marked as 'a". Sequential decrease of $\Delta T_{1/2}$ may be rationalized on the basis of the phase transitions. Results further support the surface pressure-area isotherm derived data. In case of the system with 10 mol% IPA, the monolayer exhibited more rigidity. Addition of IPA can cause the increased crystalinity for which there occurred an increase in the transition temperature and decreased $\Delta T_{1/2}$ values.

IPA produced extra hydrophobic environment in the bilayers, which caused the physical state of bilayers as with its progressive addition turn the bilayers from fluid-phase to liquid crystalline phase. Because of the most ordered orientation of acyl chains in 5:5 SLC+IPA, it produced narrower distribution curve for the phase transitions. Increasing ΔC_p with increased concentration of IPA for SLC+IPA vesicles also further support the

aforementioned explanation which is also further established by steady state fluorescence anisotropy experiment with DPH as hydrophobic probe (to be shown later).

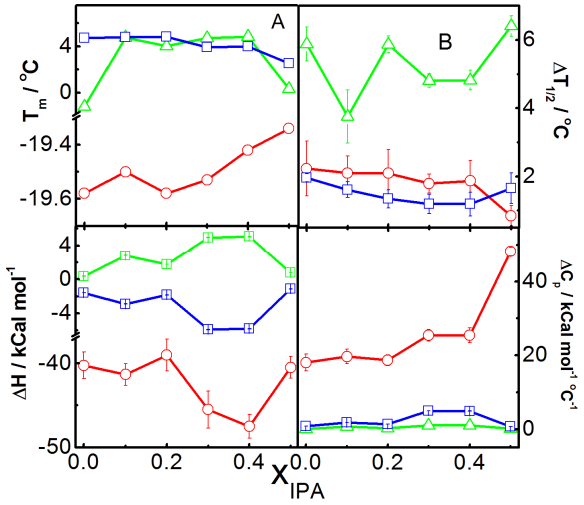

Figure 11. Variation in the transition temperature (T_m), half peak width of the transitions ($\Delta T_{1/2}$), and enthalpy changes for the melting (ΔH) and changes in the heat capacity (ΔC_p) with the composition (x_{IPA}) for SLC+IPA vesicles comprising 30 mol% cholesterol. PBS buffer at pH=7.4 was used in the preparation of vesicles.

The exothermic event 'b' was an outcome of IPA effect, as reflected from Figure 10. With increasing IPA concentration, heat change of the process was noticeably increased. This release of heat was due to the some sort of arrangement/packing of water molecule around the vesicles, which was a direct effect of IPA. Formation of an overlayer of water molecules over the lipidic head groups produces some sort of packing at temperature around 4 ^{o}C, where the density of water was supposed to be highest. T_m for 10:0 SLC+IPA was found to be −1.17 ^{o}C, which interestingly jumped up to 4.76 ^{o}C for 9:1 SLC+IPA and did not change much for 7:3 SLC+IPA. So it can be concluded that shifting of T_m from −1.17 to 4.76 ^{o}C was surely the IPA induced effect. Lower $\Delta T_{1/2}$ values for 9:1 and 7:3 SLC+IPA systems than 10:0 SLC+IPA indicate better packing of the hydrophilic overlayer as well as lipidic head

groups. This was again confirmed from the heat release (ΔH) of the process, where greater heat release for 9:1 and 7:3 SLC+IPA rather 10:0 were observed.

Appearance of neighbouring endotherm 'c' was a reverse consequence of the event 'b' where heat was absorbed. From the Figure 10 it was evident that the absorption of heat was also an IPA effect and exactly the opposite phenomenon to that of the exotherm 'b'. Endotherm 'c' was due to the disorganization of water overlayer surrounding the vesicles. At relatively higher temperature, the lipidic head groups were supposed to be vibrating. This vibration transforms the water overlayer to turn from an organized to disorganized states. Although the T_m for 10:0, 9:1 and 7:3 SLC+IPA were not changed significantly, however relatively sharp peaks were noticed for the 9:1 and 7:3 SLC+IPA systems indicating better head group packing. Higher negative heat changes associated with 9:1 and 7:3 SLC+IPA systems again support the higher order of packing. It is now been known that both the events 'b' and 'c' were the two opposite phenomenon and expected to show reverse heat change as also reflected from the Figure 11.

3.5. Fluorescence Spectroscopic Studies

Fluorescence spectroscopy is another important technique which enables to explore the subtle structure of the membrane. Packing of bilayer (in the core of the membrane) and interaction of head groups (at the palisade layer) are the two major parameters for the formation of stable vesicle. With an aim to understand the packing of head groups, fluorescence spectroscopic studies were carried out using 7-hydroxy coumarin (7-HC) as a molecular probe. 7-HC is well known as a solvatochromic dye and has a great tendency to stay on the palisade layer of the membrane.[24] Emission spectra of 7-HC in solvents of different polarity were carried out as the references in order to understand the state of polarity

of the probe at the membranous interface. Emission spectra 7-HC in the vesicles of different compositions were recorded and compared with that in the solvents of different polarities.

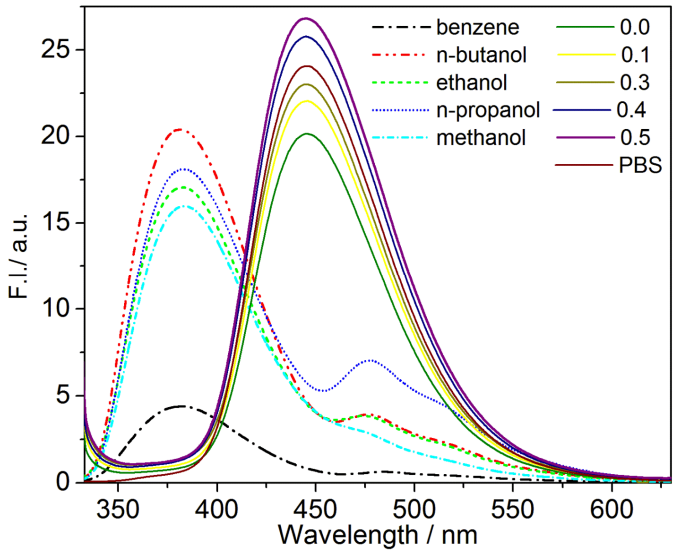

Figure 12. Fluorescence spectra of 10 μM 7HC in solvents of different polarity (dashed lines) and vesicles of varying composition (solid lines) at 25 ^{o}C. Excitation wavelength (λ_{ex}) = 330 nm. Different solvents and the mole fraction of IPA are mentioned inside the figure. Spectra was also recorded in PBS alone

Emission spectra of 10 μM 7-HC under various conditions have been graphically presented in Figure 12. Periodic declinations of intensities along with a mild red shift were observed with increasing solvent polarity. Such an observation was also reported by others.[44] While considering the spectral behaviour of 7-HC in the vesicles of different compositions, it was observed that with increasing amount of IPA in the vesicles, fluorescence intensity was enhanced along with a mild blue shift. With increasing amount of IPA the difference in polarity was thus confirmed. It is not unexpected that IPA bearing neutralized head groups will effectively result in decreasing polarity of the bilayer. Another interesting thing that additionally comes into the picture is the polarity of SLC vesicles with variant mole fractions

of IPA. Results clearly indicate that with increasing amount of IPA in the vesicles, there were increase in rigidity and decrease in the polarity of the membranous interfaces.

.

With an aim to understand the packing of the hydrocarbon chains (inside the bilayer) similar studies were carried out using l,6-diphenyl-l,3,5-hexatriene (DPH) as the molecular probe. DPH being completely hydrophobic will preferentially reside in the lipid acyl chain with parallel orientation. Emission spectra of DPH in different vesicles have been shown in Figure 13. No significant change in the fluorescence spectra of DPH in different vesicles further supported its residence in the bilayer core. Results clearly indicate no change in the polarity of the core of bilayer for different combinations. However, the change in the hydrocarbon chain packing was further investigated by measuring the fluorescence anisotropy values.

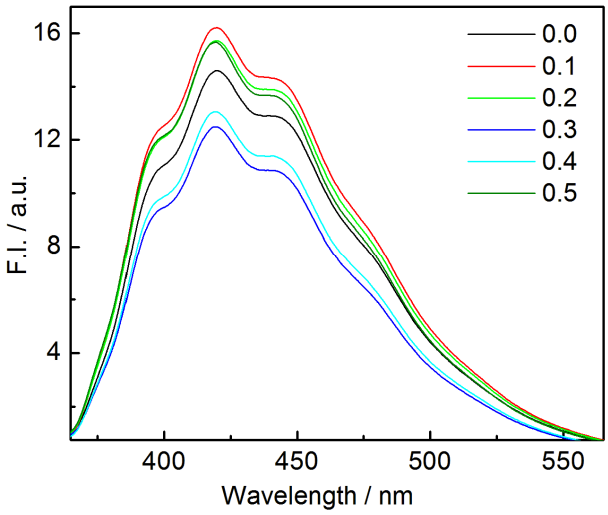

Figure 13. Fluorescence spectra of 10 µM DPH in PBS buffer (pH 7.4) in vesicles of varying composition at 25 ^{o}C. Excitation wavelength (λ_{ex}) = 357 nm. Mole fraction of IPA are mentioned inside the figure.

Variations in the fluorescence anisotropy (r) with the composition of the vesicles (x_{IPA}) have been graphically presented in Figure 14.

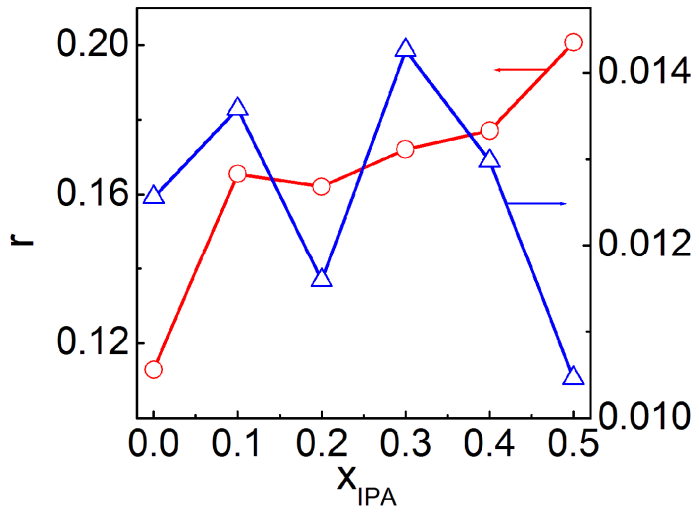

Figure 14. Variation in the fluorescence anisotropy (r) for DPH (O) and 7-HC (Δ) with the mole fraction of IPA (x_{IPA}) in the vesicles comprising SLC+IPA + 30 mol% cholesterol. Temp. 25 ^{o}C. While DPH evaluates the anisotropy value for the core hydrocarbon region of the bilayer, 7-HC monitors the anisotropy of the palisade layer.

While considering the fluorescence anisotropy variation of 7-HC with x_{IPA}, it was noted that the addition of IPA resulted an initial increase in the 'r' values followed by the appearance of a maximum. Anomalous behaviour for the system comprising 20 mol% IPA was noticed. Such anomalous behaviour was also evidenced in other measurements. Initial increment of anisotropy was due to IPA addition which forced the SLC head groups to come closer. Such an incidence was most significant in case of 30mol% IPA. Lower anisotropy value for 5:5 SLC+IPA favours repulsive forces which cause the brakeage of head group packing. Unusual behaviour for the 20% IPA system clearly indicates non-favourable packing between the components. However, further studies, *viz*., NMR, small angle neutron scattering (SANS), small angle x-ray scattering (SAXS) and molecular dynamics simulation studies could shed light in such case, which are considered as the future perspectives.

Figure 14 also represents periodic increment in the anisotropy value with progressive addition of IPA for the systems comprising DPH as the molecular probe. Vesicles with pure

SLC showed lowest value because of the fluidic nature of the membrane. However progressive addition of IPA resulted in the rigidity enhancement of hydrocarbon chains which brought some sort of crystalinity into the bilayer. Such an observation clearly implies that one can appreciably control the physical properties of vesicles through the incorporation of IPA into the SLC bilayer.

3.6. Entrapment Efficiency

Entrapment efficiency (E. E.) of the vesicles with varying mole fraction of IPA has been tabulated in Table 2. E. E. was determined for the vesicles with varying composition. It was found that the E. E. was dependent on IPA concentration and satisfactory results were found through all the vesicles comprised with different mole fraction of IPA. Anomalous behaviour was noticed for the system having 40% IPA.

Table2. Entrapment Efficiency (E. E.) of Different Sets of Vesicles with Varying Mole Fraction of SLC and IPA. Temperature 25 ^{o}C

System	Entrapment Efficiency (%)
10:0 SLC+IPA	92.5±1.41
9:1 SLC+IPA	90.0±1.30
8:2 SLC+IPA	88.7±0.45
7:3 SLC+IPA	79.2±0.79
6:4 SLC+IPA	96.5±0.87
5:5 SLC+IPA	53.9 ±1.41

The dye methylene blue is cationic in nature and expected to bind with the vesicles having negative surface potential. Pure SLC vesicles with highest negative zeta potential, showed maximum E.E. (92.50%) due to the strong electrostatic force of attraction. Progressive addition of IPA into the bilayer although decreased the E.E. mildly, yet the results were still reasonable as per as E.E. was concerned. 96.50% of E.E. was a strange result for x_{IPA} 0.4, and it was possibly due to the dissociation of IPA into corresponding cationic ($HTMA^+$) and anionic (DS^-) parts. Presence of zwitterionic choline head group and anionic DS^- could provide excess electrostatic force of attraction which leads to the high E. E. value.

4. Conclusion

SLC and IPA (HTMA- DS) in different mole fractions were used to prepare stable vesicles dispersions. Through the comprehensive investigation on the impact of IPA on the vesicles were studied from monolayer studies and it could be concluded that IPA exerts prominent influence on SLC monolayer. Associative interactions were found for some mixed monolayer however the systems with x_{IPA} ~ 0.5 did not response to produce stable vesicles dispersions. Some aberrations were noted with the systems comprising 20 and 40 mol% IPA. Dissociation of $HTMA^+$ from IPA resulted in such unusual variation. This was further scrutinized by measuring the hydrodynamic size of the hybrid vesicles and we found relatively less stable vesicular dispersions for x_{IPA} = 0.2 and 0.4. Polydispersity index values drew much attention because it unleashed the usefulness of IPA that reduce the PDI value and maintained fairly monodispersed system. TEM images of vesicles put on a view of spherical vesicular system and were well correlated to the data that obtained from DLS measurements. Packing of head groups as well as packing of the hydrocarbon chains were investigated through the combined DSC and fluorescence spectroscopy analysis where gradual incorporation of IPA into the bilayer produces rigidity or crystalinity. Systems comprising 0, 10, 20, 30 and 50 mol% IPA produce promising drug entrapment efficiency.

Thus IPA assisted vesicular system could be used as a carrier for drug delivery. The future prospective would be to characterize the system theoretically based on molecular dynamics simulation and to study the interaction through ^{1}H, ^{13}C NMR, SANS and SAXS study.

References:

References are given in BIBLIOGRAPHY under Chapter I (pp. 151-153).

CHAPTER 2

Exploring the Dual Impact of Hydrocarbon Chainlength and the Role of Piroxicam A Conventional NSAID on Soylecithin/Ion Pair Amphiphiles Mediated Hybrid Vesicles for Brain – Tumors Targeted Drug Delivery

Abstract: Development of drug delivery systems, not the drug discovery, has become more cynosures towards the efficacy of drug against the target cells. Modified hybrid cationic vesicles (HCV) were formulated using soylecithin (SLC), ion pair amphiphile (IPA, hexadecyltrimethylammonium-dodecylsulfate, $HTMA^{+}$-DS^{-}), bi-tail cationic surfactant dialkyldimethylammonium bromides (DXDABs, bis-C_{12} to C_{18}) and cholesterol. Piroxicam (Px), a conventional non steroidal anti inflammatory drug, with potent yet unexplored anticancer activity, was encapsulated in the hybrid vesicles. Dual impact of DXDABs and Px on SLC/IPA were scrutinized in the form of monolayer, bilayer and solid supported bilayer. Favourable hydrophobic interaction between SLC/IPA and dihexadecyldimethylammonium bromide (DHDAB) as well as the intercalation of Px molecules between the amphiphiles were noticed through the surface pressure area measurements. Vesicles without and with Px were fairly monodispersed with positive zeta potential (Z. P.) and considerably stable up to two months. Size of the vesicles enhanced with Px incorporation. Vesicles maintain spherical morphology as revealed from the electronic microscopic studies. Differential scanning calaorimetry and FTIR studies confirm the location of Px membrane palisade that enhances the extent of hydration by increasing the proportion of H-bonding. Bilayer thickness and the spacing between two adjacent lamellar phases were investigated by combined small angle neutron scattering and small angle X-ray scattering. Atomic force microscopic studies confirm the Px induced fluidization of membrane bilayer. The entrapment efficiency of

vesicles to host Px depends on the amount of IPA present in the bilayer. Px hosted cationic vesicles showed less than 2% hemolysis. The drug reigned supreme over human Neuroblastoma cell line (SH-SY 5Y) when encapsulated inside the membrane and was non toxic to normal human blood cell lymphocyte (PBMC) as revealed from cytotoxicity assay.

1. Introduction

Vesicles, the aggregates of amphiphiles having bilayer like structure, are widely used as potential drug delivery systems because of its tendency to fuse onto the microbial membrane bilayer. Chemical composition and structure of liposome can be controlled by considering its preparative method that could be useful in various applications. Different properties of liposome's and cell membrane mimic architect offer an useful model system for studying the membrane biophysics, colloidal interaction, photochemistry, cell function, signal transduction and many others.[1-3] Synthetic vesicles find wide range of technical applications, *viz.*, nano sensing, metal encapsulation, and drug delivery, to mention a few.[4,5] It can accumulate both hydrophilic and lipophilic drugs and transfer them to the target cells. However, vesicles suffer from major limitations like the stability and production cost. Susceptibility towards oxidation and microbial attack warrants it modulation by incorporating different substitutes.

Usually naturally occurring biological membranes have negative surface charge and hence well engineered cationic vesicles can be considered as efficient drug delivery systems. The present research group has been pursuing the physicochemical characterization of vesicles with different surrogates, which are stable up to 100 days with superiority than the conventional liposomes.[6-8] The present work endeavours to search for stable cationic vesicles with superior drug delivery capacity.[8] Over the period of time attempts have been made to

modulate cationic vesicles by using bi-tail cationic surfactant with varying chain length (bis-C_{12} to C_{18} or higher).

Ribeiro *et al.*[9] have prepared cationic vesicles in combination with DPPC and dioctadecyldimethylammonium bromide (DODAB) in solutions of different ionic strengths. Dong *et al.*[10] studied the interaction of DNA with cationic vesicle having didodecyldimethylammoniumbromide (DDDAB). Chou *et al.*[11] have made detailed investigation on the catanionic vesicles using dihexadecylphosphate (DHP) and DODAB.

Piroxicam (Px), a non steroidal anti-inflammatory drug (NSAID), can assemble with the enzyme cyclooxygenase-2 (COX-2) in the cell membrane and thereby can reduce the inflammatory function.[12-14] Its potent anticancer activity is worthy to study its efficacy towards the target cell. Its pKa values are 1.86 and 5.42 respectively. Hence in biological condition its half life and activity towards the target cell is substantially reduced. Limited activity in biological conditions, provide a scope to host or entrap Px in suitable delivery systems. Hybrid cationic vesicle (HCV) is considered as a protector as well as a vehicle, for a variety of drugs at physiological environment for better efficiency towards the target cells. However, structural properties and acid-base form of the drug molecule play crucial role and thereby govern the drug-membrane interaction. Membrane mimetic models can avoid the complexity of the biological cells, creating the platform to understand the mechanism by which it interacts with drug molecules. Different attempts have been made to understand the impact of Px or other NSAIDs on different bio-mimetic membranes.[12,14-17] Px induced fluidization of the DMPC and DPPC membranes were already reported. Basak *et al.*[12] had studied the stability of DMPC monolayer in the presence of Px. Whereas Nunes *et al.*[14] had made detail investigation on the impact of all set of oxicams in DPPC membrane. Roy *et al.* have reported the increased orientation order of the lipid chain in presence of NSAID.[17]

However no comprehensive attempts have been made so far where the interactions between hybrid cationic membrane and Px are concerned.

Limited or fragmented knowledge warrants bi-tail cationic surfactants with varying hydrocarbon chain length (bis-C_{12} to C_{18}) in combination with soy lecithin (SLC) and ion pair amphiphile (IPA). IPA, herein prepared by mixing equimolar ratio of two cationic surfactants hexadecyltrimethyalammonium bromide ($HTMA^+Br^-$) and sodium dodecyl sulfate (NaDS) (herein the IPA means $HTMA^+$-DS^-).[7] Bi-tail cationic surfactants were chosen to progressively substitute with previously established three sets of SLC/IPA combinations (1:0, HCV1; 9:1, HCV2 and 7:3, HCV3; M/M)[7] Interaction between hybrid membrane and Px were analyzed in the form of monolayer, bilayer and solid supported bilayer and finally few set of optimised px encapsulated formulations were analysed for biological activity. Mutual miscibility among the components were studied by way of the surface pressure – area measurements. Ideality, nonideality in the mixing processes, Gibbs free energy of mixing was assessed. Physicochemical characterizations of the different hybrid vesicels were assessed by combined dynamic light scattering, zeta potential, electron microscopy, atomic force microscopy, differential scanning calorimetry, FTIR, UV-VIS absorption and emission spectroscopic studies. Entrapment efficiency and the release kinetics of Px from the vesicles were also studied by conventional dialysis bag approach. Finally the toxicity and biocompatiblity of the drug loaded formulations were assessed. It is believed that such a comprehensive set of the studies would shed further light in the development of drug delivery systems in the treatment of brain – tumours targeted drug delivery.

2. Materials and Methods

2.1. Materials

L-α-phosphatidylcholinee (soylecithin, SLC, from soybean) was received from EMD Chemicals, Germany, A. R. grade sodium dodecylsulfate (SDS) [$CH_3(CH_2)_{11}SO_4Na$], hexadecyltrimethylammonium bromide (HTMAB) [$C_{16}H_{33}N(CH_3)Br$], didodecyldimethylammonium bromide (DDDAB) {$[CH_3(CH_2)_{11}]_2N(CH_3)_2Br$}, dimethylditetradecyldiammonium bromide (DTDAB) {$[CH_3(CH_2)_{13}]_2N(CH_3)_2Br$}, dihexadecyldimethylammonium bromide (DHDAB) {$[CH_3(CH_2)_{15}]_2N(CH_3)_2Br$}, dioctadecyldimethylammonium bromide (DODAB) {$[CH_3(CH_2)_{17}]_2N(CH_3)_2Br$}, (3β)-cholest-5-en-3-ol (cholesterol) 1,6-diphenyl-1,3,5-hexatriene (DPH) and piroxicam [4-Hydroxy-2-methylN-(2-pyridinyl)-2H-1,2-benzothiazine-3-carboxamide 1,1 dioxide] were purchased from Sigma-Aldrich Chemicals Pvt. Ltd. (USA). A.R. grade disodium hydrogen phosphate (Na_2HPO_4, $12H_2O$), sodium hydrogen phosphate ($NaH_2PO_4.2H_2O$), sodium chloride (NaCl) and chloroform (HPLC grade) were from Merck Specialties Pvt. Ltd, India. Double distilled water with specific conductance 2-4 μS (at 25^oC) was used for the preparation of solutions. The SH-SY 5Y cell lines were procured from National Centre for Cell Science (NCCS), Pune, India. They were maintained in DMEM F-12 Ham (Hi-Media) supplemented with 10% fetal bovine serum (FBS), 100 units/mL penicillin, 100 mg/mL streptomycin, 0.14% sodium bicarbonate and 0.1 mM sodium pyruvate.

2.2. Methods

2.2.1. Preparation and Isolation of Ion Pair Amphiphile (IPA)

IPA, also known as hexadecyltrimethylammonium-dodecylsulfate ($HTMA^+$-DS^-) was prepared by the combination of equimolar mixture of two oppositely charged surfactants in water medium.[18,19] An aquous solution of 0.1M hexadecyltrimethylammonium bromide

(HTMA) was progressively added to equimolar amount of sodium dodecyl sulfate (SDS) with constant stirring whereby a white semi solid got precipitated. The precipitate was then extracted by chloroform. After the eveporation of chloroform, the white soild powder (IPA) was dried under vacuum and thus obtaind salt free IPA. IPA was charectarised by means of ^{1}H-NMR, XRD and by FTIR.[7,18-20] Data obtaind were found to be similar with the previously published results and hence are not discussed further.

2.2.2. Preparation of Vesicles

Modified hybrid small unilamellar vesicles (SUVs) were prepared by the conventional thin film generation and rehydration technique.[4,7] Quantitative amount of SLC, IPA, bi-tail cationic surfactant and cholesterol were dissolved in chloroform: methanol (7:3, V/V) in a round bottom flask followed by solvent evaporation in a rotary evaporator. Trace amount of solvent was finally removed by the stream of nitrogen (N_2). The thin film was then rehydrated for 1h in PBS (0.1 M Na_2HPO_4, 0.1M NaH_2PO_4, 100mM NaCl, pH 7.4) at 70 ^{o}C, well above the chain melting temperature of all the lipidic components. After rehydration, freeze-thaw sonication processes were repeated for 4 cycles. Finally, it was extruded using 0.45 micron cellulose nitrate membrane filter (Whatman Gmbh, Germany). Px loaded vesicles were obtained by mixing appropriate amount of drug into the lipid mixture before the generation of the thin film such that the final ratio of lipid and dye was 200:1. Total phospholipids concentration was kept at 2 mM and was diluted depending on the type of experiment.

2.2.3. Surface Pressure (π) – Area (A) Isotherm

Surface pressure-area isotherm was constructed with a Langmuir surface balance (micro trough X, Kibron, Finland). The trough was filled with the PBS solution at pH = 7.4 with 100 mM NaCl with the barrier made of Teflon to avoid contamination.[19] Isotherms were

obtained by carefully spreading the droplets using a Hamilton (USA) micro syringe. Pure as well as mixed lipidic components were dissolved in chloroform (1.0 $mgmL^{-1}$) and were spread over the subphase with an amount of 10 μL. To prevent the entry of dust particles, a Plexiglas box was used which covered the stage and trough. Solvent was allowed to evaporate approximately 20 min. All the π – A isotherms were recorded at a subphase temperature of 25 ± 0.5 ^{o}C with a lateral compression rate of 5.0 mm min^{-1}. To ensure reliable result, each set of experiment as performed twice.

2.2.4. Dynamic Light Scattering (DLS) Studies

To get the knowledge about hydrodynamic diameter (D_h), zeta potential (Z. P.) and PDI, DLS measurement was carried out for different combination of vesicles.[21] Dynamic light scattering spectrometer (Zetasizer Nano ZS90 ZEN 3690, Malvern Instrument Ltd., U.K.) was used for such measurement. A He-Ne laser was used having emission wavelength 632.8 nm and all the data were recorded at a scattering angle 90^{o}.

2.2.5. Electron Microscopic (TEM/FF-TEM) Studies

Morphological information of the vesicles were obtained from the TEM studies, carried out in the form of both normal and freeze fractured (FF) TEM.[22, 23] For normal TEM, one drop of dilute vesicle dispersion was placed on Formver carbon-coated 300 mesh copper grid and the excess liquid was removed from the edge of the grip and the sample was allowed to dry for 10 min before performing the experiment. Hitachi H-600 transmission electron microscope (Japan) was used to view the morphology of the vesicle. For FF-TEM measurement, FR-7000A (Hitachi High Technologies Ltd., Japan) was used at -150 ^{o}C for freeze fracturing process. The sample was placed on the sample holder and frozen in liquid propane. Replication of the sample was done by evaporation using Pt-C. The replica was then

positioned on 300 mesh copper grid, dried and taken to electron microscope (H-7650, Hitachi High Technologies Ltd., Japan) with an acceleration voltage of 120 kV.

2.2.6. Scattering (SANS and SAXS) Studies

2.2.6.1. Small Angle Neutron Scattering (SANS)

Scattering intensities of the different sets of vesicles with and without drugs in D_2O were recorded by SANS instrument at the Dhruva Reactor, Trombay, India.[24] Sample-to-detector distance was set at 1.8 m. Crystalline BeO filtered beam that provides mean wavelength (λ) 0.52 nm was used. A one dimensional position sensitive detector (PSD) was used to record the angular distribution of the scattered neutron. The scattering vector Q ($Q = 4\pi\sin\theta / \lambda$) for this instrument was 0.018 to 0.35 $Å^{-1}$.

2.2.6.2. Small Angle X-ray Scattering (SAXS)

SAXS measurements were performed in NANOSTAR U SYSTEM with a detector VANTEC-2000 (Bruker AXS GmbH, Karlsruhe, Germany) to further clarify the bilayer architect.[25, 26] Samples were placed in a capillary tube and the X-ray wavelength was set to 1.5 Å with energy of the incoming beam 12 keV. Distance of the two sample detectors were set at 63.4 and 95.2 cm respectively leading to the Q range 0.01-0.3 $Å^{-1}$. The obtained raw data were first radially averaged, normalised for the acquisition time and the background correction for the PBS was done to obtain the scattering curve for the samples.

2.2.7. Differential Scanning Calorimetry (DSC) Studies

A Mettler Toledo differential scanning calorimeter (DSC 1, STARe system, Switzerland) was used where two identical pans were loaded with sample and PBS respectively.[27]

Samples were scanned with two different scan rates 5 ^{o}C and 2 ^{o}C with complete heating and cooling circle. The result so obtained was further processed with STAR^{e} software.

2.2.8. FTIR Studies

FTIR spectra of vesicles with and without drug and the drug in PBS alone were recorded with a Perkin Elmer Spectrum two FT-IR spectrophotometer equipped with a zinc selenide and a KBr beam spliter at ambient temperature (Perkin Elmer, Inc. MS, USA).[28,29]

2.2.9. Atomic Force Microscopic (AFM) Studies

The vesicular dispersion with and without drug was sonicated for ~ 7 min at 37 ^{o}C. A mica plate was placed into the cell and covered by 20 μL dispersions. After 45 min of waiting about 1000 μL of PBS was added into the cell and the AFM experiment was started using a Nanoscope III MM-AFM under ambient condition. Surface hardness and topography of the membrane was studied by adopting contact mode.

2.2.10. Determination of Entrapment Efficiency (EE)

Drug loaded vesicles dispersions were filled into the cellulose dialysis bag (MWCO 12 KDa) and dialyzed in PBS with constant stirring (60 rpm) under sink conditions for about 15 min.[30] Thus the un-entrapped drug was removed from the formulations and the absorption spectra of collected samples were recorded through UV-VIS spectrophometer (UVD-2950 Labomed Inc., USA). The EE was calculated by considering the following equation:

$$\text{E.E. (\%)} = \frac{T-C}{T} \times 100 \qquad (1)$$

where, T is the total amount of drug presents both in the sediment and supernatant, C is the amount of drug detected only in the supernatant. T and C values were determined colorimetrically.

2.2.11. In Vitro Drug Release Studies

The release of Px from the vesicular systems was quantified by measuring the Uv-VIS absorption spectra. The experiment was carried out by dialysis method as our group has been reported previously.[8]

2.2.12. Hemolysis Assay

Hemocompatability of the free and drug loaded vesicles were studied to understand the biocompatibility of the vesicles and drug.[31-33] EDTA stabilized freshly prepared blood sample was collected from human subject after obtaining the details. Guidelines provided by the Indian Council of Medical Research (ICMR), New Delhi, India was followed. Blood sample was centrifuged for 5 min at 1600 rpm to renounce the plasma, buffy coat and the top layer of the cell. The remaining RBC was then washed with sterlie isotonic PBS at least 5 times and then diluted with PBS. Dilute suspension of RBC was then mixed with PBS and distilled water as negative and positive control. Besides, the RBC suspension was mixed with different set of hybrid vesicles with or without drug. The mixture was gently vortexes and incubated for 2 h. The incubated mixtures were then allowed to centrifuge at 1600 rpm for 5 min; the supernatant was colorimetrically assessed at 541 nm.

2.2.13. In Vitro Cytotoxicity Studies on Human Blood Cell Lymphocyte (PBMC) and Human Neuroblastoma Cell Line (SH-SY 5Y)

Cells were seeded in 96-well plates at a density of 5 x 10^3 cells per well in 200 µL culture medium. After 24 h, the cells were treated with PBS, vesicles and drug encapsulated vesicles with increasing concentration of drug. After 24 h, media was replaced with MTT solution (10 µL of 5 mg/mL/well) prepared in PBS and incubated further for 3 h at 37 ^{o}C in a humidified incubator with 5% CO_2. Then 50 µL isopropanol was added to each well and plates were gently shaken for 1 min and absorbance was recorded at 595 nm (for MCF 7) and

620 nm (for SH-SY 5Y) by micro titre plate reader (Thermo). The experiments were repeated three times independently. Results were presented as mean of triplicates from three independent experiments.

3. Results and Discussion

3.1. Surface Pressure (π) – Area (A) Isotherm.

With the quest to understand the mixing of hydrocarbon chain, surface pressure (π) - area (A) isotherms of the individual as well as mixed components were obtained (Figure 1, panel A and B). A bilayer can be considered as superimposition of two monolayers. Nature of the molecular interaction between the components, lift-off area, excess free energy, film compressibility, *etc.*,[7,20] could define the nature of bilayer. The behaviour of mixed monolayer in the presence of Px would certainly be interesting over here. Px induced fluidization or repulsive interaction in lipid monolayer has already reported.[12,14,17] Interfacial behaviour of the individual components (SLC, IPA, DXDABs and cholesterol) as well as in the form of mixed monolayer was investigated by using Langmuir Balance. Monolayer isotherms for individual components were represented in Figure 1, panel A. SLC with unsaturation in one of its fatty acyl chains was in liquid-expanded state and the lift-off area was at 1.09 $nm^2 molecule^{-1}$. Being unsaturated it does not show any platue in the isotherm while undergoing transition from the gaseous to liquid phase. Lift-off area for the IPA was 1.02 $nm^2 molecule^{-1}$ because of the mismatch in its hydrocarbon chains.[7] The limiting area of IPA per molecule was 0.56 nm^2. Apparently, half of the limiting area per IPA should have been 0.28 nm^2, comparable to the limiting area per alkyl chain. The ideal limiting area per alkyl chain is 0.20 nm[34], quite lower than the value herein calculated. This implies that the bulky head groups of IPA play crucial roles in molecular packing.

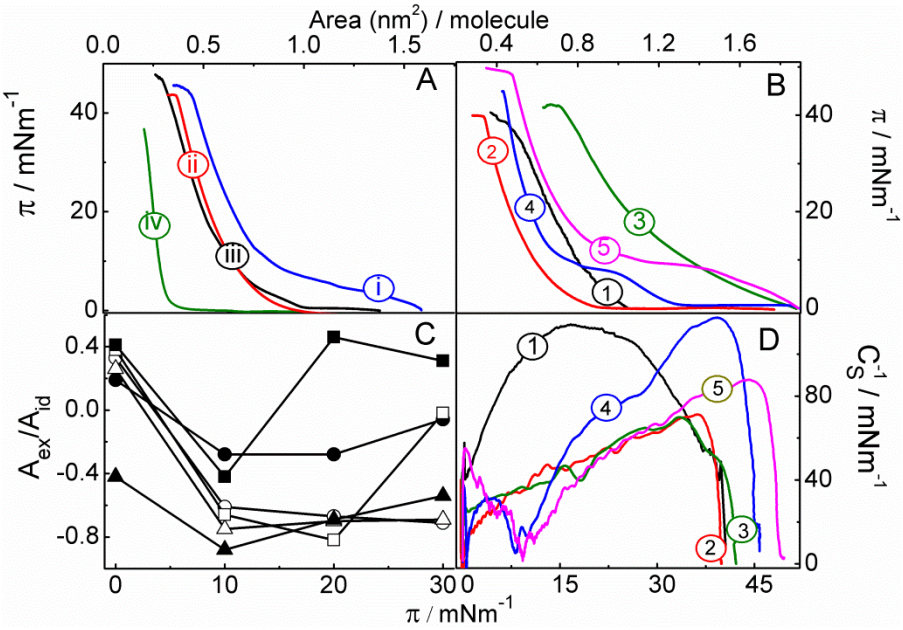

Figure 1. (A) π – A isotherms for the mono momolecular films of (i) DHDAB, (ii) SLC, (iii) IPA and (iv) cholesterol **(B)** mixed spread monolayers at the air-buffer interface: (1) HCV2, (2) 1+DDDAB, (3) 1+DTDAB, (4) 1+DHDAB and (5) 1+DODAB. Bi-tail surfactant amount was 5 mol%. **(C)** Dependence of A_{ex}/A_{id} on π for different sets of SLC/IPA with DHDAB. (○ and ●) HCV1; (Δ and ▲) HCV2 and (□ and ■) HCV3. Amount of DHDAB (○, Δ and □ 5 mole % and ●, ▲ and ■ 10 mole %). **(D)** Variation in the compressibility moduli (C_s^{-1}) with π. Surfactant amount 5 mol%: (1) HCV2; (2) 1 + DDDAB; (3) 1 + DTDAB; (4) 1 + DHDAB; (5) 1 + DODAB. Temperature 25 ºC.

DHDAB also produces SLC like expanded isotherm with lift-off at 1.59 $nm^2molecule^{-1}$. It could achieve surface pressure up to 45.4 mNm^{-1} with limiting area of 60 $nm^2molecule^{-1}$. The expanded isotherm was probably the outcome of electrostatic charge repulsion between the similar head groups.[7] Isotherms of HCV2 in combination with 5 mol% bi-tail surfactants (bis-C_{12} to C_{18}) are shown in Figure 1, panel B. Area condensation occurred with the addition of (DDDAB) (isotherm 2) and DHDAB (isotherm 4) and the vice-versa for ditetradecyldimethylammoniumbromide (DTDAB) (isotherm 3) and dioctadecyldimethylammoniumbromide (DODAB) (isotherm 5). For the isotherms 2 and 4, the limiting area was 0.34 and 0.44 $nm^2molecule^{-1}$ respectively indicating favourable area

condensation/contraction for these two mixed systems than the individual pure components. Favourable hydrophobic interaction resulted area condensation.

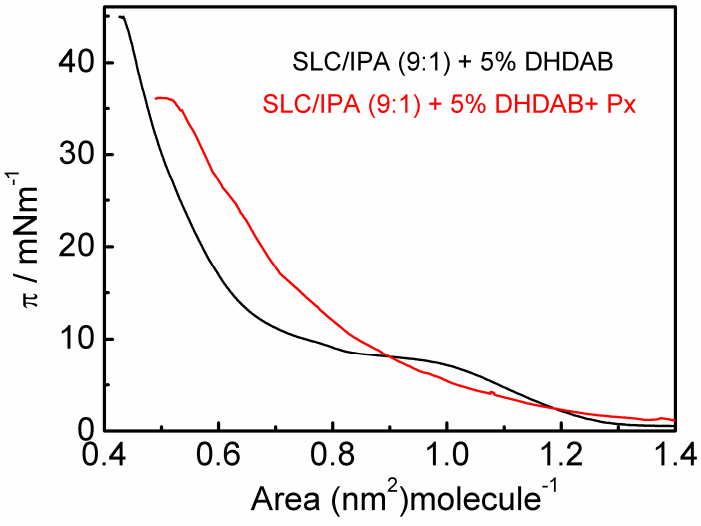

Figure 2. π – A isotherm of mixed monolayer with (Red) and without (Black) Px at 25 ºC

It is known that for acyl chains the constant segmental order parameter exists between C1 to C9. From C9 to C10 or higher, there occurs considerable disorder.[14] DDDAB and DHDAB have the major number of carbon atoms in the ordered state, which facilitate hydrophobic interaction leading to area condensation. Bi-tail cationic surfactants facilitate the dissociation of IPA[7] as the loss of $HTMA^+$ from the monolayer into the bulk. [35] This eventually leads to the area condensation. The expanded monolayer was the outcome for the systems with DODAB. Presence of C9 - C18 carbon atoms in the acyl chain brings relatively more disordered state in the monolayer, and hence produces expanded monolayer. Px significantly alters the π – A isotherms as revealed from Figure 2. Px being negatively charged (in PBS pH 7.4) occupies the bilayer region or better to say Px intercalated itself between the amphiphiles causing the expansion of the isotherm.

Variation in the compressibility modulus (C_s^{-1}), that indicates monolayer elasticity, with surface pressure for the same systems described in panel B are shown in panel D, Figure 1.

Maximum C_s^{-1} values were 113 and 117 mNm^{-1} for HCV2 and HCV2 + 5 mol% DHDAB respectively. Lower C_s^{-1} values for the other three bi-tailed surfactants were noticed when 10 % IPA was used. Fluidization[14,36] of the mixed monolayer (lower C_s^{-1} value) indicates relatively less miscibility or unfavourable packing among the components. As both the hydrocarbon chains of SLC and one chain of the IPA have sixteen carbon atoms, together they exhibit favourable hydrophobic interaction with DHDAB. However lower C_s^{-1} values for all the DXDABs, except DHDAB, were due to the disordered state of the mixed lipidic chains that promote the fluidization.

A_{ex}/A_{id} *vs.* surface pressure (π) plots (panel C, Figure 1) indicate the extent of miscibility among the amphiphiles. Ideal area of the mixed system can be calculated as:

$$A_{id} = x_1A_1 + x_2A_2 \quad (2)$$

where, A_{id} is the theoretically calculated average area per molecule. A and x represent the area per molecule and mole fraction of the components respectively. Suffices 1 and 2 represent component 1 (SLC/IPA, M/M + 30 mol% cholesterol) and component 2 (bi-tailed cationic surfactant + 30 mol% cholesterol) respectively. Deviation from the ideality (A_{id}) was calculated from the excess area (A_{ex}) as:

$$A_{ex} = A_{12} - A_{id} \quad (3)$$

where, A_{12} is the experimentally obtained area per molecule for the mixed monolayer. Positive deviation indicates repulsive interaction and vice versa. HCV1 and HCV3 with 10 mol% DHDAB execute positive A_{ex}/A_{id}. Electrostatic repulsion between the head groups result in the fluidization of the monolayer. However, HCV2 with 5 and 10 mol% DHDAB exhibited attractive interaction.

To prepare stable vesicle dispersion, one need to further consider the mixed monolayer studies and subsequent evaluation of different thermodynamic parameters of the interfacial mixing processes, viz., excess Gibbs free energy (ΔG_{ex}^{0}) that measures the extent of interaction among the components in mixed system with reference to the interaction of the components before mixing. The values of ΔG_{ex}^{0} can be determined by using the following calculation:

$$\Delta G_{ex}^{0} = \int_{0}^{\pi} (A_{12} - A_{id})\, d\pi \qquad (4)$$

Negative ΔG_{ex}^{0} indicates spontaniety of the mixing processes and vice versa. The hydrocarbon chain mixing between DxDABs with HCV2 are shown in Figure 3. In the present study, the chain mixing between component 1 (SLC/IPA/cholesterol) and component 2 (bi-tail cationic surfactants) was considered. Spontaneity of chain mixing in the absence (panel A) and presence of piroxicam (panel B) was also recorded. Magnitude of the negative free energy change was more profound for DDDAB and DHDAB, indicating better mixing of hydrocarbon chains in presence and absence of Px. However, DTDAB and DODAB exhibit less mixing between chains. Hence from monolayer study it was possible to assess the optimum stable vesicular system for carrying out the further studies. Minimum chain miscibility for DTDAB was noticed, like the other experiments, which indicates that DTDAB is not a suitable agent for the preparation of vesicles. Negligible ΔG_{ex}^{0} values for DDDAB and DHDAB in absence and presence of Px were recorded. An appreciable change in ΔG_{ex}^{0} was observed in the mixed monolayer having the drug and DODAB. The hydrophobic interaction between component 1 and DODAB in presence of Px become the predominant factor, that leads to the negative free energy change. In all the cases the maximum spontaneity was observed in 30 mNm^{-1}, which is also the pressure of the biological cell membrane. Being in the palisade layer, Px can induce expansion of the polar head groups.

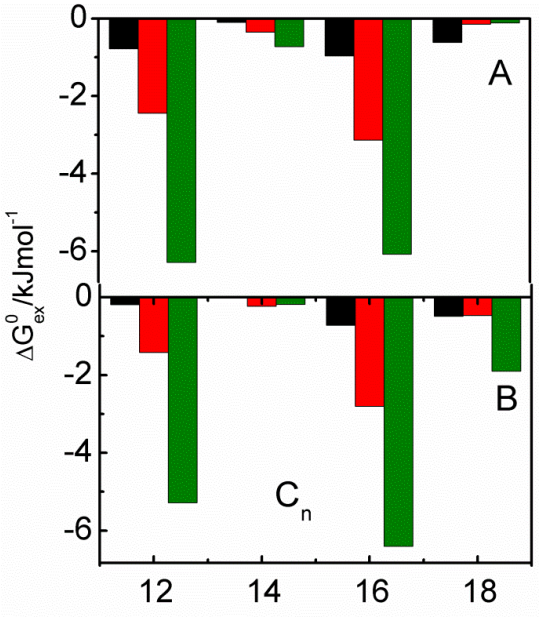

Figure 3. Gibbs excess free energy (ΔG^0_{ex}) for the interfacial mixing of lipids. Systems (HCV2) with the chain length of bi-tail cationic surfactant (5 mol%) at different surface pressures. Surface pressure (mN/m): 10 (black), 20 (red) and 30 (green). Panel A: mixed monolayer without Px. Panel B: mixed monolayer with Px.

3.2. Dynamic Light Scattering (DLS) Studies

Figure 4 describes the dependence of hydrodynamic diameter (d_h), zeta potential (Z. P.) and polydispersity index (PDI) of the vesicles on the composition and hydrocarbon chain length of the double tailed cationic surfactant. Vesicle size did not vary appreciably with the bi-tail cationic surfactant chain length for the system HCV1 and HCV2. Impacts of bi-tail cationic surfactants were insignificant upto 10 mol% IPA. However, size abruptly increased for HCV3. Excepting a few, sizes of the vesicles were in the range of 250 to 300 nm. 30% IPA in combination with SLC brings more disorder in bilayer as compared to 10% IPA. Hence added bi-tail cationic surfactant along with 10% IPA produced smaller vesicles than the 30% IPA.

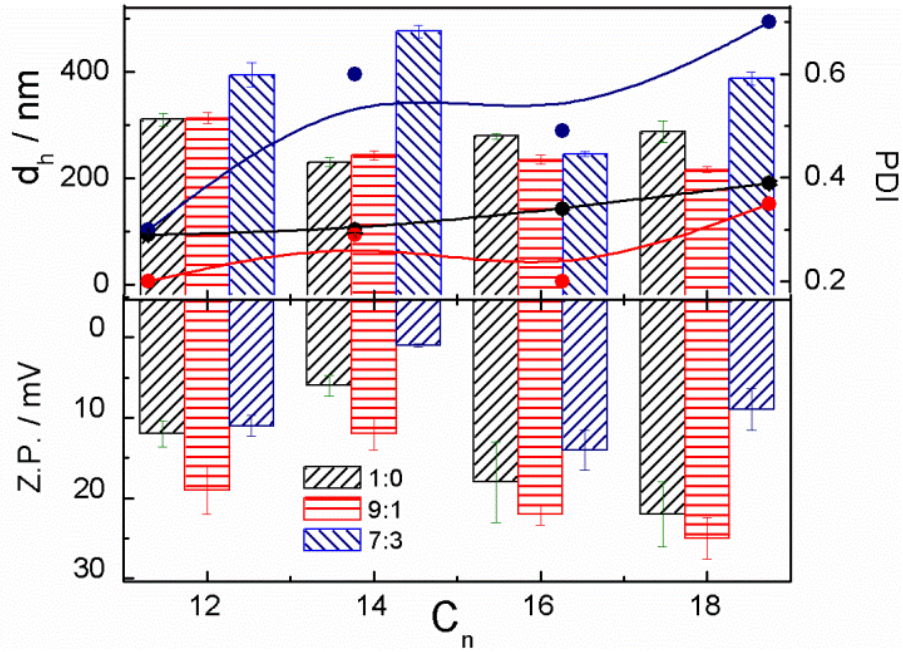

Figure 4. Variation of hydrodynamic size (d_h), zeta potential (Z. P.) and PDI of SLC/IPA hybrid vesicles with the bi tail surfactant chain length at 25 ºC. d_h and PDI were indicated by bars and solid lines respectively. SLC/IPA mole ratios are indicated in the figure and the bi-tail cationic surfactants amount was fixed to 5 mol%.

Z. P. holds the identity of the vesicles that prevents coagulation. Z. P. values were in the range of 10 to 28 mV for obvious reason. Z. P. increased with increasing hydrocarbon chain length. It is expected that with increasing chain length, inductive effect (+I effect) of the surfactant increases, which favours the charge separation between the counter ions around the polar surface leading to increased Z. P. Except 30% IPA, other vesicles were fairly monodispersed (PDI values less than 0.4). Px, being small and rigid, preferentially occupies the bilayer which causes enhanced d_h value. Although DLS studies provide the information concerning state of the vesicle with and without Px, but not adequate to come across the insight of bilayer which warrants further studies like electron microscopy.

3.3. Electron Microscopic Studies (TEM/ Freeze Fractured (FF)-TEM*)*

To figure out the size, morphology and the existence of the bilayer,[7,8,37] electron microscopic studies were performed in the form of normal TEM and freeze fractured-TEM measurements. Impact of Px could also be revealed from such studies. Representative TEM and FF-TEM microphotographs of HCV2 with 5 mol% DHDAB are shown in Figure 5, panel A_1 and B_1 respectively. Spherical morphology of the vesicle was confirmed from both the normal and FF-TEM studies. Additionally the formation of bilayer could also be established. Size of the vesicle was found to be comparable with DLS measurement.

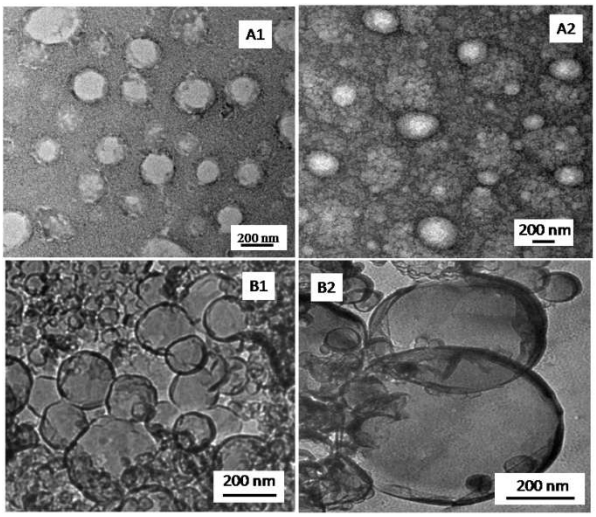

Figure 5. Conventional (A_1 and A_2) and freeze fractured (B_1 and B_2) transmission electron micrographs of HCV2/DHDAB in the absence (A1, B1) and presence (A2, B2) of piroxicam.

Influence of Px on the size as well as the morphology were revealed from the TEM and FF-TEM images shown in Figure 5 (panel A_2 and B_2). Heterogeneity in the vesicle sizes were due to the accumulation of Px in the bilayer. Thus spherically shaped vesicles offer Px an safe location in the bilayer zone.

3.4. Scattering (SANS and SAXS) Studies

3.4.1. Small Angle Neutron Scattering (SANS)

Bilayer thickness is an important parameter of the vesicles as it modulates the cellular activities by randomly altering its composition. The typical bilayer thickness under appropriate physiological condition is reported to lie in the range of 4 – 6 nm.[38-40] However, additives, like cholesterol and other amphiphile can change its thickness that eventually alter its biological function. Neutron (SANS) scattering has become one of the powerful prevalent techniques to measure the bilayer thickness.[39] Figure 6 shows some representative SANS plot, where the scattering intensity I(Q) of vesicles are plotted against scattering vector Q = 4 π Sinθ/λ; where 2θ is the scattering angle and λ is the wavelength of the neutrons. I(Q) values decreased with increasing Q that indicates lowering of scattering with the increase of scattering angle.

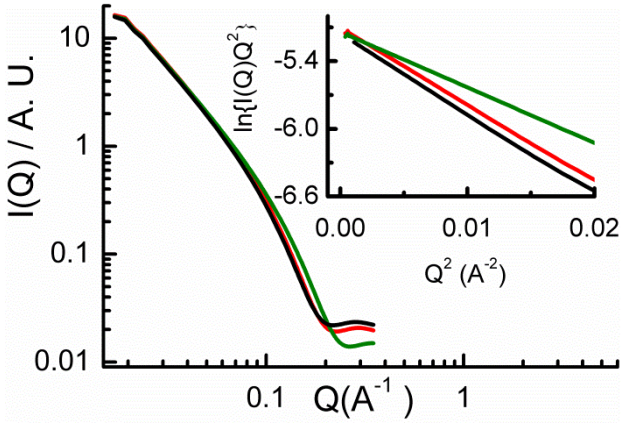

Figure 6. Variation of SANS intensity with scattering vector Q for HCV1 (black), HCV2/DHDAB (red) and HCV2/DHDAB/Px (green) at 25 ºC. Inset: Kratky plot for the same set of systems. Q value set between the region of 0.0013 Å^{-2} ≤ Q^2≤ 0.02 Å^{-2}.

3.4.2. Kratky Plot Analysis

Kratky plot is one of the important and simplest ways to get the bilayer thickness (Figure 6, inset).[41] Scattering intensity of vesicles within a small range of scattering vector can be written as:

$$I(Q) = I(0)\, Q^{-2} \exp(-Q^2 R_g^2) \quad (5)$$

where, I (0) is a constant and R_g is the radius of gyration. R_g can be calculated from the Kratky plot represented in Figure 5 B (inset). From the R_g value, one can easily evaluate the bilayer thickness parameter d_g as:

$$d_g^2 = 12\, R_g^2 \quad (6)$$

A careful assessment leads to select the region of 0.0013 $Å^{-2} \leq Q^2 \leq 0.02$ $Å^{-2}$ for fitting the experimental graphs. The driven Kratky plot from the experimental SANS data maintained the linear function and fitted well up to $Q^2 = 0.02$. At larger values of Q, deviation from linearity was observed (data not shown). The calculated values of R_g and d_g are summarized in Table 1 derived from equation 5.

Table 1. SANS data for the different cationic vesicles in the absence and presence of Px at 25 ºC. DXDAB's concentration was set to 5 mol%.

Vesicles	**R_g / Å**	**d_g / Å**
HCV1	139.25	40.87
HCV2/DDDAB	148.72	42.24
HCV2/DHDAB	156.49	43.33
HCV2/DODAB	163.72	44.32
HCV2/DHDAB/Px	158.27	63.58

3.4.3. Small Angle X-ray Scattering (SAXS)

Amphiphile molecules get self assembled spontaneously to form micro structure of different shapes. Identification of such structures like bilayer lamellar phase could be identified by SAXS studies.[40,42] SAXS data of cationic and Px loaded vesicles are graphically shown in Figure 7, where scattering intensities are plotted against the scattering vector Q.

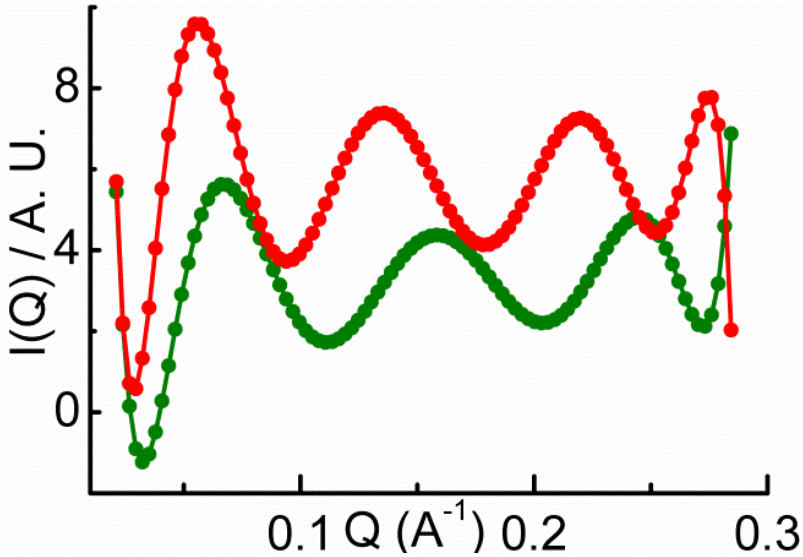

Figure 7. SAXS profiles of the cationic vesicles with and without Px. HCV2/DHDAB (red) and HCV2/DHDAB/Px (green) at 25 °C.

The periodic bilayer distance (d) can be evaluated form the equation, $d = 2\pi/Q$. The first order diffraction peak for HCV2/DHDAB and the same with Px appears at Q = 0.06 and 0.05 respectively, which correspond to d spacing of 125.7 and 104.7 Å respectively. Appearance of more than one Braggs diffraction peaks with equal spacing ($\Delta Q = 0.08$ Å^{-1}) indicate existence of vesicles.[25,42] Relative broadening of the diffraction maxima for Px loaded system (HCV2/DHDAB/Px) correspond to low electron density around the head group region due to the intercalation of the drug. Accumulation of Px in the palisade layer

causes the amphiphilic head groups to move apart from each other as already discussed in monolayer section.

3.5. Differential Scanning Calorimetry (DSC) Studies

Functionality and/or stability of vesicles are governed by the state of the lamellar phase. Exogenously added compounds can alter the activity and the state of the lamellar phase[43] which can be detected through DSC measurements. Comprehensive DSC studies on the thermotropic features of the vesicles bilayer with and without Px are expected to enable in understanding the impact of the drug on the membrane bilayer. Figure 8 describes the thermotropic features of SLC bilayer, hybrid bilayer, cationic and drug loaded cationic bilayers. Phase transition temperature (T_m) of SLC and hybrid vesicles appeared at -20 ºC,[44] that was completely abolished upon the addition of DXDABs'and Px. The disappearance of specific T_m indicates the heterogeneity of the bilayer region due to the insertion of surfactant and Px. Broadening of $\Delta T_{1/2}$ with less heat change was observed when DDDAB, DTDAB and DODAB were introduced into SLC/IPA, compared to DHDAB. The mixing of SLC/IPA with DHDAB produces relatively less compressible or more compact lamellar phase than the other three bi-tail surfactants and thus associated with lesser heat change.

Both the vesicles without and with Px exhibited exothermicity (Figure 8). Exothermic nature for HCV2/DHDAB was due to the hydration of the amphiphilic head groups around the vesicle surface. Px caused enhanced exothermicity reflecting higher extent of hydration. Results suggest the location of Px near the polar head group region (palisade layer) of the bilayer where it influences the extent of hydration by parting the polar head groups.

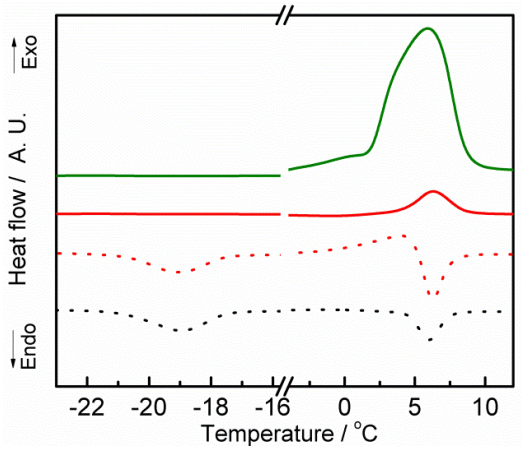

Figure 8. DSC thermograms of HCV1 (black dotted line), HCV2 (red dotted line), HCV2/DHDAB (red solid line) and HCV2/DHDAB/Px (green solid line). Scan rate: 2 ºC/min.

Other thermodynamic parameters such as changes in enthalpy (ΔH), heat capacity (ΔC_p) and half peak width ($\Delta T_{1/2}$) of SLC/IPA bilayer on addition of bi-tail cationic surfactants are shown in Figure 9. Acyl chains of DHDAB in SLC/IPA bilayer are in more order state relative to other bi-tailed cationic surfactants, the chain mismatch of DDDAB, DTDAB and DODAB with SLC/IPA causes the fluidization of the bilayer.[17]

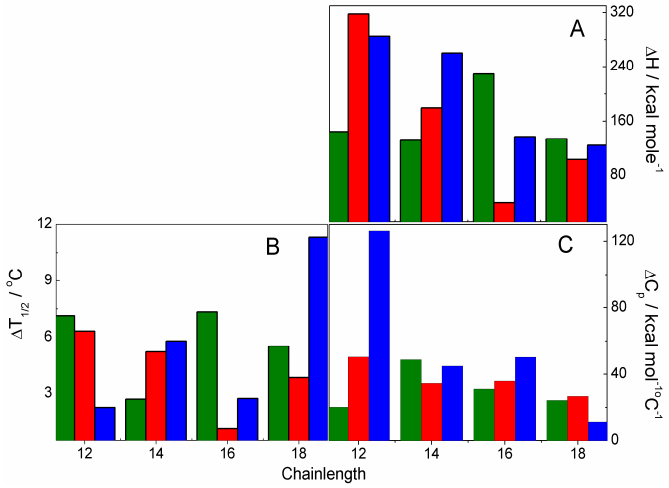

Figure 9: Variation of enthalpy (ΔH; panel A); half peak width ($\Delta T_{1/2}$, Panel B) and heat capacity (ΔC_P, Panel C) with bi-tail surfactant chainlength (bis-C_{12} to bis-C_{18}). Vesicle composition: SLC/IPA (1:0, Green); SLC/IPA (9:1, Red) and SLC/IPA (7:3, blue).

3.6. FTIR Studies

Phospholipids having different functional groups with different stretching frequencies act as the fingerprint in IR-zone.[45] Such groups are $-CH_2$, $-CH$, PO_4^{2-}, etc. FTIR spectra of SLC vesicles in combination with 5 mol% DHDAB and 5 mol% DHDAB + Px are shown in Figure 10. The antisymmetric and symmetric stretching frequencies indicate the hydrocarbon chains to move from the ordered to disordered states with the corresponding frequencies of 2918.5 and 2851.3 cm^{-1} respectively for the SLC vesicles.

The trans/gauche isomerisation needs to be considered as per as the $-CH_2$ stretching frequency is concerned. Increasing stretching frequency implies gauche conformation with more disordered state in the acyl chain.[46] Addition of DHDAB into the bilayer upshifted the antisymmetric and symmetric stretching frequency to 2925.3 and 2854.3 cm^{-1}, hence gauche conformation regain supremacy over the trans conformer. Similarly, increased stretching frequency (2927.7 cm^{-1}, antisymmetric) with relatively broad spectra was observed in case of added Px. Upshift in the $-CH_2$ stretching frequency with added DHDAB and Px make major population of the hydrocarbon chain in gauche form as depicted in the inset of Figure 10. Results suggest that the preferential position of Px was in the palisade layer of the bilayer region with disordered state.

The state of the membrane polarity could be known form the stretching frequency of phosphate group which is vital in the formation of aggregates and H-bonding. Lower is the frequency of the phosphate group higher is the extent of H-bonding with surface water molecule/hydration.[46] Zwitterionic head group of SLC is relatively less hydrated and for which a weak band appears at 1227 cm^{-1}. DHDAB downshifts the peak (1224 cm^{-1}) supporting the process of hydration as also reflected from DSC studies. Px downshifted the peak to lowest frequency (1220 cm^{-1}), reflecting greater hydration.

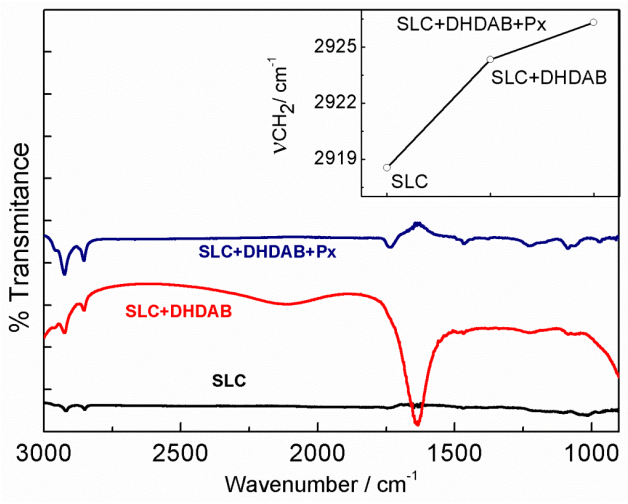

Figure 10. FTIR spectra of HCV1 (black), HCV2/ DHDAB (red) and HCV2/ DHDAB/Px (blue). Inset: Increment of $-CH_2$ stretching frequency with addition of DHDAB and Px on SLC bilayer.

Px is capable of modifying the orientation and the number of H-bonded water molecules in the palisade layer[14] and confirmed its position around the palisade layer. Px causes the formation of hole which facilitates the process of roughening the surface and causes higher extent of hydration as noticed in DSC. Thus the state of the acyl chain as well as the polar head group could be assessed when bi-tail surfactants and Px were added.

3.7. Atomic Force Microscopic (AFM) Studies

Atomic force microscopy is a direct imaging tool to visualise lipid bilayer with high resolution. It is well known that vesicles spontaneously transform into a solid supported bilayer (SSB),[47] when they are placed on freshly cleaved mica. The nanoscale properties of membrane and its ability to form solid supported bilayer (SSB) onto the mica substrate can be accessed from such studies. With an aim to understand the interaction of drug with model membrane, AFM studies were carried out as represented in Figure 11. Panel A and A1 elucidate the surface morphology and corresponding height analysis. Px occupying the palisade layer, reduces the compact packing of the lipid head groups.

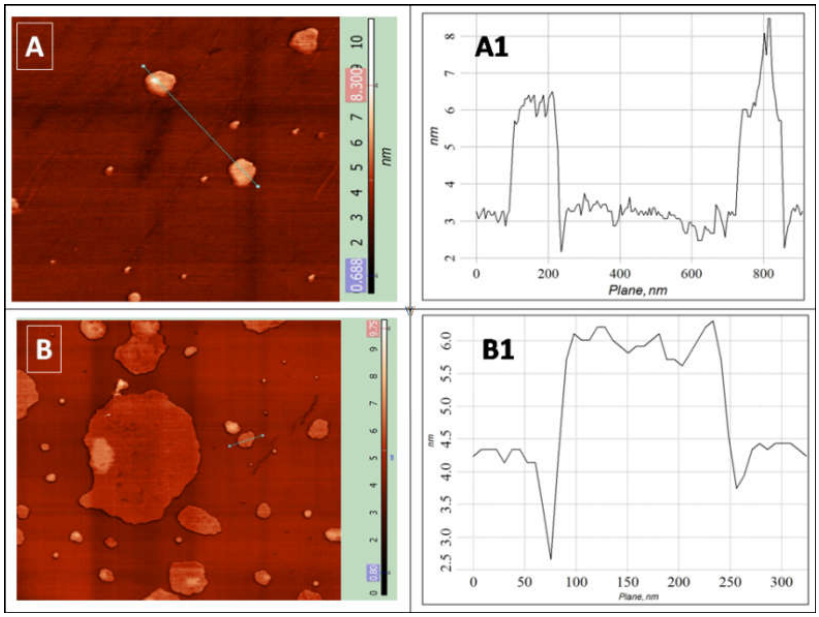

Figure 11. AFM images of solid supported bilayers. Images were recorded in liquid cell by tapping mode. Systems (A) HCV2/ DHDAB/Px (B) HCV2/DHDAB. Scan area: 2x2 μm^2. Panel A1 and B2: Height analyses of the bilayer surface of system A and B.

The height analysis of A1 shows few interesting facets. It helps to understand the rough bilayer surface due to the presence of number of amphiphiles along with unsaturated SLC. Additionally, increase in vertical height to the extent of few nanometers was also noticed. The height increment was due to the intercalation of Px between the lipidic components that pushes the polar head groups to stay away from each other and thereby resulting rough surfaces. Px could also result in the thickening of the bilayer, similarly observed in the SANS studies. Intercalation of Px between the lipid aggregates disrupts the lipid-lipid interaction and thus creates an opportunity to generate rough surface with hole formation on the surface of the bilayer domain.

AFM image of the SSB without Px has been shown in panel B Figure 11. Height analysis of the same shows the surface morphology was rather smooth than the SSB interdigited with

Px. Presence of bi-tail surfactant with similar head groups along with IPA and SLC associated with one unsaturation cause the surface slightly heterogeneous with the bilayer thickness in the range of 4 to 5 nm. The fluid domain of SSB was noticed as the consequence of the supremacy of gauche conformation of the acyl chain marking from FTIR measurement.

3.8. Entrapment Efficiency (EE)

Entrapment efficiency of different set of vesicles (HCV1, HCV2 and HCV3) to encapsulate the drug Px was tabulated in Table 2. The EE was found to be directly linked with amount of IPA and the chain length of bi-tail surfactants.

Table 2. % of EE of cationic vesicles with ascending chainlength and drug concentrations. Where HCV1, SLC/IPA (1:0) ; HCV2, SLC/IPA (9:1) and HCV3, SLC/IPA (7:3)

System	% of Entrapment Efficiency of Px / µM				
	10	**20**	**30**	**40**	**50**
HCV1 + DDDAB	36 ± 1.3	42 ± 0.9	45 ± 1.1	51 ± 1.6	52 ± 1.2
HCV1 + DTDAB	6 ± 2.2	9 ± 1.5	14 ± 1.6	17 ± 2.0	18 ± 1.9
HCV1 + DHDAB	41 ± 0.8	51 ± 1.1	59 ± 0.7	68 ± 1.4	70 ± 1.2
HCV1 + DODAB	42 ± 1.0	50 ± 1.2	58 ± 1.6	69 ± 0.9	70 ± 1.8
HCV2 + DDDAB	52 ± 0.9	59 ± 1.6	67 ± 1.2	75 ± 1.2	77 ± 1.9
HCV2 + DTDAB	7 ± 1.8	13 ± 2.3	16 ± 1.6	21 ± 1.8	23 ± 1.5
HCV2 + DHDAB	59 ± 0.5	68 ± 1.6	81 ± 1.5	92 ± 1.1	93 ± 0.6
HCV2 + DODAB	65 ± 1.2	76 ± 0.9	83 ± 0.8	96 ± 1.4	97 ± 1.8
HCV3 + DDDAB	42 ± 1.5	51 ± 1.9	60 ± 0.5	67 ± 1.6	68 ± 0.7
HCV3 + DTDAB	4 ± 1.6	10 ± 2.6	14 ± 2.6	19 ± 1.4	20 ± 1.8
HCV3 + DHDAB	52 ± 1.1	60 ± 1.4	71 ± 1.6	82 ± 1.4	82 ± 0.8
HCV3 + DODAB	60 ± 1.6	63 ± 1.1	75 ± 0.8	83 ± 0.4	85 ± 1.6

As shown in the table the EE values for the cationic vesicles comprised of DTDAB did not show any significant loading of Px. Throughout vesicle characterization, it was found that DTDAB comprising vesicles did not show any productive information as it was mostly unstable. However DDDAB, DHDAB and DODAB comprising vesicles show reasonable EE. Interestingly it was found that set of vesicles mixed with DHDAB and DODAB resulted

maximum and almost equal EE. Free energy calculation for the chain mixing derived from monolayer study suggests that systems with DHDAB and DODAB in combination with Px produced spontaneous mixing. Both DHDAB and DODAB associated with longer chainlength expected to be in more disordered state creating enough space in the bilayer region to accumulate more drug as compared to DDDAB.

To achieve the maximum E. E., we varied the drug concentration and it was found that 40 μM was the optimum loading concentration. The systems were found to be saturated beyond this concentration as reflected from Table 2. Among all, HCV2 type vesicles results maximum EE other then HCV1 and HCV3. HCV2 accompanied with 10 mol% IPA have a significant role for providing hydrophobic interaction as reflected from monolayer studies. Relatively less EE for HCV1 and HCV3 could be analyzed as the absence of IPA in HCV1 produces less hydrophobic interaction to accumulate enough drugs; whereas HCV3 was being carried with 30 mole % IPA produces rigid bilayer.

3.9. In Vitro Drug Release Studies

An excellent drug delivery must have the ability to undergo sustained release. With an aim to understand the nature of drug release from the hybrid cationic vesicles, HCV2 with varying hydrocarbon chainlength was chosen to quantify the release of Px. HCV2 was chosen on the basis of its highest EE. Figure 12 represents the cumulative release of Px for 48 hr. The results indicated that the release of Px from the vesicles was composition dependent. As one can see from the Figure 12, apart from the native Px (Px in PBS), vesicles comprised of DTDAB involved almost complete drug release with in 5 hr. Whereas other three sets of vesicles mixed with HCV2 + DDDAB, HCV2 + DHDAB and HCV2 + DODAB put on a view of 82, 92 and 60% total drug release respectively in 48 hr. It took almost 3 hr for the

native Px to completely release from PBS, indicating the superiority of hybrid cationic vesicles for the sustained release.

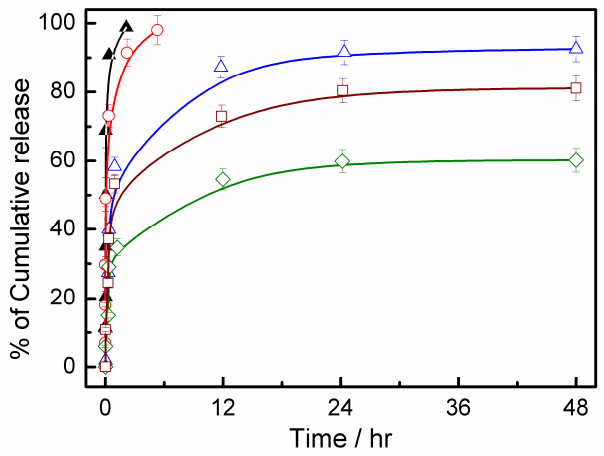

Figure 12. In Vitro release profile of Px from PBS (▲) and from SLC/IPA (9:1, M/M, HCV2) with varying hydrocarbon chainlength. DDDAB (□), DTDAB (○), DHDAB (Δ) and DODAB (◊). All the experiment was performed in PBS and repeated three times. Temperature: 25 ºC

The pattern of drug release could be classified into two steps. The first one was the burst release that happened within 1 hr followed by a sustained release. Vesicles having DTDAB produces maximum burst release (60%) as compared to other three sets of vesicle. The extent of burst release for HCV2 + DDDAB, HCV2 + DHDAB and HCV2 + DODAB were 31, 33 and 24% respectively, then followed a sustain release. The rapid release of Px from HCV2 + DTDAB was due to the instability of the vesicles as well as poor EE. From the results of EE it was found that HCV2 + DHDAB and HCV2 + DODAB have similar EE. However HCV2 + DODAB involve relatively slow release compared to the vesicles having DHDAB and DDDAB. The slow release of Px was due to the favourable hydrophobic interaction that enhanced upon the encapsulation of Px. Which further confirm free energy

calculation. But Px resides in the membrane bilayer of HCV2 + DHDAB and HCV2 + DDDAB creating enough disorder to swipe out the drug.

3.10. *In Vitro* Cytotoxicity Studies

3.10.1. On Human blood cell lymphocyte (PBMC) and Human Neuroblastoma cell line (SH-SY 5Y)

Biocompatibility of the hybrid vesicles without or with Px is one of the primary criteria once the drug delivery issue of the vesicles is concerned. RBC is one of the popular membranous systems to check the biocompatibility of drug delivery systems. However, before undertaking the above two cytotoxicity experiments, hemolysis studies were performed. Interaction between RBC and vesicles without or with the drug (positive and negative control) is depicted in Figure 13 as measured through UV-VIS absorption spectra. Hemolysis for both the systems was found to be ~ 2%. Systems having <5% hemolysis are regarded as hemocompatable and hence the studied combinations can be considered as non-toxic to human physiology[32]

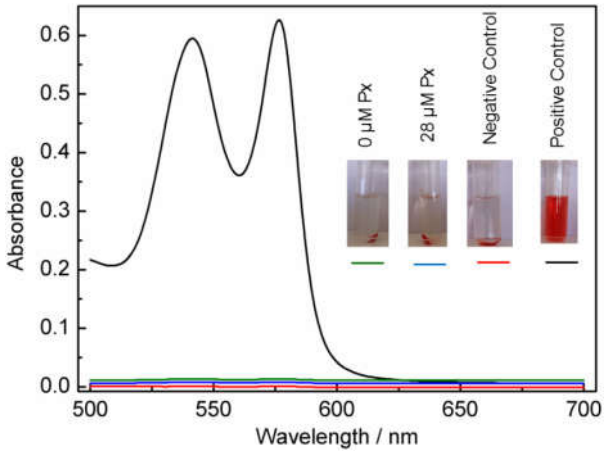

Figure 13. UV-VIS spectra of vesicles with and without Px with respect to the controls. Absorbance measured at 541 nm.

In-vitro cytotoxicity of HCV2 vesicles loaded with Px was assessed on normal human blood cell lymphocytes shown in Figure 14. Compared to the control (PBS), both the blank

and Px loaded vesicles were non-toxic towards normal human blood cell lymphocytes. Same set of formulations were taken to study the impact of Px on human Neuroblastoma cell line (SH-SY 5Y), via MTT analysis[48].

Formulations were non-toxic to normal human blood cell lymphocytes; however when the same set of samples were administered in the SH-SY 5Y cell line (cancerous cell), Px encapsulated vesicles showed substantial cytotoxicity (Figure 15). Px within the experimental concentration range, in PBS, did not show significant cytotoxicity compared to its encapsulated state.

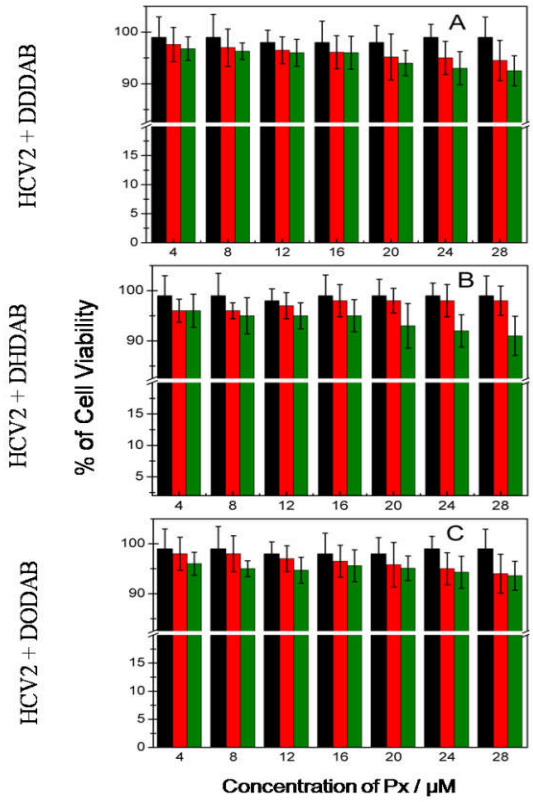

Figure 14. *In-vitro* cytotoxicity studies of vesicles with and without Piroxicam on normal human blood cell lymphocytes. PBS, control (black); HCV2/DxDAB (red) and V2/DxDAB/Px, (green). The mean standard deviations are indicated in the bar.

The activity was studied for 48 h and Px encapsulated HCV2 with varying chainlength show much smaller IC_{50} values (15.65, 21.74 and 25.32 for HCV2/DDDAB/Px, HCV2/DHDAB/Px and HCV2/DODAB) than the values of drug in PBS alone (IC_{50} = 534 μM). Vesicles without Px were substantially nontoxic as reflected from Figure 15. It reveals that the cytotoxicity nature of the drug (with respect to the cancer cell line) gets enhanced when entrapped in the vesicles.

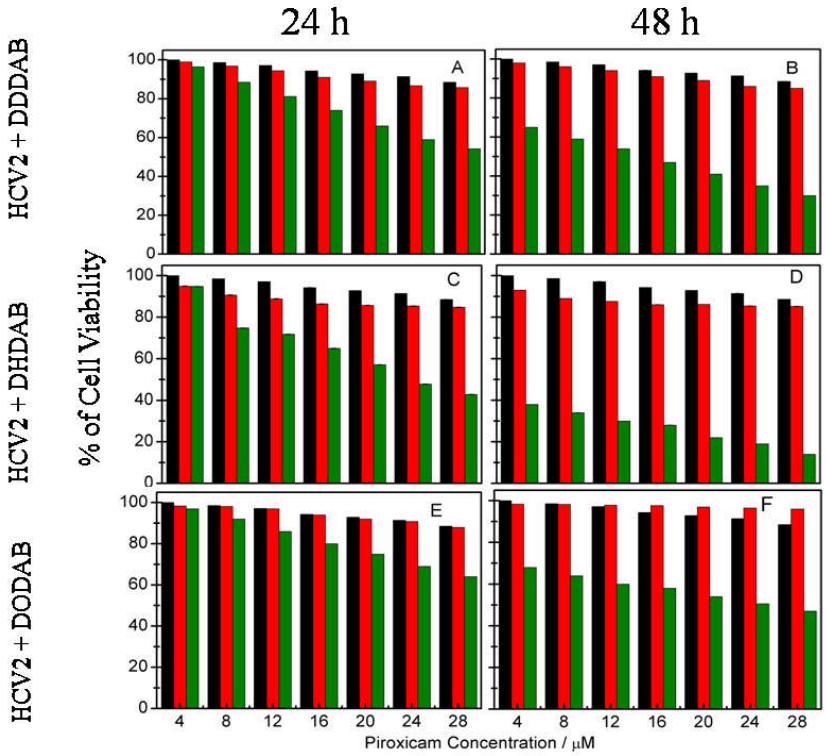

Figure 15. *In-vitro* cytotoxicity studies of vesicles with and without Piroxicam at 24 and 48 h on human Neuroblastoma cell line (SH-SY 5Y). PBS, control (black); HCV2 + 5 mol% DxDAB (red) and HCV2 + 5 mol% DxDAB + Px, (green). The mean standard deviations are indicated in the bar.

The cell line was treated with varied concentration of drug (5 to 28 μM) and HCV2/DHDAB/Px showed highest cytotoxicity. Within 24 h it achieved IC_{50} value 21.74 μM. However it took 48 h to get IC_{50} values 15.65 and 25.32 μM for the systems

HCV2/DDDAB/Px and HCV2/DODAB/Px. The time lag to achieve such values was due to the slow release of Px form the vesicles as compared to HCV2/DHDAB/Px. Such low concentration activity for Px was due to the controlled and sustained release of the entrapped drug from the vesicle.

4. Conclusion

Monolayer studies for the mixed systems (SLC/IPA/bi-tail cationic surfactant + 30 mol% cholesterol) put on a view of attractive interaction between SLC with dihexadecyldimethylammonium bromide (DHDAB) and didodecyldimethylammonium bromide (DDDAB) when 10 mol% IPA was present in the bilayer. DHDAB produce maximum spontaneity in chain mixing as calculated from free energy changes. Morphology of the vesicles with and without Px was revealed from the DLS and electron microscopic studies. Accumulation of the Px in the bilayer was noticed from FF-TEM measurement. Vesicles with positive zeta potential (Z. P.) were stable for substantial time period and maintained monodispersity, except a few combinations. Existence of unilamellar vesicles were confirmed form electron microscopy, SANS and SAXS studies. d-spacing between two adjacent lamellar phases were determined from SAXS. Both DSC and IR studies support the occupation of the palisade layer by small rigid Px molecules. Increased proportion of the gauch conformer of the acyl chains were noticed from FTIR studies. Px fluidizes the bilayer as studied by the AFM measurements. Bilayer thickness of the membrane was found to be around 5 nm as revealed from SANS studies. While the drug hosted vesicles were non-toxic to normal human blood cell lymphocyte (with less than 2% hemolysis), however, it was toxic over Human Neuroblastoma cell line (SH-SY 5Y). Because of the blood brain barrier, the drug avilibity in curing the Neuroblastoma cell line was insignificant. Vesicles of these kinds could be used as drug delivery, gene therapy or other therapeutic agents. Also the efficacy of

drug loaded vesicles towards the Neuroblastoma cell line and its impact on blood brain barrier could be considered as future perspective.

References

References are given in BIBLIOGRAPHY under Chapter II (pp. 154-157).

Ion Pair Amphiphile in preserving Bilayer Integrity: An account of PAMAM dendrimer induced Morphological adaption of Hybrid cationic vesicles.

Abstract. Universal nano-carriers with hyper branched polymeric molecules like dendrimers are serving in the field of therapeutics for number of years. However their path of interaction with the cell or plasma membrane yet to be fully understood. The complex and dynamic nature of the cell membrane hindered to fully understand the interaction. To recognize the nature of impact of dendrimer on the cell membrane, cell mimic hybrid cationic vesicles were composed using soylecithin (SLC), Ion Pair Amphiphile (IPA), dihexadecyldimethylammonium bromide (DHDAB) and their physicochemical behavior with the inclusion of negatively charged PAMAM succinamic acid dendrimers, generation 5 (G5-SA) were investigated. Adsorption of dendrimers on vesicle's surface and bilayer disruption was noticed and found to be strongly depending on bilayer composition and dendrimers concentration. Existence of dendrimers/lipid aggregates were confirmed by measuring hydrodynamic size via dynamic light scattering and TEM studies. Turbidity measurement of the mixture also confirms the presence of larger aggregates. Progressively decreased Zeta potential with increasing dendrimer concentration strongly recommends ionic interaction. Dendrimer induced vesicle disintegration kinetics illustrates the transformation of cationic bilayer to monolayer and there by exposed the role of IPA in maintaining the bilayer integrity by providing hydrophobic effect. AFM micrographs also corollary with morphological data as it confirms the adsorption as well hole formation on the bilayer. Changes in the phase transition of vesicles bilayer upon inclusion of verity of dendrimers concentration was

measure through differential scanning calorimeter which assists to recognize the point of dendrimers interaction on bilayer segment. It concludes low concentration dendrimer does not alter bilayer integrity. Anisotropy measurement confirms adsorption and bilayer disruption due to the inclusion of dendrimers.

1. Introduction

For medical therapeutics, different kinds of nanoparticles have been utilized as drug delivery vehicle. Vehicle like micro emulsion, solid lipid nanoparticle (SLN), vesicle, dendrimer *etc* have been utilizing as drug delivery medium for number of years. However the nature of interaction between nanoparticles and cell or plasma membrane is still a fundamental challenge as the mechanism of their interaction remains poorly understood. To explore such interaction one should judicially design nanoparticles with appropriate components having desire size and morphology. It should have low cytotoxicity, biodegradability and must have efficiency to transport the drug, gene or bio active molecules to the target tissue by surviving to the physiological environment. For decades vesicles comprising phospholipids in different forms have been utilized because of its flexible morphology and fascinating hydrophilic-lipophilic nature.[1-4] Similarities with biological cell membrane often help to predict its interaction with drug or other macromolecules such as dendrimers. However limitations like stability[5] has provoked researchers to develop a new class of compound that can avoid such limitations. Polyamidoamine (PAMAM) dendrimers have drawn considerable interest in the field of vaccine carriers, drug and gene delivery *etc*.[6-8] The details of dendrimers structure and its synthesis have widely been reported.[9-12] Dendrimers have a core and several units of branching which help to reside number of functional moieties on the surface. Molecular shape of dendrimer depends on the generation number. Lower generation (G4 and below)

dendrimers execute open, porous structure with ellipsoid geometry. While closed shell spherical morphology was confirmed for higher generation (G5 and above) dendrimers.[13] The architect of dendrimers is such that its generation number, units of branching and function of the surface groups can be tuned. Its versatile properties such as well defined molecular weight, spherical morphology, cage like architect, lipophilic "dendritic box" and active functional groups to the surface mark it as potential candidates for drug delivery. It is capable of encapsulating small drug molecules either in "dedritic box" or by bonding with the terminal groups. Efficiency of large number of drug molecules get abolished or suppressed as they do not reach to the target cell or may lose their original physicochemical properties in physiological conditions. Disease like viral infection, cancer requires effective drug carrying agents which efficiently can protect the labile drugs. *In vitro* drug release using cationic dendrimers are considered to be promising; because of its faster cellular uptake.[14,15] Wisely chosen dendrimers and subsequent studies on its interaction with cell mimetic systems need to be scrutinized thoroughly to explore the consequences induced by dendrimers on bilayer.

Well defined interior structure and its aqueous solubility provide opportunities to the researchers in studying dendrimers in details as an intracellular drug delivery system (DDS).[16-18] Reports on their efficacy to transfer DNA fragments,[19-21] immunioglobins[22] and anticancer drug[23,24] across the cell membrane are available in the literature. PAMAM dendrimers in the field of oral drug delivery are quite common as they are capable to pass over the intestinal barrier.[25-27] Interactions of dendrimers with Piroxicam[28], indomethacin[29] and ibuprofen[30] have also been reported. Dendrimers has also been explored in solubility improvement, catalysis[31,32], electronics[33] and many more. Hence interaction of dendrimers either with drug or with the cell membrane needs detail investigation to correlate their interaction.

Although substantial works have been carried out with dendrimers, specifically the cationic dendrimers. Cell membranes are known to be negatively charged and hence cationic dendrimers could act as an excellent carrier. PAMAM-succinamate dendrimers, 1,4-diaminobutane core, generation 5, (G5-SA) is an anionic dendrimers having succinamic acid groups on the surface. Bearing acidic group on the surface, it can survive in low pH environment. Literature studies reviled that no work have carried out so far to understand the impact between G5-SA dendrimer and hybrid cationic vesicles (HCV). The scope of this study to gain knowledge of their interaction and to get optimised aggregates of dendrimer/vesicles that can serve in the area of drug delivery.

The present work demonstrates the impact of G5-SA dendrimer on hybrid cationic vesicles (HCV). Three set of vesicles (HCV1, HCV2 and HCV3, composition has given in the methods section) were prepared using soylecithin (SLC), ion pair amphiphile (IPA) and dihexadecyldimethylammonium bromide (DHDAB) with 30 mol% cholesterol in aqueous medium. Inclusion of G5-SA dendrimer at different concentration (0.0001 – 2 μM) into the vesicular medium displayed different features of the membrane bilayer. Being oppositely charged, they interact with each other as confirmed from zeta potential measurement from DLS studies. Combined turbidity and hydrodynamic size (d_h) measurement provide the clue of dendrimer/vesicle aggregates that depend on the concentration of dendrimer. Effect of dendrimer concentration on the vesicles were scrutinized by TEM studies that confirmed dendrimer (at low concentration) adsorption on bilayer surface. Dendrimer induced hole formation and fluidization of bilayer was noticed through AFM studies. Vesicles disintegration kinetics as a function of dendrimers was also monitored. The role IPA in maintaining the bilayer integrity was also established through such studies. DSC studies confirmed both gel and liquid crystalline (LC) phase of bilayer were susceptible to dendrimer. Finally the perturbation of bilayer packing was recorded through steady state

fluorescence anisotropy measurement employing DPH and 7-hydroxy coumarin. Comprehensive studies account the diverse effect of dendrimer on bilayer and its subsequent morphological adaptation. Formation of dendrimer/vesicle aggregate encourages next set of work to study the cytotoxicity assay of such aggregate by incorporating different kind of drugs. Such aggregates known as dendriosome hence could be benefitted in drug delivery.

2. Materials and Methods

2.1. Materials

L-α-phosphatidylcholinee (soylecithin, SLC, from soybean) was purchased from EMD Chemicals, Germany, A. R. grade sodium dodecylsulfate (SDS) [$CH_3(CH_2)_{11}SO_4Na$], hexadecyltrimethylammonium bromide (HTMAB) [$C_{16}H_{33}N(CH_3)Br$], dihexadecyldimethylammonium bromide (DHDAB) {[$CH_3(CH_2)_{15}]_2N(CH_3)_2Br$}, (3β)-cholest-5-en-3-ol (cholesterol), PAMAM succinamate dendrimer, 1,4-diaminobutane core, Genaration 5,10 wt.% water solution (G5-SA), 7-hydroxycumarin (7-HC) and 1,6-diphenyl-1,3,5-hexatriene (DPH) were purchased Sigma-Aldrich Chemicals Pvt. Ltd. (USA). Double distilled water having specific conductance 2-4 μS (at 25 ^oC) was used for the preparation of solutions.

2.2. Methods

2.2.1. Preparation and Isolation of Ion Pair Amphiphile (IPA)

IPA, herein the hexadecyltrimethylammonium-dodecylsulfate ($HTMA^+$- DS^-) was synthesized by mixing stoichiometric amount of two oppositely charged aqueous surfactant solution as described in details in chapter 1. IPA was charectarised by means of ^{1}H-NMR, XRD and by FTIR[17].

2.2.2. Preparation of Vesicles

Hybrid cationic vesicles of different compositions were prepared by conventional thin film technique.[35,36] SLC: IPA (10:0, 9:1 and 7:3; M/M along with 30 mol% cholesterol) was chosen and 5 mol% DHDAB was added to prepare cationic vesicles. Quantitative amount of SLC, IPA, DHDAB and cholesterol were dissolved in 3:1 chloroform/methanol mixture in a round bottom flask and solvent was evaporated in a rotary evaporator. The flask was kept under vacuum overnight at room temperature to remove the remaining solvent. The thin film was then rehydrated for 1h in double distilled water at 70 ^{o}C, above the chain melting temperature of all the lipidic components. Finally, homogeneous dispersion was achieved through 4-5 cycles of freeze-thaw and sonication. Total concentration of lipidic component was set at 2 mM. It was extruded using 0.45 μm cellulose nitrate membrane filters (Whatman GmbH, Germany). Vesicles were diluted according to the type of experiment. For probe loaded vesicles, in the lipidic mixture 10 μM DPH and 7-HC separately in chloroform were added before the generation of the thin film. Here in three set of hybrid cationic vesicles SLC/IPA (1:0, M/M) + 5 mol% DHDAB, SLC/IPA (9:1, M/M) + 5 mol% DHDAB and SLC/IPA (7:3 M/M) + 5 mol% DHDAB are represented as HCV1, HCV2 and HCV3 respectively

2.2.3. Dynamic Light Scattering (DLS) Studies

Hydrodynamic diameter (d_h), zeta potential (Z. P.) and polydispersity index (PDI) of the vesicle/dendrimer aggregates were measured by Dynamic light scattering spectrometer (Zetasizer Nano ZS90 ZEN 3690, Malvern Instrument Ltd., U.K.). A He-Ne laser was used having emission wavelength 632.8 nm and all the data were recorded at a scattering angle of 90^{o}.

2.2.4. Turbidity Measurement

Turbidity of vesicle/dendrimer aggregates was measured through UV/VIS spectrophotometer (UVD-2950, Labomade Inc., USA), and the % transmittance of different sets of vesicle/dendrimer at 420 nm. (100-%T) was considered to be proportional to the turbidity of the medium.

2.2.5. Transmission Electron Microscopic Studies

A drop of dilute vesicular dispersion was placed on Formver carbon-coated 300 mesh copper grid and the excess liquid was removed from the edge of the grip and the sample was allowed to dry for 10 min before performing the experiment. Hitachi H-600 transmission electron microscope (Japan) was used to view the morphology with an acceleration voltage 120KV.

2.2.6 Atomic Force Microscopic (AFM) Studies

Atomic Force Microscopy (AFM) was executed in taping mode to get insight of the bilayer surface. Once the sample was placed, was washed with NaCl solution and finally placed in a liquid cell in Nanoscope III MM-AFM. Vesicular dispersion with dendrimer was sonicated for ~ 7 min. at 37 ^{o}C. The mica plate was placed into the cell and covered by 20 μL dispersions. After 50 min of the waiting about 1000 μL of distilled water was added into the cell and the AFM experiment was started. Samples were then transferred to a under ambient condition. Surface hardness and topography of the dendrimers induced membrane was studied by adopting taping mode.

2.2.7. Vesicles Disintegration Kinetics Measurement

The process of disintegration and subsequent formation of the adsorbed monolayer at the water-air interface was monitored by using Langmuir surface balance set up with a multiwell trough (micro trough X, Kibron, Finland). Langmuir adsorption type isotherms

were [Surface pressure (π) vs. time (t)] obtained by carefully adding 500 µL of the vesicle/dendrimer mixture in the trough. Plexiglass box was used to cover the stage that prevented the entry of dust particles. All the π – t isotherms were recorded at a subphase temperature of 25 ± 1 ^{o}C. To ensure reliable result, each set of experiment was performed thrice.

2.2.8. Differential Scanning Calorimetry (DSC) Studies

A Mettler Toledo differential scanning calorimeter (DSC 1, STARe system, Switzerland) was used where two identical pans were loaded with vesicles/dendrimer and water respectively. Samples were scanned with two different scan rates 5 ^{o}C and 2 ^{o}C per min with complete heating and cooling circle. The result so obtained was further processed with STAR^{e} software.

2.2.9. Steady State Fluorescence Anisotropy (r) Measurement

Fluorescence anisotropy values for the probes (DPH and 7-HC) embedded in the bilayer was obtained using the following equation:

$$r = \frac{I_{VV}-GI_{VH}}{I_{VV}+2GI_{VH}} \quad (1)$$

where, I_{VV} and I_{VH} were the fluorescence intensities, the subscripts indicate the position of the excitation and emission polarizer. $G = \frac{I_{HV}}{I_{HH}}$ was the grating correction factors. Data were recorded with a bench-top spectrofluorimeter (Quantummaster-40, Photon Technology International Inc., NJ, USA) at room temperature where excitation and the emission wavelength were set at 351 and 421nm respectively for DPH whereas the same for 7- HC were set to 330 and 379 nm respectively.

3. Results and Discussions

3.1. Combined Dynamic Light Scattering (DLS) and Turbidity Measurement

Vesicle hydrodynamic size (d_h) is a vital parameter to consider its stability. Figure 1, panel A proposes the changes in d_h of vesicles upon the addition of varying concentrations of G5-SA dendrimer. For every set of vesicle, size started increasing at 0.01 μM G5-SA concentration that indicates the onset of adsorption of dendrimer to vesicle surface which passed through a maximum.

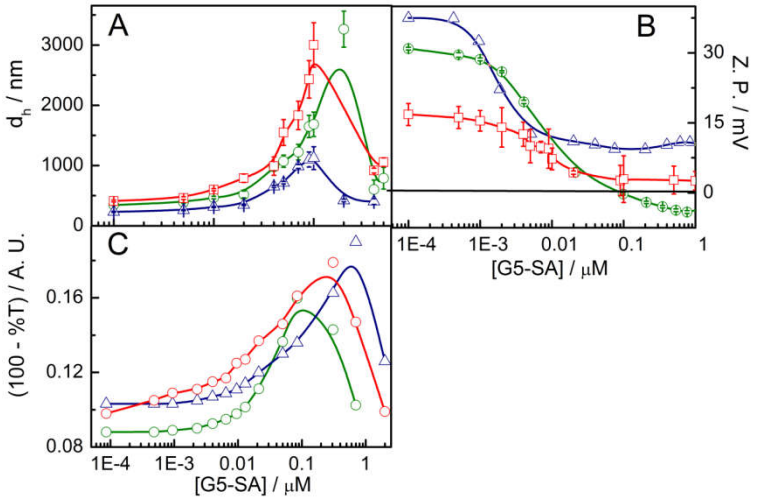

Figure 1. Variation of hydrodynamic size (d_h, panel A), zeta potential (Z. P., panel B) and turbidity (T, panel C) with G5-SA concentration at 25 ºC. Vesicles (HCV1, ○; HCV2, Δ and HCV3, □.) with 0.1 mM lipid/surfactant concentration were used.

Results suggest that the vesicle dispersions experienced the dispersion-flocculation-dispersion stages. G5-SA below 0.01 μM concentration acts as a dilute electrolyte solution (Lipid/Dendrimer ratio = 10^7:1) that does not induced enough interaction with the vesicles, leading to negligible size changes. Above this concentration increase in vesicle size with increasing G5-SA concentration indicates that onset of adsorption of dendrimer to the vesicle surface maybe through electrostatic interaction between cationic vesicles and negatively

charged dendrimer. Size enhancement was higher for HCV3 and HCV1 type vesicles compared to HCV2. HCV2 exhibits comparatively smaller size than other two, due to the presence of 10 mol% IPA that provides hydrophobic effect into the bilayer. In contrast absence of IPA in HCV1 and presence of excess 30 mol% IPA in HCV3 lead to increase in size. It was anticipated that IPA somehow plays a crucial role in maintaining bilayer morphology as it was the only variable component in the bilayer.

Charge in the vesicle surface, as monitored by zeta potential (Z. P.), provide information regarding the fate of vesicles in different condition. Figure 1 panel B demonstrate the process of charge neutralisation; where Z. P. decreased with increasing dendrimer concentration. Z. P. of HCV1, HCV2 and HCV3 in absence of G5-SA were +31, +37 and +16 mV respectively. Decrease in Z. P. primarily due to the electrostatic attraction between the oppositely charged vesicle and dendrimer. Interestingly, inversion of Z. P. from positive to negative was observed for system HCV1 being associated with SLC and DHDAB only, (without any IPA). While HCV2 (10% IPA) and HCV3 (30% IPA) having IPA as a bilayer constituting component maintained positive Z. P. Here in The neutral head group of IPA plays a decisive role. Absence of IPA in HCV1 allows dendrimer to get adsorbed on relatively more exposed polar surface compare to HCV2 and HCV3. For the later two formulations Z. P. get masked to some extent for G5-SA dendrimer due to neutral head group of IPA and hence retain their positive Z. P. These phenomena could be correlated with dispersion-flocculation-dispersion stages, where initially at low dendrimer concentration it interacts with positively charged vesicle surface as an ordinary electrolyte causes the system to maintain its dispersion behaviour. After a certain concentration is reached, electrostatic interaction becomes predominant leading to the formation of dendrimer/vesicle complex which subsequently flocculates and put on a view of bigger particles size.

Such complexes having bigger hydrodynamic size compared to normal vesicles are expected to scatter light to greater extent compared to the vesicle in absence of any dendrimers. To confirm the presence of aggregates and find out the concentration for the onset of interaction, turbidity measurement was carried out. As we know turbidity compute the point at which light scatter starts by the colloids (here in the dendrimer vesicle aggregate) upon the interaction with colloidal particles and depends on the difference of refractive index between the particles and medium. Figure 1 panel C represents the turbidity variation with dendrimer concentration for three different sets of vesicles with ascending dendrimer concentrations. Turbidity increases with increasing G5-SA concentrations passes through a maximum similar to the size measurement studies. Both DLS and turbidity measurement recommend the complex or aggregation formation between the dendrimer and vesicle scrutinized and discuss later.

3.2. Transmission Electron Microscopic Studies (TEM)

Aforementioned investigations suggest the formation of dendriosome, a dendrimers/vesicles complex at post maximal region. In order to understand the morphological changes in the vesicle structure induced by dendrimer, TEM analyses are considered to be worthwhile task. Dendrimer at very low, moderate and high concentration was studied on the vesicle through the electron microscopic analysis and the morphological changes are documented in Figure 2.

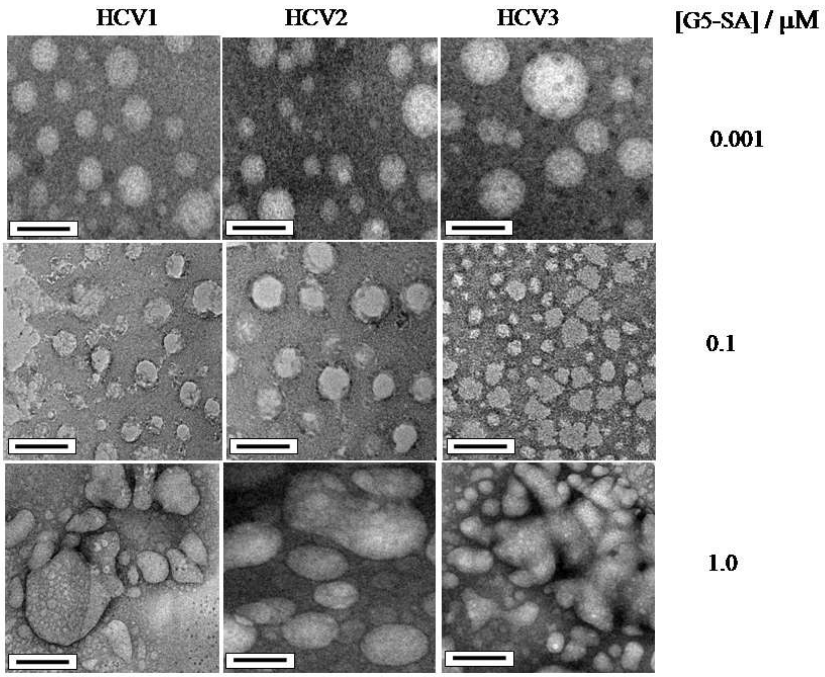

Figure 2. Morphological behaviours of vesicle formulations at different G5-SA dendrimer concentration. Scale bar: 500 nm.

Vesicle morphologies were not significantly perturbed upto 0.001 μM G5-SA added dendrimer. The middle panels of Figure 2 were the collection of micrographs of the vesicles with 0.1 μM added dendrimer. Dendrimer could significantly mark its presence being adsorbed on the vesicle surface. Dendrimer induced deformed morphology could also be viewed. The extent of morphological deformation was higher for HCV1 type vesicles in comparison to both HCV2 and HCV3 strongly recommend the superiority of IPA in maintaining the bilayer morphology. The bottom panels describe dendriosome formation due to the mixing of higher concentration (1 μM) dendrimer with vesicles. Formation of dendriosome was confirmed through the occurrence of spherical entities with substantial bigger size and/or formation of aggregated species whereby some irregular shaped species were formed. Analyses on size and Z. P. data at this concentration confirm the formation of such aggregated species; it is assumed that the bilayer encapsulated dendrimer complexes were formed. Additionally it was also found that extent of particle aggregation was higher for

HCV3 and was reasonable as it exerts relatively less Z. P. compared to other two vesicles. TEM studies, therefore was quite helpful to recognize the IPA dependent surface binding of dendrimers.

3.3. Atomic Force Microscopic (AFM) Studies

TEM study is not enough to understand the state of the vesicle surface upon dendrimer interaction because of its spherical morphology. Hence AFM study would be an ideal one where one could study the bilayer surface in molecular level as planer bilayer. Changes in the features of bilayer surface induced by dendrimer can also be studied. Its adsorption onto the bilayer surface through electrostatic interaction also assist the hydrophobic effect that tends to maximizes the impact between bilayer tail and hydrophobic core of dendrimers which leads to bilayer disruption.[37]

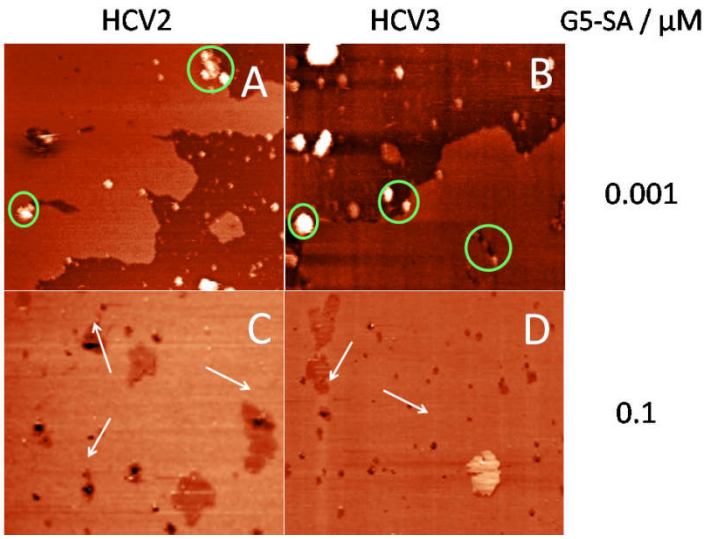

Figure 3. AFM micrographs of solid supported bilayers of HCV2 (10 mol% IPA) and HCV3 (30 mol% IPA) at 0.001(panel A and B) and 0.1 µM (panel C and D) G5-SA. Images were taken 2 h after the mixing.

A featureless AFM images were obtained for HCV1, HCV2 and HCV3 in the absence of dendrimer (images are not shown). However inclusion of 0.001 and 0.1 μM G5-SA dendrimer cause roughening the bilayer surface. Figure 3 represents micrographs of such rough surfaces caused by the dendrimers. Panel A and B display the state of the surfaces for HCV2 and HCV3 upon interaction with 0.001 μM dendrimers. Dendrimers interact with the bilayer edge where the defects were most. The accumulation of G5-SA on bilayer surface was indicated by green circle. Height analysis reviled the white patches into the green circle was about 1 – 2 nm tall and regarded as dendrimer aggregates. Electrostatic interaction most obviously plays predominant role over here.

On the other hand hydrophobic force plays crucial job when dendrimers concentration jumped up to 0.1 μM. Panel C and D represent such hydrophobic effect on the solid supported bilayer of HCV2 and HCV3. Bilayer disruption as a consequence of hole formation were resulted are indicated by the white arrows. This hole formation leads to the removal of lipidic entities causing a faster bilayer disintegration as described earlier. High dendrimer concentration facilitates the process of adsorption, as it maximizes hydrophobic effect between lipophilic dendrimer core and hydrocarbon of bilayer. These two combined force eventually lead bilayer disruption. In both cases phase and domain separation were not observed.

3.4. Vesicle Disruption and Subsequent Interfacial Adsorption Studies

It was evident form Z. P. measurement, vesicles/dendrimer interact electrostatically that predominantly occurs in the vesicle surface. This outcome was further designed to study dendrimers induced vesicle bilayer disintegration. Characteristics and formation of monolayer at the water-air interface from bilayer was extensively studied[38,39] It is known that, vesicles from the bulk subphase can transform to monolayer at the water-air interface through

the bilayer disruption. Hence using a Langmuir-Blodget surface balance, one can study such phenomena through the π–t measurement. Development of monolayer was confirmed at the water-air interface and its growth was monitored as a function of surface pressure (π) and time. Figure 4 represents the time dependent surface pressure changes, corollary of monolayer formation at the water-air interface.

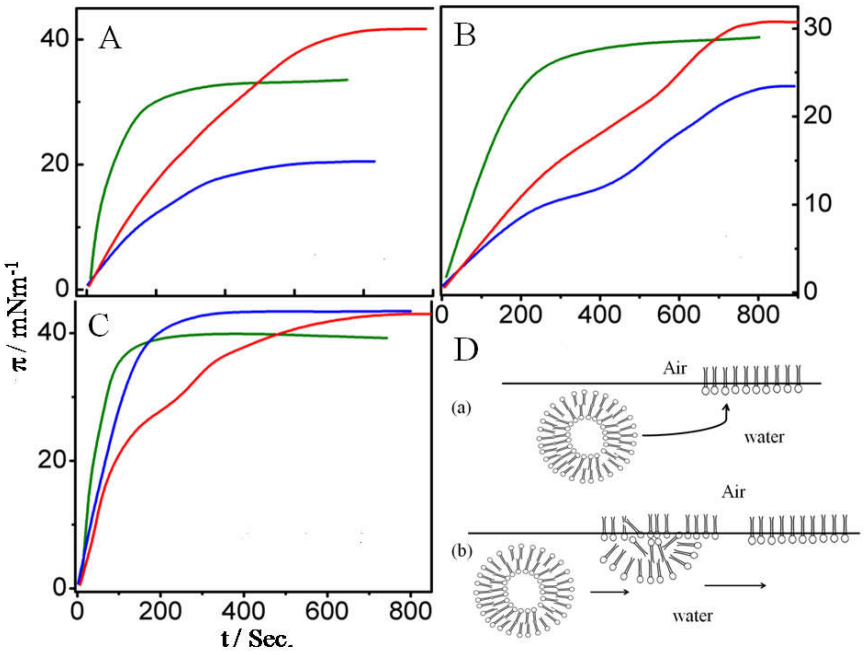

Figure 4: Formation of interracially adsorbed monolayer at water- air interface through the vesicle disintegration in the absence and presence of dendrimer at different concentration. Each panel describe changes in the value surface pressure (π) as a function of time. Dendrimer concentrations (in μM): Panel A, 0.0; Panel B, 0.001 and Panel C, 0.1. Green line; HCV1, Blue line; HCV2 and Red line; HCV3. Panel D describes two possible steps of adsorption of monolayer at the water-air interface from hybrid cationic vesicles.

Vesicles have a tendency to disintegrate where the aggregate constituting amphiphiles leave the bilayer region to some extent and preferred its orientation towards the water – air interface. Relinquish of amphiphiles from the bilayer causing its population increase onto the

water – air interface with the progress of time. Initially the surface pressure increases which eventually attains continuum as the interfacial film gets saturated.

Figure 4, panel A corresponds to the time dependent surface pressure change for vesicle HCV1 (green isotherm), HCV2 (blue isotherm) and HCV3 (red isotherm) in the aqueous medium. HCV1 having no IPA achieved equilibrium pressure 33 mN/m in 360 second. On the other hand HCV2 (10 mol% IPA) and HCV3 (30 mol% IPA) accomplished the equilibrium pressure 21 and 41 mN/m in 623 and 800 second respectively. Hence it could be concluded that the role of IPA was crucial as long as disintegration process are concerned. Limiting area per alkyl chain of IPA is reported to be 0.28 nm^2,[5] quite higher than the value of a typical saturated hydrocarbon chain (0.20 nm^2) as calculated by Li *et al*.[40] Results suggest that not only hydrocarbon region, but also relatively bulky neutralized head of IPA also played a vital role. In the absence of IPA, removal of SLC or DHDAB becomes easier for which high equilibrium pressure 33 mN/m could be achieved. On the other hand, HCV2 and HCV3 containing 10 and 30 mol% IPA exhibited slow release of the lipidic components onto the interface. It could be attributed as the lack of hydrophobic interaction as compared to IPA loaded formulations. IPA provides additional hydrophobic effect. Among all the set of formulations, HCV2 put on a view of least equilibrium pressure (21 mN/m) while vesicle HCV3 evidenced highest (41 mN/m) equilibrium pressure. To elucidate the issue, one should consider both the bulky neutral head group and hydrocarbon zone of IPA that played crucial roles. HCV2 with only 10 mole% IPA experiences more hydrophobic effect than the disturbance produced by the bulky head group which subsequently holds the bilayer more rigidly. However, the picture turns completely opposite when one consider vesicle HCV3 (30 mole% IPA). Presence of three times IPA displayed not only hydrophobic effect but also an additional steric effect produces by the head group of IPA which tries to create hole formation on the surface. This eventually leads to the disaggregation of some of the

amphiphiles of vesicle moiety very slowly and get adsorbed at the water-air interface that eventually causes an increase surface pressure. Therefore, it could be conclude that IPA brings additional hydrophobic interaction in the bilayer segment, ensuing slow and steady liberation of amphiphiles as noticed from equilibrium pressure.

Our goal was to understand the impact of dendrimer on vesicular disintegration and subsequent kinetics onto the water-air interface. Surface adsorption kinetics was studied at varied dendrimer concentration in combination with a fixed concentration of vesicles. Panel B and C represent the disintegration isotherm for the same three set of cationic vesicles in 0.001 and 0.1 μM dendrimers respectively. Z. P., hydrodynamic size and turbidity measurement as previously discussed implied to opt for 0.001 μM G5-SA dendrimer, where the stoichiometric ratio of lipid/dendrimers was 10^5:1. As reflected from Figure 3 panel B, vesicles mixed with 0.001 μM G5-SA, achieved low surface pressure compared to dendrimer free systems. HCV1, HCV2 and HCV3 achieved equilibrium pressure 28.3, 23 and 31 mN/m in 563, 824 and 821 second respectively. So we had two different consequences: (a) retarded interfacial adsorption and (b) delay in time to achieve the equilibrium pressure, due to the presence of 0.001 μM G5-SA dendrimer. Both the issues could be addressed by considering the surface charges of vesicles and dendrimers. Being oppositely charged dendrimers molecules tend to adsorb on the surface of the vesicles. It was also expected that major portion of the dendrimers would be around the surface of the vesicles and thereby reduce the process of disintegration which eventually reduces the monolayer formation at the water-air interface and endorse longer time to acquire equilibrium pressure.

The role of IPA was again fascinating here; 10 mol% IPA hold the vesicles (HCV2) identity here again. However the role of IPA head group becomes predominant for HCV3, which perturb the vesicles surface region leading to achieve 31 mN/m equilibrium pressures. During the formation of monolayer, appearance of a platue formation was noticed for the

isotherm of HCV2 and HCV3, which was completely absent for HCV1 (panel B). This conspicuous nature of the isotherm, apart from HCV1 must signify some role of IPA, which was the only parameter with varying proportion in the vesicles. Figure 4, panel D represent two alternative steps of formation of monolayer from the vesicles in bulk. Step (a) involved a direct formation of monolayer at the water-air interface whereas step (b) communicates a combination of two separate steps; first one was the formation of perturb monolayer (gaseous state) assisted with other lipidic aggregates which forms a part time monolayer island. Second step involves the adsorption of monolayer from such monolayer island until it gets saturated.

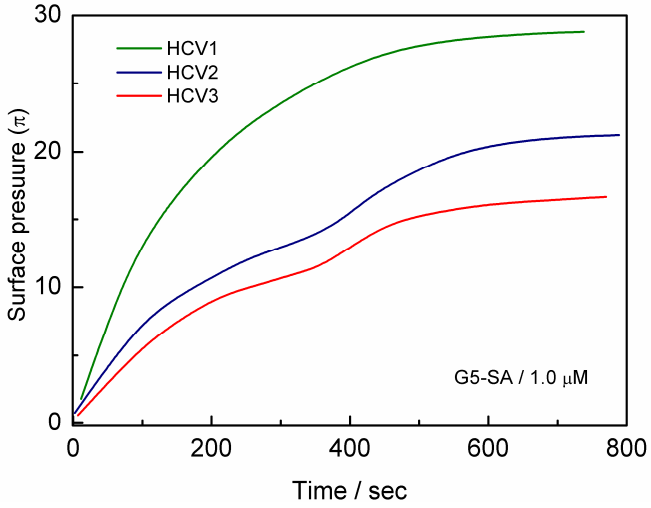

Figure 5. Changes in the surface pressure of dendrimer/vesicle complex as a function of time. Vesicles identity and dendrimer concentration were given in the figure.

Both HCV2 (10 mo% IPA) and HCV3 (30 mol% IPA) must follow the scheme (b) as confirmed form the platue. However vesicle HCV1 (0 mol% IPA) does not follow the same, rather direct formation of monolayer was noticed (scheme a). Thus it could be concluded that IPA must supports to hold the aggregates, which facilitates to form monolayer island first followed by the formation of saturated monolayer at the interface.

Figure 4, panel C illustrates adsorbed monolayer formation at 0.1 μM G5-SA concentration, where the lipid to dendrimer stoichiometric ratio was 10^3:1. The equilibrium pressure is relatively rapid, which implies quick membrane disruption induces by dendrimer as compared to the formulations in panel A and B. At higher dendrimers concentration, a slow disintegration was noticed as represented in Figure 5. It demonstrates strong affinity of G5-SA dendrimer to bind with the hybrid membranes at high concentration and lower surface pressure, which are the unique features cells enduring rapid miotic division, like cancer cell.[13]

3.4.1. Kinetics of Monolayer Formation

Formation of monolayer could be treated as the adsorption of lipidic molecules at the water-air interface. Therefore the rate kinetics of monolayer formation could help in understanding the route of interaction between dendrimers and vesicles. The rate constant (k) of vesicle disintegration and subsequent monolayer formation for the three vesicles were calculated and summarized in Figure 6. Figure 4 follow Langmuir like adsorption isotherms where the process of monolayer formation registered constancy after some time as reflected through the attainment of constant surface pressure. By employing the pseudo first order formalism one can calculate the rate constant of monolayer formation as:

$$\log \frac{\pi_f - \pi_i}{\pi_f - \pi_t} = \frac{kt}{2.303} \qquad (2)$$

where, t = time, k = rate constant, π_i = initial surface pressure, π_t = surface pressure at time t and π_f = final surface pressure of the adsorbed monolayer. Figure 5 represents three different set of vesicles and their rate kinetics for the formation of adsorbed monolayer. Linear graphs that pass through the origin imply first order rate kinetics for the formation of adsorbed monolayer.

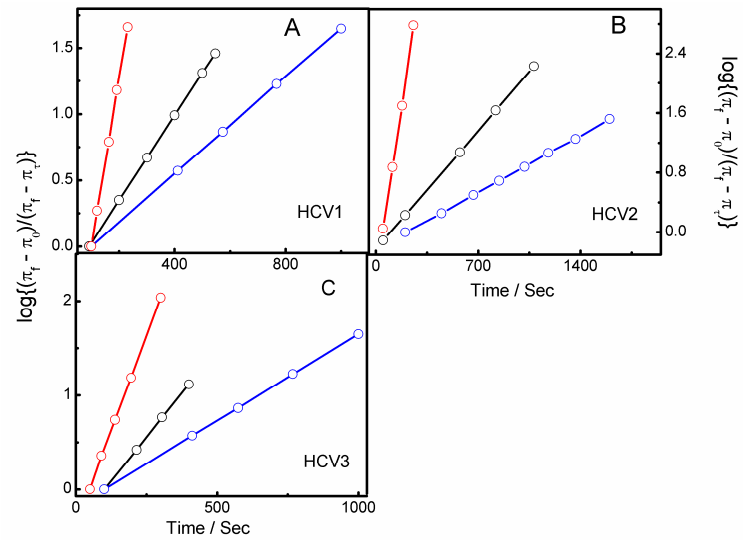

Figure 6. The rate of vesicle disintegration or monolayer formation kinetics for three different formulated cationic vesicles at different dendrimers concentrations. Dendrimers concentrations (μM): 0 (Black); 0.001 (Blue) and 0.1 (Red).

To understand more evidently, we have represented the rate constant in Figure 7 as function of IPA content in the bilayer and dendrimer concentration.

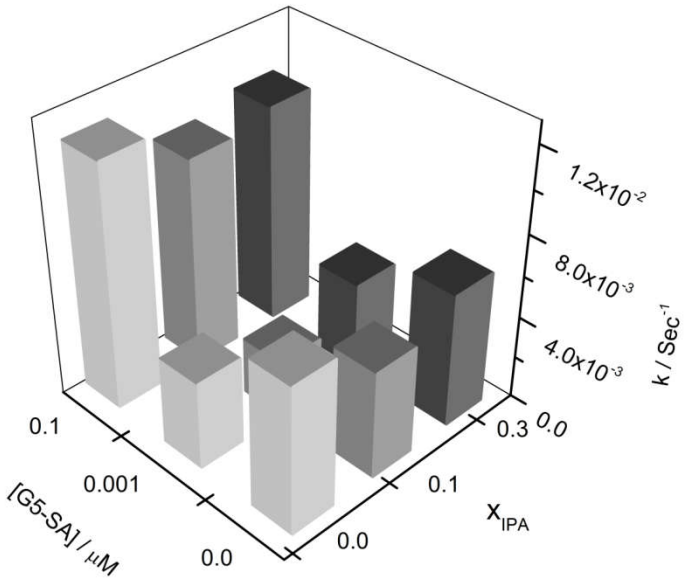

Figure 7. A comparative study of rate constant (k) for three different set of vesicles HCV1 (x_{IPA} = 0), HCV2 (x_{IPA} = 0.1) and HCV3 (x_{IPA} = 0.3) as a function of dendrimers concentrations.

Bar diagram indicates the values of k and was found to be specific with the amount of added dendrimer. For each set of formulations, values of k dropped down at 0.001 μM dendrimer concentration (as compared to dendrimers free systems). At higher concentration (0.1 μM G5-SA) it was increased by 63, 88 and 77% for HCV1, HCV2 and HCV3 respectively. Hence it would be stated that at this concentration, not only ionic interaction but hydrophobic interaction between dendrimer lipophilic branch and hydrocarbon zone also played a vital role. Combined ionic and hydrophobic interactions predominantly facilitate the process of bilayer disintegration. The values of k assist to understand a tendency of HCV2 vesicles to uphold the bilayer integrity. Threshold value to remove lipidic components, which sets disintegration kinetics, was higher for HCV2.

3.5. Differential Scanning Calorimetry (DSC) Studies

With a motive to assess the thermodynamics changes of the bilayer upon the inclusion of G5-SA dendrimer, DSC studies were carried out. It could lead us to specify the different bilayer phase and their susceptibility towards dendrimer. The role of DSC in measuring the bilayer phase transition or hydrocarbon chain melting (T_m) in presence of dendrimers were well documented.[41,42] It is known that bilayer phase transition course is highly specific and depend on the bilayer constituting entities. Exogenously added compounds or the state of the dispersion medium especially iconicity of the medium also plays crucially in the process of chain melting. With the calculation of changes in enthalpy (ΔH) and heat capacity (ΔC_p) one could understand the arrangement of hydrocarbon chains and subsequently the state of the vesicles bilayer due to the adsorption of dendrimer.

DSC thermograms of HCV2 and HCV3 vesicles mixed with 0.001 and 0.1 µM G5-SA was presented in Figure 8. SLC one of the major compounds of the bilayer contains one unsaturation in one of its hydrocarbon chain and hence renders chain melting at -20 ºC.

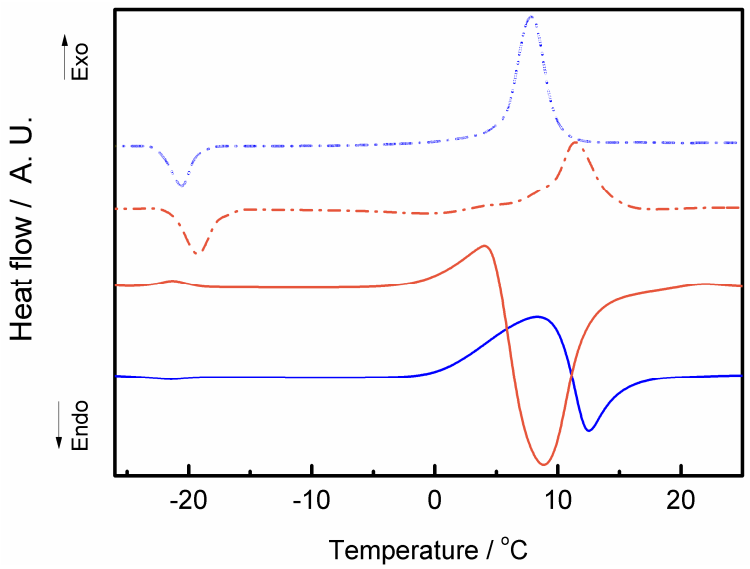

Figure 8. DSC thermograms of vesicles HCV2 (blue line), HCV3 (brown line) in presence of G5-SA Dendrimers. Dendrimer concentrations was set to 0.001 (dotted lines) and 0.1 µM (solid line). Scan rate: 2 ºC/min.

However inclusion of oppositely charged dendrimers and other substitutes (IPA, DHDAB and Cholesterol) in the bilayer may hamper the chain melting phenomena. Below chain melting, bilayer execute gel phase. Hence the temperature range was set to -30 to +30 ºC so that each formulation mast passes through gel to liquid crystalline (LC) phase. Hence the propensity of dendrimers towards gel and LC phase of the bilayer can be correlated more firmly. The thermograms could be viewed as two different segments: Segment (a) chain melting process occurred around -20 ºC and segment (b) stepwise development of exothermic event, soon converted to endothermic process at around 10 ºC.

Blue and brown dotted lines indicate the chain melting segment for HCV2 and HCV3 in presence of 0.001 μM G5-SA. The chain melting was found to be -20.23 and -19.16 ºC for HCV2 and HCV3 respectively. Although other surrogates in the bilayer slight alter the T_m, interestingly dendrimers in this case does not produce any disturbance in phase transition. Hence it could be concluded that at 0.001 μM G5-SA concentrations, the interaction manly occurred at the bilayer surface. Same set of formulations at segment b put on a view of exothermic process. Exothermic event generally displays some short of bonding or association. In our case once the temperature attains positive values, the formulations transform to liquid phase where the process of dendrimers adsorption gets facilitated. The stacking of dendrimers on vesicles surface thus create exothermic event.

The thermograms and hence the fate of the vesicle bilayer get completely changed once we add 0.1 μM G5-SA dendrimer on HCV2 (solid blue thermograms) and HCV3 (solid brown thermograms). Endothermic segment describe the chain melting process, which was abolished for HCV2. However HCV3 that has 30% IPA in the bilayer shows an exothermic event at – 21.22 ºC. That brings the possibilities of higher concentration dendrimer to interact with gel phase of the bilayer segment which was completely missing at 0.00 1μ m G5-Sa concentration. At this concentration, dendrimers could apply enough ionic interaction as well as hydrophobic force that may initially facilitate some of the dendrimers molecules to get inside of the bilayer hydrocarbon wall which was now in LC phase.[13,43] Due to this insertion, hydrophobic interaction between amphiphiles acyl chain and the core of the dendrimers becomes predominant. Segment b in this case tells a story bilayer disruption induced by oppositely charged dendrimers. The first exothermic event for the same set of formulations arises due to the adsorption of dendrimers due to ionic interaction that release heat energy. Soon after formations of endotherms indicate the deformation of ionic bonding exerts between vesicles and dendrimers, indicates a process of bilayer disruption. Thus it

could be stated that G5-SA dendrimer has a tendency to interact with both gel and LC phase depending on its concentration. Thermodynamics of bilayer phase behaviour was further determined and have presented in Table 1.

Table1. Changes in thermodynamic parameters of vesicles at different concentration of Dendrimer.

Formulations	**[Dendrimer] / µM**	**$\Delta T_{1/2}$**	**ΔH KCal/Mole**	**ΔC_p / kcal/mol/°C**
HCV2	0.001	2.22	22.56	7.51
HCV2	0.1	2.78	28.69	9.36
HCV3	0.001	-	-	-
HCV3	0.1	2.36	32.54	11.23

3.6. Fluorescence Anisotropy Measurement

Influences of dendrimer on bilayer accompanied some alteration in packing of palisade layer and hydrocarbon wall. Steady state fluorescence anisotropy measurement was carried out with an intention to get information on the issue of dendrimer induced bilayer packing using two suitable probes DPH and 7-HC. DPH being a lipophilic probe has an affinity to be inherent in non-polar hydrocarbon region, while solvatochromic probe 7-HC occupies the palisade region of the bilayer. For the vesicles HCV1, HCV2 and HCV3 Figure 9, panel A and panel B demonstrate the changes in anisotropy also known as micro viscosity of DPH and 7-HC respectively as function of G5-SA dendrimer concentration. Changes in the value of anisotropy for all set of formulations indicate the influences of dendrimer on both hydrophilic and hydrophobic part of bilayer. Panel A represent an increment of bilayer rigidity or packing with increasing G5-SA dendrimer. Enhanced packing of the bilayer hydrocarbon zone restricts the rotational motion of DPH could be the only scenario and

would only be possible if dendrimers were bonded with polar surface of the bilayer. It has also been identified that anisotropy of DPH increased with increasing IPA content in the hybrid bilayer. Hence the role of IPA in better packing by providing hydrophobic effect has also been confirmed. Sudden drops in the value of anisotropy around 0.1 μM G5-SA strongly recommend penetration of dendrimer into the bilayer hydrocarbon zone and there by loosening the packing, which was corollary with the results obtained from DSC measurement.

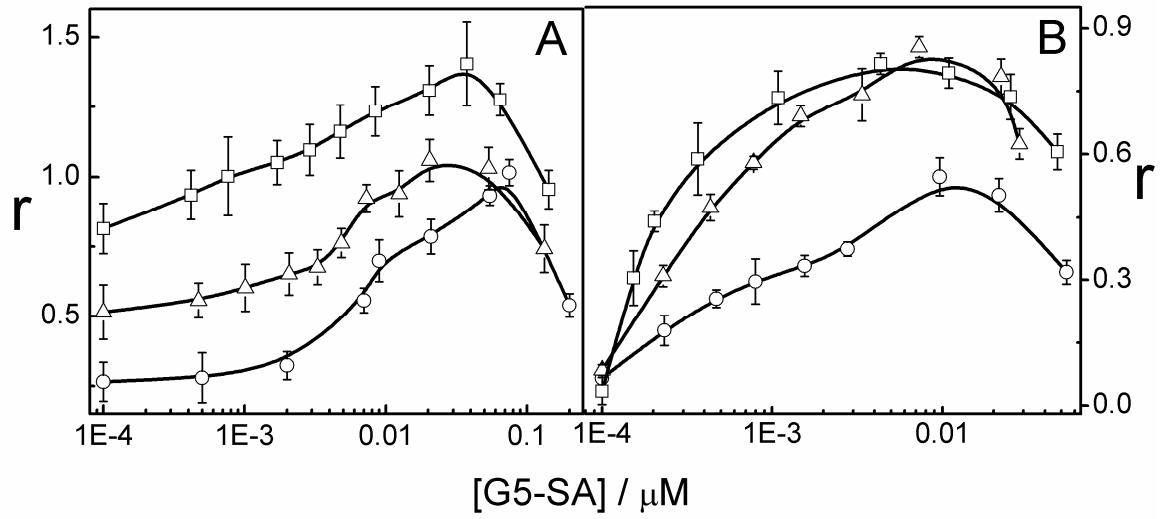

Figure 9. Variation of steady state fluorescence anisotropy (r) of DPH (panel A) and 7-HC (Panel B) as a function of dendrimer concentration at 25 ºC. HCV1 (○); HCV2 (Δ) and HCV3 (□).

To understand the packing of the interface of hydrophilic-hydrophobic part of the bilayer (palisade layer), solvatochromic probe 7-HC was embedded with hybrid bilayer and changes in the values of anisotropy was monitored as a function of dendrimer concentration (Figure 9, panel B). 7-HC being contained with oxygen moiety preferentially occupies the palisade region. Like DPH, similar trend of anisotropy increment was observed. It further confirms ionic interaction between oppositely charged vesicles and dendrimers that restrict

the motion of bilayer component and so does 7-HC. However a fall in the value of anisotropy beyond 0.01 μM G5-SA implies weak packing of palisade layer due to the dendrimer inclusion. Compare to HCV1, the anisotropy was found to be higher for HCV2 and HCV3 further confirms the novelty of IPA in maintaining bilayer rigidity or packing. Hence it would be stated that dendrimer can alter membrane fluidity depending on its concentration. At low concentration it sit on the surface of the bilayer via ionic bonding and drives the lipid hydrocarbon chain to get close to each other, consequently order in the bilayer increased. At higher concentration it penetrates into the vesicle bilayer zone and disrupts the packing of lipid acyl chain. Intercalation of dendrimer reduces the lateral packing and caused the lipid molecules to the random or radial orientation[44] and thereby increases overall fluidity.

4. Conclusion

Interaction of PAMAM-succinamate dendrimers, 1,4-diaminobutane core, generation 5 with hybrid cationic vesicles comprised of SLC, IPA and DHADB was investigated to get information of their morphological adaptation. Inclusion of dendrimers solution in vesicles displayed prominent influence of dendrimers on the vesicles morphology. Comprehensive investigation on morphologies confirms the influence of dendrimers on cationic vesicles to suffer through dispersion-flocculation-dispersion. Decreased Z. P. with increasing concentration of dendrimers also suggests some morphological changes due to the ionic bonding. The impact of dendrimers was furthers examined by studying vesicles disintegration kinetics where formation of monolayer was noticed as a consequence of bilayer disintegration. Studies confirmed the influences of dendrimers on the process of disintegration. When dendrimers concentration low, reduction of the disintegration kinetics was noticed, however higher amount of dendrimers does the opposite. AFM micrograph confirms both adsorption and the process of bilayer disruption induced by low and high amount of dendrimers respectively. Absence of any phase or domain separation for HCV2

and HCV3 vesicles upon inclusion of dendrimers confirm the novelty of IPA to sustain the bilayer integrity. Phase transition temperature was detected via DSC measurement; dendrimers at low concentration primarily interact on the surface. However we have also witnessed of the bilayer disruption mediated by higher concentration dendrimers as bilayer fail to exhibits chin melting. At this concentration dendrimer showed a tendency to interact with gel phase. Collective physicochemical investigations assists to understand the impact of negatively charged dendrimers on cationic vesicles and their morphological adaptation in depth by considering their interaction in molecular range. Encapsulation of drug molecule into the dendrimer/vesicles aggregates could be benefitted in the field of drug delivery.

5. References

References are given in BIBLIOGRAPHY under Chapter III (pp. 158-161).

Vesicles considering as novel drug delivery agent were formulated using SLC in combination with non conventional amphiphile, IPA with 30 mol% cholesterol. Formulations were investigated to understand the role of IPA in SLC bilayer. The physicochemical properties of SLC/IPA bilayer was depend on the amount of IPA. However unsaturation of hydrocarbon chain also plays a crucial role. In SLC/IPA mixed monomolecular film, chain mixing was associative upto 30 mol% of IPA. Fairly monodispersed vesicles formulations were stable over a period of 100 days and hydrodynamic sizes (d_h) were in the range of 200-300 nm. Z. P. of the formulations was decreased with increasing amount of IPA that contain neutral head group. Vesicles morphological properties was investigated by electron microscopic (normal TEM as well as FF-TEM) studies and the formation of spherical vesicles were confirmed. Thermotropic behaviours of SLC/IPA bilayers were analysed and the point of chain melting was negligibly hampered by IPA. By providing additional hydrophobic effect it helps to packed or rigidifies the SLC bilayer more efficiently. However presence of IPA must affect the bilayer and the structural changes were scrutinized by fluorescence anisotropy measurement using 1, 6-diphenyl-1, 3, 5-hexatriene (DPH) and 7-hydroxycoumarin (7HC). Anisotropy or micro viscosity was found to be higher for SLC/IPA vesicles in comparison to SLC vesicle and hence confirmed the role of IPA to rigidify the bilayer was conclude. Entrapment efficiency (E.E.) of the vesicles using cationic dye methylene blue (MB) was also evaluated and found to be dependent of IPA content. Such systems are expected to have superior properties as potent vectors for drug delivery.

As cell membranes are negatively charged, cationic vesicles could serve as an excellent drug delivery vehicle. Three set of SLC/IPA vesicles were used with a motive to formulate hybrid cationic vesicles using bi-tail cationic surfactants with varying hydrocarbon chain length (bis-C_{12} to C_{18}). Incorporation of piroxicame (Px), a NSAID and its subsequent

impact on the hybrid cationic bilayer was investigated. Optimised Px encapsulated formulations were analysed for biological activity. Mutual miscibility among the components was studied by way of the surface pressure – area measurements. Both DDDAB and DHDAB bring associative type interaction in SLC/IPA monolayer as compared to DTDAB and DODAB. Expanded monolayer was the outcome when Px was incorporated into the mixed monomolecular film of SLC/IPA/DxDAB. Z. P. for each set of formulations was found to be increased with increasing cationic surfactant chainlength. Px certainly resides into the bilayer and thereby enhances the hydrodyanamic size of the vesicles. Accumulation of Px into the spherical shape vesicles were observed via TEM studies and AFM studies further confirms such incorporation of Px into the bilayer. The process of chain melting for SLC/IPA/DXDAB vesicles was hampered which confirms the presence of DXDABs into the bilayer creates some heterogeneity. The heterogeneity mainly associated with hydrocarbon chain and was further confirmed through FTIR studies. Entrapment efficiency and the release kinetics of Px from the hybrid cationic vesicles were found to be good for all the formulations except DTDAB comprising vesicles. Within 25 hr formulations show sustains release. Both blank and drug loaded vesicles were hemocompatable and hence show the novelty. Finally the toxicity and biocompatibility of the drug loaded formulations were assessed. It was non-toxic to normal human blood lymphocytes however becomes toxic to Neuroblastoma cell line. Such formulations could shed light in the development of drug delivery systems in the treatment of brain – tumors targeted drug delivery.

Physico-chemistry between the interaction of cationic vesicles and PAMAM succinamic acid, 1, 4-diaminobutane core dendrimer generation 5 (G5-SA) which is negatively charged. Previously prepared cationic vesicle comprised of SLC, IPA and DHDAB in three different combinations was taken to investigate the impact of dendrimer. Increasing hydro dynamic size and reduced Z. P. measurement suggests the formation of

vesicle/dendrimer aggregates. Morphological state of the vesicles with and without dendrimer was analysed via TEM studies which confirmed the adsorption of dendrimer on the vesicle surface. The effect of dendrimer on solid supported cationic bilayer was further scrutinized via AFM studies that confirmed the hole formation on the bilayer at higher concentration of dendrimer. Vesicles disintegration kinetics measurement also has been done to understand the pattern of interaction using varying concentration of dendrimer. A surface pressure – time isotherm developed due to the vesicle disintegration upon the inclusion of dendrimer. The rate kinetics of such disintegration process was found to be depending on the dendrimer concentration. Finally DSC studies was performed which specifically enlighten the features of bilayer in presence of dendrimer; it describes the point of dendrimer attack on the bilayer. Overall interaction studies put IPA on the map as it tries to restore the bilayer morphology by providing hydrophobic interaction. Dendrimer certainly modulates the bilayer structure depending on its concentration. Initial adsorption of dendrimer restrict hydrocarbon chain movement and that was reflected fro anisotropy measurement. Although at higher dendrimer concentration, formation of dendrimer/vesicle complex, also known as dendriosome was noticed. Such complexes could be useful in encapsulation of drug molecules and subsequently cytotoxicity studies.

Introduction

Reference

1 C. Duval-Terrie, G. Cosette P Fau - Molle, G. Molle G Fau - Muller, E. Muller G Fau - De, E. De., *Protein Sci*. **2003**, *12*, 681-689.

2 M. Fariya, A. Jain, V. Dhawan, S. Shah, M. S. Nagarsenker, *Adv. Pharm. Bull.* **2014**, *4*, 483-491.

3 D. R. Sikwal, R. S. Kalhapure, T. Govender, *Eur. J. Pharm. Sci.* **2017**, *97*, 113-134.

4 X. B. Xiong, O. Binkhathlan Z Fau - Molavi, A. Molavi O Fau - Lavasanifar, A. Lavasanifar, *Acta Biomaterialia.* **2012**, *8*, 2017-2033.

5 J. C. Athas, C. Jun K Fau - McCafferty, O. McCafferty C Fau - Owoseni, V. T. Owoseni O Fau - John, S. R. John Vt Fau - Raghavan, S. R. Raghavan, *Langmuir* **2014**, *30*, 9285-9294.

6 K. Yamazaki, M. Imai, I. Suzuki, *Biochem. Eng. J.* **2004**, *19*, 171-179.

7 B. J. Clavijo, L. Venturini, C. Schudoma, G. G. Accinelli, G. Kaithakottil, J. Wright, P. Borrill, G. Kettleborough, D. Heavens, H. Chapman, J. Lipscombe, T. Barker, F.-H. Lu, N. McKenzie, D. Raats, R. H. Ramirez-Gonzalez, A. Coince, N. Peel, L. Percival-Alwyn, O. Duncan, J. Trösch, G. Yu, D. M. Bolser, G. Namaati, A. Kerhornou, M. Spannagl, H. Gundlach, G. Haberer, R. P. Davey, C. Fosker, F. D. Palma, A. L. Phillips, A. H. Millar, P. J. Kersey, C. Uauy, K. V. Krasileva, D. Swarbreck, M. W. Bevan, M. D. Clark, *Genome Res.* **2017**, *27*, 885-896.

8 J. H. Fendler, *Adv. Mater.* **1996**, *8*, 260-260.

9 S. Clarke, *J. Chem. Edu.* **1981**, *58*, A246.

10 C. Tanford, Editor, Krieger, Malabar, Fla, **1991**.

11 R. A. Khalil, A.-h. A. Zarari, *Appl. Surf. Sci.* **2014**, *318*, 85-89.

12 D. J. Mitchell, B. W. Ninham, *J. Chem. Soc., Faraday Trans.* **1981**, *77*, 601-629.

13 M. Wolowicz, A. Szaniawska, *Polar Res.* **1986**, *4*, 79-84.

14 L. May, A. B. Kamble, I. P. Acosta, *J. Membr. Biol.* **1970**, *2*, 192-200.

15 R. J. King, M. C. MacBeth, *Biochim. Biophys. Acta* **1981**, *647*, 159-168

16 M. Sipai altaf bhai, V. Yadav, Y. Mamtha, V. v. Prashant, *J. Pharm. Sci. innov.* **2012**, *1*, 13-21.

17 J. E. Vance, G. Tasseva, *Biochim. Biophys. Act.* **2013**, *3*, 543-54.

18 V. Bolotina, V. Omelyanenko, B. Heyes, U. Ryan, P. Bregestovski, *Pflügers Arch.* **1989**, *415*, 262-268.

19 R. A. Cooper, *J. Supramol. Struct.* **1978,** *8***,** 413-430.

20 G. Bozzuto, A. Molinari, *Int. J. Nanomed.* **2015**, *10*, 975-999.

21 H.-I. Chang, M.-K. Yeh, *Int. J. Nanomed.* **2012**, *7*, 49-60.

22 N. Weiner, S. Lieb L Fau - Niemiec, C. Niemiec S Fau - Ramachandran, Z. Ramachandran C Fau - Hu, K. Hu Z Fau - Egbaria, K. Egbaria, *J. drug Target.* **1994**, *2*, 405-410.

23 A. Akbarzadeh, R. Rezaei-Sadabady, S. Davaran, S. W. Joo, N. Zarghami, Y. Hanifehpour, M. Samiei, M. Kouhi, K. Nejati-Koshki, *Nanoscale Res. Lett.* **2013**, *8*, 102-102.

24 A. Sharma, U. S. Sharma, *Int. J. Pharm.* **1997**, *154*, 123-140.

25 E. Kaler, A. Murthy, B. Rodriguez, J. Zasadzinski, *Science* **1989**, *245*, 1371-1374

26 K. Maiti, S. Bhattacharya, S. Moulik, A. Panda, *J. Chem. Sci.* **2010**, *122*, 867-879.

27 M. H. Chung, B. Park C Fau - Chul Chun, Y.-C. Chul Chun B Fau - Chung, Y. C. Chung, **2004**. *Colloids Surf. B* **2004**, *34*, 179-184.

28 M.-H. Chung, C. Park, B. Chul Chun, Y.-C. Chung, *Colloids Surf. B* **2004**, *34*, 179-184.

29 A. Caria, O. Regev, A. Khan, *J. Colloid Interf. Sci.* **1998**, *200*, 19-30

30 A. D. Bangham, R. W. Horne, *Nature* **1962**, *196*, 952

31 A. D. Bangham, R. W. Horne, *J. Mol. Biol.* **1964**, *8*, 660-IN10

32 R. W. Horne, A. D. Bangham, V. P. Whittaker, *Nature* **1963**, *200*, 1340

33 E. Abbasi, S. F. Aval, A. Akbarzadeh, M. Milani, H. T. Nasrabadi, S. W. Joo, Y. Hanifehpour, K. Nejati-Koshki, R. Pashaei-Asl, *Nanoscale Res. Lett.* **2014**, *9*, 247

34 E. Abbasi, S. F. Aval, A. Akbarzadeh, M. Milani, H. T. Nasrabadi, S. W. Joo, Y. Hanifehpour, K. Nejati-Koshki, R. Pashaei-Asl, *Nanoscale Res. Lett.* **2014**, *9*, 247

35 A. S. Abu Lila, T. Ishida, *Biol. Pharm. Bull.* **2017**, *40*, 1-10.

36 J. O. Eloy, M. Claro de Souza, R. Petrilli, J. P. Barcellos, R. J. Lee, J. M. Marchetti, *Colloids Surf. B* **2014**, *123*, 345-63.

37 M. Alavi, N. Karimi, M. Safaei, *Adv. Pharm. Bull.* **2017**, *7*, 3-9

38 F. Ghaffar, K. Carrick, B. B. Rogers, L. R. Margraf, K. Krisher, O. Ramilo, *Pediatr. Infect. Dis. J.* **2000**, *19*, 764.

39 T. Feng, Y. Wei, R. J. Lee, L. Zhao, *Int. J. Nanomed.* **2017**, *12*, 6027-6044.

40 S. Patil, B. Choudhary, A. Rathore, K. Roy, K. Mahadik, *Phytomedicine.* **2015**, *22*, 1103-1111.

41 J. Shaji, V. Patole, *Indian J. Pharm. Sci.* **2008**, *70*, 269-277.

42 N. K. Marie, A. D. Habeeb, *Mustansiriya Med.* J. **2012**. *11*, 39-44.

43 H. Chanda, P. Das, *Int. J.Pharm. Sci. Res.* **2011**, *27*, 1-9.

44 M. Achim, C. Precup, D. Gonganăuniţu, L. B. Tudoran, A. S. Porfire, R. Scurtu, C. Ciuce, *Farma.\Cia.* **2009**, *57*, 703-710.

45 B. A, *J. Pharm. Pharmaceut. Sci.* **2004**, *7*, 252-259.

46 S. Ghanbarzadeh, H. Valizadeh, P. Zakeri-Milani, *BioImpacts.* **2013**, *3*, 75-81.

47 L. B. Lopes, M. V. Scarpa, N. L. Pereira, L. C. de Oliveira, A. G. Oliveira, *Brazilian J. Pharm. Sci.* **2006**, *42*, 497-504.

48 D. W. Deamer, *Ann. N. Y. Acad. Sci.* **1978**. *308*, 250-258.

49 C. Jaafar-Maalej, V. Diab R Fau - Andrieu, A. Andrieu V Fau - Elaissari, H. Elaissari A Fau - Fessi, H. Fessi, *J. Liposome Res.* **2010**, *20*, 228-243.

50 M. Pons, M. Foradada, J. Estelrich, *Int. J.Pharm.* **1993**, *95*, 51-56

51 T. L. Hwang, W. R. Lee, S. C. Hua, J. Y. Fang, *J. Dermatol. Sci.* **2007**, *46*, 11-20.

52 R. Cortesi, S. Esposito E Fau - Gambarin, P. Gambarin S Fau - Telloli, E. Telloli P Fau - Menegatti, C. Menegatti E Fau - Nastruzzi, C. Nastruzzi, *J. Microencapsul*. 1999, *16*, 251-256.

53 F. Szoka, F. Olson, T. Heath, W. Vail, E. Mayhew, D. Papahadjopoulos, *Biochim. Biophys. Acta* **1980**, *601*, 559-571.

54 V. A. Frolov, A. V. Shnyrova, J. Zimmerberg, *Cold Spring Harb. Perspect. Biol.* **2011**, *3*, a004747.

55 D. P. Pantazatos, S. P. Pantazatos, R. C. MacDonald, *J. Membr. Biol.* **2003**, *194*, 129-39.

56 S. P. Pantazatos, R. C. MacDonald, *J.Membr. Biol.* **2003**, *191*, 99-112.

57 T. M. Allen, *Drugs* **1997**, *54*, 8-14.

58 A. Gabizon, R. Goren D Fau - Cohen, Y. Cohen R Fau - Barenholz, Y. Barenholz, *J. Control Release* **1998,** *53*, 275-279.

59 O. Et-Thakafy, N. Delorme, C. Gaillard, C. Meriadec, F. Artzner, C. Lopez, F. Guyomarc'h, *Langmuir* **2017**, *33*, 5117-5126.

60 V. Joguparthi, T. X. Xiang, B. D. Anderson, *J. Pharm. Sci.* **2008**, *97*, 400-20.

61 K. Florine-Casteel, *Biophys. J.* **1990**, *57*, 1199-1215.

62 N. Kučerka, M.-P. Nieh, J. Katsaras, *Biochim. Biophys. Acta* **2011**, *1808*, 2761-2771

63 R. N. McElhaney, *Chem. Phys. Lipids* **1982**, *30*, 229-259.

64 J. R. Silvius, N. Mak, R. N. McElhaney, *Biochim. Biophys. Acta* **1980**, *597*, 199-215.

65 I. W. Yellin N Fau - Levin, I. W. Levin, *Biochemistry* **1977**, *16*, 642-647.

66 B. A. C. Horta, A. H. de Vries, P. H. Hünenberger, *J. Chem. Theory Comput.* **2010**, *6*, 2488-2500.

67 S. Leekumjorn, A. K. Sum, *Biochim. Biophys. Acta* **2007**, *2*, 354-65.

68 R. N. A. H. Lewis, R. N. McElhaney, *Biochim. Biophys. Acta* **2013**, *1828*, 2347-2358.

69 A. Abolfazl, Z. Nosratollah, M. Haleh, A. Davoud, G. Amir Mohammad, H. Khaksar Khiabani, D. Soodabeh, *Int. J. Nanotechnol. Sci. Environ.* **2012**, *5*.

70 A. Abolfazl, M. Samiei, D. Soodabeh, *Nanoscale Res. Lett.* **2012**, *7*.

71 A. Akbarzadeh, M. Samiei, S. W. Joo, M. Anzaby, Y. Hanifehpour, H. T. Nasrabadi, Davaran, *J. Nanobiotechnol.* **2012**, *10*.

72 L. M. Ensign, R. Cone, J. Hanes, *Adv. Drug Deliv. Rev.* **2012**, *64*, 557-570.

73 F. L. Lopez, T. B. Ernest, C. Tuleu, M. O. Gul, *Expert Opin. Drug Deliv.* **2015**, *12*, 1727-1740.

74 S. V. Sastry, J. R. Nyshadham, J. A. Fix, *Pharm. Sci. Technol. Today* **2000**, *3*, 138-145.

75 M. A. Ashwell, J. F. Bagli, T. J. Caggiano, P. S. Chan, A. J. Molinari, C. Palka, C. H. Park, J. F. Rogers, M. Sherman, E. J. Trybulski, D. K. Williams, *Bioorganic Med. Chem. Lett.* **2000**, *10*, 783-786.

76 A. Breitenbach, Y. X. Li, T. Kissel, *J. Control. Rel.* **2000**, *64*, 167-178.

77 H. Kranz, R. Bodmeier, *Int. J. Pharm.* **2007**, *332*, 107-114.

78 B. Sun, Y. Yeo, *Curr. Opi. Solid State Mater. Sci.* **2012**, *16*, 295-301.

79 M. R. Prausnitz, R. Langer, *Nat. biotechnol.* **2008**, *26*, 1261-1268.

80 M. U. Ghori, M. H. Mahdi, A. M. Smith, B. R. Conway, *Am. J. Pharmacol. Sci.* **2015**, *3*, 110-119.

81 S. Turker, Y. Onur E Fau - Ozer, Y. Ozer, *Pharm. World Sci*., **2008**, *78*, 87-90.

82 P. P. Constantinides, M. V. Chaubal, R. Shorr, *Adv. Drug Deliv. Rev.* **2008**, *60*, 757-762.

83 P. Gershkovich, K. M. Wasan, C. A. Barta, *Crit. Rev. Ther. Drug. Carrier Syst*., **2008**, *25*, 545-584.

84 B. Heidi, P. Ange, P. Bernard, V. Patrick, *Curr. Drug Deliv.* **2004**, *1*, 299-312

85 F. Kreye, J. Siepmann F Fau - Siepmann, J. Siepmann, *Expert Opin Drug Deliv.* **2008**, *5*, 291-307.

86 G. Tiwari, R. Tiwari, B. Sriwastawa, L. Bhati, S. Pandey, P. Pandey, S. K. Bannerjee, *Int. J. Pharm. Investig.* **2012**, *2*, 2-11.

87 V. Alireza, M. Haleh, S. Mohammad, F. Samad Mussa, Z. Nosratollah, K. Mohammad, A. Abolfazl, D. Soodabeh, *Nanoscale Res. Lett.* **2012**, *7*.

88 H. S. Hassan, A. M. Sule Mi Fau - Musa, K. Y. Musa Am Fau - Musa, M. S. Musa Ky Fau - Abubakar, A. S. Abubakar Ms Fau - Hassan, A. S. Hassan, *Afr. J. Tradit. Complement Altern. Med.* **2011**, *9*, 250-255.

89 M. Shahbaaz, K. Bisetty, F. Ahmad, M. I. Hassan, *OMICS,* **2015**, *19*, 416-434.

90 P. K. Ghosh, R. S. R. Murthy, *Curr. Drug Deliv.* **2006**, *3*, 167-180.

91 P. Li, A. Ghosh, R. F. Wagner, S. Krill, Y. M. Joshi, A. T. Serajuddin, *Int. J. Pharm.* **2005**, *288*, 27-34.

92 S. Trevino, R. Joubran, N. Parris, N. Berk, *Langmuir* **1994**, *10*, 4398-4398.

93 S. Benita, M. Y. Levy, *J. Pharm. Sci.* **1993**, *82*, 1069-1079.

94 F. A. Araújo, R. G. Kelmann, B. V. Araújo, R. B. Finatto, H. F. Teixeira, L. S. Koester, *Eur. J. Pharm. Sci.* **2011**, *42*, 238-245.

95 P. Kesharwani, A. K. Iyer, *Drug Discov. Today* **2015**, *20*, 536-547..

96 M. R. Bhalekar, V. Pokharkar, A. Madgulkar, N. Patil, N. Patil, *AAPS Pharm. Sci. Tech.* **2009**, *10*, 289-296.

97 S. Mukherjee, S. Ray, R. S. Thakur, *Indian J. Pharm. Sci.* **2009**, *71*, 349-358.

98 N. Naseri, H. Valizadeh, P. Zakeri-Milani, *Adv. Pharm. Bull.* **2015**, *5*, 305-313.

99 E. Buhleier, F. Vögtle, *Ber. Dtsch. Chem. Ges.* **1978**, *111*, 2729-2731.

100 B. Klajnert, M. Bryszewska, *Acta Biochim. Pol.*, **2001**, *48*, 199-208.

101 P. Xu, G. Bajaj, T. Shugg, W. G. Van Alstine, Y. Yeo, *Biomacromol.* **2010**, *11*, 2352-2358.

102 A. I. Lopez, R. Y. Reins, A. M. McDermott, B. W. Trautner, C. Cai, *Mol. biosys.* **2009**, *5*, 1148-1156.

103 P. Kesharwani, K. Jain, N. K. Jain, *Prog. Polym. Sci.* **2014**, *39*, 268-307.

104 N. Amreddy, A. Babu, R. Muralidharan, A. Munshi, R. Ramesh, *Top. Cur. Chem.* **2017**, *375*, 35-40.

105 P. Antoni, Y. Hed, A. Nordberg, D. Nyström, H. von Holst, A. Hult, M. Malkoch, *Angew. Chem.* **2009**, *121*, 2160-2164.

106 M. J. Laufersweiler, J. M. Rohde, J.-L. Chaumette, D. Sarazin, J. R. Parquette, *J. Organic Chem.* **2001**, *66*, 6440-6452.

107 J. R. McElhanon, D. R. Wheeler, *Organic Lett.* **2001**, *3*, 2681-2683.

108 J. A. Kremers, E. W. Meijer, *React. Funct. Polym.* **1995**, *26*, 137-144.

109 F. Avila-Salas, C. Sandoval, J. Caballero, S. Guiñez-Molinos, L. S. Santos, R. E. Cachau, F. D. González-Nilo, *J. Phys. Chem. B* **2012**, *116*, 2031-2039.

110 B. K. Nanjwade, H. M. Bechra, G. K. Derkar, F. V. Manvi, V. K. Nanjwade, *Eur. J. Pharm. Sci.* **2009**, *38*, 185-196.

111 D. A. Tomalia, A. M. Naylor, W. A. Goddard, *Angew. Chem.* **1990**, *29*, 138-175.

112 D. A. Tomalia, H. Baker, J. Dewald, M. Hall, G. Kallos, S. Martin, J. Roeck, J. Ryder, P. Smith, *Polym. J.* **1985**, *17*, 117-123.

113 S. K. Mastronicolis, A. Boura, A. Karaliota, P. Magiatis, N. Arvanitis, C. Litos, A. Tsakirakis, P. Paraskevas, H. Moustaka, G. Heropoulos, *Food Microbiol.* **2006**, *23*, 184-194.

114 J. M. Frechet, *Science* **1994**, *263*, 1710-1715.

115 C. Yiyun, M. Na, X. Tongwen, F. Rongqiang, W. Xueyuan, W. Xiaomin, W. Longping, *J. Pharm. Sci.* **2007**, *96*, 595-602.

116 A. S. Chauhan, K. B. Sridevi S Fau - Chalasani, A. K. Chalasani Kb Fau - Jain, S. K. Jain Ak Fau - Jain, N. K. Jain Sk Fau - Jain, P. V. Jain Nk Fau - Diwan, P. V. Diwan, *J. Control. Release*, **2003**, *93*, 335-343.

117 A. D'Emanuele, J. Jevprasesphant R Fau - Penny, D. Penny J Fau - Attwood, D. Attwood, *J. Control. Release* **2004**, *95*, 447-453.

118 S. Bai, C. Thomas, F. Ahsan, *J. Pharm. Sci.* **2003***, 96*, 2090-2106.

119 A. Myc, T. P. Majoros Ij Fau - Thomas, J. R. Thomas Tp Fau - Baker, Jr., J. R. Baker, Jr., *Biomacromol*. **2007**, *8*, 13-18.

120 Y. Choi, T. Thomas, A. Kotlyar, M. T. Islam, J. R. Baker, *Chem. Biol.* **2005**, *12*, 35-43.

121 M. A. C. Broeren, J. L. J. van Dongen, M. Pittelkow, J. B. Christensen, M. H. P. van Genderen, E. W. Meijer, *Angew. Chem.* **2004**, *43*, 3557-3562.

122 E. C. Wiener, H. Brechbiel Mw Fau - Brothers, R. L. Brothers H Fau - Magin, O. A. Magin Rl Fau - Gansow, D. A. Gansow Oa Fau - Tomalia, P. C. Tomalia Da Fau - Lauterbur, P. C. Lauterbur, *Magn. Reson. Med.* **1994**, *31*, 1-8.

123 E. Wiener, M. W. Brechbiel, H. Brothers, R. L. Magin, O. A. Gansow, D. A. Tomalia, P. C. Lauterbur, *Magn. Reson. Med.* **1994**, *31*, 1-8.

124 H. Brockman, *Curr. Opin. Struct. Biol.* **1999**, *9*, 438-443.

125 B. Ruozi, D. Belletti, A. Tombesi, G. Tosi, L. Bondioli, F. Forni, M. A. Vandelli, *Int. J. Nanomed.* **2011**, *6*, 557-563.

126 B. Ruozi, G. Tosi, F. Forni, M. Fresta, M. A. Vandelli, *Eur. J. Pharm. Sci.* **2005**, *25*, 81-89.

127 P. Balgavý, M. Dubničková, N. Kučerka, M. A. Kiselev, S. P. Yaradaikin, D. Uhríková, *Biochim. Biophys. Acta* **2001**, *1512*, 40-52.

128 J. Gallová, D. Uhríková, M. Hanulová, J. Teixeira, P. Balgavý, *Colloids Surf. B* **2004**, *38*, 11-14.

129 M. Li, H. H. Morales, J. Katsaras, N. Kučerka, Y. Yang, P. M. Macdonald, M.-P. Nieh, *Langmuir* **2013**, *29*, 15943-15957.

130 M. R. Brzustowicz, A. T. Brunger, *J. appl. Crystallogr.* **2005**, *38*, 126-131.

131 K. A. Riske, L. Q. Amaral, M. T. Lamy-Freund, *Biochim. Biophys. Acta* **2001**, *2*, 297-308.

132 E. A. Smith, C. Smith, B. Tanksley, P. K. Dea, *Biophys. Chem.* **2014**, *191*, 1-7.

133 E. N. Towns, A. N. Parikh, D. P. Land, *J. Phys. Chem. C* **2015**, *119*, 2412-2418.

134 A. K. Jain, A. Jain, N. K. Garg, A. Agarwal, S. A. Jain, R. K. Tyagi, R. K. Jain, H. Agrawal, G. P. Agrawal, *Colloids Surf. B* **2014**, *121*, 222-229.

Chapter I

Reference

1 C. Luna, K. M. Stroka, H. Bermudez, H. Aranda-Espinoza, *Colloids Surf. B.* **2011**, *85*, 293-300.

2 T. Hara, H. Kuwasawa, Y. Aramaki, S. Takada, K. Koike, K. Ishidate, H. Kato, S. Tsuchiya, *Biochim. Biophys. Acta.* **1996**, *1278*, 51-58.

3 L. E. Unates, R. N. Farias, *Biochim. Biophys. Acta.* **1979**, *568*, 363-369.

4 J. Pintschovius, K. Fendler, E. Bamberg, *Biophys. J.* **1999**, *76*, 827-836.

5 S. Parimi, T. J. Barnes, C. A. Prestidge, *Langmuir* **2008**, *24*, 13532-13539.

6 J. Lee, C.-H. Chang, *Soft Matter* **2014**, *10*, 1831-1839.

7 B. D. Isailović, I. T. Kostić, A. Zvonar, V. B. Đorđević, M. Gašperlin, V. A. Nedović, B. M. Bugarski, *Innov. Food Sci.Emerg. Technol.* **2013**, *19*, 181-189.

8 K. Kato, P. Walde, N. Koine, S. Ichikawa, T. Ishikawa, R. Nagahama, T. Ishihara, T. Tsujii, M. Shudou, Y. Omokawa, T. Kuroiwa, *Langmuir* **2008**, *24*, 10762-70.

9 A. Akbarzadeh, R. Rezaei-Sadabady, S. Davaran, S. W. Joo, N. Zarghami, Y. Hanifehpour, M. Samiei, M. Kouhi, K. Nejati-Koshki, *Nanoscale Res. Lett.* **2013**, *8*, 8-102.

10 J. Sabín, J. M. Ruso, A. González-Pérez, G. Prieto, F. Sarmiento, *Colloids Surf. B.* **2006**, *47*, 64-70.

11 M. Alexander, A. Acero Lopez, Y. Fang, M. Corredig, *Food SCi. Technol.* **2012**, *47*, 427-436.

12 P. da Silva Malheiros, Y. M. S. Micheletto, N. P. d. Silveira, A. Brandelli, *Food Res. Int.* **2010**, *43*, 1198-1203.

13 E. Kaler, A. Murthy, B. Rodriguez, J. Zasadzinski, *Science* **1989**, *245*, 1371-1374.

14 P. Ghosh, G. Han, M. De, C. K. Kim, V. M. Rotello, *Adv. Drug Deliv. Rev.* **2008**, *60*, 1307-1315.

15 Y. Gao, J. Hao, *J. Phys. Chem. B.* **2009**, *113*, 9461-71.

16 R. Dong, R. Weng, Y. Dou, L. Zhang, J. Hao, *J. Phys. Chem. B.* **2010**, *114 (6)*, 2131-2139

17 S. L. Duncan, R. G. Larson, *Biochim. Biophys. Acta.* **2010**, *1798*, 1632-1650.

18 K. Maiti, S. Bhattacharya, S. Moulik, A. Panda, *J. Chem. Sci.* **2010**, *122*, 867-879.

19 S. Takegami, K. Kitamura, T. Kitade, M. Takashima, M. Ito, E. Nakagawa, M. Sone, R. Sumitani, Y. Yasuda, *Chem. Pharm. Bull.* **2005**, *53*, 147-50.

20 L. Zhao, S.-S. Feng, *J.Colloid Interf. Sci.* **2005**, *285*, 326-335.

21 A. K. Panda, K. Nag, R. R. Harbottle, F. Possmayer, N. O. Petersen, *J.Colloid Interf. Sci.* **2007**, *311*, 551–555.

22 S. Paul, A. K. Panda, *Colloids Surf. A.* **2013**, *419*, 113-124

23 V. Gupta, R. Gupta, R. Grover, R. Khanna, V. Jangra, A. Mittal, *J. Nanosci. Nanotechnol.* **2008**, *8*, 2328-33.

24 R. Pal, W. A. Petri, Jr., V. Ben-Yashar, R. R. Wagner, Y. Barenholz, *Biochemistry* **1985**, *24*, 573-81.

25 N. Ehrlich, A. L. Christensen, D. Stamou, *Anal. Chem.* **2011**, *83*, 8169-76.

26 M. Companyo, A. Iborra, J. Villaverde, P. Martinez, A. Morros, *Biochim. Biophys. Acta.* **2007**, *9*, 19.

27 S. H. Park, S. G. Oh, J. Y. Mun, S. S. Han, *Colloids Surf. B.* **2006**, *48*, 112-8.

28 S. H. Park, S. G. Oh, K. D. Suh, S. H. Han, D. J. Chung, J. Y. Mun, S. S. Han, J. W. Kim, *Colloids Surf. B.* **2009**, *70*, 108-13.

29 A. Karewicz, D. Bielska, B. Gzyl-Malcher, M. Kepczynski, R. Lach, M. Nowakowska, *Colloids Surf. B.* **2011**, *88*, 231-9.

30 S. Kapil, R. Rekha, S. Vipin, *Int. Res. J. Pharm.* **2012**, *3 (4)*, 378-383.

31 H. Brockman, *Curr. Opin. Struct. Biolo.* **1999**, *9*, 438-443.

32 F. He, R. X. Li, D. C. Wu, *J. Colloid Interf. Sci.* **2010**, *349*, 215-23.

33 S. Nichols-Smith, S. Y. Teh, T. L. Kuhl, *Biochim. Biophys. Acta.* **2004**, *27*, 1-2.

34 A. K. Panda, K. Nag, R. R. Harbottle, F. Possmayer, N. O. Petersen, *Colloids Surf. A* **2004**, *247*, 9-17.

35 A. K. Panda, K. Nag, R. R. Harbottle, F. Possmayer, N. O. Petersen, *J. Colloid Interf. Sci.* **2007**, *311*, 551-5.

36 J. Sabín, J. M. Ruso, A. González-Pérez, G. Prieto, F. Sarmiento, *Colloids Surf. B* **2006**, *47*, 64-70.

37 M.-L. Jobin, P. Bonnafous, H. Temsamani, F. Dole, A. Grélard, E. J. Dufourc, I. D. Alves, *Biochim. Biophys. Acta* **2013**, *1828*, 1457-1470.

38 W.-T. Li, Y.-M. Yang, C.-H. Chang, *J. Colloid Interf. Sci.* **2008**, *327*, 426-432.

39 N. Škalko, J. Bouwstra, F. Spies, M. Stuart, P. M. Frederik, G. Gregoriadis, *Biochim. Biophys. Acta.***1998**, *1370*, 151-160

40 B. Söptei, J. Mihály, J. Visy, A. Wacha, A. Bóta, *J. Phys. Chem. B* **2014**, *118*, 3887-3892.

41 Y. Yan, J. Huang, Z. Li, J. Ma, H. Fu, J. Ye, *J. Phys. Chem. B* **2003**, *107*, 1479-1482.

42 I. S. de Sousa, E. M. Castanheira, J. I. Rocha Gomes, M. E. Real Oliveira, *J Liposome Res* **2011**, *21*, 151-157.

43 L. Zhao, S. S. Feng, N. Kocherginsky, I. Kostetski, *Int. J. Pharm.* **2007**, *338*, 258-66.

44 M. M. Kodape, N. D. Gawhale, D. D. Kamble, S. A. Dabhade, N. V. Awajare, *Sci. Revs. Chem. Commun.* **2012**, *2*, 201-205.

Chapter II

Reerence

1 D. Lasic, *American Scientist* **1992**, *80*, 20-31.

2 R. Lipowsky, *Nature* **1991**, *349*, 475.

3 G. Storm, S. O. Belliot, T. Daemen, D. D. Lasic, *Adv. drug deliv. rev.* **1995**, *17*, 31-48.

4 A. Akbarzadeh, R. Rezaei-Sadabady, S. Davaran, S. W. Joo, N. Zarghami, Y. Hanifehpour, M. Samiei, M. Kouhi, K. Nejati-Koshki, *Nanoscale res. lett.* **2013**, *8*, 102.

5 I. M. Henderson, W. F. Paxton, *Angew. Chemie.* **2014**, *53*, 3372-3376.

6 R. Bhattarai, T. Sutradhar, B. Roy, P. Guha, P. Chettri, A. K. Mandal, A. G. Bykov, A. V. Akentiev, B. A. Noskov, A. K. Panda, *J. Phys. Chem. B* **2016**, *120*, 10744-10756.

7 P. Guha, B. Roy, G. Karmakar, P. Nahak, S. Koirala, M. Sapkota, T. Misono, K. Torigoe, A. K. Panda, *J. Phys. Chem. B.* **2015**, *119*, 4251-4262.

8 S. Koirala, B. Roy, P. Guha, R. Bhattarai, M. Sapkota, P. Nahak, G. Karmakar, A. K. Mandal, A. Kumar, A. K. Panda, *RSC Adv.* **2016**, *6*, 13786-13796.

9 C. N. Sobral, M. A. Soto, A. M. Carmona-Ribeiro, *Chem. Phys. Lipids* **2008**, *152*, 38-45.

10 Z. Zhang, W. Huang, J. Tang, E. Wang, S. Dong, *Biophys. Chem.* **2002**, *97*, 7-16.

11 T.-H. Chou, C.-H. Liang, Y.-C. Lee, L.-H. Yeh, *Phys. Chem. Chem. Phys.* **2014**, *16*, 1545-1553.

12 U. K. Basak, A. Datta, D. Bhattacharyya, *Colloids Surf. B.* **2015**, *132*, 34-44.

13 K. Czapla, B. Korchowiec, E. Rogalska, *Langmuir* **2009**, *26*, 3485-3492.

14 C. Nunes, G. Brezesinski, C. Pereira-Leite, J. L. F. C. Lima, S. Reis, M. Lúcio, *Langmuir* **2011**, *27*, 10847-10858 10.1021/la201600y.

15 H. Chakraborty, M. Sarkar, *Langmuir* **2004**, *20*, 3551-3558.

16 H. Ferreira, T. Matamá, R. Silva, C. Silva, A. C. Gomes, A. Cavaco-Paulo, *React. Fun. Polym.* **2013**, *73*, 1328-1334.

17 S. Mondal Roy, A. S. Bansode, M. Sarkar, *Langmuir* **2010**, *26*, 18967-18975.

18 W.-T. Li, Y.-M. Yang, C.-H. Chang, *Colloids Surf. B.* **2008**, *66*, 187-194.

19 K. Maiti, S. C. Bhattacharya, S. P. Moulik, A. K. Panda, *J. chem. Sci.* **2010**, *122*, 867-879.

20 J. Lee, C.-H. Chang, *Soft matter* **2014**, *10*, 1831-1839.

21 R. Dong, R. Weng, Y. Dou, L. Zhang, J. Hao, *The J. Phys. Chem. B.* **2010**, *114*, 2131-2139.

22 H. Jung, B. Coldren, J. Zasadzinski, D. Iampietro, E. Kaler, *Proceed. Nat. Academ. Sci.* **2001**, *98*, 1353-1357.

23 Y.-Y. Won, A. K. Brannan, H. T. Davis, F. S. Bates, *J. Phys. Chem. B* **2002**, *106*, 3354-3364.

24 J. Hoque, P. Kumar, V. K. Aswal, J. Haldar, *J. Phys. Chem. B* **2012**, *116*, 9718-9726.

25 M. R. Brzustowicz, A. T. Brunger, *J. Appl. crystallogr.* **2005**, *38*, 126-131 doi:10.1107/S0021889804029206.

26 P.-W. Yang, T.-L. Lin, Y. Hu, U.-S. Jeng, *Chin. J. Phys.* **2012**, *50*, 349-356.

27 S. v. C. Lopes, M. V. Novais, D. g. S. Ferreira, F. o. C. Braga, R. r. Magalhães-Paniago, A. n. Malachias, M. n. C. Oliveira, *Langmuir* **2014**, *30*, 15083-15090.

28 G. Fetih, D. Fathalla, M. El-Badry, *Drug Dev. Res.* **2014**, *75*, 257-266.

29 S. Nagarajan, E. E. Schuler, K. Ma, J. T. Kindt, R. B. Dyer, . *Phys. Chem. B* **2012**, *116*, 13749-13756.

30 A. K. Jain, A. Jain, N. K. Garg, A. Agarwal, S. A. Jain, R. K. Tyagi, R. K. Jain, H. Agrawal, G. P. Agrawal.

31 A. Chonn, P. Cullis, D. Devine, *J. Immunol.* **1991**, *146*, 4234-4241.

32 S. K. Jana, A. K. Mandal, A. Kumar, H. Puschmann, M. Hossain, S. Dalai, *RSC Adv.* **2016**, *6*, 95888-95896.

33 I. K. Sen, A. K. Mandal, S. Chakraborti, B. Dey, R. Chakraborty, S. S. Islam, *Int. J. Biol. Macromol.* **2013**, *62*, 439-449.

34 M. J. Rosen, J. T. Kunjappu, *Surf. Interf. Phenom.* Editor, John Wiley & Sons, **2012**.

35 C.-H. Lee, Y.-M. Yang, K.-L. Leu, H.-Y. Lin, C.-H. Liang, C.-H. Chang, *Colloid Polym Sci.* **2015**, *293*, 2239-2247.

36 K. Shimizu, J. N. Canongia Lopes, A. M. P. S. Gonçalves da Silva, *Langmuir* **2015**, *31*, 8371-8378.

37 B. Klosgen, W. Helfrich, *Biophys. J.* **1997**, *73*, 3016-29.

38 P. Balgavy, M. Dubnickova, N. Kucerka, M. A. Kiselev, S. P. Yaradaikin, D. Uhrikova, *Biochim. Biophys. Acta.* **2001**, *2*, 40-52.

39 J. Gallová, D. Uhríková, M. Hanulová, J. Teixeira, P. Balgavý, *Colloids Surf. B.* **2004**, *38*, 11-14.

40 N. Kučerka, D. Uhríková, J. Teixeira, P. Balgavý, *Physica B: Condens. Mat.* **2004**, *350*, E639-E642.

41 P. Balgavý, M. Dubničková, N. Kučerka, M. A. Kiselev, S. P. Yaradaikin, D. Uhríková, *Biochim. Biophys. Acta.***2001**, *1512*, 40-52.

42 F. R. Alves, W. Loh, *J Colloid Interf. Sci.* **2012**, *368*, 292-300.

43 M.-L. Jobin, P. Bonnafous, H. Temsamani, F. Dole, A. Grélard, E. J. Dufourc, I. D. Alves, *Biochim. Biophys. Acta.* **2013**, *1828*, 1457-1470.

44 J. I. N. R. Gomes, A. L. F. Baptista, *Text. Res. J.* **2001**, *71*, 153-156.

45 K. Cieślik-Boczula, J. Szwed, A. Jaszczyszyn, K. Gasiorowski, A. Koll, *J. Phys. Chem. B* **2009**, *113*, 15495-15502.

46 E. N. Towns, A. N. Parikh, D. P. Land, *J. Phys. Chem. C.* **2015**, *119*, 2412-2418.

47 G. J. Hardy, G. C. Wong, R. Nayak, K. Anasti, M. Hirtz, J. G. Shapter, S. M. Alam, S. Zauscher, Editor, Biochim. Biophys. Acta. **2014**, *1838*, 2662-2669.

48 F. Denizot, R. Lang, *J. Immunol. Method* **1986**, *89*, 271-7.

Chapter III

Reference

1 A. Akbarzadeh, R. Rezaei-Sadabady, S. Davaran, S. W. Joo, N. Zarghami, Y. Hanifehpour, M. Samiei, M. Kouhi, K. Nejati-Koshki, *Nanoscale Res. Lett.* **2013**, *8*, 102-102.

2 P. R. Karn, W. Cho, S. J. Hwang, *Nanomed.* **2013**, *8*, 1529-48.

3 L. Sagalowicz, M. E. Leser, H. J. Watzke, M. Michel, *Trend Food Sci. Technol.* **2006**, *17*, 204-214.

4 A. Wagner, K. Vorauer-Uhl, *J. Drug Deliv.* **2011**, *591325*, 5-12.

5 P. Guha, B. Roy, G. Karmakar, P. Nahak, S. Koirala, M. Sapkota, T. Misono, K. Torigoe, A. K. Panda, *J. Phys. Chem. B.* **2015**, *119*, 4251-4262.

6 S. P. Chaplot, I. D. Rupenthal, *J. Pharm. Pharmacol.* **2014**, *66*, 542-556.

7 P. M. Heegaard, U. Boas, N. S. Sorensen, *Bioconjug. Chem.* **2010**, *21*, 405-18.

8 L. Xu, H. Zhang, Y. Wu, *ACS Chem. Neurosci.* **2014**, *5*, 2-13.

9 E. Abbasi, S. F. Aval, A. Akbarzadeh, M. Milani, H. T. Nasrabadi, S. W. Joo, Y. Hanifehpour, K. Nejati-Koshki, R. Pashaei-Asl, *Nanoscale Res. Lett.* **2014**, *9*, 247-247.

10 D. Astruc, E. Boisselier, C. Ornelas, *Chem. Rev.* **2010**, *110*, 1857-1959.

11 S. M. Grayson, J. M. J. Fréchet, *Chem. Rev.* **2001**, *101*, 3819-3868.

12 H. Sashiwa, H. Yajima, S.-i. Aiba, *Biomacromol.* **2003**, *4*, 1244-1249.

13 V. Tiriveedhi, K. M. Kitchens, K. J. Nevels, H. Ghandehari, P. Butko, *Biochim. Biophys. Acta.* **2011**, *1808*, 209-218.

14 P. Kolhe, E. Misra, R. M. Kannan, S. Kannan, M. Lieh-Lai, *Int. J. Pharm.* **2003**, *259*, 143-60.

15 M. Markowicz, P. Szymański, M. Ciszewski, A. Kłys, E. Mikiciuk-Olasik, *J. Biol. Phys.* **2012**, *38*, 637-656.

16 R. Duncan, *Nat. Rev. Drug Discov.* **2003**, *2*, 347-60.

17 K. M. Kitchens, M. E. El-Sayed, H. Ghandehari, *Adv. Drug Deliv. Rev.* **2005**, *57*, 2163-76.

18 S. Svenson, D. A. Tomalia, *Adv. Drug Deliv. Rev.* **2005**, *57*, 2106-29.

19 A. Bielinska, J. F. Kukowska-Latallo, J. Johnson, D. A. Tomalia, J. R. Baker, Jr., *Nucleic Acids Res* **1996**, *24*, 2176-82.

20 H. Kang, R. DeLong, M. H. Fisher, R. L. Juliano, *Pharm. Res.* **2005**, *22*, 2099-106.

21 H. Yoo, P. Sazani, R. L. Juliano, *Pharm. Res.* **1999**, *16*, 1799-804.

22 R. F. Barth, D. M. Adams, A. H. Soloway, F. Alam, M. V. Darby, *Bioconjug. Chem.* **1994**, *5*, 58-66.

23 C. Chittasupho, S. Anuchapreeda, N. Sarisuta, *Eur. J. Pharm. Biopharma.* **2017**, *119*, 310-321.

24 J. Singh, K. Jain, N. K. Mehra, N. K. Jain, *Artif. Cells Nanomed. Biotechnol.* **2016**, *44*, 1626-34.

25 M. El-Sayed, M. Ginski, C. Rhodes, H. Ghandehari, *J. Control Rel.* **2002**, *81*, 355-65.

26 R. Jevprasesphant, J. Penny, D. Attwood, N. B. McKeown, A. D'Emanuele, *Pharm. Res.* **2003**, *20*, 1543-50.

27 K. M. Kitchens, R. B. Kolhatkar, P. W. Swaan, N. D. Eddington, H. Ghandehari, *Pharm. Res.* **2006**, *23*, 2818-26.

28 S. Choudhary, L. Gupta, S. Rani, K. Dave, U. Gupta, *Fron. Pharmacol.* **2017**, *8*, 261.

29 M. Liu, K. Kono, J. M. Frechet, *J. Control Rel.* **2000**, *65*, 121-31.

30 O. M. Milhem, C. Myles, N. B. McKeown, D. Attwood, A. D'Emanuele, *Int. J. Pharm.* **2000**, *197*, 239-41.

31 T. Borkowski, P. Subik, A. Trzeciak, S. Wolowiec, Editor, **2011**, *16*, 427-41.

32 J. N. H. Reek, S. Arévalo, R. van Heerbeek, P. C. J. Kamer, P. W. N. M. van Leeuwen, in *Adv. Cat.*, ed. by B. C. Gates, H. Knözinger, Academic Press, **2006**, *49*, 71-151.

33 A. Adronov, J. M. J. Frechet, *Chem. Comm.* **2000**, 1701-1710.

34 K. Maiti, S. Bhattacharya, S. Moulik, A. Panda, *J. Chem. Sci.* **2010**, *122*, 867-879.

35 S. Ghanbarzadeh, H. Valizadeh, P. Zakeri-Milani, *BioImpact.***2013**, *3*, 75-81 10.5681/bi.2013.016.

36 S. Varona, Á. Martín, M. J. Cocero, *Industrial & Engineering Chemistry Research* **2011**, *50*, 2088-2097 10.1021/ie102016r.

37 B. Erickson, S. DiMaggio, D. G. Mullen, C. V. Kelly, P. R. Leroueil, S. A. Berry, J. R. Baker, B. G. Orr, M. M. Banaszak Holl, *Langmuir* **2008**, *24*, 11003-11008.

38 C. S. Vassilieff, I. Panaiotov, E. D. Manev, J. E. Proust, T. Ivanova, *Biophys. Chem.* **1996**, *58*, 97-107.

39 T. Yotsuyanagi, J. Mizutani, M. Iwata, K. Ikeda, *Biochim. Biophys. Acta* **1983**, *731*, 304-11.

40 W.-T. Li, Y.-M. Yang, C.-H. Chang, *Colloids Surf. B* **2008**, *66*, 187-194.

41 K. Gardikis, S. Hatziantoniou, K. Viras, M. Wagner, C. Demetzos, *Int. J. Pharm.* **2006**, *318*, 118-23.

42 B. Klajnert, J. Janiszewska, Z. Urbanczyk-Lipkowska, M. Bryszewska, R. M. Epand, *Int. J. Pharm.* **2006**, *327*, 145-152.

43 C. V. Kelly, P. R. Leroueil, B. G. Orr, M. M. Banaszak Holl, I. Andricioaei, *J. Phys. Chem. B* **2008**, *112*, 9346-9353.

44 P. E. Smith, J. R. Brender, U. H. Durr, J. Xu, D. G. Mullen, M. M. Banaszak Holl, A. Ramamoorthy, *J. Am. Chem. Soc.* **2010**, *132*, 8087-97.

INDEX

Reprints

THE JOURNAL OF PHYSICAL CHEMISTRY B

Article

pubs.acs.org/JPCB

Ion-Pair Amphiphile: A Neoteric Substitute That Modulates the Physicochemical Properties of Biomimetic Membranes

Pritam Guha,[†] Biplab Roy,[†] Gourab Karmakar,[†] Prasant Nahak,[†] Suraj Koirala,[‡] Manish Sapkota,[‡] Takeshi Misono,[§] Kanjiro Torigoe,[§] and Amiya Kumar Panda*[,†]

[†]Department of Chemistry, University of North Bengal, Darjeeling 734 013, West Bengal, India

[‡]Department of Pharmaceutics, Himalayan Pharmacy Institute, Majhitar, Rangpo, East Sikkim 737136, India

[§]Department of Pure and Applied Chemistry, Tokyo University of Science, 2641 Yamazaki, Noda, Tokyo 278-8510, Japan

Supporting Information

ABSTRACT: Ion-pair amphiphiles (IPAs) are neoteric pseudo-double-tailed compounds with potential as a novel substitute of phospholipid. IPA, synthesized by stoichiometric/equimolar mixing of aqueous solution of hexadecyltrimethylammonium bromide (HTMAB) and sodium dodecyl sulfate (SDS), was used as a potential substituent of naturally occurring phospholipid, soylecithin (SLC). Vesicles were prepared using SLC and IPA in different ratios along with cholesterol. The impact of IPA on SLC was examined by way of surface pressure (π)−area (A) measurements. Associated thermodynamic parameters were evaluated; interfacial miscibility between the components was found to depend on SLC/IPA ratio. Solution behavior of the bilayers, in the form of vesicles, was investigated by monitoring the hydrodynamic diameter, zeta potential, and polydispersity index over a period of 100 days. Size and morphology of the vesicles were also investigated by electron microscopic studies. Systems comprising 20 and 40 mol % IPA exhibited anomalous behavior. Thermal behavior of the vesicles, as scrutinized by differential scanning calorimetry, was correlated with the hydrocarbon chain as well as the headgroup packing. Entrapment efficiency (EE) of the vesicles toward the cationic dye methylene blue (MB) was also evaluated. Vesicles were smart enough to entrap the dye, and the efficiency was found to vary with IPA concentration. EE was found to be well above 80% for some stable dispersions. Such formulations thus could be considered to have potential as novel drug delivery systems.

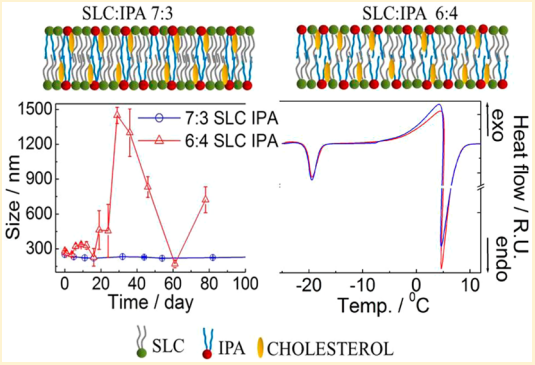

INTRODUCTION

Intracellular components are compartmentalized by thin biomembranes which commonly behave like a physical boundary to separate the respective compartments from the surrounding continuous environments.[1] Biological cells are directly responsible for numerous physicochemical processes that depend on the composition of the membrane bilayer. Research on the biological and biomimetic membranes resulted in the generation of substantial useful information in order to understand its subtle structure and its relevance in physiological environments. Biomembranes have diversity in potential because of the functional interface; it can bind to DNA, peptides, control the enzymes, etc.[2,3] Further research on the membranous components suggests that biomembranes can actively play a role in biochemical processes, e.g., adhesion, signaling, controlling the Na^+/K^+ balance, fusion, etc.[4] The resultant activity or potential of biomembrane largely depends on their components (phospholipids, cholesterol, and regulatory protein, etc.).

The major components of the cell membranes are phospholipids that are capable of forming vesicles spontaneously when they are hydrated.[5] Because of their amphiphilic nature, naturally occurring phospholipids are widely used in the synthetic formulation of vesicles in order to have further insight into their different physicochemical properties. Research on biomimetic membranes over the past few decades has revealed its potential application toward drug delivery, gene therapy, DNA transfection, etc.[6] Drug carrying capabilities arise because of its unique hydrophilic and hydrophobic charisma. So, over the past few years vesicles have been a subject of focus for their biocompatibility and stability.

Stability of the vesicles is highly dependent on the amphiphile composition, surface charge (zeta potential), and hydrodynamic size.[7] Additionally, "rigidity" and "fluidity" of the membranes' microenvironment also play a crucial role for its stability as they are highly dependent on the nature of the phospholipids and cholesterol. Cholesterol, one of the key components of the cell membranes, can judiciously control the fluidity and rigidity of the bilayer. Usually cholesterol amounts to a maximum of 30 mol % of the total lipid in mammalian cell

Received: December 8, 2014
Revised: February 11, 2015
Published: February 25, 2015

DOI: 10.1021/jp512212u
J. Phys. Chem. B 2015, 119, 4251−4262

membranes.[8] Unsaturated phospholipids from natural sources, like palmitooleylphosphatidylcholine (POPC), form less stable fluidic and permeable bilayers, whereas saturated phospholipids, viz., dipalmitoylphasphatidylcholine (DPPC) and dimyristylphosphatidylcholine (DMPC), can form rather stable, however, rigid bilayers.[9] It is reported that vesicles comprising naturally occurring phospholipids exhibit poor stability under normal conditions.[10] However, strategies have been adapted by researchers in order to improve the stability of vesicles for its better performance.

Vesicles comprising different types of phospholipids have been the research of interest for the past few decades.[7,11,12] Double-tail and single-tail surfactants which also form self-assembled structures were also introduced to produce stable vesicles dispersion. Kaler et al.[13] first reported about a neoteric phospholipid mimic amphiphile which spontaneously forms vesicles. This was synthesized from single chain mixed cationic and anionic surfactants, known as ion-pair amphiphile (IPA). Vesicles comprising catanionic surfactants, also known as catanosomes, find it excellent for drug delivery,[6] binding with DNA,[14,15] nanoparticle synthesis,[15,16] etc. Easy laboratory preparation of IPA marked its implication in membrane mimetic studies. However, the impact of IPA on naturally occurring phospholipids (unsaturated), on monolayer, and consequently on the bilayer needs some extra attention as it may produce stable vesicular dispersion for drug delivery. Such studies could shed further light on the possible yet unexplored application potentials as well as understanding of the fundamentals on the membranous interfaces.

In the present set of experiments, vesicles were prepared at different ratios of SLC and IPA with additional 30 mol % cholesterol (with respect to SLC and IPA) in physiological phosphate buffer solution. Cholesterol, which is a key component of bilayers, regulates the rigidity and fluidity of the membrane.[17] The effect of IPA on SLC in the form of monomolecular film was investigated by the Langmuir monolayer technique (surface pressure–area isotherms). Ideality/nonideality in mixing, film compressibility, and associated thermodynamic parameters were evaluated. Hydrodynamic size (d_h), zeta potential (ZP), and polydispersity index (PDI) of the vesicles were measured by the dynamic light scattering (DLS) technique. Morphological investigations on the vesicles were successfully documented by electron microscopic (normal TEM as well as FF-TEM) studies. Thermotropic behaviors of the bilayers were scrutinized by differential scanning calorimetry (DSC). Structural changes, induced by IPA, were further scrutinized by using fluorescence spectroscopy using 1,6-diphenyl-1,3,5-hexatriene (DPH) and 7-hydroxycoumarin (7HC) as the fluorescent probes. Entrapment efficiency (EE) of the vesicles toward the cationic dye methylene blue (MB) was also evaluated. The comprehensive studies can further shed light on the vesicles from the fundamental understanding point of view. Also, such systems are expected to have superior properties as potent vectors for drug delivery.

EXPERIMENTAL METHODS

Materials. L-α-Phosphatidylcholine (soylecithin, SLC, from soybean) was obtained from EMD Chemicals, Germany. A. R. grade sodium dodecyl sulfate [SDS, $CH_3(CH_2)_{11}SO_4Na$], hexadecyltrimethylammonium bromide [HTMAB, $C_{16}H_{33}N(CH_3)_3Br$], 1,6-diphenyl-1,3,5-hexatriene [DPH], 7-hydroxycoumarin [7HC], and (3β)-cholest-5-en-3-ol [cholesterol] were the products of Sigma-Aldrich Chemicals Pvt. Ltd. A.R. grade disodium hydrogen phosphate [$Na_2HPO_4{\cdot}12H_2O$], sodium dihydrogen phosphate [$NaH_2PO_4{\cdot}2H_2O$], sodium chloride [NaCl], methylene blue [MB], and chloroform (HPLC grade) were products from Merck Specialties Pvt. Ltd., India. All the chemicals were stated to be more than 99% pure and were used as received. Double-distilled water with a specific conductivity 2–4 μS cm^{-1} (at 25 °C) was used for the preparation of solutions.

Methods. Preparation and Isolation of IPA. The ion-pair amphiphile (IPA) hexadecyltrimethylammonium–dodecyl sulfate (HTMA$^+$-DS$^-$) was prepared by mixing a stoichiometric amount (equal mole ratio) of the two oppositely charged surfactants in water. Equal volume of 0.1 M aqueous HTMAB solution was progressively added to 0.1 M aqueous SDS solution under constant stirring. A white semisolid precipitate was thus obtained due to charge neutralization of the ionic surfactants; thus the IPA was formed. The mixture was then stirred and kept overnight. The IPA was extracted by chloroform using a separating funnel, where the counterions Na^+ and Br^- remained in the aqueous phase. The solvent (chloroform) was evaporated, leaving a white solid powder (HTMA$^+$-DS$^-$) that was dried under vacuum. The IPA, prepared in this work, thus can be considered as a salt-free catanionic surfactant.[18,19] IPA (HTMA$^+$-DS$^-$) powder was then characterized by means of XRD, FTIR, and ^{1}H NMR studies. Studies confirmed the formation of salt-free IPA with equimolar ratio of HTMA$^+$ and DS$^-$ ions. The obtained results were found to be similar to that of the previously published results.[6,19−23] Hence, the characterization details of the IPA are not mentioned in the present article.

Preparation of Vesicles. Small unilamellar vesicles (SUVs) of different compositions were prepared by the conventional thin film technique.[12,24−26] The mole ratio of SLC:IPA was set at 10:0, 9:1. 8:2, 7:3, 6:4, and 5:5 along with an additional 30 mol % cholesterol (with respect to the total amount of SLC and IPA). Quantitative amounts of SLC, IPA, and cholesterol were dissolved in chloroform in a round-bottom flask followed by solvent evaporation in a rotary evaporator. A trace amount of solvent was removed by the stream of nitrogen (N_2), and the flask was kept under vacuum overnight at room temperature to remove the residual solvent. The thin film obtained was then rehydrated for 1 h in PBS (0.1 M Na_2HPO_4, 0.1 M NaH_2PO_4, 100 mM NaCl, pH 7.4) at 70 °C, well above the chain melting temperature of all the lipidic components. Finally, vesicle dispersions were made homogeneous through 4–5 cycles of freeze–thaw and sonication. Total concentration of SLC and IPA was set at 2 mM. It was extruded using 0.45 μm cellulose nitrate membrane filter (Whatman GmbH, Germany). Vesicles were diluted depending on the type of experiment, e.g., 10^{-4} M dispersion was used for DLS studies. 10 μM DPH and 7-HC separately in chloroform were added into the lipidic mixture before the generation of the thin film. Exactly the same procedure was followed as mentioned above for the preparation of dye loaded vesicles. Final ratio of lipids to dye was maintained at 200:1.

Instrumentation. Surface Pressure (π)–Area (A) Isotherm. Surface pressure (π)–area (A) isotherms were recorded with a Langmuir balance (M/S Apex Instrument Co. India, Model LB2000C) with a stated resolution of 0.01 mN m^{-1}. The trough and the barrier were made up of Teflon (both hydrophobic and lyophobic) to avoid any contamination.[19] The trough was filled with the PBS solution at pH 7.4 with 100 mM NaCl. Surface of the subphase was precleaned using a

DOI: 10.1021/jp512212u
J. Phys. Chem. B 2015, 119, 4251−4262

micropipet aspirator before spreading the monomolecular film. Monomolecular film was generated by careful spreading of quantitative amount of the lipid ± IPA (with 30 mol % cholesterol) solutions dissolved in chloroform (1.0 mg mL^{-1}) with a Hamilton syringe (USA) onto the air−buffer interface. The solvent was allowed to evaporate approximately for 20 min. All the π−A isotherms were recorded at a subphase temperature of 25 ± 0.5 °C with a lateral compression rate of 5.0 mm min^{-1}. For each set of experiments, the curve was repeated at least twice to achieve the reproducible result. Further details are available in the literature.[27]

Dynamic Light Scattering (DLS) Studies. DLS studies were carried out to determine the hydrodynamic diameter (d_h), polydispersity index (PDI), and zeta potential (ZP) of different vesicle formulations.[16,28] A dynamic light scattering spectrometer (Zetasizer Nano ZS90 ZEN3690, Malvern Instruments Ltd., U.K.) was used for such studies. He−Ne laser with an emission wavelength of 632.8 nm was used, and all the data were recorded at a scattering angle of 90°. The translational diffusion coefficient (D) was actually measured by this instrument which is correlated with the diameter (d_h) of vesicles according to the Stokes−Einstein equation:[28]

$$d_h = \frac{kT}{3\pi\eta D} \quad (1)$$

where k, T, and η indicate the Boltzmann constant, temperature, and viscosity of water, respectively. The polydispersity index (PDI) is another informative parameter which could be obtained from the DLS studies. Zeta potential (ZP) values were measured using folded capillary cells. All the measurements were carried out at temperature 25 °C, and each reported zeta potential value was an average of four measurements.

Electron Microscopic Studies (TEM/FF-TEM). One drop of liposomal dispersion was placed on Formver carbon-coated 300 mesh copper grid.[29] Excess liquid was removed by using a piece of filter paper from the edge of the grid. The grid was then dried for 10 min before performing the measurement. The dry sample loaded grid was then viewed through Hitachi H-600 transmission electron microscope (Japan) using the standard procedure. The voltage was set at 80 kV. In case of FF-TEM studies, a drop of the sample was placed onto the sample holders and frozen in liquid propane. FR-7000A (Hitachi High Technologies Ltd., Japan) was used at −150 °C for the freeze-fracturing process. Samples were then replicated by evaporation using platinum−carbon.[30,31] The replica was placed on 300-mesh copper grid, dried, and examined in a transmission electron microscope (H-7650, Hitachi High Technologies Ltd., Japan) with an accelerating voltage of 120 kV.

Differential Scanning Calorimetry (DSC) Studies. DSC studies were performed to evaluate the chain melting temperature/phase transition temperature (T_m) and related thermodynamic parameters of the bilayer which eventually control the physical states of vesicles. Experiments were carried out in a Mettler Toledo differential scanning calorimeter (DSC 1, STAR^e system, Switzerland). The dry thin films were rehydrated in 40 μL sealed Al pan. Each sample was scanned two times with a scanning rate 5 °C min^{-1} and 2 °C min^{-1} for complete heating and cooling cycles. The reference pan was sealed with PBS (pH 7.4). The obtained results were calculated by STAR^e software.

Fluorescence Spectroscopic Studies. Solvatochromic dye 7-HC and hydrophobic probe DPH were employed to investigate membrane polarity and bilayer packing, respectively. Having some oxygeneous moiety, coumarin derivatives can accommodate itself into the palisade layer of vesicles.[32] Overall membrane polarity was thus determined from the steady-state spectra of 7-HC comprising systems. The spectra were recorded by using a benchtop spectrofluorometer (Quantum-master-40, Photon Technology International Inc., Birmingham, NJ). Steady-state fluorescence spectra of 7-HC under different conditions were recorded in the range 350−600 nm with an excitation wavelength of 330 nm (λ_{ex}). Fluorescence anisotropy of 7-HC was determined by recording the emission data at 379 nm. Fluorescence anisotropy values for the probe embedded in the liposomal bilayer were obtained using the equation[33,34]

$$r = \frac{I_{VV} - GI_{VH}}{I_{VV} + 2GI_{VH}} \quad (2)$$

where I_{VV} and I_{VH} are the fluorescence intensities and the subscripts indicate the position of the excitation and emission polarizer. $G = I_{HV}/I_{HH}$ is the grating correction factors. DPH, being a hydrophobic dye, is expected to reside inside the bilayer.[35−37] The steady-state fluorescence anisotropy technique was employed to measure the membrane rigidity. All the anisotropy data were recorded at room temperature with excitation wavelength 351 nm, and the emission was set to 421 nm for DPH, whereas that for 7-HC, excitation and emission wavelengths were set to 330 and 379 nm, respectively.

Entrapment Efficiency. Entrapment efficiency (EE) reveals the dye entrapment capacity of the vesicles. To determine the entrapment efficiency, lipidic components (SLC, IPA and cholesterol) were dispersed in PBS (pH 7.4) containing a known amount of methylene blue (MB).[29] Three cycles of freeze−thawing technique, as mentioned earlier, were adopted so that the dye concentration inside and outside vesicle remained the same. 40 μM MB loaded vesicles were made in such a way so that final concentration of lipid:MB becomes 50:1. MB loaded samples were centrifuged at 10 000 rpm for 2 h. The supernatant containing free MB molecules were analyzed in a UV−vis spectrophotometer (UVD-2950, Labomed Inc., USA), and the absorbance values were recorded for different sets of vesicles. The entrapment efficiency was calculated by using the equation[35]

$$\text{EE}\ (\%) = \frac{T - C}{T} \times 100 \quad (3)$$

where T is the total amount of dye presents both in the sediment and supernatant and C is the amount of drug detected only in the supernatant. T and C values were determined colorimetrically.

RESULTS AND DISCUSSION

Monomolecular Film Behavior at the Air−Buffer Interface. Surface Pressure (π)−Area (A) Isotherm. Using a Langmuir balance, pure and mixed lipidic monolayers were conveniently studied at the desired combination, which was not otherwise possible in the form of bilayer. Besides, different physicochemical parameters, viz., molecular organization and subsequent interaction between the different components, lift-off area, excess thermodynamic potential, film compressibility, etc., were evaluated from such measurements.[19] Despite the fact that the monolayers effectively were only half a bilayer, with a flat rather than curved structure, information from the monolayer studies can effectively be translated into liposome or cell membrane systems.[38] With this

DOI: 10.1021/jp512212u
J. Phys. Chem. B 2015, 119, 4251−4262

background, surface pressure−area isotherms for SLC + IPA mixtures (in the presence of 30 mol % cholesterol) were recorded at the air−PBS buffer (pH 7.4) interface. π−A isotherms for different combinations of SLC + IPA, along with 30 mol % cholesterol, are shown in Figure 1. The pure

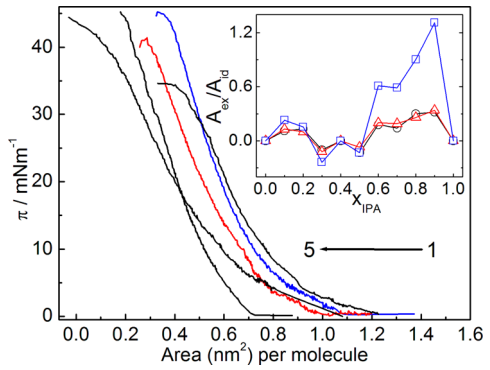

Figure 1. Surface pressure (π)−area (A) isotherm for the monomolecular films of SLC + IPA (in the presence of 30 mol % cholesterol) at the air−buffer interface at 25 °C. Amount of IPA (mol %): 1, 20; 2, 0; 3, 40; 4, 100; and 5, 50. Inset: A_{ex}/A_{id} vs x_{IPA} profile at π = (○) 0, (△) 20, and (□) 30 mN m^{-1}. A 0.1 mM PBS buffer (pH 7.4) in 100 mM NaCl was used as the subphase.

components, viz., SLC, IPA, and cholesterol, were also individually recorded as shown in Figure S1 (Supporting Information). The lift-off area for the components in their individual pure forms appeared at 1.10, 1.17, and 0.40 nm^2 molecule^{-1} for SLC, IPA, and cholesterol, respectively. While considering the effect of cholesterol on either SLC or the IPA, it was found that cholesterol exhibited condensation effect on the mixed monolayers. Lift-off area for SLC in combination with 30 mol % cholesterol appeared at 1.07 nm^2 molecule^{-1} while that for the IPA was at 1.08 nm^2 molecule^{-1}. Results were found to be comparable with the previously published reports.[19,39] Monolayers with unsaturated lipid exhibit as a single homogeneous liquid expanded (fluid) phase.[17,39,40] Lift-off area of IPA (1.08 nm^2 molecule^{-1}) was found to be significantly larger than the theoretically proposed value (~0.20 nm^2 molecule^{-1} per single chain).[40]

Results suggest that the molecular packing at the interface was somehow correlated to the bulky head groups of the IPA. Additionally, nonparallel orientations of the hydrocarbon chains were responsible for such differences. Cholesterol with a relatively smaller lift-off area (~0.4 nm^2 molecule^{-1}, from Supporting Information Figure S1) has a propensity to interdigitate itself into the bilayers with parallel orientation.[17]

Isotherms of mixed monolayers (SLC + IPA) were different from those of the individual components. Expanded isotherms were noticed for the systems with 20 mol % IPA; the lift-off area was found to be the highest, 1.21 nm^2 molecule^{-1}. Comparably condensed state for the mixed monolayer was initiated from 30 mol % IPA which continued up to 50 mol %. The isotherms for the mixed monolayers shifted to the lower area region from that of the pure isotherms with gradual increment of IPA, and indeed the lift-off area was reduced from 1.21 nm^2 molecule^{-1} (20 mol % IPA) to 0.71 nm^2 molecule^{-1} where IPA mol % was 50 as estimated from the π−A isotherms. Such studies clearly indicate the renovation/reorganization of the molecular packing at the interface to a more condensed state when the amount of IPA was higher than 20 mol %. The unusual variation with lesser IPA mol % can be rationalized as follows: the Coulombic forces of repulsion between bulky choline head groups of SLC were dominant in the presence of lower amounts of IPA leading to the expanded (fluidic) monolayer. Increasing amounts of IPA (>20 mol %) in the mixed monolayer assist the hydrogen bonding or van der Waals forces of attraction between SLC and IPA which overcome the Coulombic force exerted by the choline head groups, thus condensed mixed monolayer results.

Da-Cheng et al.[39] reported that C_8-substituted alkylaminomethylrutin (DAMR) and SLC were miscible but exhibited intermolecular repulsive force over the entire range of DMAR mole fraction. Reports on the monomolecular film studies in combination with different amphiphiles are available in the literature. Chang et al.[6] studied the monolayer behavior of IPA in the presence of double-tail cationic surfactant dihexadecyldimethylammonium bromide (DHDAB), where the dissociation of the IPA was confirmed at 50 mol %. Characterization of IPA was further reported by Panda et al.[19] where solubilization of IPA in the presence of additives like cholesterol and bile salt was confirmed and the distinguished properties of IPA with the variation of alkyl chain length were observed. In all of their studies, film functionality was found to be dependent on the composition of the lipid mixture.

Isotherms of the pure components lead to calculate ideal isotherms for the mixed systems according to the additivity rule:[41]

$$A_{id} = x_1A_1 + x_2A_2 \quad (4)$$

where A_{id} is the average theoretical area per molecule, x_1 and x_2 being mole fractions of the components 1 (SLC + 30 mol % cholesterol) and 2 (IPA + 30 mol % cholesterol), respectively. A_1 and A_1 are the corresponding area per molecule for the individual components. Deviation of the experimental value (A_{ex}) from the ideal one can be obtained through the calculation of the excess area per molecule as[27]

$$A_{ex} = A_{12} - A_{id} \quad (5)$$

where A_{12} is the experimental area per molecule of the mixed monolayer. Any deviation from linearity or any incidence of the appearance of maximum or minimum with varying composition would produce the extent of deviation from ideality.[42] In case of an ideal mixture, the calculated value (A_{id}) should be equal to that of the measured value (A_{12}) and should vary linearly with mole fraction of any components. On the other hand, for immiscible/noninteractive systems, each component hangs about as individual/clusters containing substantial/considerable amount of molecules. A negative deviation from the ideal behavior signifies associative interaction between lipidic hydrocarbon chains and the IPA. While a positive deviation (positive A_{ex}) signifies repulsive interaction.[27] Representative plots for the variation of A_{ex}/A_{id} with composition are shown in the inset of Figure 1. Initial positive deviation (for 10 and 20 mol % IPA) from the linearity was the outcome of repulsive interaction between SLC and IPA. Columbic repulsion, prevailing at low IPA mol %, causes the system to deviate positively from the ideality. However, associative interactions were validating for the systems with 30 and 50 mol % of IPA, respectively. Strong van der Waals force of interaction along with hydrogen bonding results in associative interaction which prevails the Coulombic repulsion for these systems. Significant divergence from the trend line was observed for 20 and 40 mol % IPA, suggesting some anomalous interactions than the other

DOI: 10.1021/jp512212u
J. Phys. Chem. B 2015, 119, 4251−4262

combinations. The calculated values of A_{ex}/A_{id} for the former were found to be ~0.117 and that for the latter was 0. This constancy was found for the entire range of surface pressure for the two. Loss of molecules from the surface monolayer into the subphase through the formation of vesicles and micelles could be the reason for this peculiar behavior, as been reported by Chang et al.[6] Dissociation of DS^- (because of its higher water solubility compared to $HTMA^+$) from IPA was the outcome when amphiphile concentration was higher and some sort of stress on IPA was initiated by SLC.[40] Accordingly, negatively charged phosphate group of the zwitterionic choline moiety could exert strong electrostatic interaction with the unbound $HTMA^+$ at the interface with desorption of DS^-. DS^- as the group's water-soluble characteristics would not be able to withstand high surface pressure at interface after being dispatched by the choline moiety. Reports are supporting the fact that the dissociation of excess ionic surfactant from the mixed cationic/anionic monolayers with nonequimolar ratio, whereas stably existed monolayer was confirmed with a mixture of equimolar ratio.[40] Thus, it could be inferred that dissociation of DS^- from IPA ($HTMA^+$–DS^-) was one of the reasons for the anomalous behavior that generate excess area curve.

Condensation of mixed monolayer (area contraction) at higher x_{IPA} was revealed from Figure 1, and the subtle structure of the monolayer could further be scrutinized from various factors such as ordering of chain, tilting of polar head, and molecular packing. To obtain the state of the investigated film and the consequent molecular ordering, compression modulus was calculated (according to eq 6) for different mixed monolayers. Film compressibility (C_s) is a measure of the resistance of the monolayer against compression; in other words, it can be defined as the amount of pressure needed to cause a change in the molecular area.[41] The reciprocal of compressibility, C_s^{-1} known as compression modulus, is also another route to demonstrate the phase transition.

$$C_s^{-1} = -A\left(\frac{\delta\pi}{\delta A}\right) \tag{6}$$

Such a representation is depicted in Figure 2. It is known that the monomolecular film with compressibility modulus in the range of 12.5–50 mN m^{-1} is in the liquid-expanded (LE) phase, whereas for the liquid states the value lie in the range of 50–100 mN m^{-1}.[19] In our present set of studies, all the mixed monolayers were in the LE phase as the compression modulii

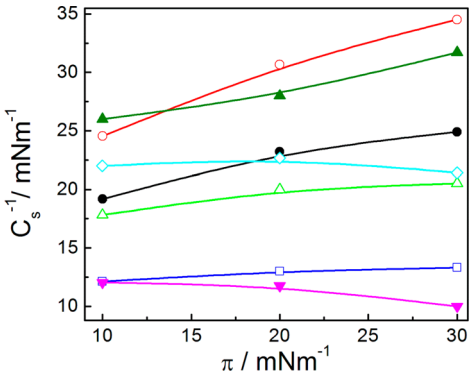

Figure 2. Variation in the compressibility modulii (C_s^{-1}) with the surface pressure for pseudo binary monomolecular films of SLC + IPA with 30 mol % cholesterol at 25 °C. Mol % of IPA: ●, 0; ○, 10; △, 20; □, 30; ◇, 40; ▲, 50; and ▼, 100.

were in between 12.5 and 50 mN m^{-1}. C_s^{-1} values were found to be larger for 10 mol % IPA and a little smaller for 50 mol %, which then increased with increasing surface pressure. Surface pressure independent of C_s^{-1} was noted for the mixed monolayer comprising 20 and 40 mol % IPA, which indeed was in good agreement with previous findings. Lowest C_s^{-1} values were found for the system comprising 30 mol % IPA as well as the system comprising IPA alone. Because of the unsaturation, these monolayers were more compressible than their saturated analogues. IPA, with the acyl chain, being saturated, experienced less compressibility than SLC. Such an observation is not uncommon.

Mixed monolayer study could be useful to formulate stable liposomal dispersions by considering different thermodynamic parameters of the interaction processes. The spontaneity associated with hydrophobic interactions between the hydrocarbons chains of SLC + IPA can also be viewed by evaluating the excess free energy change as given by the following equation:

$$\Delta G_{ex}^0 = \int_0^{\pi} (A_{12} - A_{id})\, d\pi \tag{7}$$

Quantitative assessment of the magnitude of the mutual interaction between SLC and IPA could be best studied by considering ΔG_{ex}^0 values. Figure 3 describes the variation in the

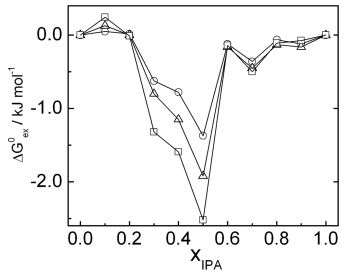

Figure 3. Variation of excess free energy (ΔG_{ex}^0) for the SLC + IPA mixed monolayer systems (in the presence of 30 mol % cholesterol) with the mole fraction of IPA (x_{IPA}) at different surface pressure (mN m^{-1}): ○, 10 ; △, 20; and □, 30 at 25 °C.

excess free energy with the composition of the mixed monolayer (x_{IPA}). Nonideal mixing behavior between SLC and IPA was confirmed from the run of the curves; positive deviation from the ideal behavior was observed for the system comprising <20 mol % IPA. Coulombic force of repulsive interaction between the polar head groups and the dissociation of DS^- from IPA could be associated in the process of mixing. Again, the cis orientation of one of the fatty acyl chains of SLC could resist the IPA to get condensed and subsequent nonspontaneity in the mixing processes was observed. Negative values of ΔG_{ex}^0 for 30, 40, and 50 mol % IPA indicate that the supplement of IPA into SLC monolayer grounds the formation of stable monolayer at their favorable arrangement. Because of the saturation of IPA, strong van der Waals force of interaction and hydrogen bonding among SLC and IPA result in an associative manner.

Thus, stable mixed monolayer resulted when IPA content was high. Unlike the systems with 30 and 50 mol % IPA, monolayer with 40 mol % IPA did not follow the same trend and produced relatively lower negative value of ΔG_{ex}^0 compared to the other two. Unfavorable interaction between SLC and IPA could be the reason as DS^- has a propensity to dissociate

DOI: 10.1021/jp512212u
J. Phys. Chem. B 2015, 119, 4251–4262

(when x_{IPA} is higher) in the presence of negatively charged phosphate ion of the choline group and get solublized into the subphase. Thus, the small negative ΔG^0_{ex} that originate for the system with 40 mol % IPA could be due to the associative electrostatic interaction between phosphate ion and $HTMA^+$.

In order to further scrutinize the interaction between SLC and IPA in their monolayer forms, apart from conventional monolayer thermodynamic parameters, regular solution theory was adopted. The interaction parameter (IP) describes the extent of interaction between SLC and IPA in mixed monolayer state and can be derived by using the following equation:[39]

$$w = \frac{\Delta G^0_{ex}}{x_1 x_2} \quad (8)$$

$$\mathrm{IP} = \frac{w}{RT} \quad (9)$$

IP as a function of π is plotted in Figure 4 and shows some fascinating points regarding the interaction process. Figure 4

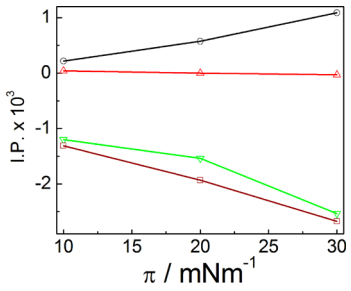

Figure 4. Relationship between interaction energy (IP) and surface pressure (π) at different IPA mol %: ○, 10; △, 20; ▽, 30; and □, 40. Temperature was set at 25 °C.

indicates that interaction was maximum for 10 mol % IPA and increasing linearly with π, whereas for 30 and 40 mol % IPA, IP is decreased with surface pressure. The system comprising 20 mol % IPA further established anomaly through its parallel propagation along the *X*-axis proving the interaction is surface pressure independent. A relatively high extent of interaction for 10 mol % IPA was due the presence of least amount of IPA in the monolayer. The presence of one IPA molecule for nine other combinations was a state where IPA was assumed to be interdigitated by huge amount of SLC. Cholesterol, being an additive, plays an important role for the interaction process.

With increasing π, cholesterol pushes the acyl chains of SLC which in turn hold the saturated hydrocarbon chain of IPA firmly to produce reasonable IP for this mixed monolayer. It could be stated as "arresting the IPA by lipids assembly through the lyophilic solvation in monolayer". On the contrary, we noticed relatively lower IP values for the systems with higher proportion of IPA. To address the corollary, one must need to consider the influence of headgroup packing between SLC and IPA. It is now known that IPA constitutes bulky head groups which produce lesser tight packing when mixed with SLC (as choline group is also a bulky headgroup). Again, desorption of DS^- from IPA and its subsequent solubilization was the reason that we could not find any changes in the values of I.P.

Lipid assemblies in the monolayer and bilayer forms are different. While the former having linear orientation, while the latter show curvature. Although there are some structural differences, mixed monolayer studies could be informative to explain the stability and biodiversity of SLC–IPA vesicles. It was concluded from π–*A* study that increasing proportion of IPA made the system more rigid although 10 mol % of IPA exhibited repulsive interaction. Some aberrations for 20 and 40 mol % of IPA were observed. Such anomalous behaviors are beyond explanation with the present level of knowledge. The mechanisms of such interactions are yet to be clear and could be explained on the basis of molecular dynamics simulation which is considered as one of the future perspectives.

Solution/Dispersion Behavior of the Vesicles in PBS Buffer at pH 7.4. Vesicles of different compositions were prepared in PBS buffer, and their solution properties were studied using a number of techniques in order to understand the bilayer packing of the components.

Dynamic Light Scattering (DLS) Studies. Hydrodynamic diameter (d_h) is an important parameter toward the direction of stability and biodistribution of vesicle formulations. Apart from the size, polydispersity index (PDI) is considered to be another important parameter as it describes the size distribution of dispersions having range from zero for a monodisperse system up to unity for completely polydispersed systems. Stability of the vesicles with different compositions of SLC and IPA, in combination with 30 mol % cholesterol, was investigated through the size measurement for a time period over 100 days starting from the day of sample preparation. Representative sizes vs time (day) profiles are presented in Figure 5. Size of the

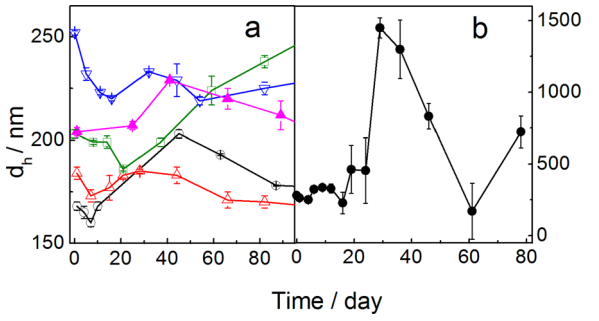

Figure 5. Variation in the hydrodynamic diameter (d_h) for SLC + IPA (in the presence of 30 mol % cholesterol) vesicles with time at 25 °C. Concentration of IPA (mol %): Panel a: ○, 0; △, 10; □, 20; ▽, 30; ▲, 50. Panel b: ●, 40.

vesicles passed through minima at ~10–12 days (except the system with 20 mol % IPA), which depended on the composition. This time period may be viewed as the equilibration time of the vesicles. Flipping and reorganization of components of vesicles occurred during this time period which led to the decrease in size. Initial observation shows that progressive addition of IPA to the SLC resulted in the size increment of vesicles. System with 40 mol % IPA exhibited inconsistent behavior compared to the other systems.

Such unambiguous variation was probably due to the mismatch in the packing of SLC and IPA in the form of bilayer. Because of the size constriction in IPA and subsequent loss of compactness in the packing of SLC and IPA, larger number of water molecules can occupy the palisade layer of vesicles. As a consequence, the extent of hydration increased[43] which eventually resulted in the overall size increment of the vesicles. Additionally, it is proposed that at this particular composition (40 mol % IPA) the SLC molecules can induce dissociation of the IPA ($HTMA^+$ and DS^- ions).[6] It subsequently results in the release of DS^- ions into the dispersion medium. However, further studies are warranted to

DOI: 10.1021/jp512212u
J. Phys. Chem. B 2015, 119, 4251–4262

bit final nail on this issue. Additionally, it was observed that the equilibration time increased with increasing amount of IPA. Initial size contraction for equilibration (systems with 10, 20, and 30 mol % IPA) may be attributed to the presence of saturated hydrocarbon chain of IPA which produces more hydrophobic environment in the bilayers. However, permanent size contraction was involved for the liposome with 10 mol % IPA, as also reflected from highest C_s^{-1} and IP (shown earlier) that demonstrate the strong interaction between SLC and IPA. Vesicles with 30 and 50 mol % IPA showed exceptional stability up to 100 days; the spontaneity of the interaction that arise for these two systems, as revealed from the excess Gibbs potential (ΔG_{ex}^0) value from monolayer study, also support the fact. Size of the vesicles with 20 mol % IPA monotonously increased with time; such systems also exhibited relatively higher PDI value. Such a different behavior could be rationalized through the surface pressure independent repulsive interaction between SLC and IPA as already reflected from the monolayer studies. Dissociation of DS^- from IPA could lead unfavorable orientation for lipid acyl chain which could lead the way of destabilization. However, the modes of interactions for these two sets of vesicles are yet to be revealed and cannot be explained with the present level of knowledge. Change in the PDI values with time have been graphically presented in the Supporting Information (Figure S3). Results on the DLS data recorded on day 45 are shown in Table 1 as representative.

Table 1. Hydrodynamic Diameter (d_h), Zeta Potential (ZP), and Polydispersity Index (PDI) Values for the Different Vesicle Formulations at 25 °C[a]

SLC:IPA	d_h/nm	ZP/mV	PDI
10:0	203.0 ± 2	−20.7 ± 1.41	0.28 ± 0.03
9:1	182.4 ± 4	−7.17 ± 1.30	0.20 ± 0.02
8:2	207.8 ± 2	−1.59 ± 0.45	0.28 ± 0.03
7:3	227.8 ± 8	−1.53 ± 0.79	0.24 ± 0.006
6:4	877.5 ± 8	+3.02 ± 0.87	0.95 ± 0.07
5:5	228.4 ± 1	−1.71 ± 1.41	0.31 ± 0.04

[a]Values correspond to the data acquired on day 45 of the sample preparation.

Stable liposomal dispersions were formed for the systems with the following compositions of SLC/IPA (M/M): 10:0, 9:1, 7:3, and for 5:5. It could therefore be concluded that the IPA plays an important role in stabilizing the vesicles by imparting monodispersity for which the IPA could be considered as novel substitutes of the conventional phospholipids.

Zeta potential (ZP) is another major parameter that holds the physical stability and subtle structure of vesicles as it determines the electrostatic repulsion between the vesicles.[12] Table 1 represents the zeta potential values of the vesicles with different SLC + IPA molar ratio recorded on day 45 of the sample preparation. Like the size measurements, ZP values varied nonsystematically up to 15 days, after which the values did not change appreciably until they became physically unstable. Generally, the zeta potential values were found to be negative, which accounts for the electrostatic stabilization among the lipidic dispersion and thus prevent vesicles from fusion or aggregation (the mean size did not change much as reflected from hydrodynamic size measurement study). With gradually increasing proportion of IPA in the vesicles (with respect to SLC), negative zeta potential values are found moved toward the positive range. SLC, a naturally occurring phospholipid, exhibited ZP ∼ −20.7 mV. The negative value of ZP was found to decrease with increasing IPA mol % in a nonlinear fashion. Except the vesicle with 40 mol % IPA, all other sets of vesicles exhibited negative ZP. Vesicles with 40 mol % IPA showed positive zeta potential; however, it was certainly a discrepancy which has already been explained on the basis of the dissociation of IPA and subsequent dissolution of DS^- ion into the bulk.[6] Dissociation of DS^- from IPA (for 40 mol % IPA) leaves $HTMA^+$ ion in the bilayer with SLC which effectively increased the overall positive ZP. The instability of the vesicle having 40 mol % IPA now could well be realized and could be correlated from the monolayer studies.

Electron Microscopic Studies. Both normal TEM and freeze-fractured TEM (FF-TEM) studies were carried out with an aim to confirm the formation of vesicles as well as their morphologies;[21,30,31,44] also, the impact of IPA on vesicles size could be evidenced from such measurements.[21,44,42] Representative TEM image of the vesicle with 30 mol % IPA has been shown in Figure 6. Spherical morphology and bilayer

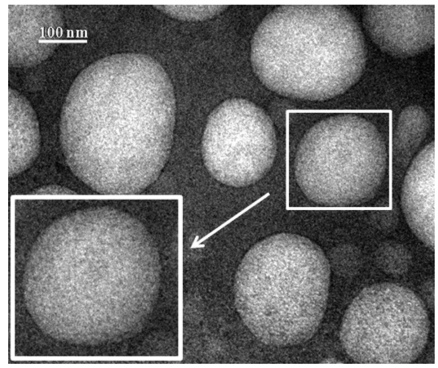

Figure 6. Representative TEM image of SLC + IPA (7:3, M/M) vesicles. Inset: magnified image of the selected area.

structure of the vesicles were confirmed from the image. In the inset, the magnified image of the selected vesicle further revealed the existence of the bilayer. Thus, TEM measurement could be considered as a useful tool to characterize a vesicular system.

FF-TEM studies were carried out to further support the normal TEM measurements, presented in Figure 7 as representatives.[30,31,45] Both the images in panel A (pure SLC) and B (7:3 SLC + IPA system) put on a view of spherical morphology as well as bilayer section around the vesicles. A distinct bilayer structure could be visualized as shown in the inset of panel A.

Vesicle sizes were found to be comparable in both normal TEM and in FF-TEM. Impact of IPA on SLC bilayer have been explored by means of different instrumentation, like DLS study; the fate of the vesicles were found to be same here also as we have witnessed minor size enhancement for 7:3 SLC + IPA. Spherical morphology of the vesicles was confirmed from the images and the clustered form so obtained was not uncommon for the vesicular systems.

Differential Scanning Calorimetry (DSC) Studies. Chain melting temperature (T_m) of the bilayer dispersion, its crystallinity, enthalpy of the transition processes (ΔH), and the heat capacity values (ΔC_p), etc., can suitably be evaluated by DSC studies. Such studies are exceedingly responsive in the presence of exogenously added compounds (herein the IPA).[44]

DOI: 10.1021/jp512212u
J. Phys. Chem. B 2015, 119, 4251−4262

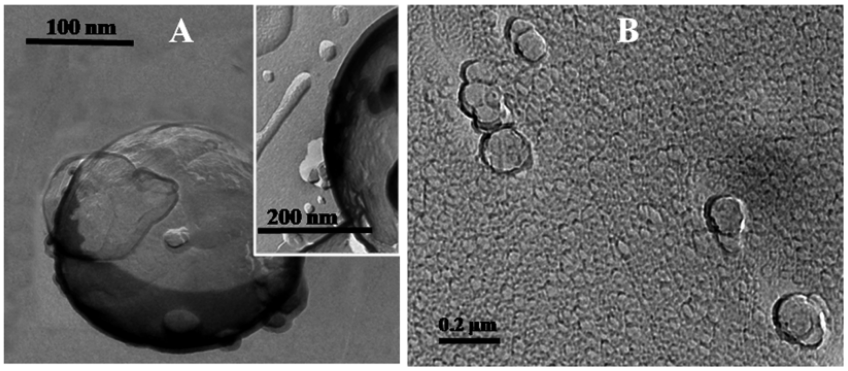

Figure 7. Freeze fractured TEM images of SLC + IPA (10:0, M/M, panel A) and SLC + IPA (7:3, M/M, panel B) vesicles.

Exogeneously added compound may alter the half peak width ($\Delta T_{1/2}$).

In the present set of studies, DSC measurements were carried out in the temperature range −25 to 25 °C with a scan rate of 2 °C min^{-1}. Representative thermograms are shown in Figure 8. Vesicles of different compositions with 30 mol % of

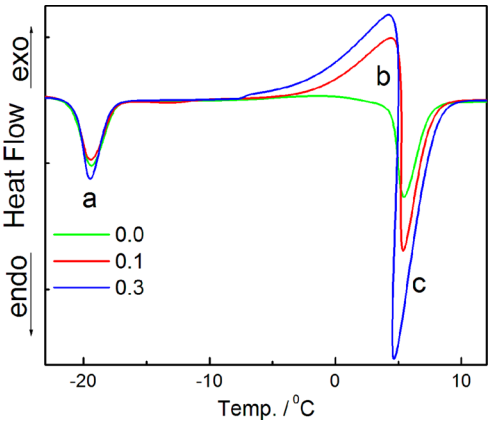

Figure 8. DSC thermograms of SLC + IPA vesicles at different SLC/IPA ratio (in the presence of 30 mol % cholesterol). Scan rate: 2 °C min^{-1}. Mole fractions of IPA are mentioned inside the figure.

cholesterol generated three distinct separate events. Two endotherms appeared at "a" in the temperature range −20 to −19 °C and another at "c" in the temperature range 3−6 °C, respectively. The exothermic one, "b", appeared in the temperature range 0−3 °C. SLC, with an unsaturation in one of its fatty acyl chains, exhibited the T_m at around −20 °C.The value was found to be comparable with the previously published report.[46] Endotherm "a" was due to the "phase transition" or "chain melting" of mixed acyl chains of SLC.[46] IPA has discrete effect on the thermogram. The bilayer chain melting temperature (T_m), width at half-peak height ($\Delta T_{1/2}$),[47] enthalpy change (ΔH), and corresponding heat capacities (ΔC_p) for the different formulations have been summarized in Figure 9. Incorporation of 10 mol % IPA enhanced T_m (0.8%) and lowered the $\Delta T_{1/2}$ (1.3%) values at ∼−20 °C, but a significant increase in the negative value of ΔH (11%) and positive value of ΔC_p (16%) were noticed. It was found that progressive addition of IPA into the SLC bilayers decreased the $\Delta T_{1/2}$ while increased ΔC_p in the transition region marked as "a". Sequential decrease of $\Delta T_{1/2}$ may be rationalized on the basis of the phase transitions. Results further support the surface pressure−area isotherm derived data. In case of the

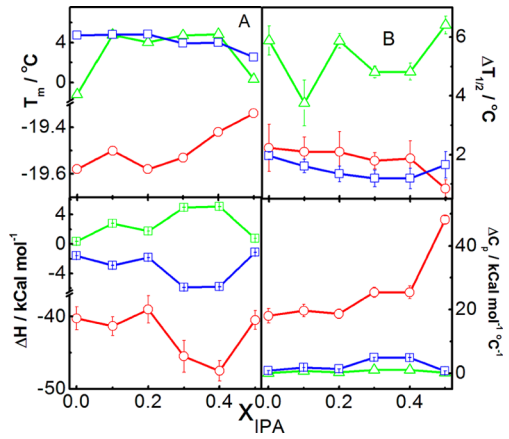

Figure 9. Variation in the transition temperature (T_m), half-peak width of the transitions ($\Delta T_{1/2}$), and enthalpy changes for the melting (ΔH) and changes in the heat capacity (ΔC_p) with the composition (mol % of IPA) for SLC + IPA vesicles comprising 30 mol % cholesterol. PBS buffer at pH 7.4 was used in the preparation of vesicles.

system with 10 mol % IPA, the monolayer exhibited more rigidity. Addition of IPA can cause the increased crystallinity for which there occurred an increase in the transition temperature and decreased $\Delta T_{1/2}$ values. IPA produced extra hydrophobic environment in the bilayers, which caused the physical state of bilayers as with its progressive addition turn the bilayers from fluid phase to gel phase. Because of the most ordered orientation of acyl chains in 5:5 SLC + IPA, it produced narrower distribution curve for the phase transitions. Increasing ΔC_p with increased concentration of IPA for SLC + IPA vesicles also further support the aforementioned explanation which is also further established by steady state fluorescence anisotropy experiment with DPH as hydrophobic probe (to be shown later).

The exothermic event "b" is an outcome of IPA effect, as reflected from Figure 8. With increasing IPA concentration, heat change of the process was noticeably increased. This release of heat is due to arrangement/packing of water molecule around the vesicles, which is a direct effect of IPA. Formation of an overlayer of water molecules over the lipidic head groups produces some sort of packing at temperature around 4 °C, where the density of water is at a maximum. Recently, Bhargava et al.[43] reported the enhanced membrane hydration for the hybrid vesicles, where one of its lipidic head groups was hydrophobic in nature and the extent of hydration was found to be increased with increasing headgroup hydrophobicity.

DOI: 10.1021/jp512212u
J. Phys. Chem. B 2015, 119, 4251−4262

IPA having an electrically neutral headgroup, induced more loose packing of the lipids in the vesicle, which eventually allowed more water molecule to penetrate into the surface and hence extent of hydration increased. An expected trend was observed from Figure 8, as with increasing amount of IPA, formation of water overlayer was also increased.

T_m for 10:0 SLC + IPA was found to be −1.17 °C, which interestingly jumped up to 4.76 °C for 9:1 SLC + IPA and did not change much for 7:3 SLC + IPA. So it can be concluded that shifting of T_m from −1.17 to 4.76 °C was surely the IPA induced effect. Lower $\Delta T_{1/2}$ values for 9:1 and 7:3 SLC + IPA systems than 10:0 SLC + IPA indicate better packing of the hydrophilic overlayer as well as lipidic head groups. This was again confirmed from the heat release (ΔH) of the process, where greater heat release for 9:1 and 7:3 SLC + IPA rather 10:0 were observed.

Appearance of neighboring endotherm "c" was a reverse consequence of the event "b" where heat was absorbed. From Figure 8 it is evident that the absorption of heat was also an IPA effect and exactly the opposite phenomenon to that of the exotherm "b". Endotherm "c" was due to the disorganization of water overlayer surrounding the vesicles. At relatively higher temperature, the lipidic head groups were supposed to be vibrating. This vibration transforms the water overlayer to turn from an organized to disorganized states. Although the T_m for 10:0, 9:1, and 7:3 SLC + IPA were not changed significantly, however relatively sharp peaks were noticed for the 9:1 and 7:3 SLC + IPA systems indicating better headgroup packing. Larger negative heat changes associated with 9:1 and 7:3 SLC + IPA systems again support the higher order of packing. It is known that both the events "b" and "c" are the two opposite phenomena and expected to show reverse heat change as also reflected from Figure 9.

Fluorescence Spectroscopic Studies. Fluorescence spectroscopy is another important technique which enables to explore the subtle structure of the membrane. Packing of bilayer (in the core of the membrane) and interaction of head groups (at the palisade layer) are the two major parameters for the formation of stable vesicle. With an aim to understand the packing of head groups, fluorescence spectroscopic studies were carried out using 7-hydroxycoumarine (7-HC) as a molecular probe. 7-HC is well-known as a solvatochromic dye and has a great tendency to stay on the palisade layer of the membrane.[32] Emission spectra of 7-HC in solvents of different polarity were carried out as the references in order to understand the state of polarity of the probe at the membranous interface. Emission spectra 7-HC in the vesicles of different compositions were recorded and compared with that in the solvents of different polarities. Emission spectra of 10 μM 7-HC under various conditions have been graphically presented in Figure 10.

Periodic declinations of intensities along with a mild red-shift were observed with increasing solvent polarity. Such an observation was also reported by others.[48] While considering the spectral behavior of 7-HC in the vesicles of different compositions, it was observed that with increasing amount of IPA in the vesicles, fluorescence intensity was enhanced along with a mild blue-shift. With increasing amount of IPA the difference in polarity was thus confirmed. It is not unexpected that IPA bearing neutralized head groups will effectively result in decreasing polarity of the bilayer.

Another interesting thing that additionally comes into the picture is the polarity of SLC vesicles with variant contents of IPA. Results clearly indicate that with increasing amount of IPA

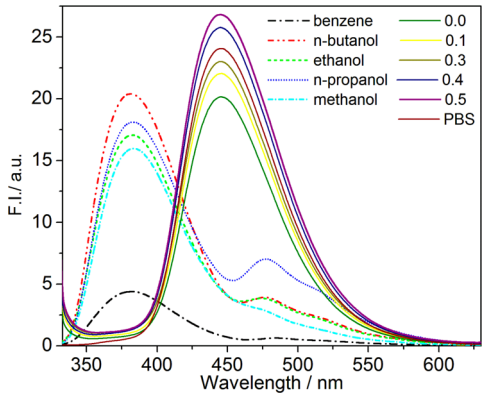

Figure 10. Fluorescence spectra of 10 μM 7-HC in solvents of different polarity (dashed lines) and vesicles of varying composition (solid lines) at 25 °C. Excitation wavelength (λ_{ex}) = 330 nm. Different solvents and the mole fraction of IPA are mentioned inside the figure. Spectra were also recorded in PBS alone.

in the vesicles, there were increase in rigidity and decrease in the polarity of the membranous interfaces. With an aim to understand the packing of the hydrocarbon chains (inside the bilayer) similar studies were carried out using 1,6-diphenyl-1,3,5-hexatriene (DPH) as the molecular probe. DPH being completely hydrophobic will preferentially reside in the lipid acyl chain with parallel orientation. Emission spectra of DPH in different vesicles have been shown in the Supporting Information (Figure S4). No significant change in the fluorescence spectra of DPH in different vesicles further supported its residence in the bilayer core. Results clearly indicate no change in the polarity of the core of bilayer for different combinations. However, the change in the hydrocarbon chain packing was further investigated by measuring the fluorescence anisotropy values.

A variation in the fluorescence anisotropy (r) with the composition of the vesicles has been graphically presented in Figure 11.

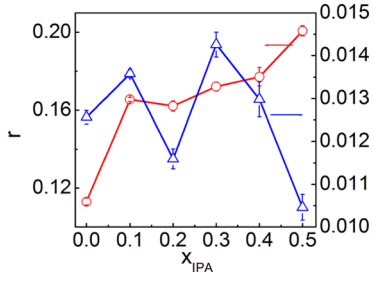

Figure 11. Variation in the fluorescence anisotropy (r) for DPH (○) and 7-HC (△) with IPA mol % in the vesicles comprising SLC + IPA + 30 mol % cholesterol. Temperature was set on 25 °C. While DPH evaluates the anisotropy value for the core hydrocarbon region of the bilayer, 7-HC monitors the anisotropy of the palisade layer.

While considering the fluorescence anisotropy variation of 7-HC with IPA mol %, it was noted that the addition of IPA resulted in an initial increase in the r values followed by the appearance of a maximum. Anomalous behavior for the system comprising 20 mol % IPA was noticed. Such anomalous behavior was also evidenced in other measurements. Initial increment of anisotropy was due to IPA addition which forced the SLC head groups to come closer. Such an incidence was

DOI: 10.1021/jp512212u
J. Phys. Chem. B 2015, 119, 4251−4262

most significant in the case of 30 mol % IPA. Lower anisotropy value for 5:5 SLC + IPA favors repulsive forces which causes the breakage of headgroup packing. Unusual behavior for the 20 mol % IPA system clearly indicates nonfavorable packing between the components. However, further studies, viz., NMR, small-angle neutron scattering (SANS), small-angle X-ray scattering (SAXS), and molecular dynamics simulation studies, could shed light in such a case, which are considered as the future perspectives. Figure 11 also represents periodic increment in the anisotropy value with progressive addition of IPA for the systems comprising DPH as the molecular probe. Vesicles with pure SLC showed least value because of the fluidic nature of the membrane. However, progressive addition of IPA resulted in the rigidity enhancement of hydrocarbon chains which brought some sort of crystallinity into the bilayer. Such an observation clearly implies that one can appreciably control the physical properties of vesicles through the incorporation of IPA into the SLC bilayer.

Entrapment Efficiency. Entrapment efficiency (EE) of the vesicles with varying amount of IPA has been tabulated in Table 2. EE was determined for the vesicles with varying composition. It was found that the EE was dependent on IPA concentration and satisfactory results were found through all the vesicles comprised with different mol % of IPA. Anomalous behavior was noticed for the system having 40 mol % IPA. The dye methylene blue is cationic in nature and expected to bind with the vesicles having negative surface potential. Pure SLC vesicles with highest negative zeta potential, showed maximum EE (92.50%) due to the strong electrostatic force of attraction. Progressive addition of IPA into the bilayer although decreased the EE mildly, yet the results were still reasonable as per as EE was concerned. 96.50% of EE was a strange result for 40 mol % IPA, and it was possibly due to the dissociation of IPA into corresponding cationic ($HTMA^+$) and anionic (DS^-) parts. The presence of zwitterionic choline headgroup and cationic $HTMA^+$ could provide excess electrostatic force of attraction which leads to the high EE value.

Table 2. Entrapment Efficiency (EE) of Different Sets of Vesicles with Varying mol % of SLC and IPA and Temperature at 25 °C[a]

system	entrapment efficiency (%)	system	entrapment efficiency (%)
10:0 SLC + IPA	92.5 ± 1.41	7:3 SLC + IPA	79.2 ± 0.79
9:1 SLC + IPA	90.0 ± 1.30	6:4 SLC + IPA	96.5 ± 0.87
8:2 SLC + IPA	88.7 ± 0.45	5:5 SLC + IPA	53.9 ± 1.41

[a] 4.0×10^{-4} M MB was used as the probe. MB:lipid ratio was fixed at 1:200.

CONCLUSIONS

SLC and IPA ($HTMA^+$–DS^-) in different sets of combination were used to prepare stable vesicles dispersions. Through the comprehensive investigation on the impact of IPA on the vesicles were evaluated from monolayer studies where it was concluded that IPA exerts prominent influence on SLC monolayer. Associative interactions were found for some mixed monolayers; however, the system with 50 mol % IPA did not respond to produce stable vesicles dispersions. Some aberrations were noted with the systems comprising 20 and 40 mol % IPA. Dissociation of DS^- ion from the vesicle resulted in such unusual variation. This was further scrutinized by measuring the hydrodynamic size of the hybrid vesicles, and we found relatively less stable vesicular dispersions for 20 and 40 mol % IPA. PDI values drew much attention because it unleashed the usefulness of IPA that reduce the PDI value and maintained fairly monodisperse systems. TEM and FF-TEM images of vesicles put on a view of spherical vesicle morphology and were well correlated to the data that obtained from DLS measurements. Packing of head groups as well as packing of the hydrocarbon chains were investigated through the combined DSC and fluorescence spectroscopic analysis where gradual incorporation of IPA into the bilayer produces rigidity or crystallinity. Systems comprising 0, 10, 20, 30, and 50 mol % IPA produce promising drug entrapment efficiency. Thus, IPA assisted vesicular system could be used as a carrier for drug delivery. The future prospective would be to characterize the systems theoretically based on molecular dynamics simulation and to study the interaction through ^1H, ^{13}C NMR, SANS, SAXS, and cryo-TEM studies.

ASSOCIATED CONTENT

Supporting Information

Four figures displaying surface-pressure area isotherms for SLC, IPA, and cholesterol in pure form (Figure S1), free energy of mixing (ΔG_{mix}) of SLC and IPA (Figure S2), PDI of different sets of vesicles as a function of time (Figure S3), and steady state fluorescence spectra of DPH incorporated into varying molar ratio of SLC + IPA in PBS (pH 7.4) (Figure S4). This material is available free of charge via the Internet at http://pubs.acs.org.

AUTHOR INFORMATION

Corresponding Author

*E-mail: akpanda1@yahoo.com (A.K.P.).

Notes

The authors declare no competing financial interest.

ACKNOWLEDGMENTS

The research project is funded by Council of Scientific & Industrial Research, Govt. of India, New Delhi, India (Project No.-01(2533)/11/EMR-II), India. Our sincere thanks to the Centre for Surface Science, Department of Chemistry, Jadavpur University, Kolkata, India, for the monolayer study. All the members under TEM unit, Sophisticated Analytical Instrument Facility, North Eastern Hill University are sincerely acknowledged for the TEM measurements. Also our heartfelt gratitude to the Department of Pure and Applied Chemistry, Tokyo University of Science, Japan, for the FF-TEM studies. P.G. acknowledges the University Grants Commission (UGC) Govt. of India, New Delhi, India - Basic Scientific Research (BSR) for a research fellowship.

DEDICATION

The manuscript is dedicated to Prof. Satya Priya Moulik, one of the mentors of A.K.P., on his 79th birthday.

REFERENCES

(1) Luna, C.; Stroka, K. M.; Bermudez, H.; Aranda-Espinoza, H. Thermodynamics of Monolayers formed by Mixtures of Phosphatidylcholine/Phosphatidylserine. *Colloids Surf., B* **2011**, *85*, 293–300.

(2) Hara, T.; Kuwasawa, H.; Aramaki, Y.; Takada, S.; Koike, K.; Ishidate, K.; Kato, H.; Tsuchiya, S. Effects of Fusogenic and DNA-Binding Amphiphilic Compounds on the Receptor-Mediated Gene

DOI: 10.1021/jp512212u
J. Phys. Chem. B 2015, 119, 4251–4262

Transfer into Hepatic Cells by Asialofetuin-Labeled Liposomes. *Biochim. Biophys. Acta* **1996**, *1278*, 51−58.
(3) Unates, L. E.; Farias, R. N. Biomembrane Cooperative Enzymes. *In Vivo* Modulation of Rat Erythrocyte Acetylcholinesterase by Insulin in Normal and Diabetic Conditions. *Biochim. Biophys. Acta* **1979**, *568*, 363−369.
(4) Pintschovius, J.; Fendler, K.; Bamberg, E. Charge Translocation by The Na+/K+-Atpase Investigated on Solid Supported Membranes: Cytoplasmic Cation Binding and Release. *Biophys. J.* **1999**, *76*, 827−836.
(5) Parimi, S.; Barnes, T. J.; Prestidge, C. A. PAMAM Dendrimer Interactions with Supported Lipid Bilayers: A Kinetic and Mechanistic Investigation. *Langmuir* **2008**, *24*, 13532−13539.
(6) Lee, J.; Chang, C.-H. The Interaction Between the Outer Layer of a Mixed Ion Pair Amphiphile/Double-Chained Cationic Surfactant Vesicle and DNA: A Langmuir Monolayer Study. *Soft Matter* **2014**, *10*, 1831−1839.
(7) Isailović, B. D.; Kostić, I. T.; Zvonar, A.; Đorđević, V. B.; ašperlin, M.; Nedović, V. A.; Bugarski, B. M. Resveratrol Loaded Liposomes Produced by Different Techniques. *Innov. Food Sci. Emerg. Technol.* **2013**, *19*, 181−189.
(8) Kato, K.; Walde, P.; Koine, N.; Ichikawa, S.; Ishikawa, T.; Nagahama, R.; Ishihara, T.; Tsujii, T.; Shudou, M.; Omokawa, Y.; Kuroiwa, T. Temperature-Sensitive Nonionic Vesicles Prepared from Span 80 (Sorbitan Monooleate). *Langmuir* **2008**, *24*, 10762−10770.
(9) Akbarzadeh, A.; Rezaei-Sadabady, R.; Davaran, S.; Joo, S. W.; Zarghami, N.; Hanifehpour, Y.; Samiei, M.; Kouhi, M.; Nejati-Koshki, K. Liposome: Classification, Preparation, and Applications. *Nanoscale Res. Lett.* **2013**, *8*, 8−102.
(10) Sabín, J.; Ruso, J. M.; González-Pérez, A.; Prieto, G.; Sarmiento, F. Characterization of Phospholipid + Semifluorinated Alkane Vesicle System. *Colloids Surf., B* **2006**, *47*, 64−70.
(11) Alexander, M.; Acero Lopez, A.; Fang, Y.; Corredig, M. Incorporation of Phytosterols in Soy Phospholipids Nanoliposomes: Encapsulation Efficiency and Stability. *LWT—Food Sci. Technol.* **2012**, *47*, 427−436.
(12) da Silva Malheiros, P.; Micheletto, Y. M. S.; Silveira, N. P. d.; Brandelli, A. Development and Characterization of Phosphatidylcholine Nanovesicles Containing the Antimicrobial Peptide Nisin. *Food Res. Int.* **2010**, *43*, 1198−1203.
(13) Kaler, E.; Murthy, A.; Rodriguez, B.; Zasadzinski, J. Spontaneous Vesicle Formation in Aqueous Mixtures of Single-Tailed Surfactants. *Science* **1989**, *245*, 1371−1374.
(14) Ghosh, P.; Han, G.; De, M.; Kim, C. K.; Rotello, V. M. Gold Nanoparticles in Delivery Applications. *Adv. Drug Delivery Rev.* **2008**, *60*, 1307−1315.
(15) Gao, Y.; Hao, J. Electrochemical Synthesis of Zinc Nanoparticles via a Metal-Ligand-Coordinated Vesicle Phase. *J. Phys. Chem. B* **2009**, *113*, 9461−9471.
(16) Dong, R.; Weng, R.; Dou, Y.; Zhang, L.; Hao, J. Preparation of Calcium Oxalate by Vesicle Modification in the Catanionic Surfactant System CDS/TTABr/H_2O. *J. Phys. Chem. B* **2010**, *114*, 2131−2139.
(17) Duncan, S. L.; Larson, R. G. Folding of Lipid Monolayers Containing Lung Surfactant Proteins SP-B1−25 and SP-C Studied via Coarse-Grained Molecular Dynamics Simulations. *Biochim. Biophys. Acta* **2010**, *1798*, 1632−1650.
(18) Kuo, A.-T.; Chang, C.-H. Cholesterol-Induced Condensing and Disordering Effects on a Rigid Catanionic Bilayer: A Molecular Dynamics Study. *Langmuir* **2013**, *30*, 55−62.
(19) Maiti, K.; Bhattacharya, S.; Moulik, S.; Panda, A. Physicochemical Studies on Ion-Pair Amphiphiles: Solution and Interfacial Behaviour of Systems Derived from Sodium Dodecylsulfate and N-alkyltrimethylammonium Bromide Homologues. *J. Chem. Sci.* **2010**, *122*, 867−879.
(20) Kuo, A.-T.; Chang, C.-H.; Shinoda, W. Molecular Dynamics Study of Catanionic Bilayers Composed of Ion Pair Amphiphile with Double-Tailed Cationic Surfactant. *Langmuir* **2012**, *28*, 8156−8164.
(21) Li, W.-T.; Yang, Y.-M.; Chang, C.-H. Stability Enhancement Effect of Normal Long-Chain Alcohols on Ion Pair Amphiphile Monolayers at the Air/Water Interface. *J. Colloid Interface Sci.* **2008**, *327*, 426−432.
(22) Li, W.-T.; Yang, Y.-M.; Chang, C.-H. Langmuir Monolayer Behavior of an Ion Pair Amphiphile with a Double-Tailed Cationic Surfactant. *Colloids Surf., B* **2008**, *66*, 187−194.
(23) Panda, A. K.; Possmayer, F.; Petersen, N. O.; Nag, K.; Moulik, S. P. Physico-Chemical Studies on Mixed Oppositely Charged Surfactants: Their Uses in the Preparation of Surfactant Ion Selective Membrane and Monolayer Behavior at the Air-Water Interface. *Colloids Surf., A* **2005**, *264*, 106−113.
(24) Carvalho, C. A.; Olivares-Ortega, C.; Soto-Arriaza, M. A.; Carmona-Ribeiro, A. M. Interaction of Gramicidin with DPPC/DODAB Bilayer Fragments. *Biochim. Biophys. Acta* **2012**, *12*, 3064−3071.
(25) Hungerford, G.; Baptista, A. L. F.; Coutinho, P. J. G.; Castanheira, E. M. S.; Oliveira, M. E. C. D. R. Interaction of DODAB with Neutral Phospholipids and Cholesterol Studied using Fluorescence Anisotropy. *J. Photochem. Photobiol., B* **2006**, *181*, 99−105.
(26) Takegami, S.; Kitamura, K.; Kitade, T.; Takashima, M.; Ito, M.; Nakagawa, E.; Sone, M.; Sumitani, R.; Yasuda, Y. Effects of Phosphatidylserine and Phosphatidylethanolamine Content on Partitioning of Triflupromazine and Chlorpromazine between Phosphatidylcholine-Aminophospholipid Bilayer Vesicles and Water Studied by Second-Derivative Spectrophotometry. *Chem. Pharm. Bull.* **2005**, *53*, 147−150.
(27) Panda, A. K.; Nag, K.; Harbottle, R. R.; Possmayer, F.; Petersen, N. O. Thermodynamic Studies of Bovine Lung Surfactant Extract Mixing with Cholesterol and its Palmitate Derivative. *J. Colloid Interface Sci.* **2007**, *311*, 551−555.
(28) Paul, S.; Panda, A. K. Physico-chemical Studies on Ionic Liquid Microemulsion: Phase Manifestation, Formation Dynamics, Size, Viscosity, Percolation Of Electrical Conductance and Spectroscopic Investigations on 1-butyl-3-methyl imidazolium methanesulfonate +water/Tween 20 + *n*-pentanol/n-heptane Pseudoternary System. *Colloids Surf., A* **2013**, *419*, 113−124.
(29) Gupta, V.; Gupta, R.; Grover, R.; Khanna, R.; Jangra, V.; Mittal, A. Delivery of Molecules to Cancer Cells Using Liposomes from Bacterial Cultures. *J. Nanosci. Nanotechnol.* **2008**, *8*, 2328−2333.
(30) Škalko, N.; Bouwstra, J.; Spies, F.; Stuart, M.; Frederik, P. M.; Gregoriadis, G. Morphological Observations on Liposomes Bearing Covalently Bound Protein: Studies with Freeze-Fracture and Cryo Electron Microscopy and Small Angle X-ray Scattering Techniques. *Biochim. Biophys. Acta* **1998**, *1370*, 151−160.
(31) Söptei, B.; Mihály, J.; Visy, J.; Wacha, A.; Bóta, A. Intercalation of Bovine Serum Albumin Coated Gold Clusters between Phospholipid Bilayers: Temperature-Dependent Behavior of Lipid-AuQC@BSA Assemblies with Red Emission and Superlattice Structure. *J. Phys. Chem. B* **2014**, *118*, 3887−3892.
(32) Pal, R.; Petri, W. A., Jr.; Ben-Yashar, V.; Wagner, R. R.; Barenholz, Y. Characterization of the Fluorophore 4-heptadecyl-7-hydroxycoumarin: A Probe for the Head-Group Region of Lipid Bilayers and Biological Membranes. *Biochemistry* **1985**, *24*, 573−581.
(33) Ehrlich, N.; Christensen, A. L.; Stamou, D. Fluorescence Anisotropy Based Single Liposome Assay to Measure Molecule-Membrane Interactions. *Anal. Chem.* **2011**, *83*, 8169−8176.
(34) Companyo, M.; Iborra, A.; Villaverde, J.; Martinez, P.; Morros, A. Membrane Fluidity Changes in Goat Sperm Induced by Cholesterol Depletion using Beta-Cyclodextrin. *Biochim. Biophys. Acta* **2007**, *9*, 2246−2255.
(35) Kapil, S.; Rekha, R.; Vipin, S. Preparation and Evaluation of Lornoxicam Niosomal Gel. *Int. Res. J. Pharm.* **2012**, *3*, 378−383.
(36) Park, S. H.; Oh, S. G.; Mun, J. Y.; Han, S. S. Loading of Gold Nanoparticles inside the DPPC Bilayers of Liposome and their Effects on Membrane Fluidities. *Colloids Surf., B* **2006**, *48*, 112−118.
(37) Park, S. H.; Oh, S. G.; Suh, K. D.; Han, S. H.; Chung, D. J.; Mun, J. Y.; Han, S. S.; Kim, J. W. Control over Micro-Fluidity of Liposomal Membranes by Hybridizing Metal Nanoparticles. *Colloids Surf., B* **2009**, *70*, 108−113.

DOI: 10.1021/jp512212u
J. Phys. Chem. B 2015, 119, 4251−4262

(38) Brockman, H. Lipid Monolayers: Why Use Half a Membrane to Characterize Protein-Membrane Interactions? *Curr. Opin. Struct. Biol.* **1999**, *9*, 438−443.
(39) He, F.; Li, R. X.; Wu, D. C. Monolayers of Mixture of Alkylaminomethyl Rutin and Lecithin at the Air/Water Interface. *J. Colloid Interface Sci.* **2010**, *349*, 215−23.
(40) Zhao, L.; Feng, S.-S. Effects of Lipid Chain Unsaturation and Headgroup Type on Molecular Interactions between Paclitaxel and Phospholipid within Model Biomembrane. *J. Colloid Interface Sci.* **2005**, *285*, 326−335.
(41) Nichols-Smith, S.; Teh, S. Y.; Kuhl, T. L. Thermodynamic and Mechanical Properties of Model Mitochondrial Membranes. *Biochim. Biophys. Acta* **2004**, *27*, 1−2.
(42) Panda, A. K.; Nag, K.; Harbottle, R. R.; Possmayer, F.; Petersen, N. O. Thermodynamic Studies on Mixed Molecular Langmuir Films: Part 2. Mutual Mixing of DPPC and Bovine Lung Surfactant Extract with Long-Chain Fatty Acids. *Colloids Surf., A* **2004**, *247*, 9−17.
(43) Bhargava, P.; Singh, M.; Sreekanth, V.; Bajaj, A. Nature of the Charged Headgroup Determines the Fusogenic Potential and Membrane Properties of Lithocholic Acid Phospholipids. *J. Phys. Chem. B* **2014**, *118*, 9341−9348.
(44) Jobin, M.-L.; Bonnafous, P.; Temsamani, H.; Dole, F.; Grélard, A.; Dufourc, E. J.; Alves, I. D. The Enhanced Membrane Interaction and Perturbation of a Cell Penetrating Peptide in the Presence of Anionic Lipids: Toward an Understanding of its Selectivity for Cancer Cells. *Biochim. Biophys. Acta* **2013**, *1828*, 1457−1470.
(45) Yan, Y.; Huang, J.; Li, Z.; Ma, J.; Fu, H.; Ye, J. Vesicles with Superior Stability at High Temperature. *J. Phys. Chem. B* **2003**, *107*, 1479−1482.
(46) de Sousa, I. S.; Castanheira, E. M.; Rocha Gomes, J. I.; Real Oliveira, M. E. Study of the Release of a Microencapsulated Acid Dye in Polyamide Dyeing Using Mixed Cationic Liposomes. *J. Liposome Res.* **2011**, *21*, 151−157.
(47) Zhao, L.; Feng, S. S.; Kocherginsky, N.; Kostetski, I.; DSC, E. P. R. Investigations on Effects of Cholesterol Component on Molecular Interactions between Paclitaxel and Phospholipid Within Lipid Bilayer Membrane. *Int. J. Pharm.* **2007**, *338*, 258−266.
(48) Kodape, M. M.; Gawhale, N. D.; Kamble, D. D.; Dabhade, S. A.; Awajare, N. V. Green Chemistery Approach for Synthesis of Derivatives of Coumarin and Comparative Study by Fluorescence Spectrophotometer. *Sci. Rev. Chem. Commun.* **2012**, *2*, 201−205.

DOI: 10.1021/jp512212u
J. Phys. Chem. B 2015, 119, 4251−4262